INFORMATION TO USERS

This manuscript has been reproduced from the microfilm master. UMI films the text directly from the original or copy submitted. Thus, some thesis and dissertation copies are in typewriter face, while others may be from any type of computer printer.

The quality of this reproduction is dependent upon the quality of the copy submitted. Broken or indistinct print, colored or poor quality illustrations and photographs, print bleedthrough, substandard margins, and improper alignment can adversely affect reproduction.

In the unlikely event that the author did not send UMI a complete manuscript and there are missing pages, these will be noted. Also, if unauthorized copyright material had to be removed, a note will indicate the deletion.

Oversize materials (e.g., maps, drawings, charts) are reproduced by sectioning the original, beginning at the upper left-hand corner and continuing from left to right in equal sections with small overlaps.

Photographs included in the original manuscript have been reproduced xerographically in this copy. Higher quality 6" x 9" black and white photographic prints are available for any photographs or illustrations appearing in this copy for an additional charge. Contact UMI directly to order.

ProQuest Information and Learning
300 North Zeeb Road, Ann Arbor, MI 48106-1346 USA
800-521-0600

UMI®

Coherently pumped micromasers

by

István Németh

A dissertation submitted to the Graduate Faculty in Physics in partial fulfillment of the requirements for the degree of Doctor of Philosophy, The City University of New York

2002

This manuscript has been read and accepted for the Graduate Faculty in Physics in satisfaction of the dissertation requirement for the degree of Doctor of Philosophy.

01/22/02
Date

Chair of Examining Committee
Professor János A. Bergou

01/16/02
Date

Executive Officer
Professor Louis S. Celenza

Professor Mark Hillery

Professor Ying–Chih Chen

Professor Edward A. Whittaker
Supervisory Committee

THE CITY UNIVERSITY OF NEW YORK

Abstract

Coherently pumped micromasers

by

István Németh

Adviser: Professor János A. Bergou

There are few systems in physics which can be investigated under clean experimental conditions and at the same time can be studied starting from first principles, using exact theoretical methods. The single-atom maser or micromaser is one of these remarkable systems, it allows us a detailed study of the atom-field interaction. The situation realized in a micromaser is very close to the ideal case of a single two-level atom interacting with a single quantized mode of a superconducting cavity. Considerable amount of work, both theoretical and experimental, has been devoted to the study of this system. However, it remains to be established how the system behaves under coherent pumping. In this work our goal is to provide a comprehensive study of the coherently pumped micromaser. We derive the master equation governing the time evolution of the field inside the coherently pumped micromaser. We then solve the resulting equation of motion, first by using the semiclassical approximation which we extend to handle the case of the coherently pumped micromaser. Then we develop a new analytical method to obtain the full quantum mechanical solution. We

also generalize the trapping states of the micromaser for the case of the coherently pumped micromaser and provide a clear physical picture of the full quantum mechanical solution. Finally we derive the phase density function describing the result of an optimal measurement of the phase of the coherently pumped micromaser's field. With the help of this density function we study the phase properties of the steady state field and determine bistable and multistable regions of operation.

Acknowledgments

I wish to express my deepest gratitude and appreciation to my adviser Professor János A. Bergou. His support, guidance and encouragement were invaluable and his warm and friendly interaction were indispensable. I am grateful to Professor Mark Hillery for the many inspiring discussions we had, and thankful for the seminars he organized over the years. I would like to thank to the other members of my dissertation supervisory committee, Professor Ying–Chih Chen and Professor Edward A. Whittaker for agreeing to serve on my committee, for their careful reading of this manuscript and for their helpful advice. My thanks also belong to my dear friend and colleague Jozef Škvarček for being a true friend and for building our parallel cluster which made the numerical parts of this work possible.

I also wish to acknowledge with gratitude the Department of Physics of Hunter College for providing me with this opportunity and support.

My sincere gratitude and great appreciation to my wife Zsuzsanna and to my parents is beyond description. Without their support, understanding and sacrifice during the years of my graduate study this work would never have been possible. I dedicate this work to them.

To my family...

Table of Contents

List of Tables

List of Figures

1

Introduction

There are few systems in physics which can be investigated under clean experimental conditions and at the same time can be studied starting from first principles, using exact theoretical methods. The single-atom maser or micromaser is one of these remarkable systems, it allows us a detailed study of the atom-field interaction. The situation realized in a micromaser is very close to the ideal case of a single two-level atom interacting with a single quantized mode of a superconducting cavity.

The story of the micromaser began with the papers published by Filipowicz *et al.* [1, 2] on the theory of the microscopic maser (for a recent review see [3]). They investigated the case where the two-level atoms before interaction were all excited to their upper level and found that the field inside the cavity goes through thresholds that resemble first-order phase transitions, as the pump rate increases. This remarkably simple system which exhibits a rich structure of phase transitions caught the attention of experimentalists who, in turn, soon came up with various realizations of this system [4–8]. The modern techniques of experimental physics made it possible to build superconducting high-Q niobium microcavities which could maintain large photon numbers. In the most recent experiments, values of the quality factor as high as

3×10^{10} have been achieved for the resonant mode, corresponding to an average lifetime of a photon in the cavity of 0.2s. A consequence of the high-Q value is that the photon lifetime is much longer than the interaction time of an atom with the maser field. Therefore during the time the atom passes through the cavity the only change in the cavity field is due to the atom-field interaction which than can be simply treated using the Jaynes–Cummings model [9, 10]. The atoms used in these micromaser experiments are rubidium Rydberg atoms pumped by laser excitation into the upper level of the maser transition. The theory of the micromaser flourished, remarkable quantum effects have been discovered such as the quantum clock [11], maser action without inversion [12] and the collapse and revival of Rabi oscillations [6]. Also, various uniquely quantum-mechanical states of the field, including entangled states [13], trapping states [2, 14], tangent and cotangent states [15, 16], sub-Poissonian photon statistics [7] and even the Fock state [17], have been generated. All these theoretical and experimental findings indicated the great importance of the study of the micromaser.

Although considerable work, both theoretical and experimental, has been carried out on this system, with a few exceptions noted below, most cases involved injecting atoms into the micromaser cavity in their excited state. An implication of this condition was that the density matrix describing the field remained diagonal in the case when it was initially diagonal. (An initial condition experimentally realizable, allowing the system to relax until no transient non-diagonal elements are left.) Therefore, investigations of phase diffusion [18, 19] and the spectrum [20–26] of the micromaser

involved both the creation of non-diagonal density matrix elements and the study of their decay. The creation of the non-diagonal elements of the density matrix can be achieved in two ways, either by injecting a preselected phase into the micromaser or by post-selecting a phase via the detection of the exiting atoms [27–30]. In our work we use the preselection of phase, which is achieved by injecting atoms, initially prepared in a proper form of the atomic coherence, into the micromaser cavity. Although investigations of the coherently pumped micromaser progressed, e.g. Krause *et al.* described how, the phase of the atomic coherence is transferred to the field in the limit of weak atom-field coupling, and Slosser *et al.* [15, 16] found that the field of a coherently pumped lossless micromaser evolves toward pure states, called tangent and cotangent states, a comprehensive study of the coherently pumped micromasers is yet to be given. Especially interesting problems are the relation of the phase of the steady state field to that of the driving atomic dipoles under general conditions, even in the case of off-resonant pumping, and developing analytical methods which can successfully handle this highly non-linear system. In this work our goal is to provide a comprehensive study of the coherently pumped micromasers focusing on these questions.

The work is organized as follows. In chapter 2 we derive the master equation governing the time evolution of the field inside the coherently pumped micromaser. In chapter 3 we solve the equation of motion using the semiclassical approximation [31, 32] which we extend to handle the case of the coherently pumped micromaser. In chapter 4 we provide a new method to obtain the full quantum mechanical solution.

In chapter 5 we generalize the trapping states of the micromaser for the case of the coherently pumped micromaser and in chapter 6 we provide a clear physical picture of the full quantum mechanical solution. In chapter 7 we derive the phase density function describing the result of an optimal phase measurement on the phase of the micromaser field and in chapter 8 we study the properties of the phase of the steady state field.

2

Model and the field master equation

In this chapter our goal is to introduce the model of a coherently pumped micromaser and to derive the master equation controlling the time evolution of the electromagnetic field inside the micromaser cavity.

Our model, illustrated in Fig. 1, consists of a stream of two-level atoms (upper

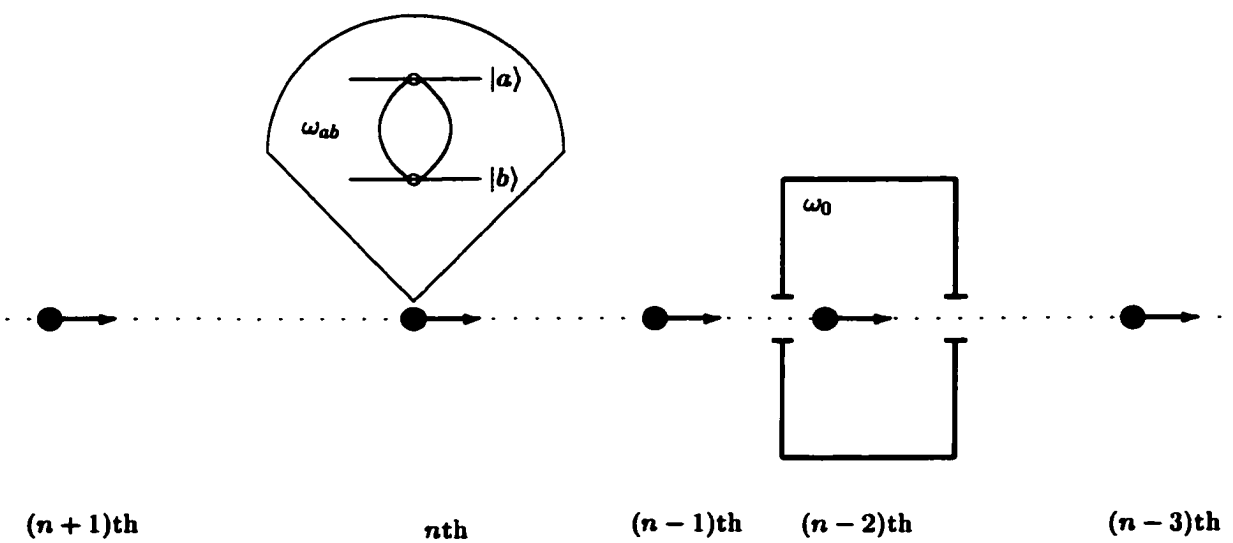

Figure 1: Micromaser pumped by two-level atoms initially prepared in coherent superposition of their upper $|a\rangle$ and lower $|b\rangle$ levels.

level a and lower level b) and a single mode of a high-Q micromaser cavity. The atoms, initially prepared in a proper form of the atomic coherence, are randomly

injected into the micromaser cavity at a rate r low enough that at most one atom at a time is present inside the cavity. In the cavity they interact with a single mode of the micromaser field for a time period of $\tau \ll 1/r$ where τ is the transit time of the atoms through the micromaser cavity. We assume that the nth atom is injected into the micromaser cavity at time t_n with the initial density matrix

$$\rho_{atom}^{(n)}(t_n) = \begin{pmatrix} \rho_{aa} & \lambda\rho_{ab}\mathrm{e}^{-i\nu t_n} \\ \lambda\rho_{ba}\mathrm{e}^{i\nu t_n} & \rho_{bb} \end{pmatrix}, \tag{2.1}$$

for a discussion on the preparation of atoms in such a state see the article by Lu and Bergou [33]. In Eq. (2.1)

$$\rho_{ab} = \rho_{ba}^{*} = |\rho_{ab}|\,\mathrm{e}^{i\varphi_{ab}}, \tag{2.2}$$

$$|\rho_{ab}| = \sqrt{\rho_{aa}\rho_{bb}}, \tag{2.3}$$

and

$$\rho_{bb} = 1 - \rho_{aa}. \tag{2.4}$$

Furthermore ν is the injected signal frequency and $\lambda \in [0, 1]$ is the parameter which determines the degree of the injected coherence (i.e. if $\lambda = 0$ no atomic coherence is injected since the non-diagonal elements of the atomic density matrix vanish and if $\lambda = 1$ the maximal atomic coherence determined by Eq. (2.2) and Eq. (2.3) is injected into the micromaser). Introducing λ allowed us to continuously scale our model to describe both the coherently and incoherently pumped micromaser.

In order to derive the master equation describing the time evolution of the single-mode electromagnetic field inside the micromaser cavity we follow the proce-

dure outlined by Cresser [34]. In the random process of pumping the micromaser the atomic arrival times t_n obey Poisson statistics. The basic assumption for the Poisson process is that the behavior of the process after the arrival of an atom should be independent of the behavior of the process before the arrival and probabilistically like the original process (regeneration). In particular, the general regeneration assumption means that the times between arrivals, $X_{n+1} = t_{n+1} - t_n$, known as interarrival times, must be independent, identically distributed random variables. Moreover, using the general regeneration assumption it is also easy to show that the random variable X describing the interarrival times has exponential distribution. Therefore the conditional probability that the $n+1$st atom arrives at t_{n+1}, given that the nth arrived at t_n, is

$$P(t_{n+1}|t_n) = \frac{1}{T}\mathrm{e}^{-\frac{t_{n+1}-t_n}{T}}, \tag{2.5}$$

where T is the mean time between the atoms ($T = 1/r$). (More on the Poisson process can be found in [35].) Since in our model the pumping of the micromaser is a random process, it is clear that we must use a statistical method to describe the field within the micromaser. Therefore we will define an average field density matrix $\bar{\rho}(t)$ and determine the master equation controlling its time evolution. To see how to define such an average field density matrix we examine the two processes controlling the time evolution of the cavity field $\rho_f(t)$ (this is not the average field it only represents the field within the micromaser for one given set $\{t_n\}_{n=1}^{\infty}$ of the random variable t_n) in Schrödinger picture.

During the time interval $t_n + \tau < t < t_{n+1}$, when no atom is inside the cavity (the

nth atom exited the cavity at $t_n + \tau$ and the $n+1$st atom did not arrive until t_{n+1}), the cavity field $\rho_f(t)$ evolves according to

$$\frac{d\rho_f(t)}{dt} = -\frac{i}{\hbar}[\mathbf{H}_{free}, \rho_f(t)] + \mathcal{L}_f\rho_f(t) = (\mathcal{H}_{free} + \mathcal{L}_f)\rho_f(t). \tag{2.6}$$

Here the action of the super operator $\mathcal{H}_{free}$ is defined by

$$\mathcal{H}_{free}\rho_f(t) = -\frac{i}{\hbar}[\mathbf{H}_{free}, \rho_f(t)], \tag{2.7}$$

where

$$\mathbf{H}_{free} = \hbar\omega_0\mathbf{a}^\dagger\mathbf{a}, \tag{2.8}$$

and ω_0 is the frequency of the empty cavity field eigenmode, $\mathbf{a}$ ($\mathbf{a}^\dagger$) is the field annihilation (creation) operator obeying the standard commutation relations

$$[\mathbf{a}^\dagger, \mathbf{a}] = 1, \quad [\mathbf{a}, \mathbf{a}] = [\mathbf{a}^\dagger, \mathbf{a}^\dagger] = 0. \tag{2.9}$$

The overall losses of the field are due to the coupling of the cavity field to the environment, which we modeled by a reservoir in thermal equilibrium. Therefore the damping of the micromaser field can be described by the term $\mathcal{L}_f\rho_f(t)$ in Eq. (2.6) where the action of the superoperator $\mathcal{L}_f$ is defined as

$$\begin{aligned}\mathcal{L}_f\rho_f(t) &= -\frac{\Gamma}{2}\bar{n}_{th}\left(\mathbf{a}\mathbf{a}^\dagger\rho_f(t) - 2\mathbf{a}^\dagger\rho_f(t)\mathbf{a} + \rho_f(t)\mathbf{a}\mathbf{a}^\dagger\right) \\ &\quad - \frac{\Gamma}{2}(\bar{n}_{th}+1)\left(\mathbf{a}^\dagger\mathbf{a}\rho_f(t) - 2\mathbf{a}\rho_f(t)\mathbf{a}^\dagger + \rho_f(t)\mathbf{a}^\dagger\mathbf{a}\right).\end{aligned} \tag{2.10}$$

Here, Γ is the cavity-damping constant, and $\bar{n}_{th}$ denotes the mean number of thermal photons in the cavity. The time evolution equation Eq. (2.6) has the formal solution

$$\rho_f(t) = \mathrm{e}^{(\mathcal{H}_{free}+\mathcal{L}_f)(t-(t_n+\tau))}\rho_f(t_n+\tau). \tag{2.11}$$

During the time interval $t_n < t < t_n + \tau$ when the nth atom is inside the cavity, the field-atom system given by tensor product $\rho_f(t) \otimes \rho_{atom}^{(n)}(t)$ evolves according to

$$\begin{aligned} \frac{d}{dt}\left(\rho_f(t) \otimes \rho_{atom}^{(n)}(t)\right) &= -\frac{i}{\hbar}\left[\mathbf{H}, \rho_f(t) \otimes \rho_{atom}^{(n)}(t)\right] + \left(\mathcal{L}_f + \mathcal{L}_a\right)\rho_f(t) \otimes \rho_{atom}^{(n)}(t) \\ &= \left(\mathcal{H} + \mathcal{L}_f + \mathcal{L}_a\right)\rho_f(t) \otimes \rho_{atom}^{(n)}(t). \end{aligned} \tag{2.12}$$

Here the action of the super operator $\mathcal{H}$ is defined by

$$\mathcal{H}\rho_f(t) \otimes \rho_{atom}^{(n)}(t) = -\frac{i}{\hbar}\left[\mathbf{H}, \rho_f(t) \otimes \rho_{atom}^{(n)}(t)\right], \tag{2.13}$$

where $\mathbf{H}$ is the Jaynes-Cummings Hamiltonian within the rotating-wave approximation (RWA) given by

$$\begin{aligned} \mathbf{H} &= \hbar\frac{\omega_a + \omega_b}{2}\mathbf{1} \otimes \mathbf{1} + \hbar\frac{\omega_{ab}}{2}\mathbf{1} \otimes \boldsymbol{\sigma}_z + \hbar\omega_0 \mathbf{a}^\dagger\mathbf{a} \otimes \mathbf{1} \\ &+ \hbar\left(g^*\mathbf{a}^\dagger \otimes \boldsymbol{\sigma}_- + g\mathbf{a} \otimes \boldsymbol{\sigma}_+\right). \end{aligned} \tag{2.14}$$

(For detailed review of the Jaynes-Cummings model see [9] and for a study of the micromaser field without the rotating-wave approximation see [36].) In Eq. (2.14) we used the following notations, $\omega_a = \mathrm{E}_a/\hbar$, $\omega_b = \mathrm{E}_b/\hbar$, $\omega_{ab} = \omega_a - \omega_b$, where E_a (E_b) is the energy eigenvalue corresponding to the energy eigenstate $|a\rangle$ ($|b\rangle$). Furthermore $\boldsymbol{\sigma}_+$ ($\boldsymbol{\sigma}_-$) is the atomic raising (lowering) operator

$$\boldsymbol{\sigma}_+|b\rangle = |a\rangle, \quad \boldsymbol{\sigma}_-|a\rangle = |b\rangle, \tag{2.15}$$

$\boldsymbol{\sigma}_z$ is the third Pauli spin matrix, and

$$g = |g|\mathrm{e}^{i\varphi_g} \tag{2.16}$$

is the complex atom field coupling constant. The damping of the field, as before, is given by the $\mathcal{L}_f\rho_f(t)\otimes\rho^{(n)}_{atom}(t)$ term. The decay of the atomic states during the interaction is given by a similar term $\mathcal{L}_a\rho_f(t)\otimes\rho^{(n)}_{atom}(t)$, where the action of the superoperator $\mathcal{L}_a$ is defined as

$$\begin{aligned}\mathcal{L}_a\rho^{(n)}_{atom}(t) &= -\frac{\gamma}{2}(\bar{n}_{th}+1)\left(\boldsymbol{\sigma}_+\boldsymbol{\sigma}_-\rho^{(n)}_{atom}(t)-2\boldsymbol{\sigma}_-\rho^{(n)}_{atom}(t)\boldsymbol{\sigma}_+ +\rho^{(n)}_{atom}(t)\boldsymbol{\sigma}_+\boldsymbol{\sigma}_-\right)\\ &- \frac{\gamma}{2}\bar{n}_{th}\left(\boldsymbol{\sigma}_-\boldsymbol{\sigma}_+\rho^{(n)}_{atom}(t)-2\boldsymbol{\sigma}_+\rho^{(n)}_{atom}(t)\boldsymbol{\sigma}_- +\rho^{(n)}_{atom}(t)\boldsymbol{\sigma}_-\boldsymbol{\sigma}_+\right), \qquad (2.17)\end{aligned}$$

here γ is the atomic decay rate. The time evolution equation of the coupled field-atom system Eq. (2.12) has the formal solution

$$\rho_f(t)\otimes\rho^{(n)}_{atom}(t)=\mathrm{e}^{(\mathcal{H}+\mathcal{L}_f+\mathcal{L}_a)(t-t_n)}\rho_f(t_n)\otimes\rho^{(n)}_{atom}(t_n). \qquad (2.18)$$

From Eq. (2.18) we obtain the cavity field at time t by tracing over the atomic variables

$$\rho_f(t)=\mathrm{Tr}_{atom}\left[\mathrm{e}^{(\mathcal{H}+\mathcal{L}_f+\mathcal{L}_a)(t-t_n)}\rho_f(t_n)\otimes\rho^{(n)}_{atom}(t_n)\right]. \qquad (2.19)$$

Now using Eq. (2.5), (2.11), (2.19) we define the average field density matrix as

$$\bar{\rho}(t)=\sum_{n=0}^{\infty}\rho^{(n)}_f(t). \qquad (2.20)$$

Here

$$\begin{aligned}\rho^{(n)}_f(t) &= \left(\frac{1}{T}\right)^n\mathrm{e}^{-t/T}\int_0^t dt_n\int_0^{t_n}dt_{n-1}\cdots\int_0^{t_2}dt_1\\ &\mathrm{e}^{(\mathcal{H}_{free}+\mathcal{L}_f)(t-(t_n+\tau))}\mathrm{Tr}_{atom}\left[\mathrm{e}^{(\mathcal{H}+\mathcal{L}_f+\mathcal{L}_a)\tau}\mathrm{e}^{(\mathcal{H}_{free}+\mathcal{L}_f)(t_n-(t_{n-1}+\tau))}\mathrm{Tr}_{atom}\left[\cdots\right.\right.\\ &\left.\cdots\mathrm{Tr}_{atom}\left[\mathrm{e}^{(\mathcal{H}+\mathcal{L}_f+\mathcal{L}_a)\tau}\mathrm{e}^{(\mathcal{H}_{free}+\mathcal{L}_f)t_1}\rho_f(0)\otimes\rho^{(1)}_{atom}(t_1)\right]\cdots\right.\\ &\left.\left.\cdots\right]\otimes\rho^{(n)}_{atom}(t_n)\right], \qquad (2.21)\end{aligned}$$

where $\rho_f(0)$ represents the field density matrix at $t = 0$ when the pumping begins. As we can see from Eq. (2.21) in the definition of the average field density matrix Eq. (2.20) the term $\rho_f^{(n)}(t)$ represents the field density matrix which is the result of the process in which exactly n atoms have passed through the cavity during time t multiplied by the probability of this event thus the average field density matrix we have defined is a proper statistical average.

In order to obtain the master equation controlling the time evolution of the average field density matrix we shall calculate the time derivative of Eq. (2.20). First, we determine the time derivative of $\rho_f^{(n)}(t)$, after some algebra this can be given as

$$\begin{aligned}\frac{d\rho_f^{(n)}(t)}{dt} &= (\mathcal{H}_{free} + \mathcal{L}_f)\rho_f^{(n)}(t) - \frac{1}{T}\rho_f^{(n)}(t) \\ &+ \frac{1}{T}e^{-(\mathcal{H}_{free}+\mathcal{L}_f)\tau}\mathrm{Tr}_{atom}\left[e^{(\mathcal{H}+\mathcal{L}_f+\mathcal{L}_a)\tau}\rho_f^{(n-1)}(t)\otimes\rho_{atom}^{(n)}(t)\right]. \qquad (2.22)\end{aligned}$$

Then using Eq. (2.22) and Eq. (2.7) we calculate the time derivative of the average field density matrix

$$\begin{aligned}\frac{d\bar{\rho}(t)}{dt} &= \sum_{n=0}^{\infty}\frac{d\rho_f^{(n)}(t)}{dt} \\ &= -\frac{i}{\hbar}[\mathbf{H}_{free},\bar{\rho}(t)] + \mathcal{L}_f\bar{\rho}(t) - \frac{1}{T}\bar{\rho}(t) \\ &+ \frac{1}{T}e^{-(\mathcal{H}_{free}+\mathcal{L}_f)\tau}\mathrm{Tr}_{atom}\left[e^{(\mathcal{H}+\mathcal{L}_f+\mathcal{L}_a)\tau}\sum_{n=1}^{\infty}\left(\rho_f^{(n-1)}(t)\otimes\rho_{atom}^{(n)}(t)\right)\right]. \qquad (2.23)\end{aligned}$$

In order to simplify this equation we take into account that each atom entering into the cavity was identically prepared, therefore we can drop the superscript distinguishing them and write

$$\rho_{atom}^{(n)}(t) = \rho_{atom}(t) \qquad \text{for all } n. \qquad (2.24)$$

Then using Eq. (2.24) we obtain that

$$\sum_{n=1}^{\infty}\left(\rho_f^{(n-1)}(t)\otimes\rho_{atom}^{(n)}(t)\right)=\left(\sum_{n=0}^{\infty}\rho_f^{(n)}(t)\right)\otimes\rho_{atom}(t)=\bar{\rho}(t)\otimes\rho_{atom}(t). \tag{2.25}$$

Using Eq. (2.25) now we can simplify Eq. (2.23) and obtain the master equation for the average field density matrix

$$\begin{aligned}\frac{d\bar{\rho}(t)}{dt} &= -\frac{i}{\hbar}\left[\mathbf{H}_{free},\bar{\rho}(t)\right]+\mathcal{L}_f\bar{\rho}(t)-\frac{1}{T}\bar{\rho}(t)\\ &+\frac{1}{T}e^{-(\mathcal{H}_{free}+\mathcal{L}_f)\tau}\mathrm{Tr}_{atom}\left[e^{(\mathcal{H}+\mathcal{L}_f+\mathcal{L}_a)\tau}\bar{\rho}(t)\otimes\rho_{atom}(t)\right].\end{aligned} \tag{2.26}$$

In the next step we will make some approximations in order to simplify the master equation given by Eq. (2.26). First we assume that the interaction time τ is so short and the cavity Q is so high that we can safely neglect the decay of the field during the interaction. Similarly, we suppose that also the atomic decay times are much longer than the interaction time τ, which means we can safely neglect the decay of the atomic states during the interaction as well. These assumptions together with Eq. (2.7) and Eq. (2.13) lead to the following approximations

$$e^{-(\mathcal{H}_{free}+\mathcal{L}_f)\tau}\bar{\rho}(t)\approx e^{i\omega_0\mathbf{a}^\dagger\mathbf{a}\tau}\bar{\rho}(t)e^{-i\omega_0\mathbf{a}^\dagger\mathbf{a}\tau}, \tag{2.27a}$$

$$e^{(\mathcal{H}+\mathcal{L}_f+\mathcal{L}_a)\tau}\bar{\rho}(t)\otimes\rho_{atom}(t)\approx e^{-\frac{i}{\hbar}\mathbf{H}\tau}\bar{\rho}(t)\otimes\rho_{atom}(t)e^{\frac{i}{\hbar}\mathbf{H}\tau}. \tag{2.27b}$$

Using Eq. (2.7) and the approximations given by Eq. (2.27) we simplify the master equation and obtain

$$\begin{aligned}\frac{d\bar{\rho}(t)}{dt} &= -i\omega_0\left[\mathbf{a}^\dagger\mathbf{a},\bar{\rho}(t)\right]+\mathcal{L}_f\bar{\rho}(t)-\frac{1}{T}\bar{\rho}(t)\\ &+\frac{1}{T}\mathrm{Tr}_{atom}\left[e^{i\omega_0\mathbf{a}^\dagger\mathbf{a}\tau}e^{-\frac{i}{\hbar}\mathbf{H}\tau}\bar{\rho}(t)\otimes\rho_{atom}(t)e^{\frac{i}{\hbar}\mathbf{H}\tau}e^{-i\omega_0\mathbf{a}^\dagger\mathbf{a}\tau}\right].\end{aligned} \tag{2.28}$$

As we see from Eq. (2.28) all of the effects of the passing atoms are included in the last term of Eq. (2.28). Our next step is to evaluate this term. To do so we need to determine the operator which represents $e^{i\omega_0 \mathbf{a}^\dagger \mathbf{a}\tau} e^{-\frac{i}{\hbar}\mathbf{H}\tau}$. After some algebra we obtain

$$e^{i\omega_0 \mathbf{a}^\dagger \mathbf{a}\tau} e^{-\frac{i}{\hbar}\mathbf{H}\tau} = \mathbf{U}_{atomic} \cdot \mathbf{U} =$$

$$\begin{pmatrix} e^{-i(\omega_a+\omega_b+\omega_0)\tau/2} & 0 \\ 0 & e^{-i(\omega_a+\omega_b-\omega_0)\tau/2} \end{pmatrix} \cdot \begin{pmatrix} C(\mathbf{\Omega}) & -ie^{i\varphi_g} S(\mathbf{\Omega})\mathbf{a} \\ -ie^{-i\varphi_g} \mathbf{a}^\dagger S(\mathbf{\Omega}) & C^*(\bar{\mathbf{\Omega}}) \end{pmatrix}, \quad (2.29)$$

where we defined the following terms

$$C(\mathbf{\Omega}) = \cos(\mathbf{\Omega}\Theta) + i\frac{n_0}{\mathbf{\Omega}}\sin(\mathbf{\Omega}\Theta), \quad (2.30a)$$

$$S(\mathbf{\Omega}) = \frac{1}{\mathbf{\Omega}}\sin(\mathbf{\Omega}\Theta), \quad (2.30b)$$

$$\mathbf{\Omega} = \sqrt{n_0^2 + \mathbf{a}\mathbf{a}^\dagger}, \quad (2.30c)$$

$$\bar{\mathbf{\Omega}} = \sqrt{n_0^2 + \mathbf{a}^\dagger\mathbf{a}}, \quad (2.30d)$$

$$\Theta = |g|\tau, \quad (2.30e)$$

$$n_0 = \frac{\omega_0 - \omega_{ab}}{2|g|}. \quad (2.30f)$$

In Eq. (2.30e) and Eq. (2.30f) we have introduced two parameters, Θ and n_0. As we can see from Eq. (2.30) parameter Θ determines the interaction phase and n_0^2 determines the effective photon number shift due to the detuning $\omega_0 - \omega_{ab}$. It reduces to zero in the case when $\omega_0 = \omega_{ab}$. Also observe that $\mathbf{U}_{atomic}$ in Eq. (2.29) does not contain any field operator. Therefore, it can be cyclically permuted in the argument of the trace in Eq. (2.28) in such a way that it will cancel out with its Hermitian

adjoint, reducing the trace term in Eq. (2.28) to

$$\begin{aligned}
\mathrm{Tr}_{atom}\left[\mathbf{U}\bar{\rho}(t)\otimes\rho_{atom}(t)\mathbf{U}^{\dagger}\right] &= \rho_{aa}C(\mathbf{\Omega})\bar{\rho}(t)C^{*}(\mathbf{\Omega})+\rho_{bb}C^{*}(\bar{\mathbf{\Omega}})\bar{\rho}(t)C(\bar{\mathbf{\Omega}}) \\
&- \lambda|\rho_{ab}|\mathrm{e}^{-i(\nu t+\varphi_g-\varphi_{ab}+\pi/2)}C(\mathbf{\Omega})\bar{\rho}(t)\mathbf{a}^{\dagger}S(\mathbf{\Omega}) \\
&- \lambda|\rho_{ba}|\mathrm{e}^{i(\nu t+\varphi_g-\varphi_{ab}+\pi/2)}S(\mathbf{\Omega})\mathbf{a}\bar{\rho}(t)C^{*}(\mathbf{\Omega}) \\
&+ \rho_{bb}S(\mathbf{\Omega})\mathbf{a}\bar{\rho}(t)\mathbf{a}^{\dagger}S(\mathbf{\Omega})+\rho_{aa}S(\bar{\mathbf{\Omega}})\mathbf{a}^{\dagger}\bar{\rho}(t)\mathbf{a}S(\bar{\mathbf{\Omega}}) \\
&+ \lambda|\rho_{ab}|\mathrm{e}^{-i(\nu t+\varphi_g-\varphi_{ab}+\pi/2)}S(\bar{\mathbf{\Omega}})\mathbf{a}^{\dagger}\bar{\rho}(t)C(\bar{\mathbf{\Omega}}) \\
&+ \lambda|\rho_{ba}|\mathrm{e}^{i(\nu t+\varphi_g-\varphi_{ab}+\pi/2)}C^{*}(\bar{\mathbf{\Omega}})\bar{\rho}(t)\mathbf{a}S(\bar{\mathbf{\Omega}}). \qquad (2.31)
\end{aligned}$$

After substituting Eq. (2.31) into Eq. (2.28) we obtain the final form of the master equation describing the time evolution of the field inside a micromaser which is pumped off-resonantly and coherently by two-level atoms,

$$\begin{aligned}
\frac{d\bar{\rho}(t)}{dt} &= -i\omega_0\left[\mathbf{a}^{\dagger}\mathbf{a},\bar{\rho}(t)\right]+\mathcal{L}_f\bar{\rho}(t) \\
&+ \frac{1}{T}\Big(\rho_{aa}C(\mathbf{\Omega})\bar{\rho}(t)C^{*}(\mathbf{\Omega})+\rho_{bb}C^{*}(\bar{\mathbf{\Omega}})\bar{\rho}(t)C(\bar{\mathbf{\Omega}})-\bar{\rho}(t) \\
&- \lambda|\rho_{ab}|\mathrm{e}^{-i(\nu t+\varphi_g-\varphi_{ab}+\pi/2)}C(\mathbf{\Omega})\bar{\rho}(t)\mathbf{a}^{\dagger}S(\mathbf{\Omega}) \\
&- \lambda|\rho_{ba}|\mathrm{e}^{i(\nu t+\varphi_g-\varphi_{ab}+\pi/2)}S(\mathbf{\Omega})\mathbf{a}\bar{\rho}(t)C^{*}(\mathbf{\Omega}) \\
&+ \rho_{bb}S(\mathbf{\Omega})\mathbf{a}\bar{\rho}(t)\mathbf{a}^{\dagger}S(\mathbf{\Omega})+\rho_{aa}S(\bar{\mathbf{\Omega}})\mathbf{a}^{\dagger}\bar{\rho}(t)\mathbf{a}S(\bar{\mathbf{\Omega}}) \\
&+ \lambda|\rho_{ab}|\mathrm{e}^{-i(\nu t+\varphi_g-\varphi_{ab}+\pi/2)}S(\bar{\mathbf{\Omega}})\mathbf{a}^{\dagger}\bar{\rho}(t)C(\bar{\mathbf{\Omega}}) \\
&+ \lambda|\rho_{ba}|\mathrm{e}^{i(\nu t+\varphi_g-\varphi_{ab}+\pi/2)}C^{*}(\bar{\mathbf{\Omega}})\bar{\rho}(t)\mathbf{a}S(\bar{\mathbf{\Omega}})\Big). \qquad (2.32)
\end{aligned}$$

This equation will be the basis of our further investigations. After some algebra we can rewrite Eq. (2.32) in the form which includes only commutators, assuring that

the normalization of the initial state of the field $\rho_f(0)$ is preserved all the time,

$$\begin{aligned}\frac{d\bar{\rho}(t)}{dt} &= -i\omega_0[\mathbf{a}^\dagger\mathbf{a},\bar{\rho}(t)] + \mathcal{L}_f\bar{\rho}(t) + \lambda\Big([\mathbf{C},\bar{\rho}(t)\mathbf{C}^\dagger] + [\mathbf{D}^\dagger,\bar{\rho}(t)\mathbf{D}]\Big) \\ &+ (1-\lambda)\Big(\rho_{bb}\Big([S(\boldsymbol{\Omega})\mathbf{a},\bar{\rho}(t)\mathbf{a}^\dagger S(\boldsymbol{\Omega})] + [C^*(\bar{\boldsymbol{\Omega}}),\bar{\rho}(t)C(\bar{\boldsymbol{\Omega}})]\Big) \\ &+ \rho_{aa}\Big([S(\bar{\boldsymbol{\Omega}})\mathbf{a}^\dagger,\bar{\rho}(t)\mathbf{a}S(\bar{\boldsymbol{\Omega}})] + [C(\boldsymbol{\Omega}),\bar{\rho}(t)C^*(\boldsymbol{\Omega})]\Big)\Big). \qquad (2.33)\end{aligned}$$

Here the operators **C**, **D** are defined as

$$\mathbf{C} = \sqrt{\rho_{aa}}e^{i\alpha}C(\boldsymbol{\Omega}) - \sqrt{\rho_{bb}}e^{-i\alpha}S(\boldsymbol{\Omega})\mathbf{a}, \qquad (2.34a)$$

$$\mathbf{D} = \sqrt{\rho_{bb}}e^{i\alpha}C(\bar{\boldsymbol{\Omega}}) + \sqrt{\rho_{aa}}e^{-i\alpha}\mathbf{a}S(\bar{\boldsymbol{\Omega}}), \qquad (2.34b)$$

where

$$\alpha = -(\nu t + \varphi_g - \varphi_{ab} + \pi/2), \qquad (2.35)$$

and **C** and **D** obey

$$\mathbf{C}^\dagger\mathbf{C} + \mathbf{D}\mathbf{D}^\dagger = \mathbb{1}. \qquad (2.36)$$

In order to further simplify Eq. (2.32) we now introduce the following substitution

$$\bar{\rho}(t) = e^{-i\mathbf{a}^\dagger\mathbf{a}(\nu t+\varphi_g-\varphi_{ab}+\pi/2)}\tilde{\rho}(t)e^{i\mathbf{a}^\dagger\mathbf{a}(\nu t+\varphi_g-\varphi_{ab}+\pi/2)}. \qquad (2.37)$$

Using Eq. (2.37) we separate the rapidly oscillating term from $\bar{\rho}(t)$. Observe that the frequency used in Eq. (2.37) is the injected signal frequency ν. This choice was suggested by the theory of the classical forced oscillations (see for example [37]), where a system is driven by an external force and the frequency of the resultant steady oscillation equals that of the driving. Also observe that using Eq. (2.37) we

introduce a $\varphi_g - \varphi_{ab} + \pi/2$ phase difference between the initial values $\bar{\rho}(0)$ and $\tilde{\rho}(0)$. Now by substituting Eq. (2.37) into Eq. (2.32) and using the relations

$$e^{ia^\dagger a(\nu t+\varphi_g-\varphi_{ab}+\pi/2)}a^\dagger e^{-ia^\dagger a(\nu t+\varphi_g-\varphi_{ab}+\pi/2)} = e^{i(\nu t+\varphi_g-\varphi_{ab}+\pi/2)}a^\dagger, \quad (2.38a)$$

$$e^{ia^\dagger a(\nu t+\varphi_g-\varphi_{ab}+\pi/2)}ae^{-ia^\dagger a(\nu t+\varphi_g-\varphi_{ab}+\pi/2)} = e^{-i(\nu t+\varphi_g-\varphi_{ab}+\pi/2)}a, \quad (2.38b)$$

we obtain the master equation for $\tilde{\rho}(t)$

$$\begin{aligned}\frac{d\tilde{\rho}(t)}{dt} &= -i(\omega_0-\nu)\left[a^\dagger a,\tilde{\rho}(t)\right]+\mathcal{L}_f\tilde{\rho}(t)\\ &+\frac{1}{T}\Big(\rho_{aa}C(\Omega)\tilde{\rho}(t)C^*(\Omega)+\rho_{bb}C^*(\bar{\Omega})\tilde{\rho}(t)C(\bar{\Omega})-\tilde{\rho}(t)\\ &-\lambda|\rho_{ab}|C(\Omega)\tilde{\rho}(t)a^\dagger S(\Omega)-\lambda|\rho_{ba}|S(\Omega)a\tilde{\rho}(t)C^*(\Omega)\\ &+\rho_{bb}S(\Omega)a\tilde{\rho}(t)a^\dagger S(\Omega)+\rho_{aa}S(\bar{\Omega})a^\dagger\tilde{\rho}(t)aS(\bar{\Omega})\\ &+\lambda|\rho_{ab}|S(\bar{\Omega})a^\dagger\tilde{\rho}(t)C(\bar{\Omega})+\lambda|\rho_{ba}|C^*(\bar{\Omega})\tilde{\rho}(t)aS(\bar{\Omega})\Big), \quad (2.39)\end{aligned}$$

where the only time dependent term is $\tilde{\rho}(t)$ itself.

For the sake of simplicity, in the followings we assume that the thermal reservoir, our system is coupled to, is at $T = 0$K temperature. Therefore the mean number of thermal photons in the cavity is equal to zero and the loss term defined by Eq. (2.10) reduces to

$$\mathcal{L}_f\tilde{\rho}(t) = -\frac{\Gamma}{2}\left(a^\dagger a\tilde{\rho}(t)-2a\tilde{\rho}(t)a^\dagger+\tilde{\rho}(t)a^\dagger a\right). \quad (2.40)$$

Also to further reduce the number of the parameters in Eq. (2.39) we rescale the time according to the cavity decay time by introducing

$$t' = \Gamma t, \quad (2.41)$$

and the parameter

$$N_{ex} = \frac{r}{\Gamma} = \frac{1}{\Gamma T}, \tag{2.42}$$

which is the number of atoms passing through the cavity during the cavity decay time $1/\Gamma$. We also introduce the atomic inversion parameter

$$u = \rho_{aa} - \rho_{bb}, \tag{2.43}$$

thus

$$\rho_{aa} = \frac{1+u}{2}, \tag{2.44}$$

$$\rho_{bb} = \frac{1-u}{2}, \tag{2.45}$$

$$|\rho_{ab}| = |\rho_{ba}| = \frac{1}{2}\sqrt{1-u^2}, \tag{2.46}$$

and

$$\Delta = \frac{\omega_0 - \nu}{\Gamma}, \tag{2.47}$$

which gives the phase shift occurring during the cavity decay time between the oscillation of the empty cavity's field and the injected signal or, simply, the scaled detuning. Using Eqs. (2.40–2.47) the master equation for $\tilde{\rho}(t)$ can be simplified as

$$\begin{aligned}
\frac{d\tilde{\rho}(t')}{dt'} &= -i\Delta\left[\mathbf{a}^\dagger\mathbf{a}, \tilde{\rho}(t')\right] - \frac{1}{2}\left(\mathbf{a}^\dagger\mathbf{a}\tilde{\rho}(t') - 2\mathbf{a}\tilde{\rho}(t')\mathbf{a}^\dagger + \tilde{\rho}(t')\mathbf{a}^\dagger\mathbf{a}\right) \\
&+ \frac{N_{ex}}{2}\Big((1+u)C(\mathbf{\Omega})\tilde{\rho}(t')C^*(\mathbf{\Omega}) + (1-u)C^*(\bar{\mathbf{\Omega}})\tilde{\rho}(t')C(\bar{\mathbf{\Omega}}) - 2\tilde{\rho}(t') \\
&- \lambda\sqrt{1-u^2}\left(C(\mathbf{\Omega})\tilde{\rho}(t')\mathbf{a}^\dagger S(\mathbf{\Omega}) + S(\mathbf{\Omega})\mathbf{a}\tilde{\rho}(t')C^*(\mathbf{\Omega})\right) \\
&+ (1-u)S(\mathbf{\Omega})\mathbf{a}\tilde{\rho}(t')\mathbf{a}^\dagger S(\mathbf{\Omega}) + (1+u)S(\bar{\mathbf{\Omega}})\mathbf{a}^\dagger\tilde{\rho}(t')\mathbf{a}S(\bar{\mathbf{\Omega}}) \\
&+ \lambda\sqrt{1-u^2}\left(S(\bar{\mathbf{\Omega}})\mathbf{a}^\dagger\tilde{\rho}(t')C(\bar{\mathbf{\Omega}}) + C^*(\bar{\mathbf{\Omega}})\tilde{\rho}(t')\mathbf{a}S(\bar{\mathbf{\Omega}})\right)\Big).
\end{aligned} \tag{2.48}$$

We would like to take a moment now and emphasize that our model contains two parameters related to detuning. The first parameter n_0 was introduced by Eqs. (2.30f) as a result of the frequency mismatch of ω_0 and ω_{ab} describing the frequency of the empty cavity field eigenmode and the atomic transition frequency respectively. The result of n_0 is an effective photon number shift as it can be seen from Eq. (2.30). The other detuning related parameter is Δ which is the result of the frequency mismatch between the empty cavity field eigenmode ω_0 and the frequency of the injected signal ν. The parameters n_0 and Δ are independent, their value can be chosen independently to control different aspects of the model. However, for the model to be experimentally feasible

$$\omega_{ab} = \nu, \tag{2.49}$$

must be satisfied. Equation (2.49) will assure that non-diagonal elements of the atomic density matrix Eq. (2.1) carry the maximum possible coherence value when injected into the micromaser cavity. In the case Equation (2.49) is satisfied the number of the detuning related parameter is reduced to one since

$$n_0 = \frac{\Gamma}{2|g|}\Delta. \tag{2.50}$$

In the rest of this work we will treat n_0 and Δ as independent parameters to preserve the generality of the model. When condition Eq. (2.49) is invoked it will be specified explicitly.

Before we proceed any further, we list all the parameters our model depends on:

$$\rho_{aa},\ \varphi_{ab},\ \omega_{ab},\ \nu,\ \lambda,\ |g|,\ \varphi_g,\ \omega_0,\ \tau,\ r,\ \Gamma. \tag{2.51}$$

However, as we can see from Eq. (2.48), $\tilde{\rho}(t')$ does not depend directly on all of these 11 parameters, some only appear in combinations with other parameters. Therefore it is important to identify the real control parameters of our model, the minimal set of parameters which uniquely determines $\tilde{\rho}(t')$. These control parameters can be read out from Eq. (2.48). They are N_{ex}, u, λ, Θ, n_0 and Δ introduced by Eqs. (2.42), (2.43), (2.1), (2.30e), (2.30f) and (2.47). Also observe the role of φ_{ab} and φ_g is very simple. As we can see from Eq. (2.37), they only introduce a constant phase shift between the initial values $\tilde{\rho}(0)$ and $\tilde{\rho}(0)$, therefore they can be eliminated from our further investigation (they can be simply set to zero). In conclusion we can say that the solution to Eq. (2.48), besides time, depends on

$$\boldsymbol{\beta} = (N_{ex}, u, \lambda, \Theta, n_0, \Delta), \tag{2.52}$$

where $\boldsymbol{\beta}$ is a vector in the 6 dimensional parameter space of the model. We can summarize this by writing $\tilde{\rho}(t') = \tilde{\rho}(\boldsymbol{\beta}, t')$. Also observe that in $\boldsymbol{\beta}$ we have two parameters, λ and Δ, which are exclusive to the coherent pumping, they do not occur in the case of the incoherent pumping.

In the next chapters we will provide two different approaches to solve Eq. (2.48). First we use the semiclassical approximation to obtain an approximate solution, then we discuss the full quantum mechanical solution of Eq. (2.48)

3

The semiclassical solution

In this chapter we employ the semiclassical approach to the coherently pumped micromaser. The semiclassical approach was originally developed by Guzman [31] for the case of the incoherently pumped micromaser and later used by Škvarček and Hillery [32] to investigate the phase distribution and the mean photon number of the coherently pumped micromaser. However all these works were restricted by the assumption that the square of the amplitude of the electric field is equal to the intensity of the field, thereby severely restricting their scope of validity. In this chapter we extend the semiclassical theory to overcome this limitation.

We describe the electromagnetic field inside the cavity as a complex vector $\varepsilon(t)$ and study its magnitude and phase along with the intensity of the field. Here we will see major differences between the coherently and incoherently pumped micromasers. Namely in the case of the incoherently pumped micromaser the phase of the field is totally random due to phase diffusion, as a result of small changes in the phase due to spontaneous emission events. Therefore the magnitude of the average electric field is zero even though the average intensity, which is immune to phase diffusion, remains finite. In the case of the coherently pumped micromaser, as we show in this

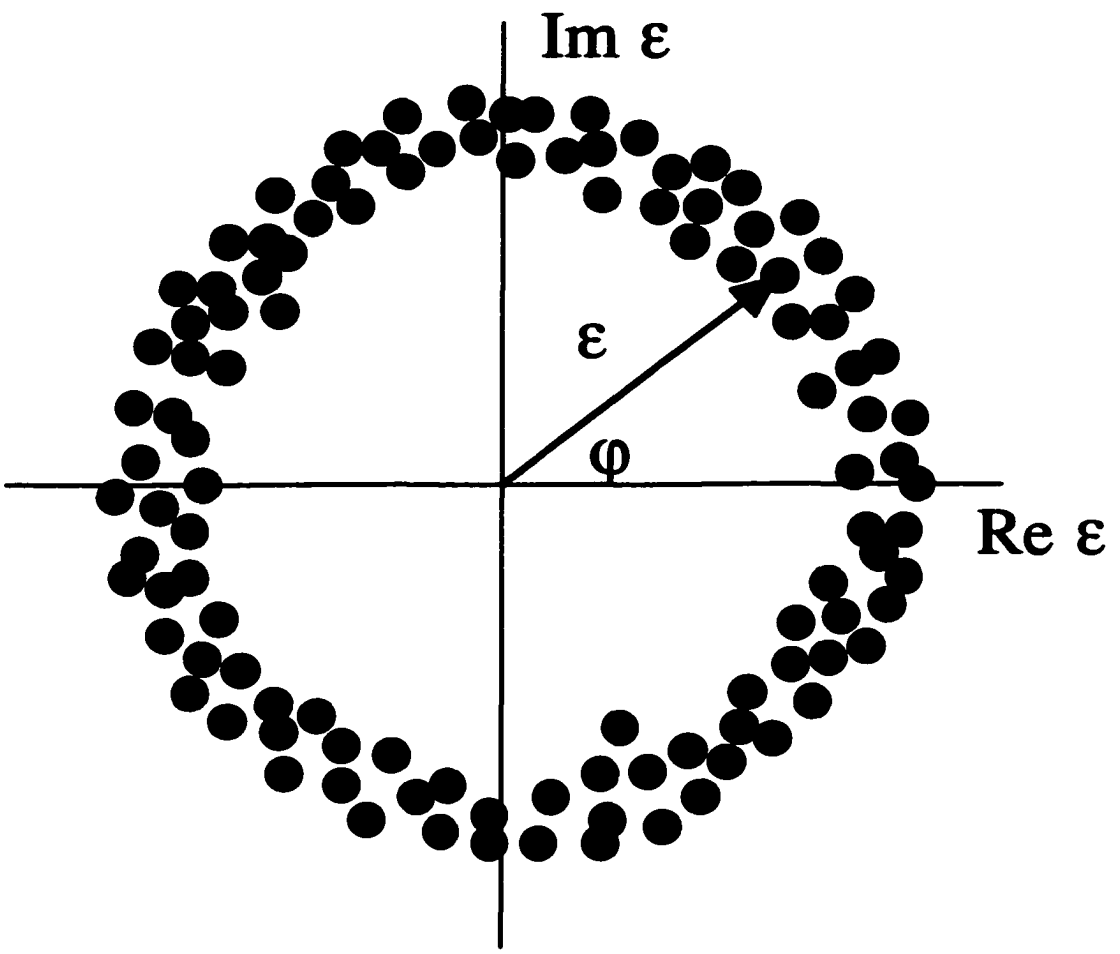

Figure 2: The electromagnetic field in the case of an incoherently pumped micromaser. The black dots are representing the possible values of the electromagnetic field after spontaneous emission events. The phase diffuses due to these spontaneous emission events. The magnitude of the average field is zero.

chapter, the effect of the injected coherence is manifest in the decrease or even total elimination of the phase diffusion thereby providing well defined phase values for the average field. We see examples where the phase of the field is uniquely determined (locked) and therefore the square of the average field's magnitude is close to the average intensity of the field. We also see examples where the phase of the field is not uniquely determined, but restricted to certain well defined values, in this case the

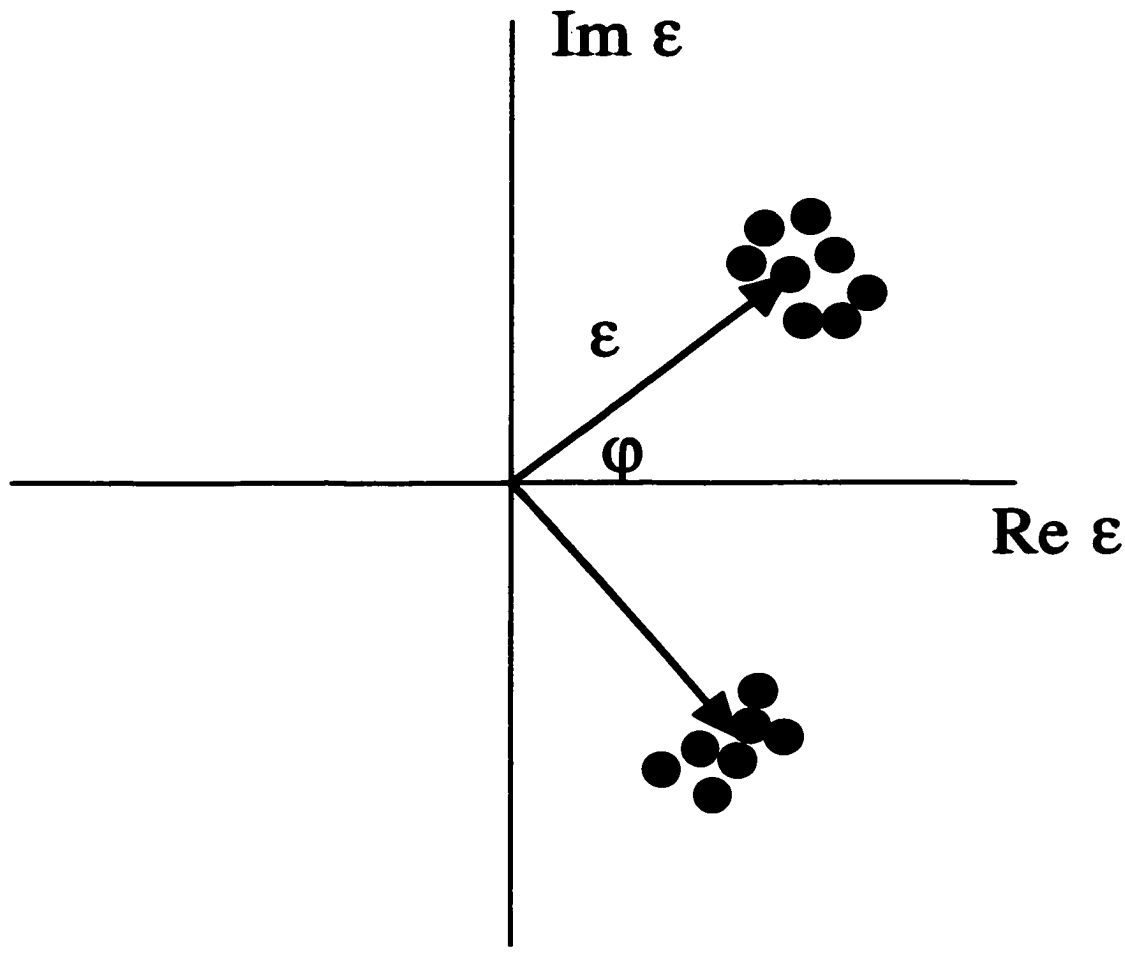

Figure 3: The electromagnetic field in the case of a coherently pumped micromaser. The phase diffusion is reduced due to the injected atomic coherence. The phase of the field is restricted to certain well defined values. The square of the average field's magnitude is smaller than the average intensity but it is not zero. The phase of the field exhibits bistability.

square of the average field magnitude is smaller than the average intensity but it is not zero unlike in the case of the incoherently pumped micromasers. The different phase locking cases we described are illustrated in Fig. 2–4.

To determine the complex vector describing the electric field inside the cavity we

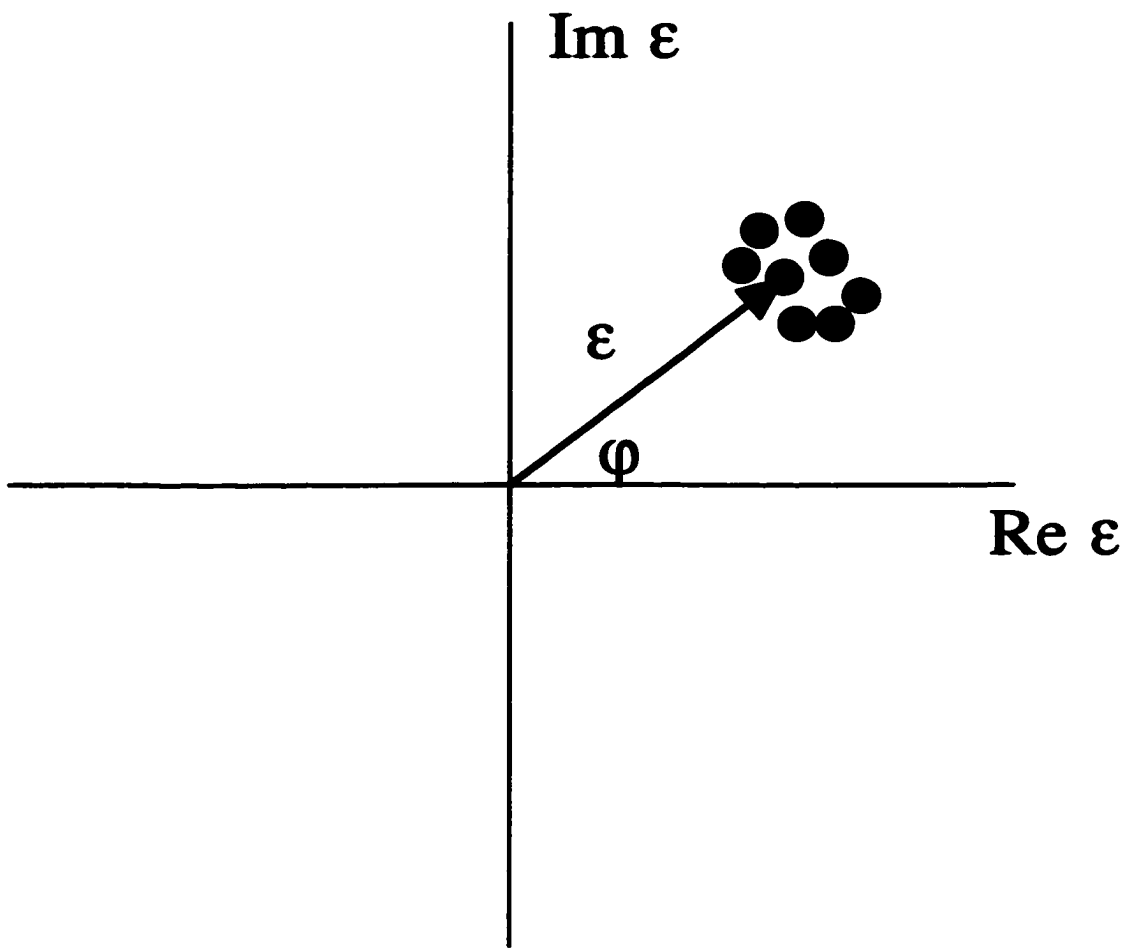

Figure 4: The electromagnetic field in the case of a coherently pumped micromaser. The phase diffusion is reduced due to the injected atomic coherence. The phase of the field is locked and the square of the average field's magnitude is equal to the intensity of the field.

must evaluate the following expectation value

$$\varepsilon(t) = \mathrm{Tr}_{field}\left[\mathbf{a}\bar{\rho}(t)\right]. \tag{3.1}$$

Using Eq. (2.37) and Eq. (2.38) we now separate the rapidly oscillating term and write

$$\varepsilon(t) = \mathrm{e}^{-i(\nu t+\varphi_g-\varphi_{ab}+\pi/2)}\mathrm{Tr}_{field}\left[\mathbf{a}\tilde{\rho}(t)\right] = \mathrm{e}^{-i(\nu t+\varphi_g-\varphi_{ab}+\pi/2)}\tilde{\varepsilon}(t). \tag{3.2}$$

The differential equation describing the time evolution of the slowly varying amplitude

given by $\tilde{\varepsilon}(t)$ can be obtained from Eq. (2.48) as follows

$$\begin{aligned}\frac{d\tilde{\varepsilon}(t')}{dt'} &= \mathrm{Tr}_{field}\left[\mathbf{a}\frac{d\tilde{\rho}(t')}{dt'}\right] = -i\Delta\tilde{\varepsilon} - \frac{1}{2}\tilde{\varepsilon} - N_{ex}\tilde{\varepsilon} \\ &+ \frac{N_{ex}}{2}\sum_{j=0}^{\infty}\left(C_{j+1}^{*}(C_j + C_{j+2}) + S_{j+1}((j+2)S_{j+2} + jS_j)\right)\sqrt{j+1}\tilde{\rho}_{j+1,j} \\ &+ u\frac{N_{ex}}{2}\sum_{j=0}^{\infty}\left(C_{j+1}^{*}(C_{j+2} - C_j) + S_{j+1}((j+2)S_{j+2} - jS_j)\right)\sqrt{j+1}\tilde{\rho}_{j+1,j} \\ &+ \lambda\frac{N_{ex}}{2}\sqrt{1-u^2}\sum_{j=0}^{\infty}\left((j+1)S_{j+1}C_j - jS_jC_{j+1}\right)\tilde{\rho}_{j,j} \\ &+ \lambda\frac{N_{ex}}{2}\sqrt{1-u^2}\sum_{j=0}^{\infty}\left(S_{j+1}C_{j+2}^{*} - C_{j+1}^{*}S_{j+2}\right)\sqrt{j+1}\sqrt{j+2}\tilde{\rho}_{j+2,j}. \qquad (3.3)\end{aligned}$$

Here we have used the notations

$$C_j = \cos\left(\sqrt{n_0^2 + j}\Theta\right) + i\frac{n_0}{\sqrt{n_0^2+j}}\sin\left(\sqrt{n_0^2+j}\Theta\right), \qquad (3.4a)$$

$$S_j = \frac{1}{\sqrt{n_0^2+j}}\sin\left(\sqrt{n_0^2+j}\Theta\right), \qquad (3.4b)$$

which obey the relation

$$C_j^{*}C_j + jS_j^2 = 1. \qquad (3.5)$$

We want to relate the sums in Eq. (3.3) to the slowly varying amplitude of the electric field $\tilde{\varepsilon}(t')$, making Eq. (3.3) an ordinary differential equation. To this end, we apply the following approximations. We assume that the photon distribution described by the diagonal $\tilde{\rho}_{j,j}$ elements of the density matrix is sharply peaked about n, also assume that the values given by $\sqrt{j+1}\tilde{\rho}_{j+1,j}$ peak at $\sqrt{n+1}\tilde{\rho}_{n+1,n}$ and the values $\sqrt{j+1}\sqrt{j+2}\tilde{\rho}_{j+2,j}$ peak at $\sqrt{n+1}\sqrt{n+2}\tilde{\rho}_{n+2,n}$. The later two assumptions follow from our first assumption, that the photon distribution is sharply peaked about n, at

least in the case of pure states when

$$\tilde{\rho}_{i,i}\tilde{\rho}_{j,j} = |\tilde{\rho}_{i,j}|^2. \tag{3.6}$$

The proof of Eq. (3.6) will be given in the next chapter. Assuming our conditions are met we approximate Eq. (3.3) as

$$\frac{d\tilde{\varepsilon}(t')}{dt'} = \Big(-i\Delta - \frac{1}{2} + N_{ex}\mathcal{D} + N_{ex}u\mathcal{F} - N_{ex}\Big)\tilde{\varepsilon} + \lambda\frac{N_{ex}}{2}\sqrt{1-u^2}\Big(\mathcal{G} + \mathcal{H}\tilde{\varepsilon}^2\Big), \tag{3.7}$$

where the coefficients are

$$\mathcal{D} = \frac{1}{2}\left(C^*_{n+1}(C_{n+2} + C_n) + S_{n+1}\big((n+2)S_{n+2} + nS_n\big)\right), \tag{3.8a}$$

$$\mathcal{F} = \frac{1}{2}\left(C^*_{n+1}(C_{n+2} - C_n) + S_{n+1}\big((n+2)S_{n+2} - nS_n\big)\right), \tag{3.8b}$$

$$\mathcal{G} = (n+1)S_{n+1}C_n - nS_nC_{n+1}, \tag{3.8c}$$

$$\mathcal{H} = S_{n+1}C^*_{n+2} - C^*_{n+1}S_{n+2}. \tag{3.8d}$$

In a similar way, we now determine the differential equation describing the intensity of the electric field inside the cavity. The intensity of the field is obtained by evaluating the following expectation value

$$n(t) = \mathrm{Tr}_{field}\big[\mathbf{a}^\dagger\mathbf{a}\tilde{\rho}(t)\big] = \mathrm{Tr}_{field}\big[\mathbf{a}^\dagger\mathbf{a}\tilde{\rho}(t)\big]. \tag{3.9}$$

The differential equation describing the time evolution of $n(t)$ can be derived from Eq. (2.48). Using the same assumptions we made earlier in deriving Eq. (3.7), we obtain

$$\begin{aligned}\frac{dn(t')}{dt'} &= -n + \frac{N_{ex}}{2}\Big((n+1)S^2_{n+1} - nS^2_n\Big) + u\frac{N_{ex}}{2}\Big((n+1)S^2_{n+1} + nS^2_n\Big) \\ &+ \lambda N_{ex}\sqrt{1-u^2}\mathrm{Re}\Big[S_{n+1}C^*_{n+1}\tilde{\varepsilon}(t')\Big].\end{aligned} \tag{3.10}$$

Equations (3.7) and (3.10) provide the basis of our semiclassical model for the coherently pumped micromasers. They form a coupled system where the coupling is established through the slowly varying amplitude of the electric field $\tilde{\varepsilon}(t')$. Also please note in the case of the incoherent pumping when $\lambda = 0$ the two equations Eq. (3.7) and Eq. (3.10) are no longer coupled, Eq. (3.10) independently determines the intensity of the field $n(t')$ which then can be used in Eq. (3.7) to determine $\tilde{\varepsilon}(t')$. Another note should be made about Eq. (3.7) namely that it is a complex equation therefore by itself represents two coupled equations.

For the sake of simplicity we shall restrict our further consideration to the case of

$$n_0 = 0. \tag{3.11}$$

Then C_n and S_n simplify to the following real expressions

$$C_n = \cos(\sqrt{n}\Theta), \tag{3.12a}$$

$$S_n = \frac{1}{\sqrt{n}}\sin(\sqrt{n}\Theta), \tag{3.12b}$$

reducing the coefficients $\mathcal{D}$, $\mathcal{F}$, $\mathcal{G}$, and $\mathcal{H}$ to real expressions. Next, we will derive separate equations for the magnitude and the phase of the electric field starting from Eq. (3.7). It is useful to introduce a new quantity,

$$\hat{\varepsilon}(t') = -i\tilde{\varepsilon}(t'), \tag{3.13}$$

since in our quantum mechanical solution we will provide the phase distribution of $\hat{\varepsilon}(t')$ and not the phase distribution of $\tilde{\varepsilon}(t')$. Therefore the direct comparison of the predictions of the two models is easier using $\hat{\varepsilon}(t')$. Using $\hat{\varepsilon}(t')$, the electric field can

be written as

$$\varepsilon(t') = \mathrm{e}^{-i(\frac{\nu}{\Gamma}t' + \varphi_g - \varphi_{ab})}\hat{\varepsilon}(t'). \tag{3.14}$$

To obtain the separate phase and magnitude equations now we write $\hat{\varepsilon}(t')$ in the form

$$\hat{\varepsilon}(t') = |\hat{\varepsilon}|\mathrm{e}^{i\varphi}. \tag{3.15}$$

After substituting Eq. (3.15) and Eq. (3.13) into Eq. (3.7) and Eq. (3.10) and doing the algebra, we obtain

$$\begin{aligned}\frac{d|\hat{\varepsilon}|}{dt'} &= \Big(-\frac{1}{2} + N_{ex}\mathcal{D} + N_{ex}u\mathcal{F} - N_{ex}\Big)|\hat{\varepsilon}| \\ &\quad - \lambda\frac{N_{ex}}{2}\sqrt{1-u^2}\Big(\mathcal{G} + \mathcal{H}|\hat{\varepsilon}|^2\Big)\sin(\varphi), \qquad (3.16a)\\ |\hat{\varepsilon}|\frac{d\varphi}{dt'} &= -\Delta|\hat{\varepsilon}| - \lambda\frac{N_{ex}}{2}\sqrt{1-u^2}\Big(\mathcal{G} - \mathcal{H}|\hat{\varepsilon}|^2\Big)\cos(\varphi), \qquad (3.16b)\end{aligned}$$

for the magnitude and the phase of the field, and

$$\begin{aligned}\frac{dn(t')}{dt'} &= -n + \frac{N_{ex}}{2}\Big((n+1)S_{n+1}^2 - nS_n^2\Big) + u\frac{N_{ex}}{2}\Big((n+1)S_{n+1}^2 + nS_n^2\Big) \\ &\quad - \lambda N_{ex}\sqrt{1-u^2}S_{n+1}C_{n+1}|\hat{\varepsilon}|\sin(\varphi),\end{aligned} \tag{3.17}$$

for the intensity of the field. From Eqs. (3.16) and (3.17) it is easy to see the major differences between the coherently and incoherently pumped micromasers. First let us see what happens in the case of the incoherently pumped micromasers. In this case either $\lambda = 0$ or $u = \pm 1$ which reduces the magnitude and phase equations to

$$\begin{aligned}\frac{d|\hat{\varepsilon}|}{dt'} &= \Big(-\frac{1}{2} + N_{ex}\mathcal{D} + N_{ex}u\mathcal{F} - N_{ex}\Big)|\hat{\varepsilon}|, \qquad (3.18a)\\ \frac{d\varphi}{dt'} &= -\Delta, \qquad (3.18b)\end{aligned}$$

and the intensity equation to

$$\frac{dn(t')}{dt'} = -n + \frac{N_{ex}}{2}\Big((n+1)S_{n+1}^2 - nS_n^2\Big) + u\frac{N_{ex}}{2}\Big((n+1)S_{n+1}^2 + nS_n^2\Big). \tag{3.19}$$

Now a very important feature of the incoherently pumped micromasers can be seen from Eqs. (3.18a) and (3.18b). The equations determining the magnitude and the phase of the field are not coupled. Thus, these equations can be solved separately. After solving Eq. (3.18b), we obtain

$$\varphi(t') = -\Delta t' + \varphi_0, \tag{3.20}$$

where the integration constant φ_0 can be chosen arbitrarily. Now using Eq. (3.14) the electric field can be written as

$$\begin{aligned} \varepsilon(t') &= \mathrm{e}^{-i\left(\left(\frac{\nu}{\Gamma}+\Delta\right)t'+\varphi_g-\varphi_{ab}-\varphi_0\right)}|\hat{\varepsilon}| \\ &= \mathrm{e}^{-i(\omega_0 t'+\varphi_g-\varphi_{ab}-\varphi_0)}|\hat{\varepsilon}|. \end{aligned} \tag{3.21}$$

This means in the case of the incoherently pumped micromaser the phase of the field is not well determined, it is arbitrary up to an integration constant. In practice this means the integration constant can and will be randomly changed by each occurring spontaneous emission event. As these small changes are totally random the phase gradually diffuses and becomes equally distributed over 2π making the average electric field to disappear. The intensity however, which is immune to this diffusion, will not vanish. Its value will be determined by Eq. (3.19). Now, what does Eq. (3.18a) tell us? To answer this question we have to see clearly what $|\hat{\varepsilon}|$ represents. Does $|\hat{\varepsilon}|$ simply stand for the square root of the intensity $n(t)$? The answer to this question is

no. If we take a look at the definition of $\hat{\varepsilon}(t')$ we see that

$$|\hat{\varepsilon}| = |\mathrm{Tr}\left[\mathbf{a}\tilde{\rho}(t')\right]|. \tag{3.22}$$

On the other hand the intensity of the field is defined as

$$n(t') = \mathrm{Tr}\left[\mathbf{a}^{\dagger}\mathbf{a}\tilde{\rho}(t')\right]. \tag{3.23}$$

The major difference between Eq. (3.22) and Eq. (3.23) is in the phase information content. In Eq. (3.22) the trace is taken using the annihilation operator **a**. This means we sum over values including not only magnitude but phase information, as well. In Eq. (3.23), however, the only retained information is the square of the magnitude and no phase information is present. This is why the intensity is immune to phase diffusion and why the value of $|\hat{\varepsilon}|$ and $\sqrt{n(t')}$ can be so different. As we will see later from the quantum mechanical solution $|\hat{\varepsilon}| \to 0$ when $\lambda \to 0$ even though the intensity remains finite, as determined by Eq. (3.19). But in general, even in the case of $\lambda = 1$, it is true that

$$|\hat{\varepsilon}|^2 \leq n. \tag{3.24}$$

Next we will investigate the case of the coherently pumped micromaser. In this case we assume $\lambda \neq 0$ and $u \neq \pm 1$. Therefore, to obtain the proper values of $|\hat{\varepsilon}|$, φ and n, we have to solve the set of three coupled differential equations represented by Eqs. (3.16a), (3.16b) and (3.17). We focus our attention on the steady state solution determined by these equations. In steady state the time derivatives of the quantities

vanish and we obtain

$$0 = \left(-\frac{1}{2} + N_{ex}\mathcal{D} + N_{ex}u\mathcal{F} - N_{ex}\right)|\hat{\varepsilon}| - \lambda\frac{N_{ex}}{2}\sqrt{1-u^2}\left(\mathcal{G} + \mathcal{H}|\hat{\varepsilon}|^2\right)\sin(\varphi), \tag{3.25a}$$

$$0 = -\Delta|\hat{\varepsilon}| - \lambda\frac{N_{ex}}{2}\sqrt{1-u^2}\left(\mathcal{G} - \mathcal{H}|\hat{\varepsilon}|^2\right)\cos(\varphi), \tag{3.25b}$$

and

$$0 = -n + \frac{N_{ex}}{2}\left((n+1)S_{n+1}^2 - nS_n^2\right) + u\frac{N_{ex}}{2}\left((n+1)S_{n+1}^2 + nS_n^2\right) - \lambda N_{ex}\sqrt{1-u^2}S_{n+1}C_{n+1}|\hat{\varepsilon}|\sin(\varphi). \tag{3.26}$$

In general, each of these three equations Eq. (3.25a), Eq. (3.25b) and Eq. (3.26) defines a surface in the 3-dimensional space spanned by $|\hat{\varepsilon}|$, φ, and n. The coordinates of those points where all three surfaces intersect will represent a set of the possible steady state values of $|\hat{\varepsilon}|$, φ, n. However, to decide whether the given point is really representing a steady state solution we have to do stability analysis. To do so we use the following theorem [38].

Consider a set of differential equations in the following form

$$\frac{dx_1}{dt} = f_1(x_1, x_2, x_3), \tag{3.27a}$$

$$\frac{dx_2}{dt} = f_2(x_1, x_2, x_3), \tag{3.27b}$$

$$\frac{dx_3}{dt} = f_3(x_1, x_2, x_3). \tag{3.27c}$$

The Jacobian of the system is given by

$$\mathrm{D}f = \begin{bmatrix} \frac{\partial f_1}{\partial x_1} & \frac{\partial f_1}{\partial x_2} & \frac{\partial f_1}{\partial x_3} \\ \frac{\partial f_2}{\partial x_1} & \frac{\partial f_2}{\partial x_2} & \frac{\partial f_2}{\partial x_3} \\ \frac{\partial f_3}{\partial x_1} & \frac{\partial f_3}{\partial x_2} & \frac{\partial f_3}{\partial x_3} \end{bmatrix}. \tag{3.28}$$

Now let $\bar{x} = (x_1, x_2, x_3)$ be a point where

$$f_1(\bar{x}) = f_2(\bar{x}) = f_3(\bar{x}) = 0. \tag{3.29}$$

Calculate the Jacobian $\mathrm{D}f\Big|_{\bar{x}}$, at this point and determine its eigenvalues, λ_1, λ_2, λ_3. If

$$\mathrm{Re}\,[\lambda_i] < 0 \tag{3.30}$$

for all eigenvalues then $\bar{x}$ represents a stable point. If for any eigenvalue $\mathrm{Re}\,[\lambda_i] = 0$ we must use some other method (for example Liapunov-method [38]) to establish the behavior of the system at that point.

Next we will provide a simple example on which we can study how the method, we just described, works. Let us suppose for the sake of simplicity that

$$\Delta = 0. \tag{3.31}$$

In this case the phase equation, Eq. (3.25b), reduces to

$$0 = \lambda \frac{N_{ex}}{2} \sqrt{1 - u^2} \left(\mathcal{G} - \mathcal{H} |\hat{\varepsilon}|^2 \right) \cos(\varphi). \tag{3.32}$$

To satisfy this equation we must satisfy either of the following conditions

$$\cos(\varphi) = 0, \tag{3.33}$$

or

$$\mathcal{G} - \mathcal{H}|\hat{\varepsilon}|^2 = 0. \tag{3.34}$$

Let us now investigate both cases starting with Eq. (3.33).

If Eq. (3.33) holds then the phase of the steady state field is well determined. It locks to either $\frac{\pi}{2}$ or $-\frac{\pi}{2}$ therefore

$$\sin(\varphi) = \pm 1. \tag{3.35}$$

Assuming Eq. (3.35) is satisfied, from Eq. (3.25a) and Eq. (3.26) we obtain

$$0 = \Big(-1 + 2N_{ex}\mathcal{D} + 2N_{ex}u\mathcal{F} - 2N_{ex}\Big)|\hat{\varepsilon}|^2 \mp \lambda N_{ex}\sqrt{1-u^2}\Big(\mathcal{G} + \mathcal{H}|\hat{\varepsilon}|^2\Big)|\hat{\varepsilon}|, \tag{3.36}$$

$$\begin{aligned} 0 \;=\; & -n + \frac{N_{ex}}{2}\Big((n+1)S_{n+1}^2 - nS_n^2\Big) + u\frac{N_{ex}}{2}\Big((n+1)S_{n+1}^2 + nS_n^2\Big) \\ & \mp \lambda N_{ex}\sqrt{1-u^2}S_{n+1}C_{n+1}|\hat{\varepsilon}|. \end{aligned} \tag{3.37}$$

The steady state values of n and $|\hat{\varepsilon}|^2$ can be obtained from these equations. Since these are non-algebraic equations we will determine the solutions using a graphical method. In the following pictures we plot those points which satisfy Eq. (3.36) and Eq. (3.37) separately. The intersections of the two graphs represent the possible steady state values of n and $|\hat{\varepsilon}|^2$. To decide which of these points really represent a steady state solution we carried out the stability analysis, we described earlier. Stable points in the semiclassical graphs are denoted by black dots and the steady state values of n and $|\hat{\varepsilon}|^2$ are printed right next to them. For comparison, along with the semiclassical graphs, we also printed the quantum mechanical distributions for n and φ obtained

from the solution of the fully quantum mechanical model. (See the next chapter for further details on the quantum model.)

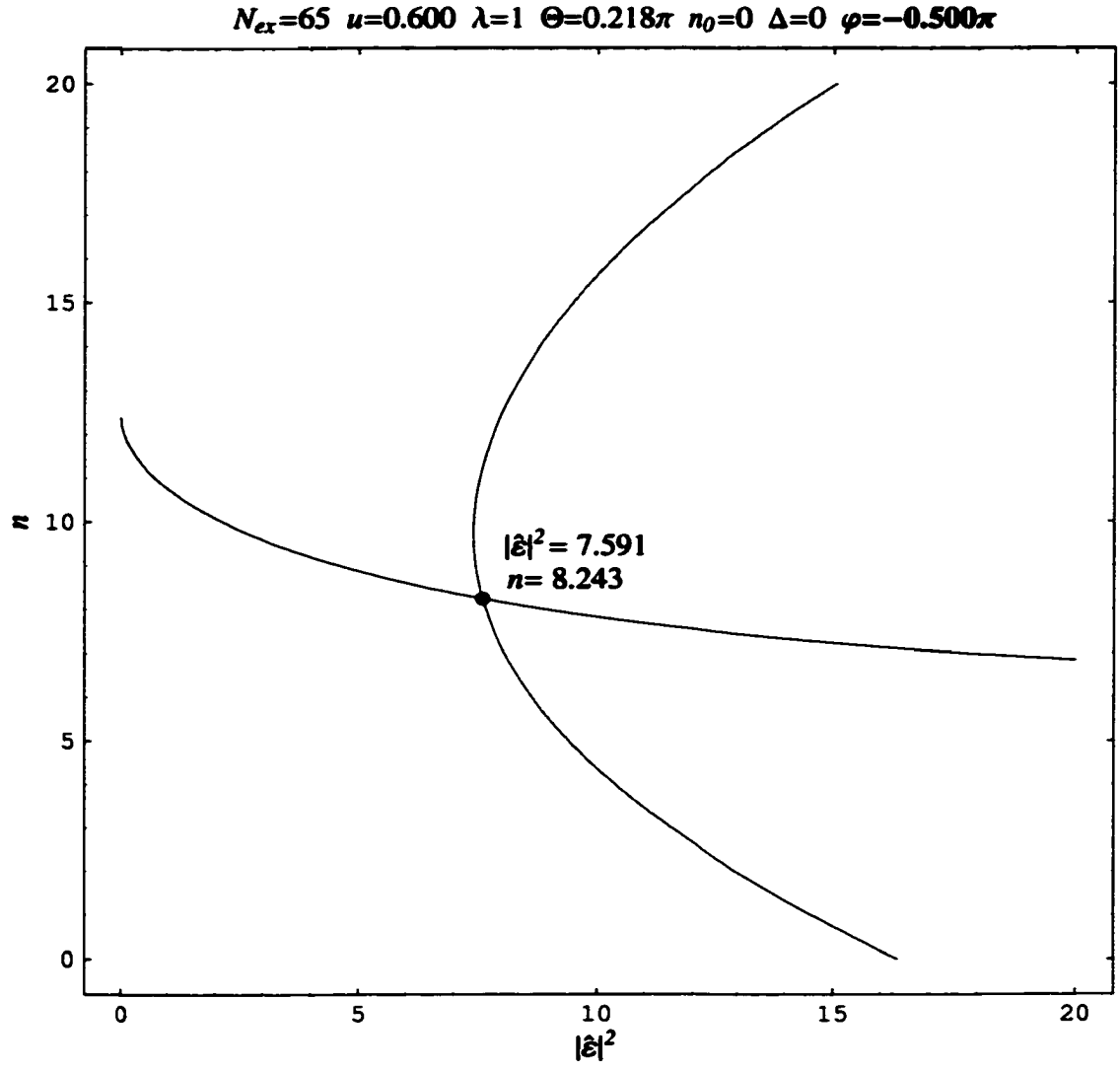

Figure 5: The predictions of the semiclassical model for a single peaked photon distribution. The points satisfying Eq. (3.36) are represented by the graph going vertically and the points satisfying Eq. (3.37) by the graph running horizontally, assuming phase locking $\varphi = -\frac{\pi}{2}$.

In Figs. 5–8 we see how well the semiclassical approximation works for a single peaked photon distribution. The values of n and $|\hat{\varepsilon}|^2$, obtained from the semiclassical

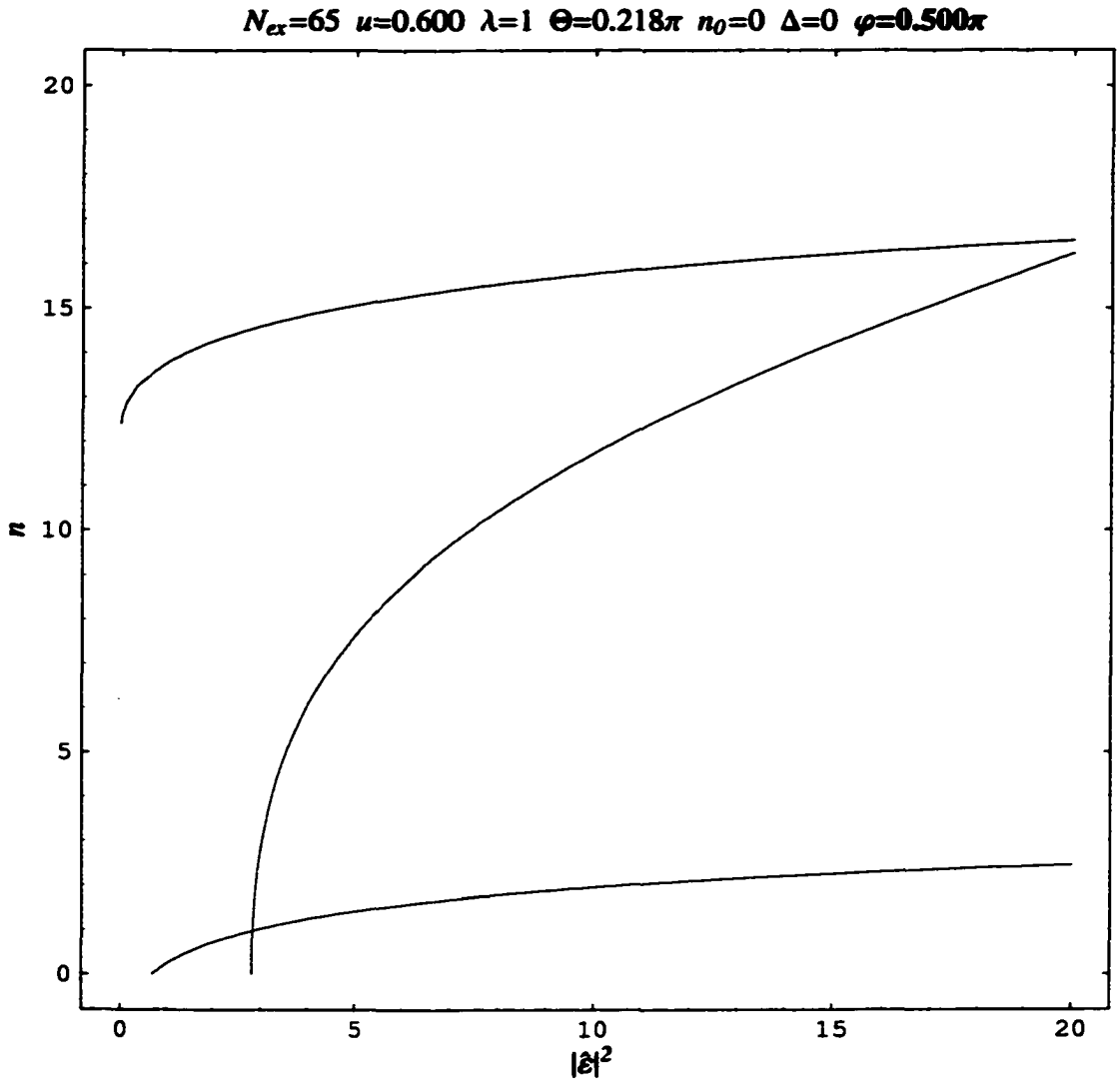

Figure 6: The predictions of the semiclassical model for a single peaked photon distribution. The points satisfying Eq. (3.36) are represented by the graph going vertically and the points satisfying Eq. (3.37) by the graphs running horizontally, assuming phase locking $\varphi = \frac{\pi}{2}$.

theory and the fully quantum model are close to each other. Note that the only stable solution predicted by the semiclassical model, has its phase locked to $-\frac{\pi}{2}$. This phase locking can also be observed in the phase density function provided by the fully quantum mechanical model and pictured in Fig. 8. Here we can see a sharp

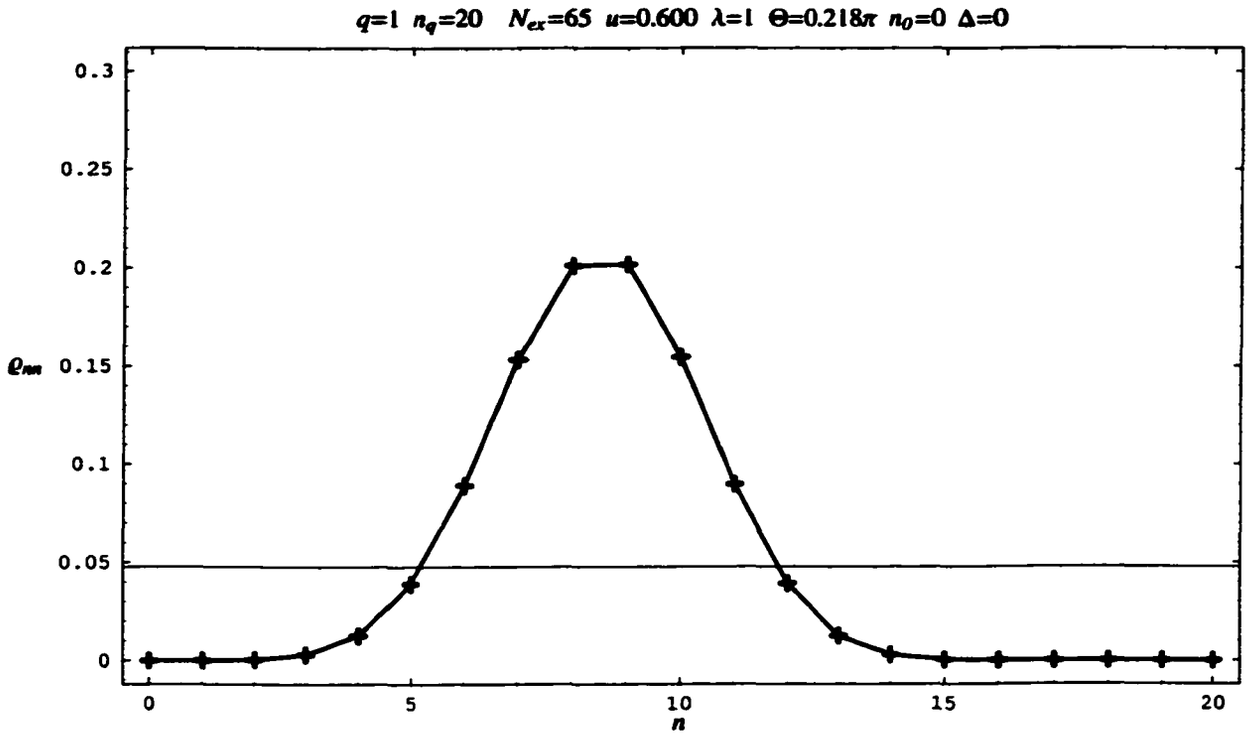

Figure 7: The predictions of the quantum mechanical model for a single peaked photon distribution. The photon distribution is obtained by solving the fully quantum mechanical model. The average photon number is $\langle n \rangle = 8.503$, and the square of the average field's magnitude is $|\langle \hat{\varepsilon} \rangle|^2 = 8.241$. On the figure we also indicated, with the thin line, the uniform photon distribution.

peak in the phase density function at $-\frac{\pi}{2}$. In the case $\varphi = \frac{\pi}{2}$ the semiclassical model predicted no stable solution. This can be easily understood from Fig. 6, where we can see that for all intersection points in the graph $|\hat{\varepsilon}|^2 > n$ and if these points represented a steady state they would violate Eq. (3.24). Also note since the phase density function, pictured in Fig. 8, is sharply peaked the corresponding steady state values of n and $|\hat{\varepsilon}|^2$ are fairly close to each other. They would be the same only if the phase density function were represented by a Dirac delta function $\delta(\varphi - \varphi_0)$ where φ_0 represents the value the phase of the field locks to. By observing the spread

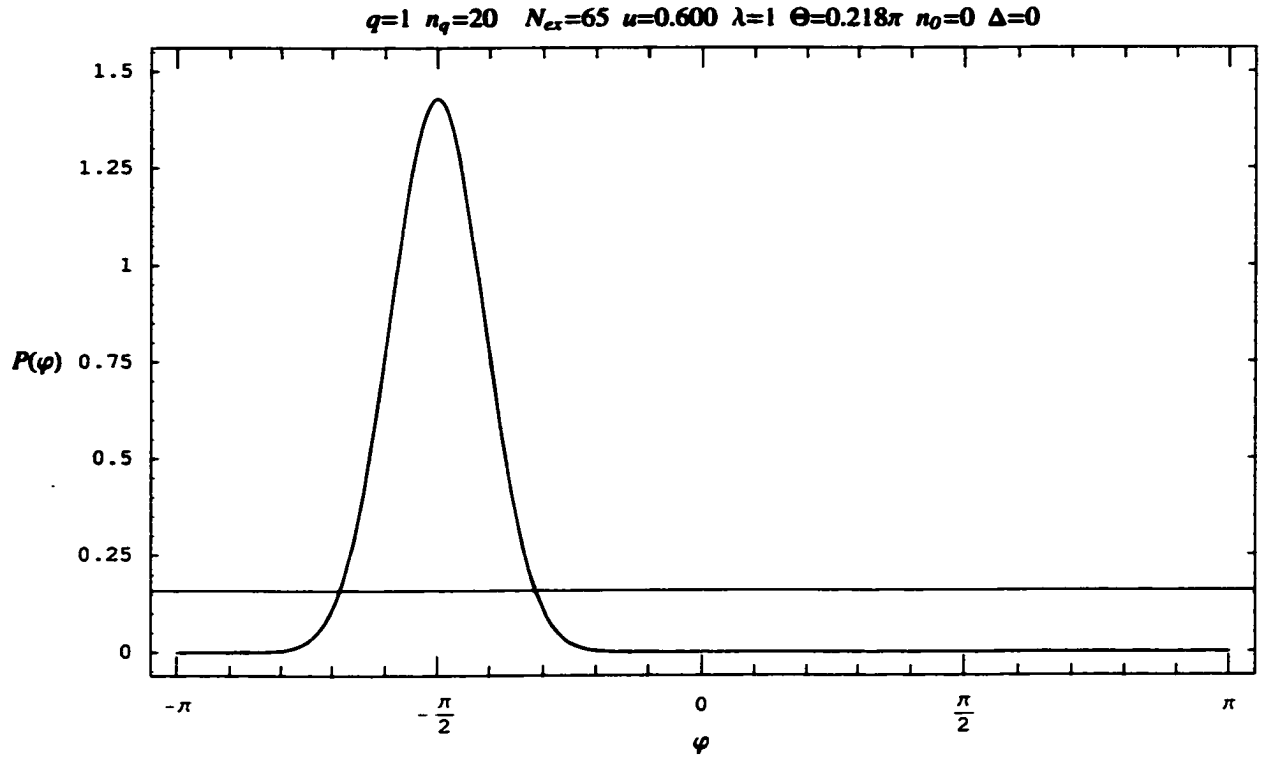

Figure 8: The predictions of the quantum mechanical model for a single peaked photon distribution. The phase density function is obtained by solving the fully quantum mechanical model. On the figure we also indicated the density function corresponding to the uniformly distributed phase.

of the phase density function pictured in Fig. 8 we can conclude that the effect of the injected atomic coherence is manifest in the significant reduction of the phase diffusion observed in the case of the incoherently pumped micromaser.

In the following set of pictures, Figs. 9–24, we show how the semiclassical approximation works for multiple peaked photon distributions. Even though in deriving Eq. (3.36) and Eq. (3.37) we assumed a single peaked photon distribution, the equations work for multiple peaked photon distributions as well. This we can see from Figs. 9–24, provided that the peaks of the photon distribution are well separated from each other. But as we can see from these pictures the values of the average photon

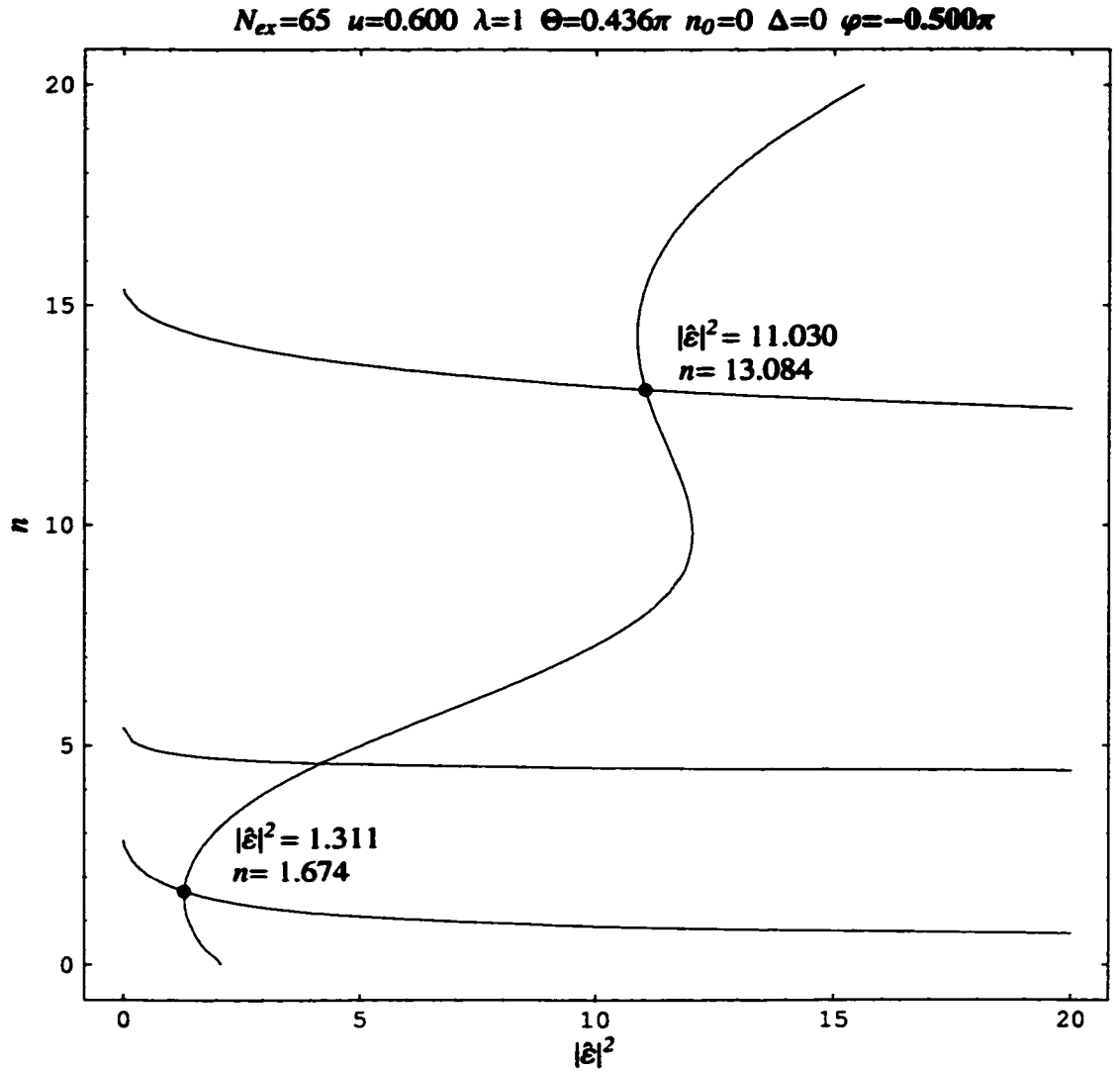

Figure 9: The predictions of the semiclassical model for a double peaked photon distribution. The points satisfying Eq. (3.36) are represented by the graph going vertically and the points satisfying Eq. (3.37) by the graphs running horizontally, assuming phase locking $\varphi = -\frac{\pi}{2}$.

numbers in steady state, provided by the fully quantum mechanical model, and the steady state values of n, provided by the semiclassical model, are no longer close to each other. However, the peaks in the photon distribution of the steady state, provided by the fully quantum mechanical model, are close to the values obtained

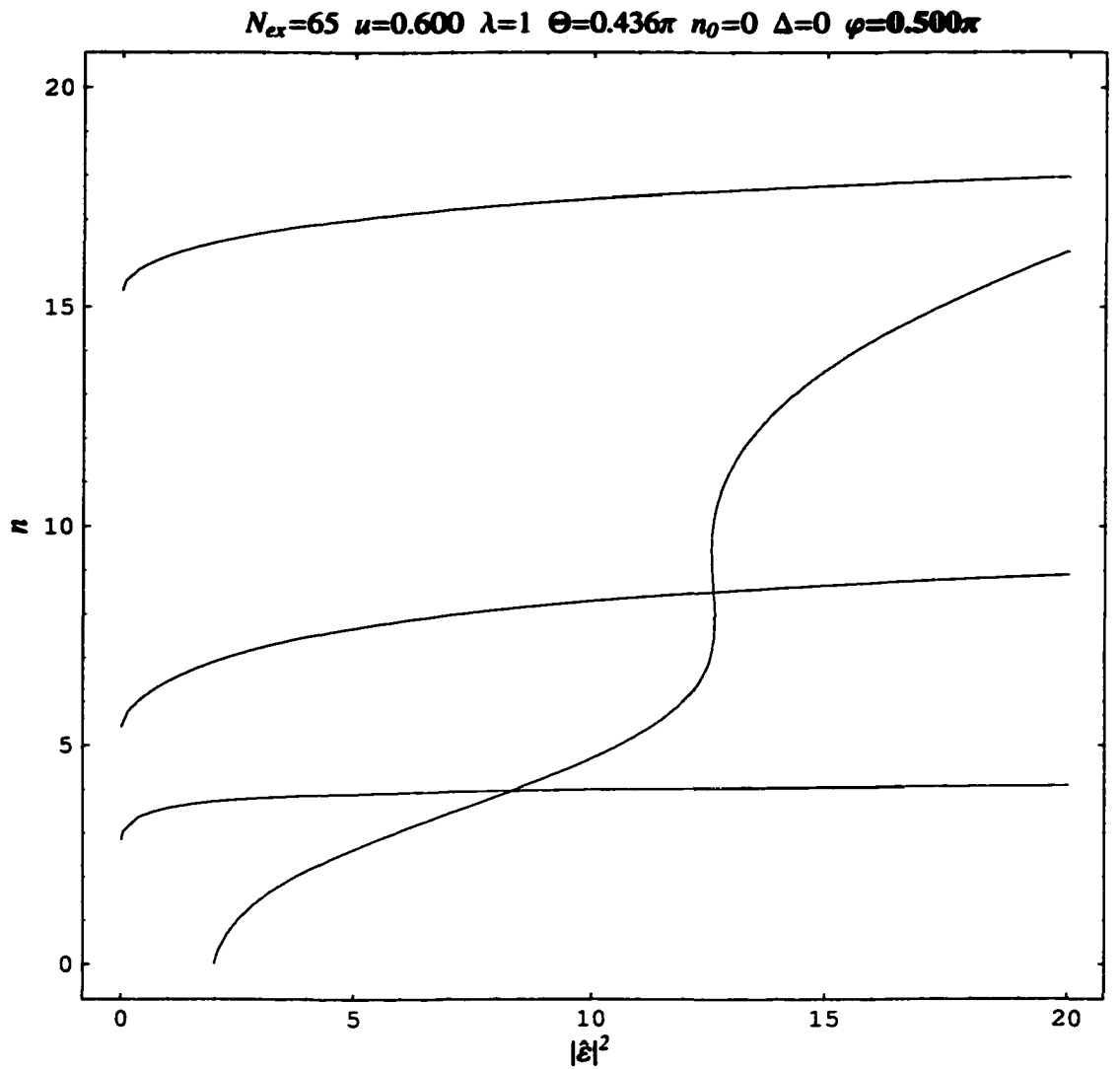

Figure 10: The predictions of the semiclassical model for a double peaked photon distribution. The points satisfying Eq. (3.36) are represented by the graph going vertically and the points satisfying Eq. (3.37) by the graphs running horizontally, assuming phase locking $\varphi = \frac{\pi}{2}$.

for the steady state value of n from the semiclassical model. The main difference between the two models is that even though the semiclassical solution, provides the positions of the peaks in the photon distribution fairly well, it can not provide the statistical weight of these peaks. Therefore it is unable to give a precise answer for

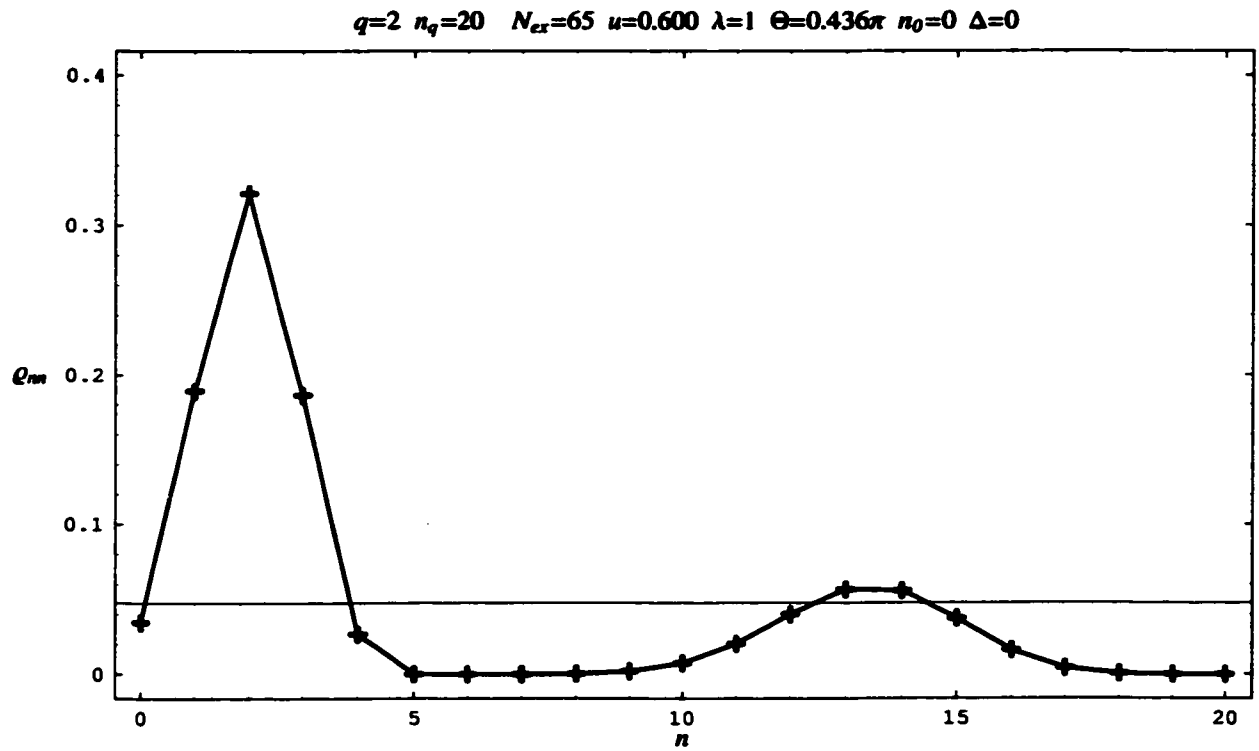

Figure 11: The predictions of the quantum mechanical model for a double peaked photon distribution. The photon distribution is obtained by solving the fully quantum mechanical model. The average photon number is $\langle n \rangle = 4.725$, and the square of the average field's magnitude is $|\langle \hat{\varepsilon} \rangle|^2 = 3.375$. On the figure we also indicated, with the thin line, the uniform photon distribution.

the average photon number. Also please note from the phase density graphs Figs. 12, 16, 20, and 24 how they spread wider in the case of more peaks in the photon distribution resulting in lesser reduction of the phase diffusion. As the phase density graphs spread wider the corresponding steady state values of n and $|\hat{\varepsilon}|^2$ are getting more and more separated. Ultimately, in the case when the phase density function is represented by the uniform distribution ($P(\varphi) = \frac{1}{2\pi}$), the case of the incoherently pumped micromaser, the steady state value of $|\hat{\varepsilon}|^2$ becomes equal to zero.

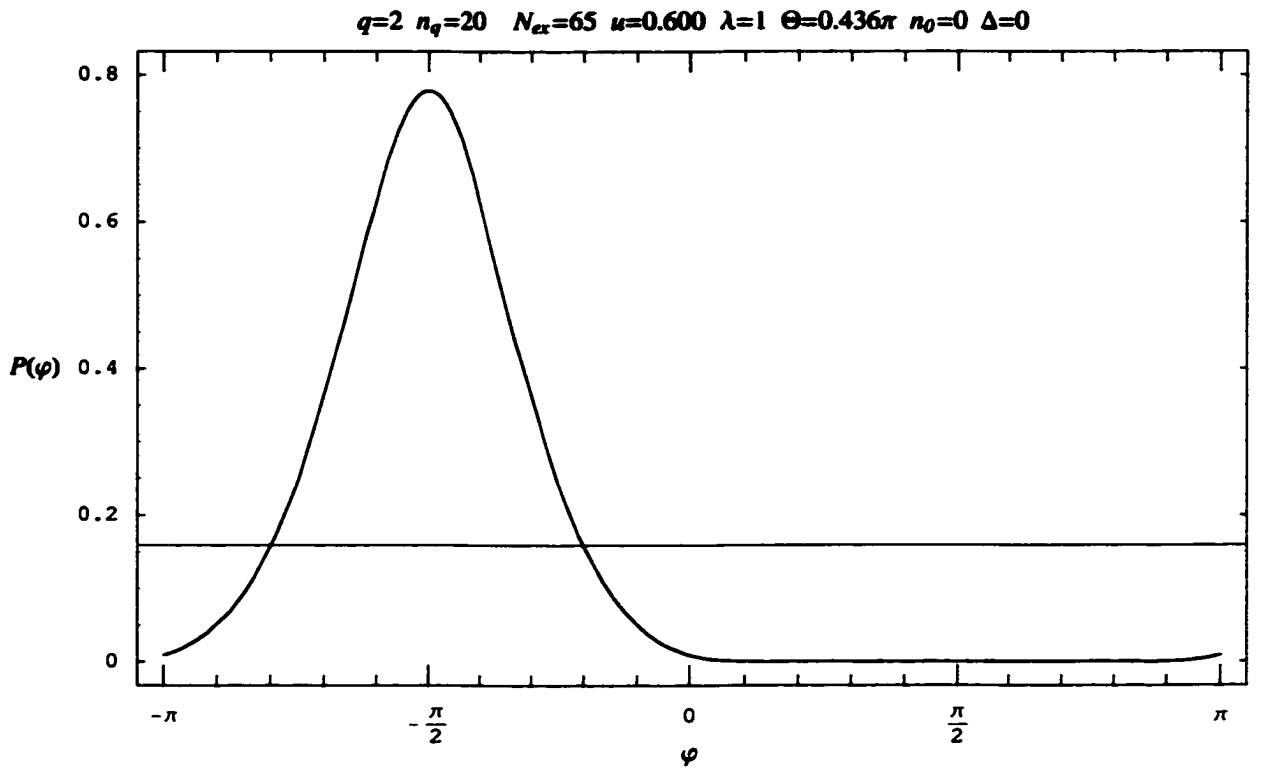

Figure 12: The predictions of the quantum mechanical model for a double peaked photon distribution. The phase density function is obtained by solving the fully quantum mechanical model. On the figure we also indicated the density function corresponding to the uniformly distributed phase.

In Figs. 25–28 we present an exciting result of the semiclassical model. We can see in Figs. 25 and Figs. 26 that stable solutions of the semiclassical model exist in both phase locking cases. Therefore, we expect that the quantum mechanical model will predict not only a multiple peaked photon distribution but a double peaked phase distribution, as well. However, the phase density function Fig. 28 obtained by solving the fully quantum mechanical model is an unexpected sight at first. It shows a triple rather than a double peaked phase distribution. The underlying principle of this phenomena is interference. Since the wave function, describing the quantum mechanical system, contains a coherent superposition of both phase locked solutions with differ-

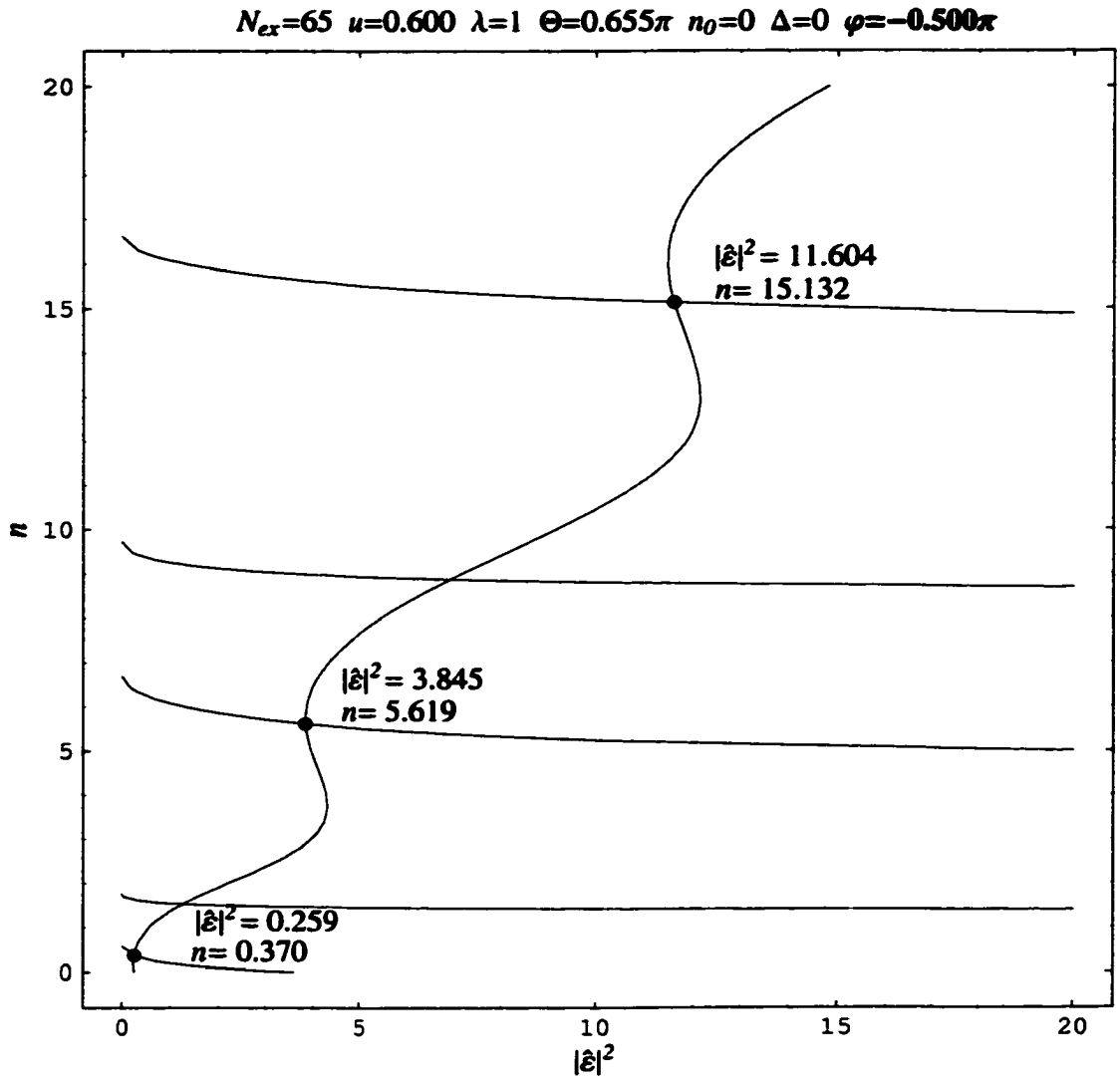

Figure 13: The predictions of the semiclassical model for a triple peaked photon distribution. The points satisfying Eq. (3.36) are represented by the graph going vertically and the points satisfying Eq. (3.37) by the graphs running horizontally, assuming phase locking $\varphi = -\frac{\pi}{2}$.

ent statistical weights, the measurement statistics of observables will contain terms which are related to interference between the two phase locking schemes. In our case, we can see from the photon distribution Fig. 27 that the highest statistical weight corresponds to the case when $n = 1$. This we can identify with two semiclassical

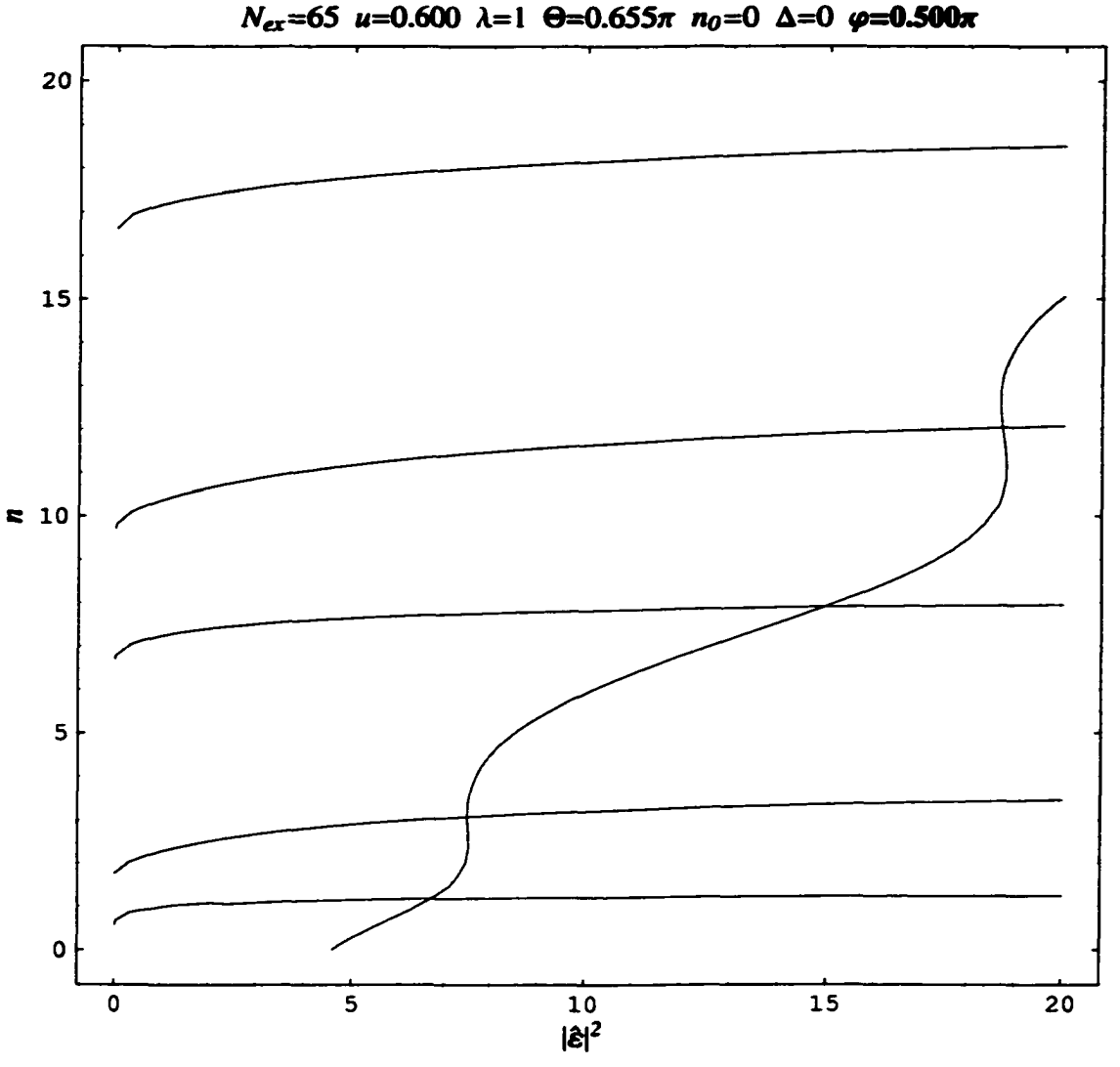

Figure 14: The predictions of the semiclassical model for a triple peaked photon distribution. The points satisfying Eq. (3.36) are represented by the graph going vertically and the points satisfying Eq. (3.37) by the graphs running horizontally, assuming phase locking $\varphi = \frac{\pi}{2}$.

branches corresponding to $n = 0.730$ and $n = 1.343$ both belonging to the $\varphi = \frac{\pi}{2}$ phase locking scheme. This is why the density function describing the measurement statistics of the phase Fig. 28 is centered around $\frac{\pi}{2}$. We can also see in the photon distribution Fig. 27 another significant peak which is located at $n = 5$. The semiclas-

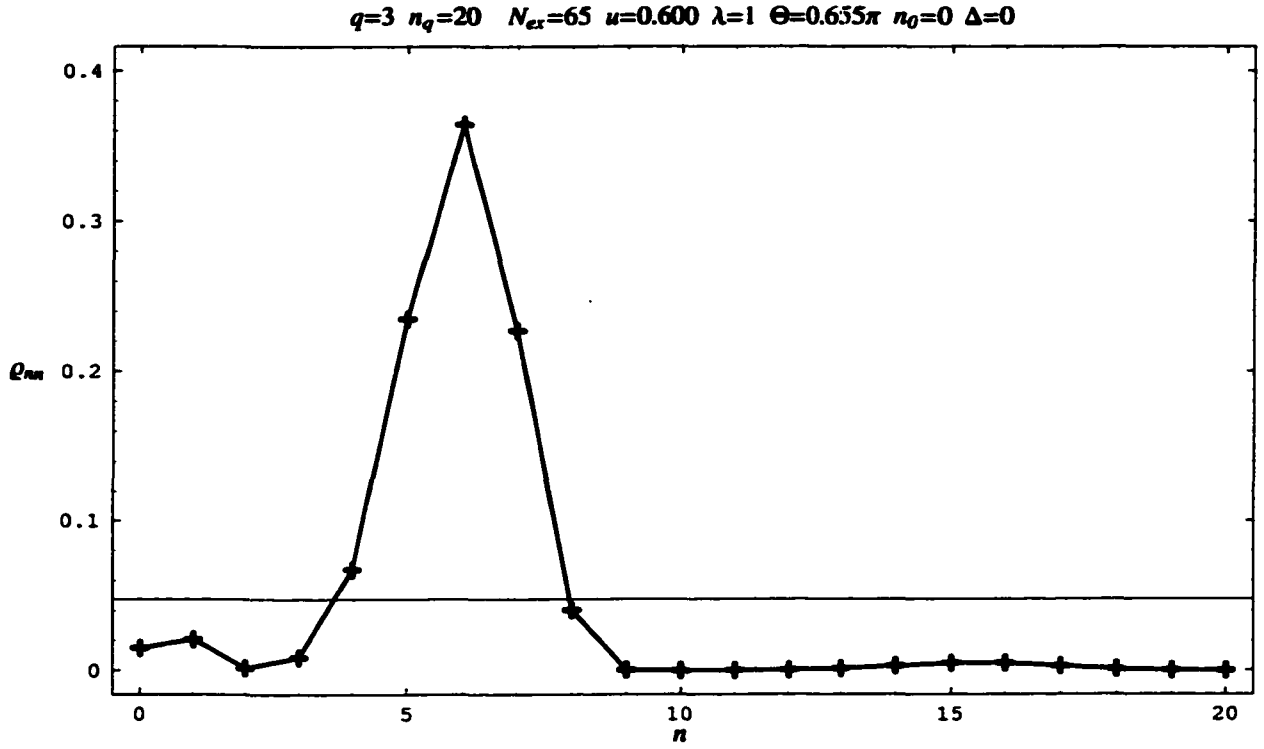

Figure 15: The predictions of the quantum mechanical model for a triple peaked photon distribution. The photon distribution is obtained by solving the fully quantum mechanical model. The average photon number is $\langle n \rangle = 5.886$, and the square of the average field's magnitude is $|\langle \hat{\varepsilon} \rangle|^2 = 4.606$. On the figure we also indicated, with the thin line, the uniform photon distribution.

sical model predicts the only solutions where the photon number is approximately equal to 5 are belonging to the $\varphi = -\frac{\pi}{2}$ phase locking scheme. Since the statistical weight of these solutions is much smaller than the statistical weight corresponding to the other phase locking scheme they do not pull the phase distribution away from being centered around $\frac{\pi}{2}$, rather they cause a symmetrical splitting of it, as shown in Fig. 28. This example is an exciting result of our extended semiclassical theory, as well it provides a simple explanation of the multistable behavior of the phase of a coherently pumped micromaser. We will see more examples of the multistable behavior

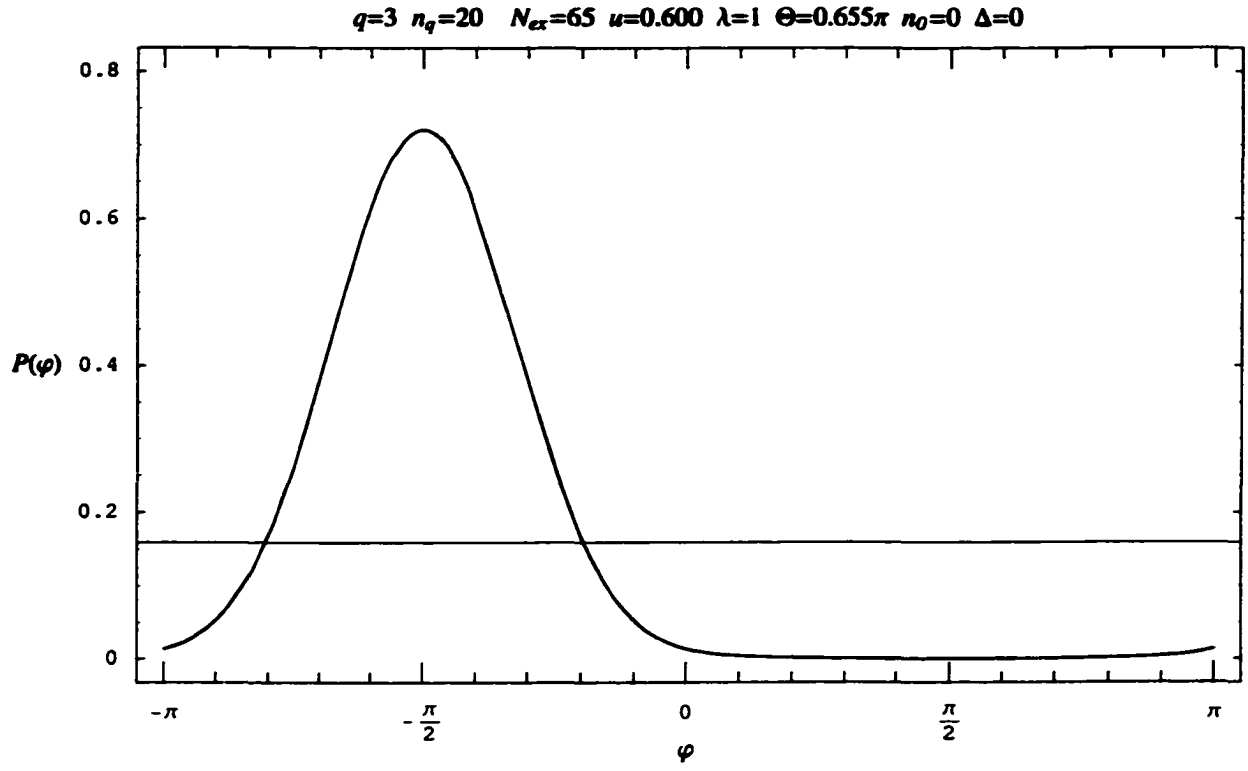

Figure 16: The predictions of the quantum mechanical model for a triple peaked photon distribution. The phase density function is obtained by solving the fully quantum mechanical model. On the figure we also indicated the density function corresponding to the uniformly distributed phase.

of the phase after discussing the fully quantum mechanical model of the coherently pumped micromaser.

Closing this chapter now we discuss the condition represented by Eq. (3.34). If it is satisfied then the steady state value of $|\langle\hat{\varepsilon}\rangle|^2$ is given by

$$|\hat{\varepsilon}|^2 = \frac{\mathcal{G}}{\mathcal{H}}. \tag{3.38}$$

However caution must be taken when applying this condition since both $\mathcal{G}$ and $\mathcal{H}$ can be either positive or negative but $|\hat{\varepsilon}|^2$ must always be positive. Therefore Eq. (3.38) can only be applied if using it leads to a steady state value of n which satisfies the

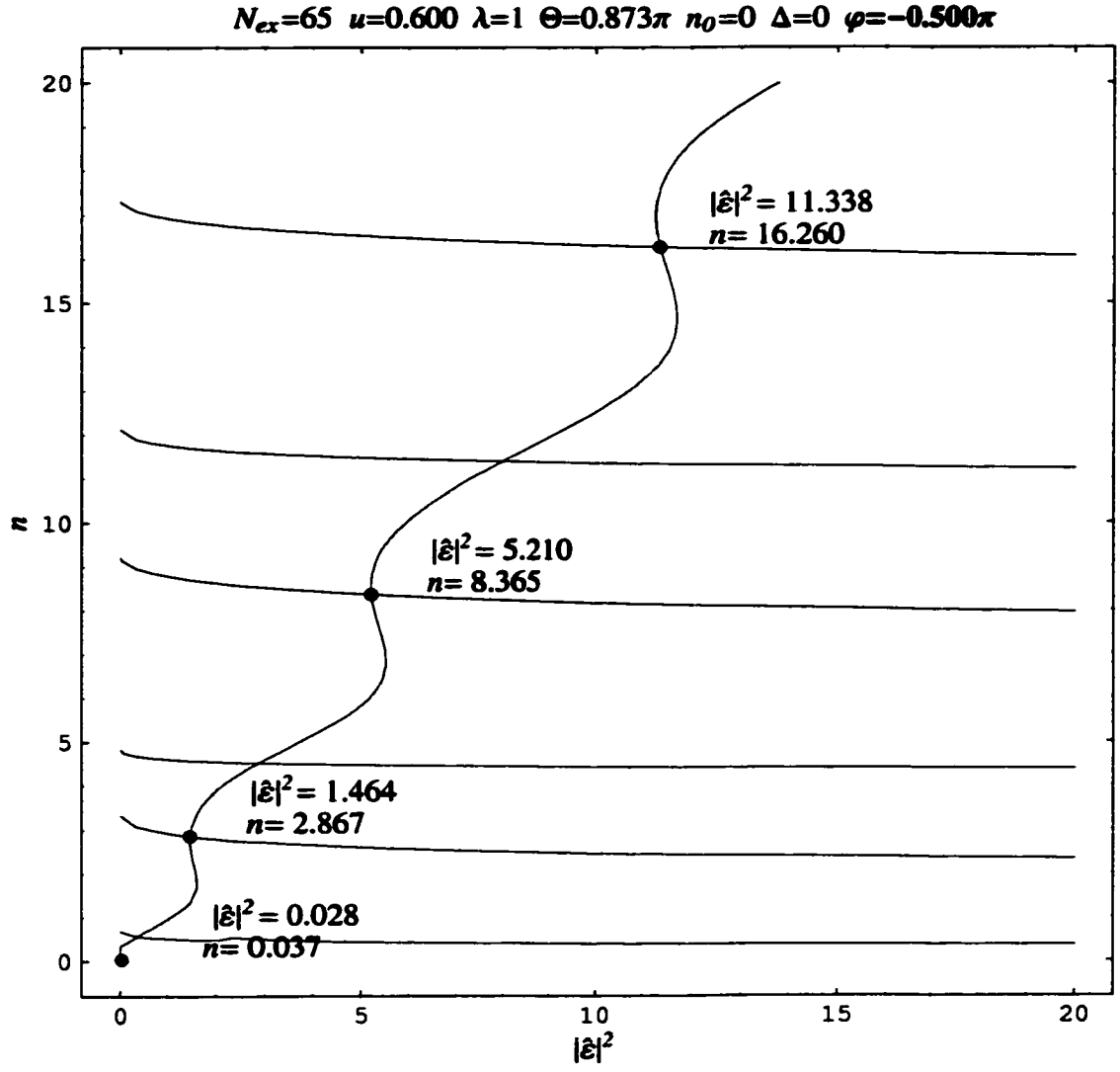

Figure 17: The predictions of the semiclassical model for a multiple peaked photon distribution. The points satisfying Eq. (3.36) are represented by the graph going vertically and the points satisfying Eq. (3.37) by the graphs running horizontally, assuming phase locking $\varphi = -\frac{\pi}{2}$.

following condition

$$\frac{\mathcal{G}}{\mathcal{H}} \geq 0. \tag{3.39}$$

Assuming we have satisfied Eq. (3.39), we can use Eq. (3.38) to simplify Eq. (3.25a) and Eq. (3.26) and obtain the coupled equations determining the steady state value

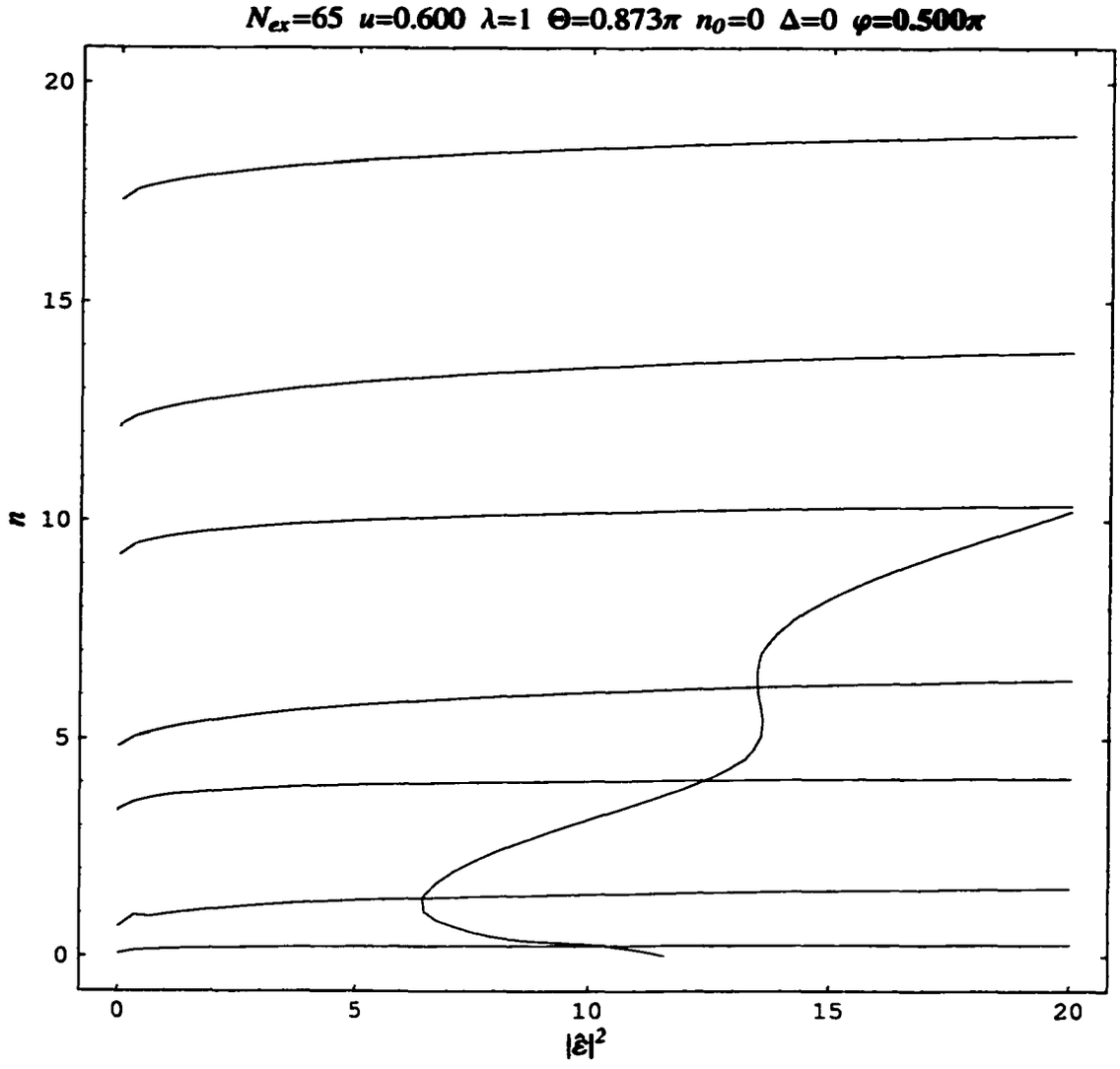

Figure 18: The predictions of the semiclassical model for a multiple peaked photon distribution. The points satisfying Eq. (3.36) are represented by the graph going vertically and the points satisfying Eq. (3.37) by the graphs running horizontally, assuming phase locking $\varphi = \frac{\pi}{2}$.

of n and φ

$$0 = \left(-1 + 2N_{ex}\left(\mathcal{D} + u\mathcal{F} - 1\right)\right)\frac{\mathcal{G}}{\mathcal{H}} - 2\lambda N_{ex}\sqrt{1-u^2}\mathcal{G}\sqrt{\frac{\mathcal{G}}{\mathcal{H}}}\sin(\varphi), \qquad (3.40)$$

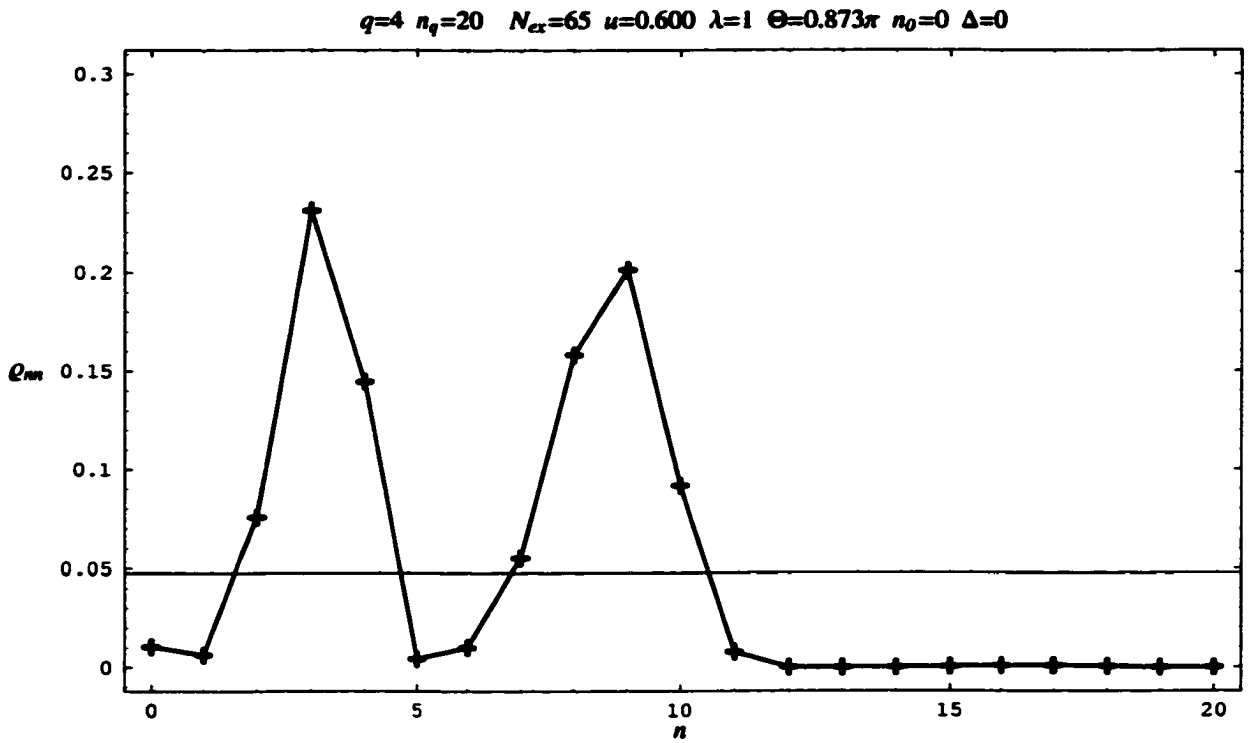

Figure 19: The predictions of the quantum mechanical model for a multiple peaked photon distribution. The photon distribution is obtained by solving the fully quantum mechanical model. The average photon number is $\langle n \rangle = 6.029$, and the square of the average field's magnitude is $|\langle \hat{\varepsilon} \rangle|^2 = 3.983$. On the figure we also indicated, with the thin line, the uniform photon distribution.

$$\begin{aligned} 0 &= -n + \frac{N_{ex}}{2}\Big((1+u)\sin^2(\sqrt{n+1}\Theta) - (1-u)\sin^2(\sqrt{n}\Theta)\Big) \\ &- \lambda N_{ex}\sqrt{1-u^2}\frac{\sin(2\sqrt{n+1}\Theta)}{2\sqrt{n+1}}\sqrt{\frac{\mathcal{G}}{\mathcal{H}}}\sin(\varphi) \end{aligned} \tag{3.41}$$

By eliminating $\sin(\varphi)$ from Eq. (3.40) and Eq. (3.41) we derived the equation determining the steady state value of n

$$\begin{aligned} 0 &= -n + \frac{N_{ex}}{2}\Big((1+u)\sin^2(\sqrt{n+1}\Theta) - (1-u)\sin^2(\sqrt{n}\Theta)\Big) \\ &- \frac{\sin(2\sqrt{n+1}\Theta)}{2\sqrt{n+1}}\Big(-\frac{1}{2\mathcal{H}} + \frac{N_{ex}}{\mathcal{H}}(\mathcal{D} + u\mathcal{F} - 1)\Big) \end{aligned} \tag{3.42}$$

Solving Eq. (3.42) provides the possible steady state values of n. However not all n

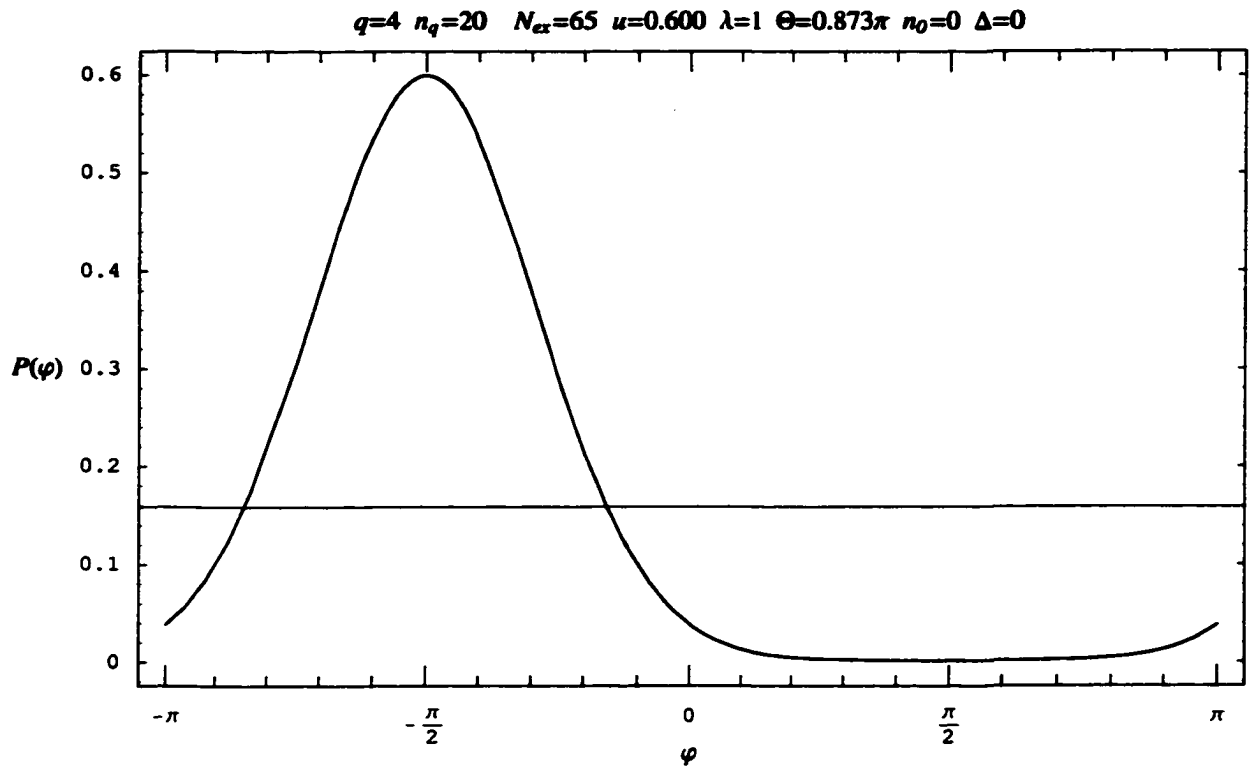

Figure 20: The predictions of the quantum mechanical model for a multiple peaked photon distribution. The phase density function is obtained by solving the fully quantum mechanical model. On the figure we also indicated the density function corresponding to the uniformly distributed phase.

values will represent real steady states. The only acceptable solutions will be those which satisfy all the following conditions. Since n is representing an intensity value it must be positive

$$n \geq 0. \tag{3.43}$$

Furthermore, using the steady state value of n from Eq. (3.40) we can determine the sine of the steady state's phase

$$\sin(\varphi) = \frac{-\frac{1}{2N_{ex}} + (\mathcal{D} + u\mathcal{F} - 1)}{\lambda\sqrt{1-u^2}\sqrt{\mathcal{G}\mathcal{H}}}, \tag{3.44}$$

which should fall between -1 and 1. Moreover, using the steady state value of

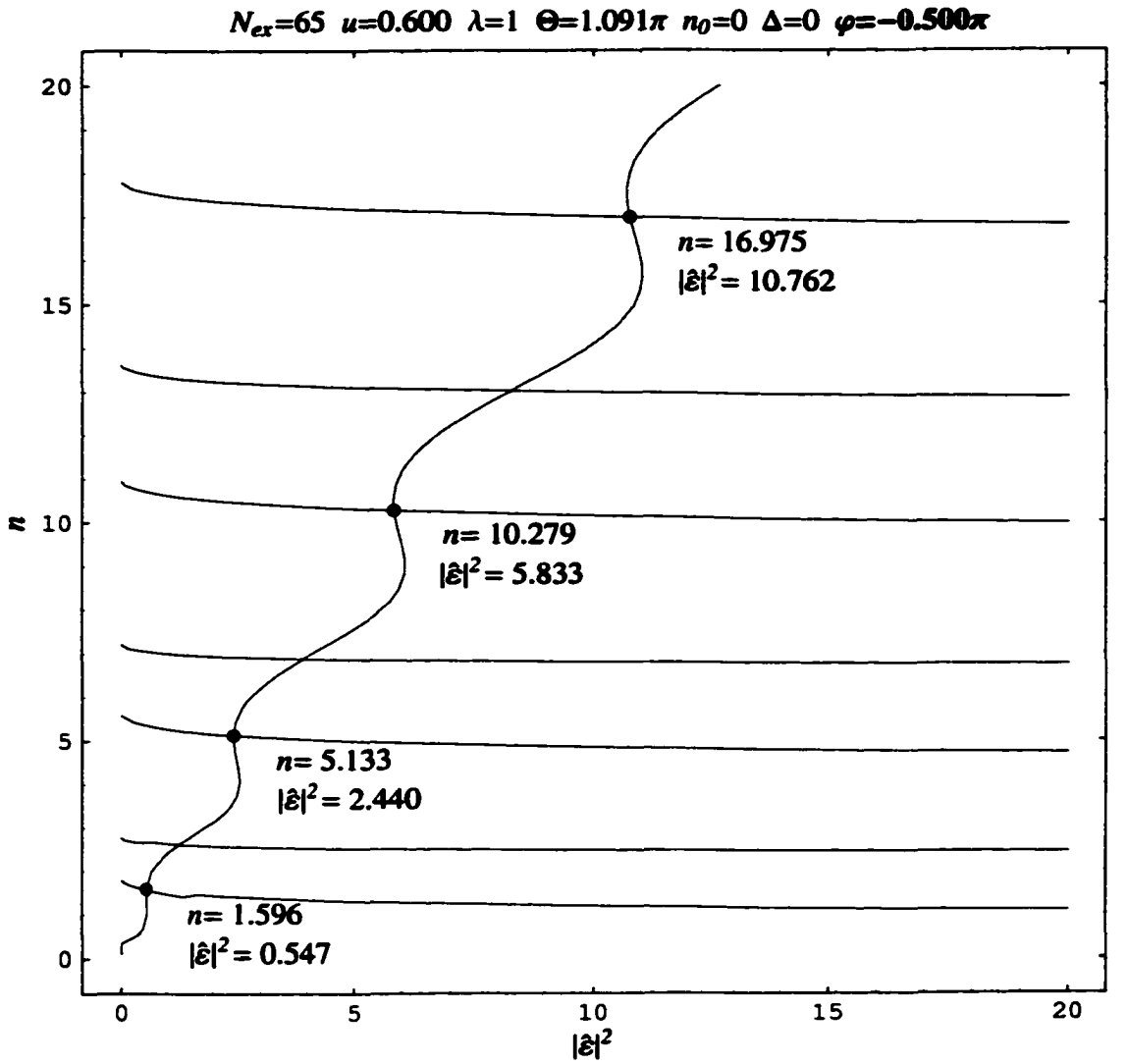

Figure 21: The predictions of the semiclassical model for a multiple peaked photon distribution. The points satisfying Eq. (3.36) are represented by the graph going vertically and the points satisfying Eq. (3.37) by the graphs running horizontally, assuming $\varphi = -\frac{\pi}{2}$.

n obtained from Eq. (3.42), we must also satisfy the initial assumption given in Eq. (3.39). If all three conditions are met and the stability analysis evaluates the point, given by the values of φ, $|\langle\hat{\varepsilon}\rangle|^2$ and n, as a stable point then we have a steady state solution. Since Eq. (3.42) is a non-algebraic equation we determined its solution

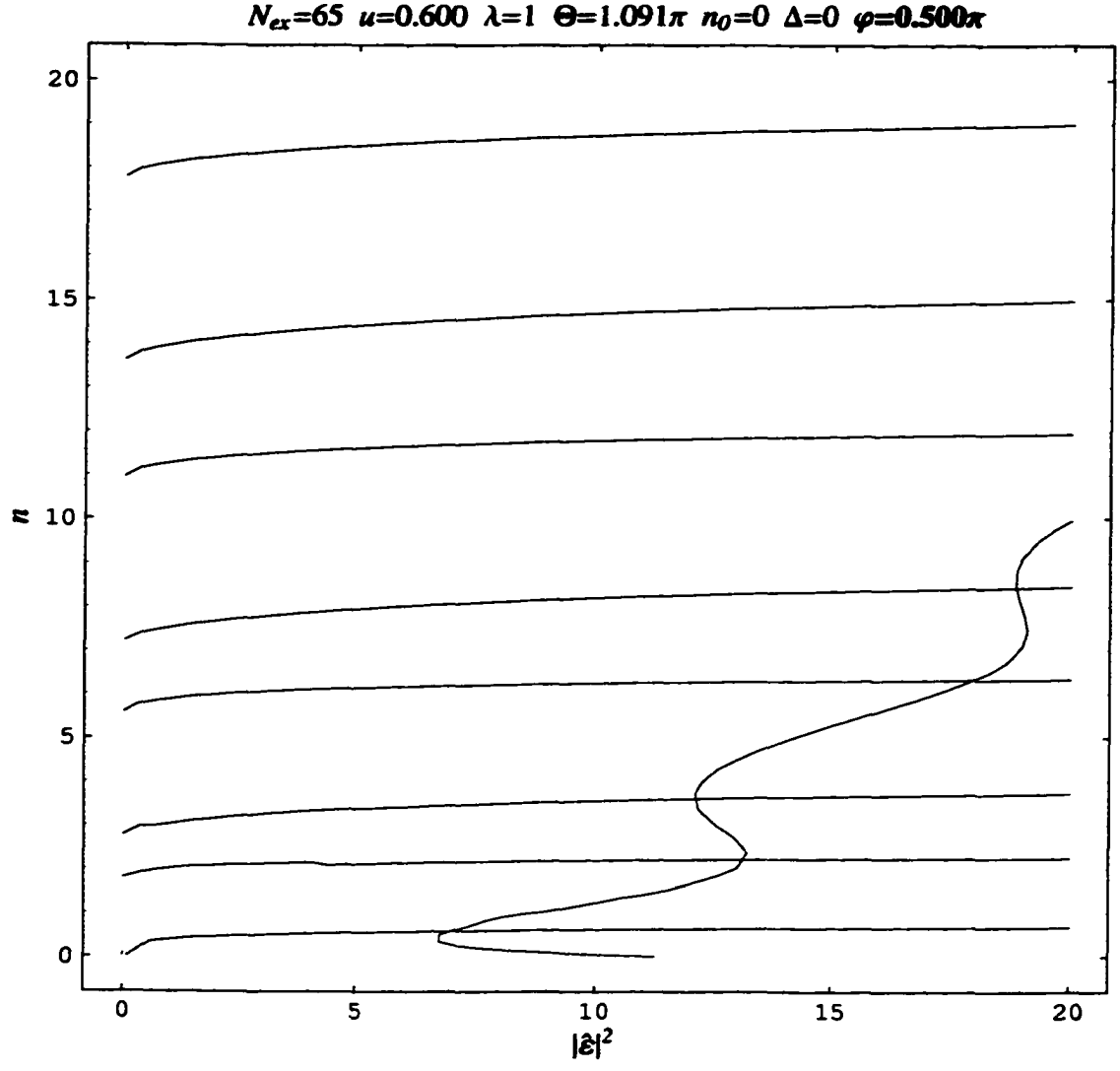

Figure 22: The predictions of the semiclassical model for a multiple peaked photon distribution. The points satisfying Eq. (3.36) are represented by the graph going vertically and the points satisfying Eq. (3.37) by the graphs running horizontally, assuming $\varphi = \frac{\pi}{2}$.

using numerical methods. We found that in general this condition provides stable solutions rarely, only in the case when the interaction phase Θ is quite high. The phase of the steady state in all of these cases evaluated to a value very close to zero. To give examples we list some of our numerical results in Table 1.

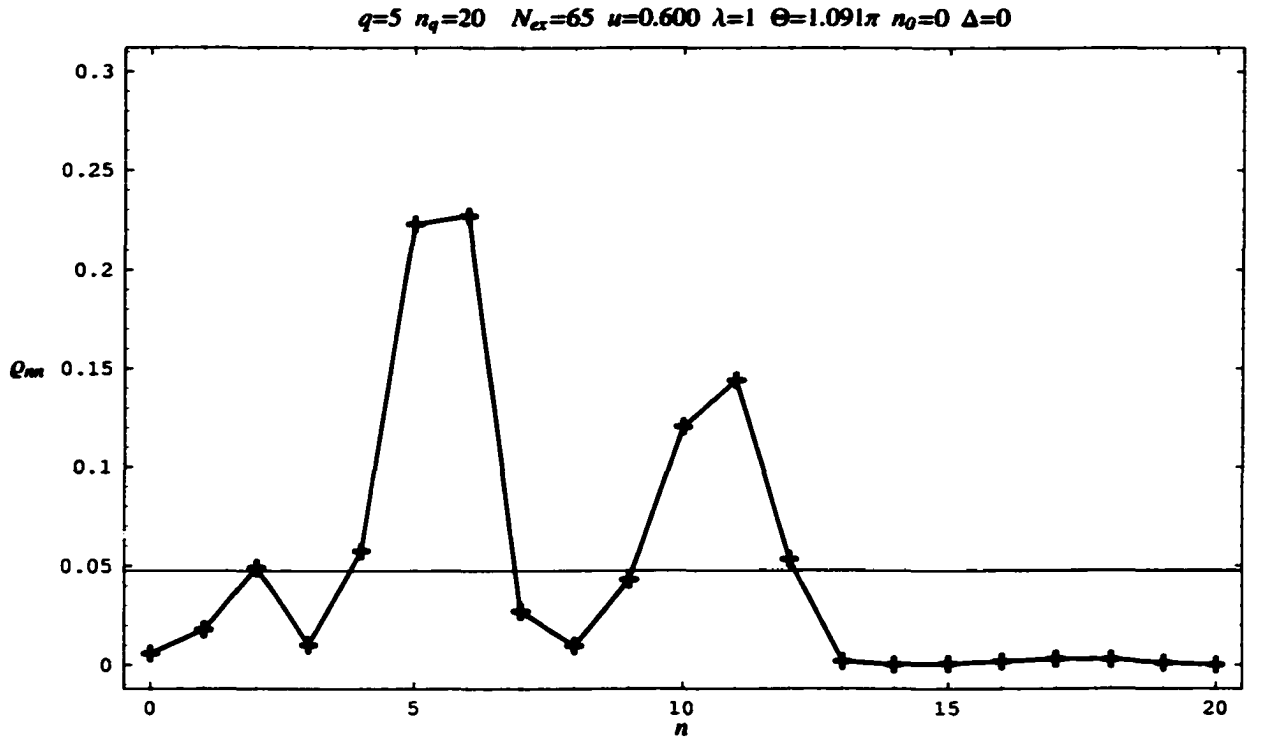

Figure 23: The predictions of the quantum mechanical model for a multiple peaked photon distribution. The photon distribution is obtained by solving the fully quantum mechanical model. The average photon number is $\langle n \rangle = 7.132$, and square of the average electric field's magnitude is $|\langle \hat{\varepsilon} \rangle|^2 = 4.324$. On the figure we also indicated, with the thin line, the uniform photon distribution.

Parameters						*Steady state values*		
q	n_q	N_{ex}	u	λ	Θ	n	$\lvert\hat{\varepsilon}\rvert^2$	φ
46	20	65	0	1	10.038π	5.42189	4.69701	-0.053722π
45	20	65	0	1	9.820π	5.19248	3.87434	-0.058086π
38	20	65	0	1	8.292π	3.44900	3.07784	-0.075403π
38	20	65	−0.07	1	8.292π	3.42931	3.38247	-0.076921π

Table 1: Numerical results for the case when $|\hat{\varepsilon}|^2 = \frac{G}{\mathcal{H}}$.

After discussing the semiclassical method of solving Eq. (2.48) we now have some knowledge about the system at hand. Next we will present the fully quantum mechanical way of solving Eq. (2.48) which will provide much more details about the

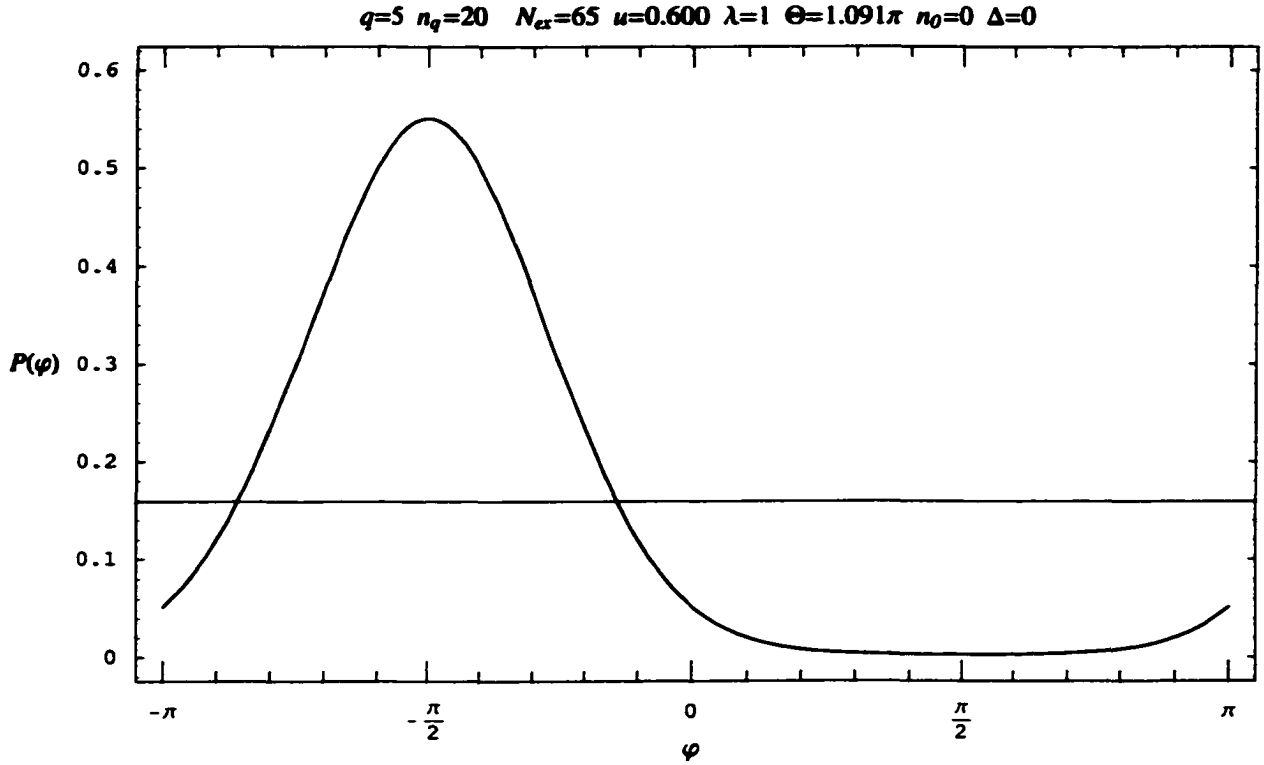

Figure 24: The predictions of the quantum mechanical model for a multiple peaked photon distribution. The phase density function obtained by solving the fully quantum mechanical model. On the figure we also indicated the density function corresponding to the uniformly distributed phase.

coherently pumped micromaser, further enhancing our knowledge about the phase and intensity of the field inside the micromaser cavity.

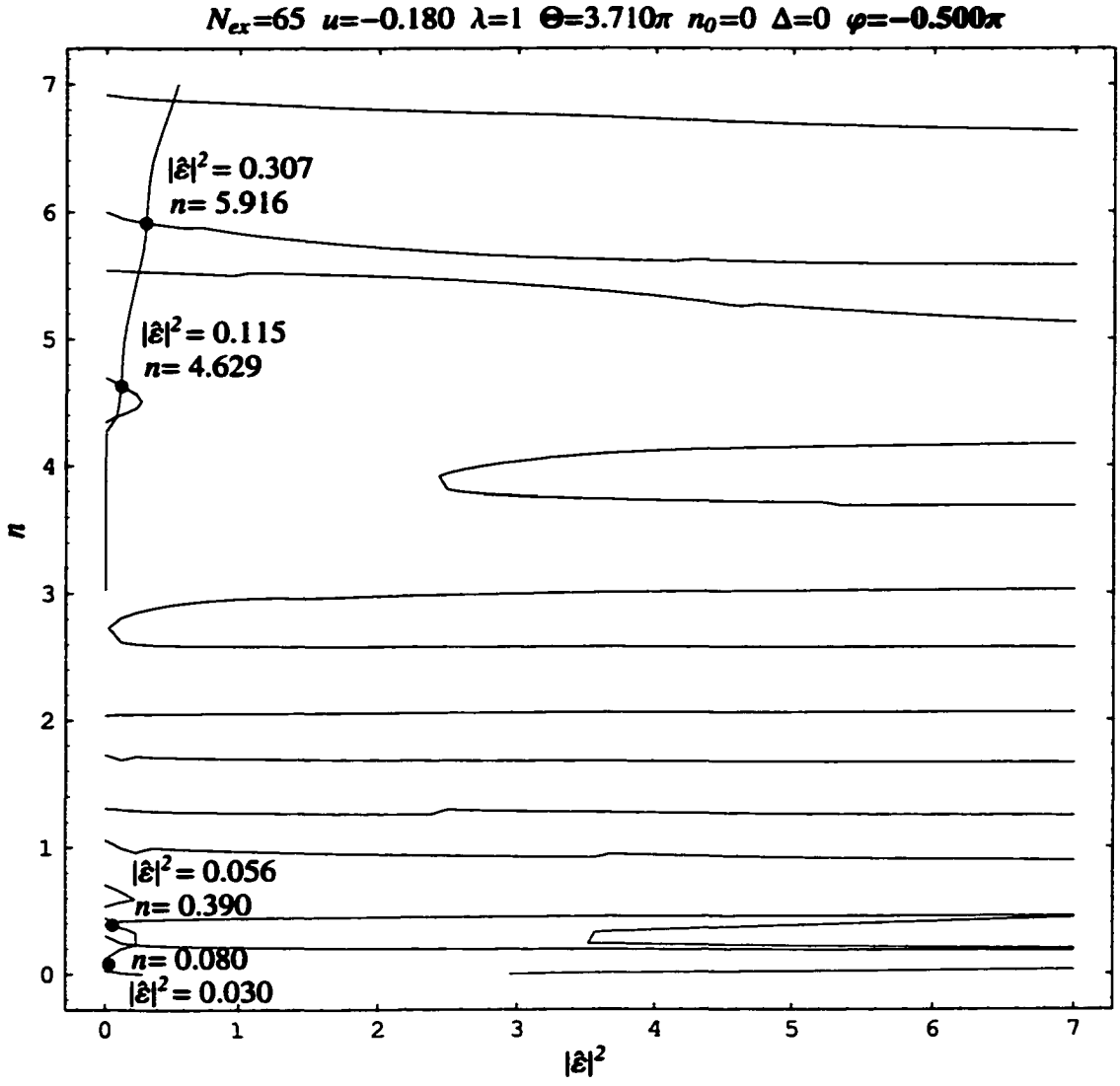

Figure 25: The predictions of the semiclassical model for a multiple peaked photon distribution. The points satisfying Eq. (3.36) are represented by the graphs going vertically and the points satisfying Eq. (3.37) by the graphs running horizontally, assuming $\varphi = -\frac{\pi}{2}$.

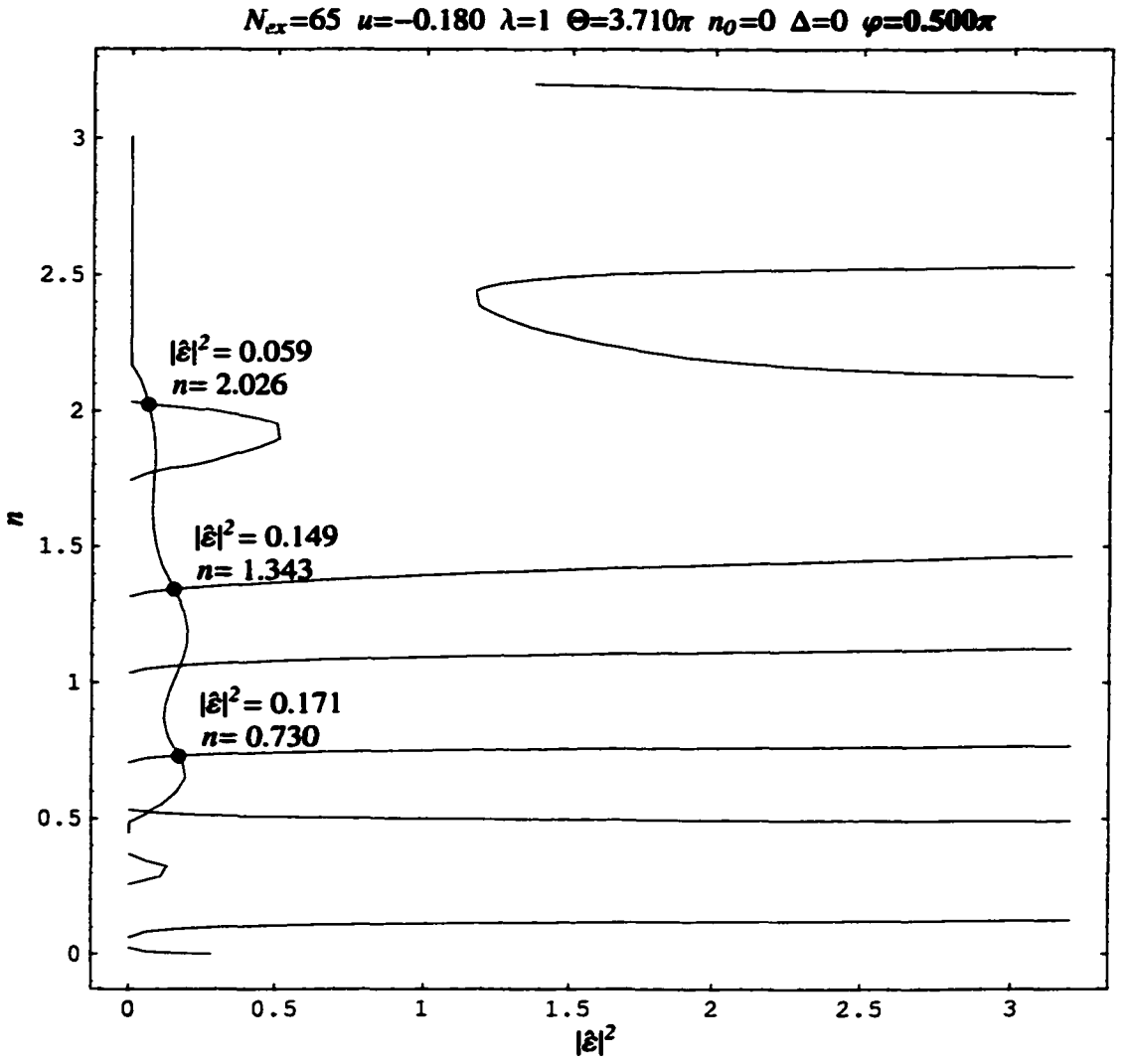

Figure 26: The predictions of the semiclassical model for a multiple peaked photon distribution. The points satisfying Eq. (3.36) are represented by the graph going vertically and the points satisfying Eq. (3.37) by the graphs running horizontally, assuming $\varphi = \frac{\pi}{2}$.

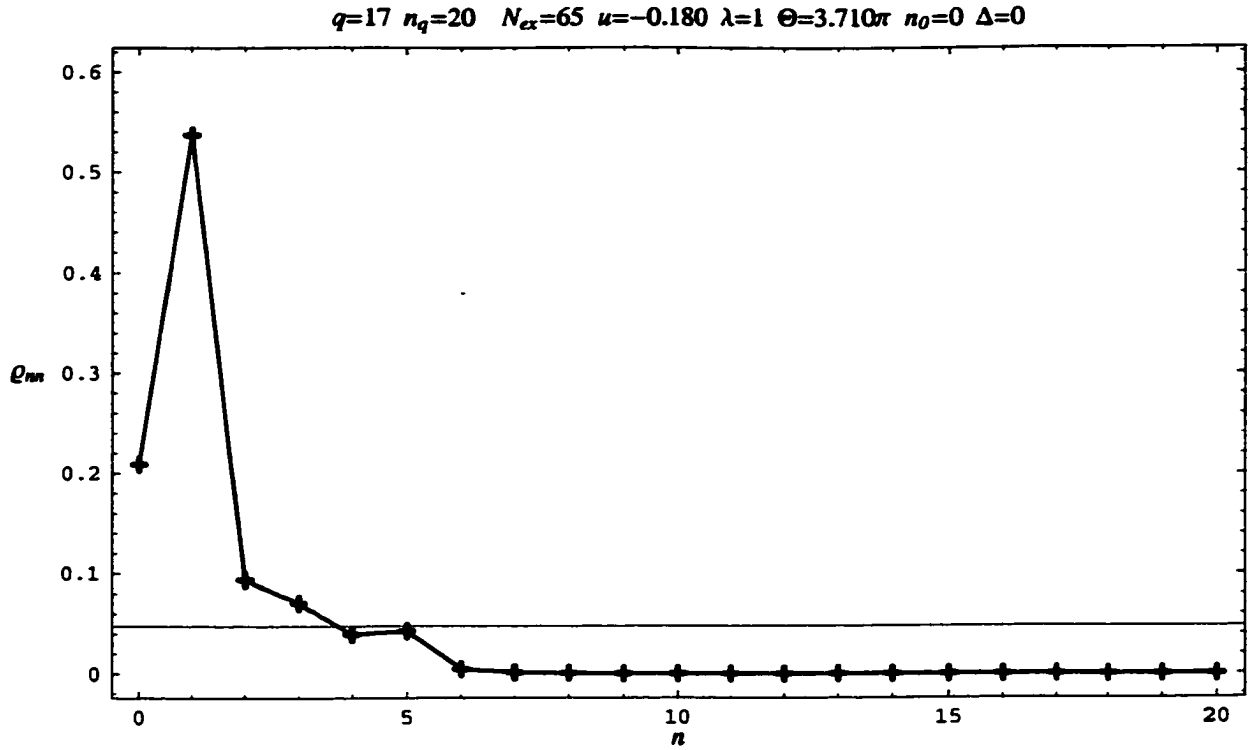

Figure 27: The predictions of the quantum mechanical model for a multiple peaked photon distribution. The photon distribution is obtained by solving the fully quantum mechanical model. The average photon number is $\langle n \rangle = 1.353$, and square of the average electric field's magnitude is $|\langle \hat{\varepsilon} \rangle|^2 = 0.229$. On the figure we also indicated, with the thin line, the uniform photon distribution.

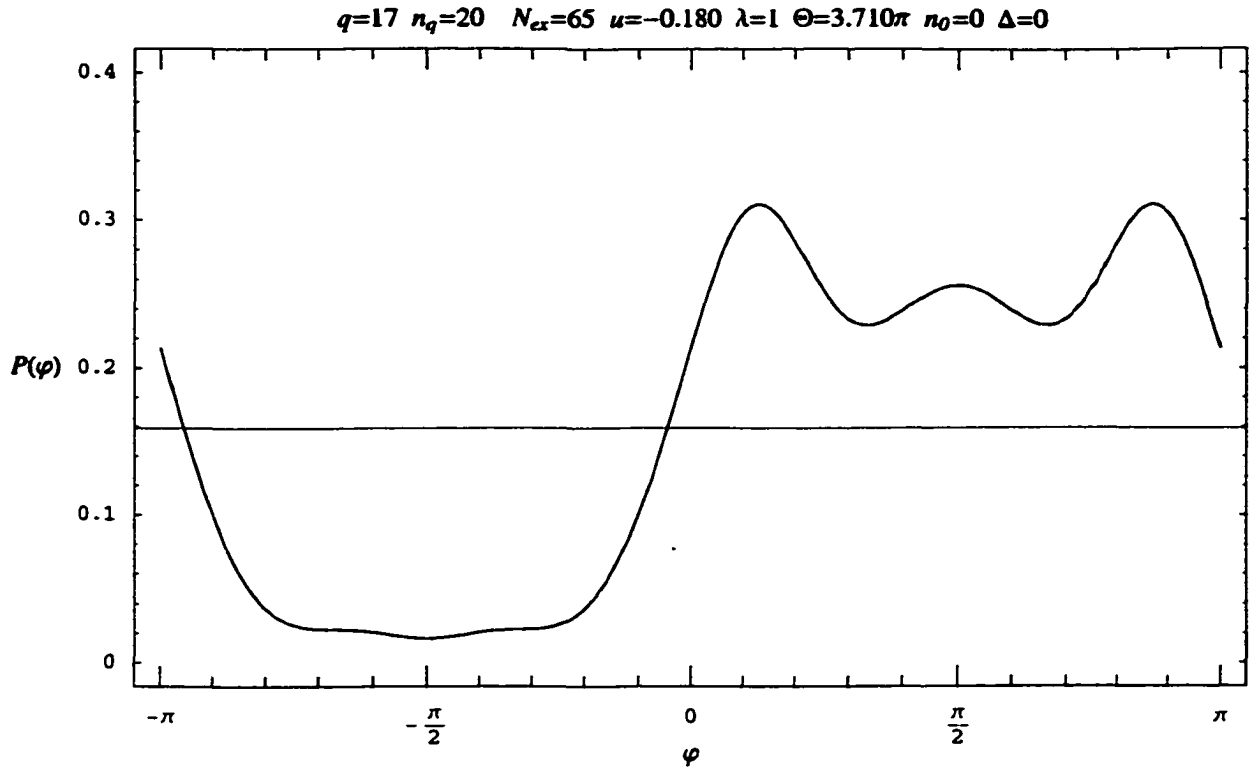

Figure 28: The predictions of the quantum mechanical model for a multiple peaked photon distribution. The phase density function obtained by solving the fully quantum mechanical model. On the figure we also indicated the density function corresponding to the uniformly distributed phase.

4

Quantum mechanical solution

In this chapter we present the full quantum mechanical solution of Eq. (2.48). There have been numerous previous attempts to solve the quantum model of the coherently pumped micromaser analytically but so far all methods fell short of this goal. The most noticeable attempt is due to McGowan and Schieve [25] who used perturbation theory to solve the problem. However, as we will show in this chapter, in many cases due to the strong coupling between the elements of the field density matrix, introduced by the coherent pumping, this approach will not provide an adequate answer. The method we introduce here works even in the case of strong coupling and it reveals intimate details about the inner structure of the density matrix describing the cavity field.

Our approach is based on a specific representation of the field density matrix. We convert the whole field density matrix into a vector called $\mathbf{x}(\beta, t')$ which is an element of the infinite dimensional complex vector space $\mathcal{V}$. The time evolution of $\mathbf{x}(\beta, t')$ will be determined by a linear operator which we will call $\mathbf{A}(\beta)$. After finding the eigenvalues and eigenvectors of $\mathbf{A}(\beta)$ we use them to describe the time evolution of the density matrix represented by $\mathbf{x}(\beta, t')$. This method is similar to the one used in

the determination of the normal modes of coupled physical systems (see for example [39]).

Before we start presenting our method we would like to point out why it is so hard to solve the master equation, Eq. (2.48), describing the time evolution of the field inside the cavity of a coherently pumped micromaser. To this end, we write down the time evolution equation for the matrix elements of $\tilde{\rho}(\beta, t')$ as determined by the master equation, Eq. (2.48), in the photon number representation,

$$\begin{aligned}
\tilde{\rho}'_{k,l}(\beta,t') &= -i\Delta(k-l)\tilde{\rho}_{k,l}(\beta,t') - \frac{k+l}{2}\tilde{\rho}_{k,l}(\beta,t') + \sqrt{(k+1)(l+1)}\tilde{\rho}_{k+1,l+1}(\beta,t') \\
&+ \frac{N_{ex}}{2}\Big((1+u)\Big((C_{k+1}C^*_{l+1}-1)\tilde{\rho}_{k,l}(\beta,t') + S_kS_l\tilde{\rho}_{k-1,l-1}(\beta,t')\Big) \\
&+ (1-u)\Big((C^*_kC_l-1)\tilde{\rho}_{k,l}(\beta,t') + S_{k+1}S_{l+1}\tilde{\rho}_{k+1,l+1}(\beta,t')\Big) \\
&+ \lambda\sqrt{1-u^2}\Big(S_kC_l\tilde{\rho}_{k-1,l}(\beta,t') - C_{k+1}S_{l+1}\tilde{\rho}_{k,l+1}(\beta,t') \\
&+ C^*_kS_l\tilde{\rho}_{k,l-1}(\beta,t') - S_{k+1}C^*_{l+1}\tilde{\rho}_{k+1,l}(\beta,t')\Big)\Big),
\end{aligned} \tag{4.1}$$

where

$$C_k = \cos(\sqrt{n_0^2+k}\Theta) + i\frac{n_0}{\sqrt{n_0^2+k}}\sin(\sqrt{n_0^2+k}\Theta), \tag{4.2a}$$

$$S_k = \frac{\sqrt{k}}{\sqrt{n_0^2+k}}\sin(\sqrt{n_0^2+k}\Theta), \tag{4.2b}$$

with k, l non-negative integers. In the case of incoherent pumping ($\lambda = 0$), as we see from Eq. (4.1), $\tilde{\rho}_{k,l}(\beta, t')$ is only coupled to the elements in the same diagonal. On the other hand, with coherent pumping ($\lambda \neq 0$) the field density matrix element $\tilde{\rho}_{k,l}(\beta, t')$ will also be coupled to the elements in the neighboring diagonals ($\tilde{\rho}_{k-1,l}(\beta, t')$ and $\tilde{\rho}_{k,l+1}(\beta, t')$, and $\tilde{\rho}_{k,l-1}(\beta, t')$ and $\tilde{\rho}_{k+1,l}(\beta, t')$), making it impossible to use the

technique of solution of the incoherently pumped micromaser, since this technique only considered the coupling between the elements in the same diagonal. Therefore, in the case of the coherent pumping, we have to develop a new method which can handle the field density matrix as a whole during all calculations, thus preserving the couplings between the elements in different diagonals. Throughout the rest of this work we will use the following convention, we will call $\tilde{\rho}_{k,l}(\beta, t')$ as an element of the nth diagonal of the density matrix $\tilde{\rho}(\beta, t')$ if $k - l = n$. The 0th diagonal in our convention is just the diagonal of the density matrix, and the elements just below the diagonal form the 1st diagonal using our convention.

To start we define the mapping of the field density matrix $\tilde{\rho}(\beta, t')$ onto the infinite dimensional complex vector space $\mathcal{V}$. We map the field density matrix using its photon number representation, given by the $\tilde{\rho}_{k,l}(\beta, t')$ elements, onto the components of $\mathbf{x}^{\mathrm{E}}(\beta, t')$ which is the representation of $\mathbf{x}(\beta, t')$ with respect to the standard basis of $\mathcal{V}$. This vector, $\mathbf{x}^{\mathrm{E}}(\beta, t')$, is also called the coordinate vector of $\mathbf{x}(\beta, t')$ with respect to the standard basis of $\mathcal{V}$. The standard basis E of $\mathcal{V}$ is composed of the column vectors $\mathbf{v}_n$,

$$(\mathbf{v}_1, \mathbf{v}_2, \ldots, \mathbf{v}_n, \ldots) = \mathrm{E}, \tag{4.3}$$

where $\mathbf{v}_n$ has a 1 in the nth position as its single nonzero entry and therefore

$$\mathbf{x}(\beta, t') = \mathrm{E}\mathbf{x}^{\mathrm{E}}(\beta, t'). \tag{4.4}$$

The actual mapping is now defined by M, a transformation which will provide the one-to-one mapping of the indexes of the elements of the field density matrix (k, l)

onto the component index, j, of $\mathbf{x}^{\mathrm{E}}(\beta, t')$, the mapping is illustrated in Fig. 29 and given by

$$(k,l) \overset{M}{\longmapsto} j = 1 + \frac{(k+l)^2 + (k+3l)}{2}, \tag{4.5}$$

and

$$x_j^{\mathrm{E}}(\beta, t') = \tilde{\rho}_{k,l}(\beta, t'). \tag{4.6}$$

To complete the mapping of the problem, using Eq. (4.1), we now determine the

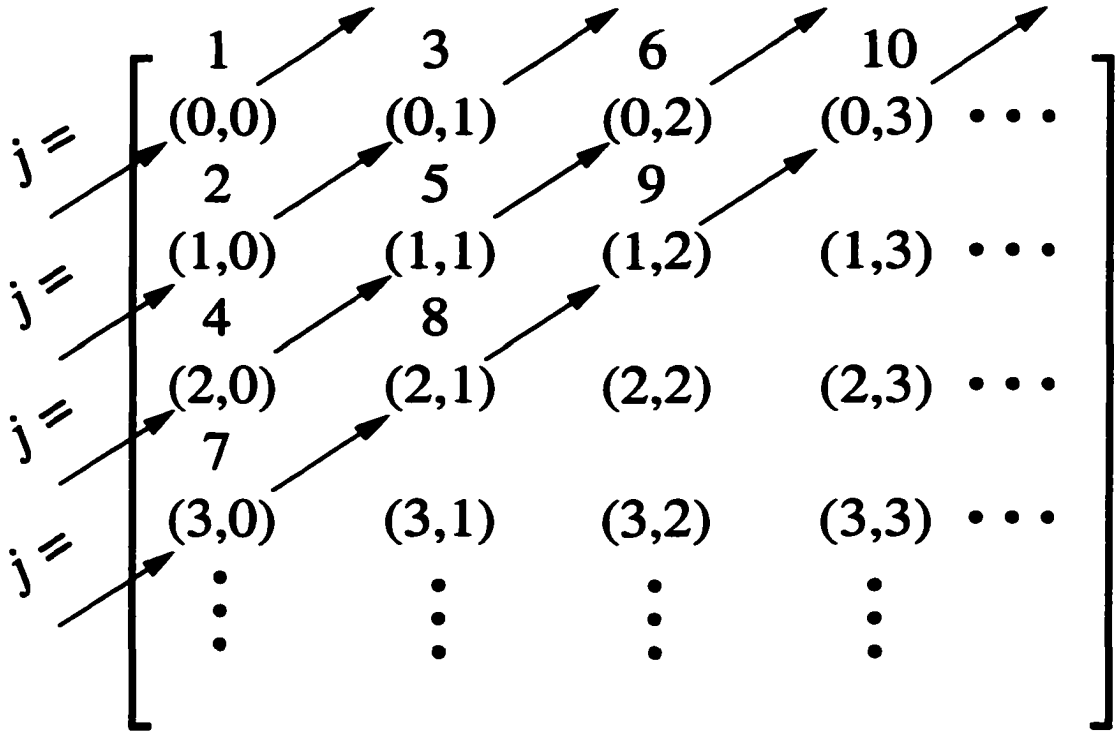

Figure 29: The mapping of the indexes of the elements of the field density matrix (k,l) onto the component index, j, of $\mathbf{x}^{\mathrm{E}}(\beta, t')$. Over the index of each element of the field density matrix, (k,l), we printed the corresponding value of j.

time evolution of $\mathbf{x}(\beta, t')$. Since Eq. (4.1) is linear in the elements of the field density matrix it can be rewritten in the following linear form

$$\frac{d\mathbf{x}(\beta, t')}{dt'} = \mathbf{A}(\beta)\mathbf{x}(\beta, t'), \tag{4.7}$$

where $\mathbf{A}(\boldsymbol{\beta})$ is a linear operator over $\mathcal{V}$. It is independent of the time and depends only on the position $\boldsymbol{\beta}$ in the parameter space. The components, $A_{i,j}(\boldsymbol{\beta})$, of the matrix of $\mathbf{A}(\boldsymbol{\beta})$ with respect to the standard basis can be determined using the index mapping, Eq. (4.5), and the time evolution equation, Eq. (4.1). The solution to Eq. (4.7), with respect to the standard basis is given by

$$\mathbf{x}^{\mathrm{E}}(\boldsymbol{\beta}, t') = \mathrm{e}^{\mathrm{A}(\boldsymbol{\beta})t'}\mathbf{x}^{\mathrm{E}}(0), \tag{4.8}$$

where $\mathbf{x}^{\mathrm{E}}(0)$ represents the initial value of the field density matrix. Using the vector notation of the density matrix, in Eq. (4.8) we obtained a formal solution to Eq. (4.1). However, the problem which arises now is to determine the exponential of the matrix $\mathrm{A}(\boldsymbol{\beta})$. This is an extremely hard problem, unless $\mathrm{A}(\boldsymbol{\beta})$ is in its Jordan form.

A matrix is said to be in Jordan form or to be a Jordan matrix if it is composed of diagonal blocks

$$\begin{bmatrix} \mathrm{J}_1 & 0 & \dots & 0 \\ 0 & \mathrm{J}_2 & \dots & 0 \\ \dots & \dots & \dots & \dots \\ 0 & 0 & \dots & \mathrm{J}_m \end{bmatrix}, \tag{4.9}$$

where each of the diagonal blocks is a Jordan block, a matrix of one of these forms

$$\begin{bmatrix} \kappa \end{bmatrix}, \begin{bmatrix} \kappa & 0 \\ 1 & \kappa \end{bmatrix}, \begin{bmatrix} \kappa & 0 & 0 \\ 1 & \kappa & 0 \\ 0 & 1 & \kappa \end{bmatrix}, \dots \tag{4.10}$$

where κ is a complex number. A theorem from algebra [40] proves that for every linear operator $\mathbf{A}$ on a complex vector space $\mathcal{V}$ there is a basis such that the matrix of $\mathbf{A}$ with respect to this basis is in Jordan form. Given our $\mathrm{A}(\boldsymbol{\beta})$ square complex matrix the

theorem asserts that $P(\beta)A(\beta)P^{-1}(\beta)$ is in Jordan form for some invertible matrix $P(\beta)$. We will refer to $P(\beta)A(\beta)P^{-1}(\beta)$ as the Jordan form for $A(\beta)$ and denote it with $A^J(\beta)$. The Jordan form of $A(\beta)$ is unique only up to a permutation of the blocks, because only the terms in the direct sum decomposition of $A(\beta)$ are unique and not their ordering. Using the Jordan form of $A(\beta)$ we can write that

$$A(\beta) = P^{-1}(\beta)A^J(\beta)P(\beta). \tag{4.11}$$

Further, corresponding to every Jordan block in $A^J(\beta)$ there are unique eigenvectors in $\mathcal{V}$. These eigenvectors are only unique up to a normalization constant. This constant can be chosen arbitrarily but it must be the same for all eigenvectors belonging to the same Jordan block. Therefore, there exists an invertible matrix N whose inverse, N^{-1}, normalizes the chosen basis in $\mathcal{V}$ such that

$$A(\beta) = P^{-1}(\beta)N^{-1}A^J(\beta)NP(\beta), \tag{4.12}$$

where

$$[N^{-1}, A^J(\beta)] = [N, A^J(\beta)] = 0. \tag{4.13}$$

Now with the aid of the Jordan decomposition, Eq. (4.11), we can rewrite Eq. (4.8) and obtain

$$\mathbf{x}^E(\beta, t') = P^{-1}(\beta)e^{A^J(\beta)t'}P(\beta)\mathbf{x}^E(0). \tag{4.14}$$

The exponential of the Jordan form can be easily calculated now since for an arbitrary $k \times k$ Jordan block

$$\mathrm{J} = \begin{bmatrix} \kappa & 0 & 0 & \dots & 0 \\ 1 & \kappa & 0 & \dots & 0 \\ 0 & 1 & \kappa & \dots & 0 \\ \dots & \dots & \dots & \dots & \dots \\ 0 & 0 & 0 & \dots & \kappa \end{bmatrix}, \tag{4.15}$$

we can write its exponential in the following form

$$\mathrm{e}^{\mathrm{J}t} = \mathrm{e}^{\kappa \mathbb{1} t}\mathrm{e}^{\mathrm{J}_0 t} = \mathrm{e}^{\kappa \mathbb{1} t}\left(\mathbb{1} + \mathrm{J}_0 \frac{t}{1!} + \cdots + \mathrm{J}_0^{k-1}\frac{t^{k-1}}{(k-1)!}\right), \tag{4.16}$$

where J_0 is a $k \times k$ matrix obtained by substituting $\kappa = 0$ into the Jordan block in Eq. (4.15). Here are some simple examples:

1. The exponential of a 1×1 Jordan block is simply $\mathrm{e}^{\kappa t}$ where κ is the complex value corresponding to the unique vector of the Jordan block.

2. The exponential of a 3×3 Jordan block J is

$$\mathrm{e}^{\mathrm{J}t'} = \begin{bmatrix} \mathrm{e}^{\kappa t'} & 0 & 0 \\ t'\mathrm{e}^{\kappa t'} & \mathrm{e}^{\kappa t'} & 0 \\ \frac{1}{2}t'^2\mathrm{e}^{\kappa t'} & t'\mathrm{e}^{\kappa t'} & \mathrm{e}^{\kappa t'} \end{bmatrix}. \tag{4.17}$$

To understand the physics behind Eq. (4.14) let us rewrite it in the following form

$$\mathrm{P}(\boldsymbol{\beta})\mathbf{x}^{\mathrm{E}}(\boldsymbol{\beta}, t') = \mathrm{e}^{\mathrm{A}^J(\boldsymbol{\beta})t'}\mathrm{P}(\boldsymbol{\beta})\mathbf{x}^{\mathrm{E}}(0), \tag{4.18}$$

and recognize that

$$\mathbf{x}^{\mathrm{B}'}(\boldsymbol{\beta}, t') = \mathrm{P}(\boldsymbol{\beta})\mathbf{x}^{\mathrm{E}}(\boldsymbol{\beta}, t') \tag{4.19}$$

is the coordinate vector of $\mathbf{x}(\boldsymbol{\beta}, t')$ when it is computed with respect to the basis spanned by the vectors $\mathbf{v}'_n$ where, in turn, $\mathbf{v}'_n$ is formed from the columns of the

matrix $\mathrm{P}^{-1}(\boldsymbol{\beta})$,

$$\mathrm{P}^{-1}(\boldsymbol{\beta}) = (\mathbf{v}'_1, \mathbf{v}'_2, \ldots, \mathbf{v}'_n, \ldots) = \mathrm{B}'. \tag{4.20}$$

The time evolution of the coordinate vector $\mathbf{x}^{\mathrm{B}'}(\boldsymbol{\beta}, t')$ can be obtained from Eq. (4.18) namely

$$\mathbf{x}^{\mathrm{B}'}(\boldsymbol{\beta}, t') = \mathrm{e}^{\mathrm{A}^J(\boldsymbol{\beta})t'}\mathbf{x}^{\mathrm{B}'}(0). \tag{4.21}$$

From Eq. (4.21) we see the coordinates corresponding to basis vectors which belong to different Jordan blocks evolve independently. Therefore these vectors represent the independent modes of the 'motion' of the density matrix. The power of our method lies in this independent mode decomposition of the density matrix, since using this technique we will preserve all couplings between various elements of the density matrix and still be able to give a physical interpretation of the time evolution of our system. The method in its essence is similar to the one used to provide the possible independent oscillation modes of interacting mechanical systems.

Using Eq. (4.20) and Eq. (4.21), we obtain the solution of Eq. (4.7) as

$$\begin{aligned} \mathbf{x}(\boldsymbol{\beta}, t') &= \mathrm{P}^{-1}(\boldsymbol{\beta})\mathbf{x}^{\mathrm{B}'}(\boldsymbol{\beta}, t') = \mathrm{P}^{-1}(\boldsymbol{\beta})\mathrm{e}^{\mathrm{A}^J(\boldsymbol{\beta})t'}\mathbf{x}^{\mathrm{B}'}(0) \\ &= \sum_{j=1}^{\infty}\sum_{k=1}^{\infty}\mathbf{v}'_j\left(\mathrm{e}^{\mathrm{A}^J(\boldsymbol{\beta})t'}\right)_{j,k}x_k^{\mathrm{B}'}(0). \end{aligned} \tag{4.22}$$

With the help of Eq. (4.16) this solution can also be written in the form which does not include the exponent of the Jordan block matrix $\mathrm{A}^J(\boldsymbol{\beta})$ namely

$$\mathbf{x}(\boldsymbol{\beta}, t') = \sum_{\kappa}\sum_{l=1}^{n_\kappa}\left(\mathrm{e}^{\kappa(\boldsymbol{\beta})t'}\sum_{m=l}^{n_\kappa}\mathbf{v}'_{(\kappa,m)}\frac{(t')^{m-l}}{(m-l)!}\right)x_{(\kappa,l)}^{\mathrm{B}'}(0). \tag{4.23}$$

In Eq. (4.23) we used the index pair (κ, l) instead of the single index k to label the basis vectors of B'. The index κ is referring to the Jordan blocks of $\mathrm{A}^J(\boldsymbol{\beta})$ by specifying

the value corresponding to a given block. It is running over the set of the eigenvalues of $A(\beta)$. The other summation index l is indexing the vectors corresponding to the Jordan block with the specified κ value. It is running over the integer numbers from 1 to the dimension of the given Jordan block which is denoted with n_κ.

Next we will examine our solution from a physical point of view. We will list the necessary conditions which must be satisfied by any physically possible solution and investigate the implications of such conditions. To start let us recall that each vector in $\mathcal{V}$ represents a unique density matrix which can be obtained using the coordinates of the given vector with respect to the standard basis E of $\mathcal{V}$ and the coordinate mapping given by Eq. (4.5) and Eq. (4.6). The following conditions are imposed on the density matrix of any proper physical state by the rules of quantum mechanics

$$\rho(t) = \rho^\dagger(t), \tag{4.24a}$$

$$\mathrm{Tr}\,[\rho(t)] = 1, \tag{4.24b}$$

$$\rho_{ii}(t)\rho_{jj}(t) \geq |\rho_{ij}(t)|^2, \quad \text{for all } i,j \in \mathbf{N}. \tag{4.24c}$$

The first two conditions, Eqs. (4.24a) and (4.24b), ensure that the density matrix describing a physical state is Hermitian and normalized. The third condition, Eq. (4.24c), can be proved as follows. By definition the general form of the density operator describing a physical state is

$$\rho = \sum_n p_n |\Psi_n\rangle \langle\Psi_n|, \tag{4.25}$$

where the summation is over a set of states and it can be discrete or continuous. The

ρ_{ij} element of the density matrix therefore can be obtained as

$$\rho_{ij} = \langle i|\,\rho\,|j\rangle = \sum_n p_n \langle i|\Psi_n\rangle \langle \Psi_n|j\rangle = \sum_n p_n c_i^n c_j^{n*}. \tag{4.26}$$

Using Eq. (4.26) we can directly evaluate the following difference

$$\begin{aligned}
\rho_{ii}\rho_{jj} - |\rho_{ij}|^2 &= \sum_{n,m} p_n p_m \left(|c_i^n|^2 |c_j^m|^2 - c_i^n c_j^{n*} c_j^m c_i^{m*}\right) \\
&= \sum_{n,m} p_n p_m \left(|c_i^n|^2 |c_j^m|^2 - |c_i^n|\,|c_j^n|\,|c_j^m|\,|c_i^m|\, e^{i(\varphi_i^n - \varphi_j^n)} e^{-i(\varphi_i^m - \varphi_j^m)}\right) \\
&= \sum_{\substack{n,m \\ n>m}} p_n p_m \Big(|c_i^n|^2 |c_j^m|^2 + |c_i^m|^2 |c_j^n|^2 \\
&\quad -2\,|c_i^n|\,|c_j^n|\,|c_j^m|\,|c_i^m| \cos\left((\varphi_i^n - \varphi_j^n) - (\varphi_i^m - \varphi_j^m)\right)\Big) \\
&\geq \sum_{\substack{n,m \\ n>m}} p_n p_m \left(|c_i^n||c_j^m| - |c_i^m||c_j^n|\right)^2 \geq 0,
\end{aligned} \tag{4.27}$$

which proves the validity of the third condition Eq. (4.24c). From Eq. (4.27) we can also see that equality only holds for pure states where

$$\rho = |\Psi\rangle \langle \Psi|\,. \tag{4.28}$$

We list some of the other consequences of Eq. (4.24c):

1. Combining Eq. (4.24b) with Eq. (4.24c) we immediately see that all diagonal elements of a density matrix representing a physically possible state must be positive or zero

$$\rho_{ii} \geq 0. \tag{4.29}$$

2. The trace of ρ^n ($n \in \mathbf{N}$ and $n \geq 2$) must be less than or equal to 1

$$\mathrm{Tr}\,[\rho^n] \leq 1, \tag{4.30}$$

and the equality only holds for pure states.

We show now for $n = 2$ that Eq. (4.30) is the consequence of Eq. (4.24c).

$$\begin{aligned} \mathrm{Tr}\left[\rho^2\right] - 1 &= \sum_{i,j} |\rho_{ij}|^2 - 1 = \sum_i {\rho_{ii}}^2 + \sum_{\substack{i,j \\ i \neq j}} |\rho_{ij}|^2 - \left(\sum_i \rho_{ii}\right)^2 \\ &= \sum_{\substack{i,j \\ i \neq j}} \left(|\rho_{ij}|^2 - \rho_{ii}\rho_{jj}\right) \leq 0, \end{aligned} \tag{4.31}$$

where in the last step we used Eq. (4.24c). Similarly, it can be shown to hold for any $n \geq 2$ integer, as well.

After reviewing the general conditions, Eq. (4.24), on the density matrices of proper physical states, we will now show that they also hold for $\tilde{\rho}(\beta, t')$, the slowly varying amplitude of the solution defined by Eq. (2.37). Using Eq. (2.37) we can write

$$\tilde{\rho}(\beta, t') = \mathrm{e}^{i\mathbf{a}^\dagger \mathbf{a}(\frac{\nu}{\Gamma} t' + \varphi_g - \varphi_{ab} + \pi/2)} \bar{\rho}(\beta, t') \mathrm{e}^{-i\mathbf{a}^\dagger \mathbf{a}(\frac{\nu}{\Gamma} t' + \varphi_g - \varphi_{ab} + \pi/2)}. \tag{4.32}$$

From Eq. (4.32), however, we immediately see that $\tilde{\rho}(\beta, t')$ will satisfy the conditions Eq. (4.24) as long as $\bar{\rho}(\beta, t')$ satisfy them. Therefore we conclude here that $\tilde{\rho}(\beta, t')$, the slowly varying amplitude of our solution, must satisfy the same conditions as the density matrix of a proper physical state. Since all conditions imposed on $\tilde{\rho}(\beta, t')$ can also be formulated as restrictions on the coordinate vector $\mathbf{x}^{\mathrm{E}}(\beta, t')$, corresponding to $\tilde{\rho}(\beta, t')$, quantum mechanics restrict the motion of $\mathbf{x}^{\mathrm{E}}(\beta, t')$ to only a physically accessible region of $\mathcal{V}$. Using the mapping equations, Eq. (4.5) and Eq. (4.6), we can

express these restrictions as

$$\mathbf{x}^{\mathrm{E}}(\beta,t') = \mathrm{T}(\mathbf{x}^{\mathrm{E}}(\beta,t'))^{*}, \tag{4.33a}$$

$$\mathbf{n}^{\mathrm{E}}\mathbf{x}^{\mathrm{E}}(\beta,t') = 1, \tag{4.33b}$$

$$x^{\mathrm{E}}_{(i+1)^2+i^2}(\beta,t')x^{\mathrm{E}}_{(j+1)^2+j^2}(\beta,t') \geq \left|x^{\mathrm{E}}_{1+\frac{(i+j)^2+(i+3j)}{2}}(\beta,t')\right|^2. \tag{4.33c}$$

Here $\mathbf{n}^{\mathrm{E}}$ is the row vector which provides the norm on $\mathcal{V}$. It is defined as

$$n^{\mathrm{E}}_i = \begin{cases} 1 & \text{if } i = n^2+(n+1)^2 \text{ for some } n \in \mathbf{N}, \\ 0 & \text{otherwise.} \end{cases} \tag{4.34}$$

The norm of a vector in $\mathcal{V}$ is therefore defined as the trace of the corresponding density matrix. Furthermore, T represents the matrix of $\mathbf{T}$ with respect to the standard basis, E, of $\mathcal{V}$. The operation $\mathbf{T}$ is defined as a vector-vector operation on $\mathcal{V}$ which results in the vector, $\mathbf{Tx}(\beta,t')$, which describes the transpose of the density matrix corresponding to $\mathbf{Tx}(\beta,t')$. Since the transpose of the transpose is equal to the original density matrix we have that

$$\mathbf{TT} = \mathbf{1} \tag{4.35}$$

which means the matrix of $\mathbf{T}$ with respect to the standard basis, E, of $\mathcal{V}$ satisfies

$$\mathrm{T} = \mathrm{T}^{-1}. \tag{4.36}$$

Using the conditions, Eq. (4.33), we are going to investigate our solution given by Eq. (4.23) and determine key properties of the independent modes $\mathbf{v}'_{(\kappa,m)}$ from which it is composed of. First, let us see what are the consequences of the Hermitian

property of $\tilde{\rho}(\beta, t')$. From Eq. (4.7) it follows that

$$\frac{d\mathbf{x}^{\mathrm{E}}(\beta, t')}{dt'} = \mathrm{A}(\beta)\mathbf{x}^{\mathrm{E}}(\beta, t'). \tag{4.37}$$

Taking the complex conjugate of Eq. (4.37) and using Eq. (4.33a), we obtain

$$\mathrm{T}\frac{d\mathbf{x}^{\mathrm{E}}(\beta, t')}{dt'} = \mathrm{A}^*(\beta)\mathrm{T}\mathbf{x}^{\mathrm{E}}(\beta, t'). \tag{4.38}$$

By multiplying both sides of the equation with T from the left and using Eq. (4.36), we get

$$\frac{d\mathbf{x}^{\mathrm{E}}(\beta, t')}{dt'} = \mathrm{T}\mathrm{A}^*(\beta)\mathrm{T}\mathbf{x}^{\mathrm{E}}(\beta, t'). \tag{4.39}$$

Now, by comparing Eq. (4.37) and Eq. (4.39), we can read out that

$$\mathrm{A}(\beta) = \mathrm{T}\mathrm{A}^*(\beta)\mathrm{T}. \tag{4.40}$$

This equation points out a very important feature of the $\mathrm{A}(\beta)$ matrix, viz. it is similar to its complex conjugate. An implication of this feature is that the Jordan form of $\mathrm{A}(\beta)$ is also similar to its complex conjugate,

$$\begin{aligned} \mathrm{A}^J(\beta) &= \mathrm{P}(\beta)\mathrm{T}\left(\mathrm{P}^{-1}(\beta)\right)^* \left(\mathrm{A}^J(\beta)\right)^* \mathrm{P}^*(\beta)\mathrm{T}\mathrm{P}^{-1}(\beta) \\ &= \mathrm{Q}(\beta)\left(\mathrm{A}^J(\beta)\right)^* \mathrm{Q}^{-1}(\beta). \end{aligned} \tag{4.41}$$

In other words, if $\mathrm{A}^J(\beta)$ includes a Jordan block J_κ with value κ then it must include the Jordan block J_{κ^*} corresponding to κ^*, and

$$\mathrm{J}_{\kappa^*} = \mathrm{J}_\kappa^*. \tag{4.42}$$

To each Jordan block there correspond unique eigenvectors in $\mathcal{V}$. We will now determine how the eigenvectors corresponding to complex conjugate blocks are related to

each other. Using Eq. (4.11) and Eq. (4.40), we can write

$$\mathrm{A}(\beta) = \mathrm{P}^{-1}(\beta)\mathrm{A}^{J}(\beta)\mathrm{P}(\beta) = \mathrm{T}\left(\mathrm{P}^{-1}(\beta)\right)^{*}\left(\mathrm{A}^{J}(\beta)\right)^{*}\mathrm{P}^{*}(\beta)\mathrm{T}. \tag{4.43}$$

From here we can read out that if $\mathrm{P}_{\kappa}^{-1}(\beta)$ contains the basis vectors corresponding to the J_{κ} Jordan block then $\mathrm{T}\left(\mathrm{P}_{\kappa}^{-1}(\beta)\right)^{*}$ will contain the basis vectors corresponding to the J_{κ^*} block. Using Eq. (4.20) this means

$$\mathbf{v}'_{(\kappa^*,m)} = \mathrm{T}\left(\mathbf{v}'_{(\kappa,m)}\right)^{*}. \tag{4.44}$$

Earlier we have defined $\mathbf{x}^{\mathrm{B}'}(\beta,t')$, Eq. (4.19), the coordinate vector describing our system in the B′ basis. Now let us work out how the coordinates in this basis corresponding to basis vectors of complex conjugate Jordan blocks are related to each other. To obtain the relation let us take the complex conjugate of $\mathbf{x}^{\mathrm{B}'}(\beta,t')$, Eq. (4.19), and get

$$\begin{aligned}\left(\mathbf{x}^{\mathrm{B}'}(\beta,t')\right)^{*} &= \left(\mathrm{P}(\beta)\mathbf{x}^{\mathrm{E}}(\beta,t')\right)^{*} = \mathrm{P}^{*}(\beta)\mathrm{T}\mathbf{x}^{\mathrm{E}}(\beta,t') \\ &= \mathrm{P}^{*}(\beta)\mathrm{T}\mathrm{P}^{-1}(\beta)\mathbf{x}^{\mathrm{B}'}(\beta,t').\end{aligned} \tag{4.45}$$

From here

$$\mathrm{P}^{-1}(\beta)\mathbf{x}^{\mathrm{B}'}(\beta,t') = \mathrm{T}\left(\mathrm{P}^{-1}(\beta)\right)^{*}\left(\mathbf{x}^{\mathrm{B}'}(\beta,t')\right)^{*}, \tag{4.46}$$

which means the coordinates corresponding to basis vectors of conjugate Jordan blocks are complex conjugates of each other at any given time. If we apply Eq. (4.46) to the initial values of the coordinates we obtain

$$x^{\mathrm{B}'}_{(\kappa^*,l)}(0) = \left(x^{\mathrm{B}'}_{(\kappa,l)}(0)\right)^{*}. \tag{4.47}$$

From Eq. (4.47) we also see the coordinates corresponding to real κ values are real as well. To summarize the results we obtained so far let us incorporate them into the general solution, Eq. (4.23), and write

$$\begin{aligned}\mathbf{x}(\beta,t') &= \frac{1}{2}\Big(\mathbf{x}(\beta,t')+\mathbf{T}\mathbf{x}^*(\beta,t')\Big)\\ &= \frac{1}{2}\sum_{\kappa}\sum_{l=1}^{n_\kappa}\Bigg[e^{\kappa t'}\left(\sum_{m=l}^{n_\kappa}\mathbf{v}'_{(\kappa,m)}\frac{(t')^{m-l}}{(m-l)!}\right)x^{\mathrm{B}'}_{(\kappa,l)}(0)\\ &\quad +e^{\kappa^* t'}\left(\sum_{m=l}^{n_\kappa}\mathrm{T}\left(\mathbf{v}'_{(\kappa,m)}\right)^*\frac{(t')^{m-l}}{(m-l)!}\right)\left(x^{\mathrm{B}'}_{(\kappa,l)}(0)\right)^*\Bigg].\end{aligned} \tag{4.48}$$

If we introduce now the following notation

$$x^{\mathrm{B}'}_{(\kappa,l)}(0) = \left|x^{\mathrm{B}'}_{(\kappa,l)}(0)\right| e^{i\varphi^{\mathrm{B}'}_{(\kappa,l)}}, \tag{4.49}$$

and use Eq. (4.44), Eq. (4.48) simplifies to

$$\begin{aligned}&\mathbf{x}(\beta,t') =\\ &=\sum_{\substack{\kappa\in\mathbf{C}\\ \mathrm{Im}\kappa>0}}\sum_{m=1}^{n_\kappa}\Bigg[\left(\mathbf{v}'_{(\kappa,m)}+\mathbf{v}'_{(\kappa^*,m)}\right)e^{\mathrm{Re}\kappa t'}\left(\sum_{l=l}^{m}\left|x^{\mathrm{B}'}_{(\kappa,l)}(0)\right|\frac{(t')^{m-l}}{(m-l)!}\cos\left(\mathrm{Im}\kappa t'+\varphi^{\mathrm{B}'}_{(\kappa,l)}\right)\right)\\ &+i\left(\mathbf{v}'_{(\kappa,m)}-\mathbf{v}'_{(\kappa^*,m)}\right)e^{\mathrm{Re}\kappa t'}\left(\sum_{l=l}^{m}\left|x^{\mathrm{B}'}_{(\kappa,l)}(0)\right|\frac{(t')^{m-l}}{(m-l)!}\sin\left(\mathrm{Im}\kappa t'+\varphi^{\mathrm{B}'}_{(\kappa,l)}\right)\right)\Bigg]\\ &+\sum_{\kappa\in\mathbf{R}}\sum_{m=1}^{n_\kappa}\left(\mathbf{v}'_{(\kappa,m)}e^{\kappa t'}\left(\sum_{l=l}^{m}x^{\mathrm{B}'}_{(\kappa,l)}(0)\frac{(t')^{m-l}}{(m-l)!}\right)\right).\end{aligned} \tag{4.50}$$

We can now read out the following important properties of the solution from Eq. (4.50).

1. The combinations of the basis vectors appearing in Eq. (4.50) represent Hermitian matrices, as seen from Eq. (4.44).

2. The density matrix corresponding to $\mathbf{x}(\beta, t')$ can be represented at any time as a linear combination of these Hermitian matrices.

3. The time evolution of the coordinates corresponding to these Hermitian matrices is independent of each other.

Based on these facts we can conclude in Eq. (4.50) we have obtained a Hermitian independent mode decomposition of the density matrix $\mathbf{x}(\beta, t')$. The independent modes of the 'motion' of the density matrix are given by the following Hermitian combinations of the basis vectors

$$\left(\mathbf{v}'_{(\kappa,m)} + \mathbf{v}'_{(\kappa^*,m)}\right); \quad i\left(\mathbf{v}'_{(\kappa,m)} - \mathbf{v}'_{(\kappa^*,m)}\right), \qquad \text{for } \kappa \in \mathbb{C} \text{ and } \mathrm{Im}\kappa > 0, \tag{4.51a}$$

and

$$\mathbf{v}'_{(\kappa,m)}, \qquad \text{for } \kappa \in \mathbb{R}. \tag{4.51b}$$

Next we will determine some important properties of these Hermitian modes of the motion. We will use the condition given by Eq. (4.33b) which states the density matrix must preserve its norm as it evolves in time. Thus

$$\mathbf{n}^{\mathrm{E}}\mathbf{x}^{\mathrm{E}}(0) = \mathbf{n}^{\mathrm{E}}\mathbf{x}^{\mathrm{E}}(\beta, t') = 1. \tag{4.52}$$

Since the Hermitian modes listed in Eq. (4.51) are linearly independent of each other, which follows from $\det \mathrm{P}^{-1}(\beta) \neq 0$, to satisfy Eq. (4.52) we must have the following statements to be true

$$\mathbf{n}^{\mathrm{E}}\left(\mathbf{v}'_{(\kappa,m)} + \mathbf{v}'_{(\kappa^*,m)}\right) = 0, \qquad \text{if } \kappa \in \mathbb{C} \text{ and } \mathrm{Im}\kappa > 0, \tag{4.53a}$$

$$\mathbf{n}^{\mathrm{E}} i \left(\mathbf{v}'_{(\kappa,m)} - \mathbf{v}'_{(\kappa^*,m)}\right) = 0, \qquad \text{if } \kappa \in \mathbb{C} \text{ and } \mathrm{Im}\kappa > 0, \tag{4.53b}$$

$$\mathbf{n}^{\mathrm{E}} \mathbf{v}'_{(\kappa,m)} = 0, \qquad \text{if } \kappa \in \mathbf{R} \text{ and } \kappa \neq 0 \text{ or } m \neq 1, \tag{4.53c}$$

$$\mathbf{n}^{\mathrm{E}} \mathbf{v}'_{(\kappa,m)} = \text{const.}, \qquad \text{if } \kappa \in \mathbf{R} \text{ and } \kappa = 0 \text{ and } m = 1. \tag{4.53d}$$

This means all but one Hermitian mode corresponding to every Jordan block with the value $\kappa = 0$ are represented by Hermitian matrices with zero trace. The Hermitian modes with non-vanishing trace can be renormalized using Eq. (4.12) and Eq. (4.13) to have a trace equal to one. Thus we can write

$$\mathbf{n}^{\mathrm{E}} \mathbf{v}'_{(\kappa,m)} = \begin{cases} 1 & \text{for } \kappa \in \mathbf{R} \text{ and } \kappa = 0 \text{ and } m = 1, \\ 0 & \text{otherwise.} \end{cases} \tag{4.54}$$

From Eq. (4.52) and Eq. (4.54) we can immediately conclude that, in order to preserve the norm we must have at least one Jordan block corresponding to the $\kappa = 0$ value.

Now let us determine the consequences of the remaining physical condition, Eq. (4.33c). One important implication would be that every Jordan block corresponding to a κ value with $\mathrm{Re}\kappa = 0$ must be a 1×1 block, which also means that only one basis vector will correspond to each of these blocks. To prove this statement let us assume that one of the Jordan blocks corresponding to a κ value with $\mathrm{Re}\kappa = 0$ is a 2×2 or larger block. In this case we can choose the initial state of the system in such a way that $x^{\mathrm{B}'}_{(\mathrm{Re}\kappa=0,1)}(0) \neq 0$. However, this would also mean the solution, Eq. (4.50), will include terms like

$$\mathbf{v}'_{(\mathrm{Re}\kappa=0,m>1)} c_{(\mathrm{Re}\kappa=0,m>1)}(t'), \tag{4.55}$$

where the coefficient diverges

$$\lim_{t'\to\infty} c_{(\mathrm{Re}\kappa=0,m>1)}(t') = \infty. \tag{4.56}$$

But terms like Eq. (4.56) would violate our third condition, Eq. (4.33c). Since the norms of the $\mathbf{v}'_{(\mathrm{Re}\kappa=0,m\neq1)}$ basis vectors are zero from Eq. (4.54), therefore if they have any positive diagonal elements they should have negative elements as well. However, these elements multiplied with the coefficients $c_{(\mathrm{Re}\kappa=0,m>1)}$ which, as time evolves go to infinity, would eventually produce negative elements in the diagonal of our solution $\mathbf{x}^{\mathrm{E}}(\beta,t')$ and violate Eq. (4.33c). But what if all the diagonal elements of the $\mathbf{v}'_{(\mathrm{Re}\kappa=0,m\neq1)}$ vectors are zero? Would we still violate the third condition, Eq. (4.33c)? The answer is yes because any non-zero element of the density matrix corresponding to the term $\mathbf{v}'_{(\mathrm{Re}\kappa=0,m\neq1)}$ would still outgrow the limit imposed by Eq. (4.24c), namely

$$\rho_{ii}(t')\rho_{jj}(t') \geq |\rho_{ij}(t')|^2, \tag{4.57}$$

since the product of the diagonal elements in Eq. (4.24c) would be a constant over time and $|\rho_{ij}(t)|^2$ would increase over time thereby violating the inequality. Because of this violation we must conclude that our assumption about the size of the Jordan block corresponding to a κ with $\mathrm{Re}\kappa = 0$ was incorrect. Therefore the correct size of the Jordan blocks corresponding to a κ with $\mathrm{Re}\kappa = 0$ is always 1×1.

Following the same argument as above, we can prove that all κ's must have non-positive real parts. To prove this, first assume we have a Jordan block corresponding to a κ with $\mathrm{Re}\kappa > 0$. Then, following the same argument as above, it is easy to see this condition violates the inequality given by Eq. (4.24c). To summarize

this important finding we write

$$\mathrm{Re}\kappa \leq 0, \qquad \text{for all } \kappa. \tag{4.58}$$

To incorporate our latest findings into the general solution we now rewrite Eq. (4.50) in the following form

$$\begin{aligned}
&\mathbf{x}(\beta, t') = \\
&= \sum_{\substack{\kappa\in\mathbf{C}\\ \mathrm{Re}\kappa<0\\ \mathrm{Im}\kappa>0}} \sum_{m=1}^{n_\kappa} \Bigg[\left(\mathbf{v}'_{(\kappa,m)} + \mathbf{v}'_{(\kappa^*,m)}\right) \mathrm{e}^{\mathrm{Re}\kappa t'} \left(\sum_{l=l}^{m} \left| x^{\mathrm{B}'}_{(\kappa,l)}(0) \right| \frac{(t')^{m-l}}{(m-l)!} \cos\left(\mathrm{Im}\kappa t' + \varphi^{\mathrm{B}'}_{(\kappa,l)}\right) \right) \\
&+ i \left(\mathbf{v}'_{(\kappa,m)} - \mathbf{v}'_{(\kappa^*,m)}\right) \mathrm{e}^{\mathrm{Re}\kappa t'} \left(\sum_{l=l}^{m} \left| x^{\mathrm{B}'}_{(\kappa,l)}(0) \right| \frac{(t')^{m-l}}{(m-l)!} \sin\left(\mathrm{Im}\kappa t' + \varphi^{\mathrm{B}'}_{(\kappa,l)}\right) \right) \Bigg] \\
&+ \sum_{\substack{\kappa\in\mathbf{C}\\ \mathrm{Re}\kappa=0\\ \mathrm{Im}\kappa>0}} \Bigg[\left(\mathbf{v}'_{(\kappa,1)} + \mathbf{v}'_{(\kappa^*,1)}\right) \left| x^{\mathrm{B}'}_{(\kappa,1)}(0) \right| \cos\left(\mathrm{Im}\kappa t' + \varphi^{\mathrm{B}'}_{(\kappa,1)}\right) \\
&+ i \left(\mathbf{v}'_{(\kappa,1)} - \mathbf{v}'_{(\kappa^*,1)}\right) \left| x^{\mathrm{B}'}_{(\kappa,1)}(0) \right| \sin\left(\mathrm{Im}\kappa t' + \varphi^{\mathrm{B}'}_{(\kappa,1)}\right) \Bigg] \\
&+ \sum_{\substack{\kappa\in\mathbf{R}\\ \kappa<0}} \sum_{m=1}^{n_\kappa} \left(\mathbf{v}'_{(\kappa,m)} \mathrm{e}^{\kappa t'} \left(\sum_{l=l}^{m} x^{\mathrm{B}'}_{(\kappa,l)}(0) \frac{(t')^{m-l}}{(m-l)!} \right) \right) \\
&+ \sum_{\substack{\kappa\in\mathbf{R}\\ \kappa=0}} \mathbf{v}'_{(\kappa,1)} x^{\mathrm{B}'}_{(\kappa,1)}(0).
\end{aligned} \tag{4.59}$$

In Eq. (4.59) all but those Hermitian modes in the last sum have zero norms and the last sum must include at least one term.

Next we will focus our attention on the steady state solution of our model. To do so first let us define what we mean when we talk about the steady state of the field inside the micromaser cavity. Are we talking about a field which does not change at all over time? No, we would like to allow periodic processes in our investigation.

Then how do we define a steady state? In our understanding a steady state will mean such a state which is not decaying over time. This is of course a generalization of what we usually understand under steady since it can also include periodic changes in the state of the system. A mathematical definition of such a state $\bar{\rho}_S(\beta, t')$ could be given as follows (see [38]). Since our solution, as we have shown earlier, is only composed of decaying, periodic and constant terms, it can always be written in the following form

$$\bar{\rho}(\beta, t') = \bar{\rho}_0(\beta, t') + \bar{\epsilon}(\beta, t'), \tag{4.60}$$

where $\bar{\epsilon}(\beta, t')$ contains all terms decaying in time. Thus

$$\lim_{t' \to \infty} \bar{\epsilon}(\beta, t') = 0, \tag{4.61}$$

and $\bar{\rho}_0(\beta, t')$ includes all terms which are constant or periodic over time. This of course does not mean automatically that $\bar{\rho}_0(\beta, t')$ is also periodic over time but if it is we will call it a steady state solution. To summarize, if

$$\bar{\rho}_0(\beta, t' + T) = \bar{\rho}_0(\beta, t'), \tag{4.62}$$

then

$$\bar{\rho}_S(\beta, t') = \bar{\rho}_0(\beta, t'), \tag{4.63}$$

else we do not have a steady state solution because the density matrix describing the field inside the micromaser cavity is changing over time without any periodicity. Using Eq. (2.37) from Eq. (4.60) we obtain the decomposition of the slowly varying amplitude $\tilde{\rho}(\beta, t')$ as

$$\tilde{\rho}(\beta, t') = \tilde{\rho}_0(\beta, t') + \tilde{\epsilon}(\beta, t'), \tag{4.64}$$

which can also be expressed in the vector form

$$\mathbf{x}(\boldsymbol{\beta}, t') = \mathbf{x}_0(\boldsymbol{\beta}, t') + \mathbf{x}_\epsilon(\boldsymbol{\beta}, t'). \tag{4.65}$$

Here $\tilde{\epsilon}(\boldsymbol{\beta}, t')$ ($\mathbf{x}_\epsilon(\boldsymbol{\beta}, t')$) contains all terms decaying over time. Therefore

$$\lim_{t'\to\infty} \tilde{\epsilon}(\boldsymbol{\beta}, t') = 0, \tag{4.66}$$

$$\lim_{t'\to\infty} \mathbf{x}_\epsilon(\boldsymbol{\beta}, t') = 0, \tag{4.67}$$

and $\tilde{\rho}_0(\boldsymbol{\beta}, t')$ ($\mathbf{x}_0(\boldsymbol{\beta}, t')$) includes all terms which are constant or periodic over time. By comparing Eq. (4.65) and Eq. (4.59), now we can determine the non-decaying part of the solution $\mathbf{x}_0(\boldsymbol{\beta}, t')$, namely

$$\begin{aligned}\mathbf{x}_0(\boldsymbol{\beta}, t') = \sum_{\substack{\kappa\in\mathbf{C}\\ \mathrm{Re}\kappa=0\\ \mathrm{Im}\kappa>0}} \Big[& \left(\mathbf{v}'_{(\kappa,1)} + \mathbf{v}'_{(\kappa^*,1)}\right) \left|x^{\mathrm{B}'}_{(\kappa,1)}(0)\right| \cos\left(\mathrm{Im}\kappa t' + \varphi^{\mathrm{B}'}_{(\kappa,1)}\right) \\ & + i\left(\mathbf{v}'_{(\kappa,1)} - \mathbf{v}'_{(\kappa^*,1)}\right) \left|x^{\mathrm{B}'}_{(\kappa,1)}(0)\right| \sin\left(\mathrm{Im}\kappa t' + \varphi^{\mathrm{B}'}_{(\kappa,1)}\right) \Big] \\ & + \sum_{\substack{\kappa\in\mathbf{R}\\ \kappa=0}} \mathbf{v}'_{(\kappa,1)} x^{\mathrm{B}'}_{(\kappa,1)}(0).\end{aligned} \tag{4.68}$$

Please note Eq. (4.68) contains two sums. The first one includes all oscillating non-decaying terms and the other sum contains all the time independent terms. Also remember, the last sum must contain at least one term in order to preserve the norm.

Now we will determine how the steady state condition, Eq. (4.62), can be met. Using Eqs. (2.37) and (4.62), we can determine that a steady state solution is equivalent to satisfying the condition

$$\left(\tilde{\rho}_0(\boldsymbol{\beta}, t' + T)\right)_{k,l} \mathrm{e}^{-i(k-l)\nu T} = \left(\tilde{\rho}_0(\boldsymbol{\beta}, t')\right)_{k,l}, \tag{4.69}$$

for all

$$k, l = 0, 1, 2, \ldots. \tag{4.70}$$

How can we satisfy this condition? Before we answer this question we must realize a very important fact, namely if $\tilde{\rho}_0(\boldsymbol{\beta}, t')$ is periodic then its period does not depend on the indexes k, l. It is solely determined by the κ values obtained from the Jordan decomposition of $\mathrm{A}(\boldsymbol{\beta})$. The κ values are of course some functions of the configuration vector $\boldsymbol{\beta}$ therefore through the κ values the time period T is determined as $T(\boldsymbol{\beta})$ depending only on the configuration vector $\boldsymbol{\beta}$. This simple fact can be easily seen from Eq. (4.68). Now to discuss how to satisfy Eq. (4.69) we have to distinguish two different cases. The first one is when the slowly varying amplitude does not depend on time

$$\tilde{\rho}_0(\boldsymbol{\beta}, t') = constant, \tag{4.71}$$

which means we did not obtain any κ value located on the imaginary axis from the Jordan decomposition. In this case Eq. (4.69) is immediately satisfied and the time evolution of $\tilde{\rho}_0(\boldsymbol{\beta}, t')$ is characterized by the time period

$$T_\nu = \frac{2\pi}{\nu}. \tag{4.72}$$

This also means in this case we have a steady state solution and it is given by

$$(\tilde{\rho}_{\mathrm{S}}(\boldsymbol{\beta}, t'))_{k,l} = (\tilde{\rho}_0(\boldsymbol{\beta}))_{k,l}\, \mathrm{e}^{-\mathrm{i}(k-l)\nu t'} \tag{4.73}$$

The second case is when the slowly varying amplitude is periodic over time. In this instance as we discussed the period of the slowly varying amplitude is solely

determined by the configuration vector β and can be given as $T(\beta)$. However, to have a steady state solution, we must also satisfy Eq. (4.69) from which it follows that

$$(k-l)\nu T(\beta) = m2\pi \tag{4.74}$$

must be true for all k and l indexes with some appropriately chosen m integer value. But Eq. (4.74) introduces a new restriction on $T(\beta)$, namely

$$T(\beta) = m\frac{2\pi}{\nu} = mT_{\nu}. \tag{4.75}$$

This means the time period of the slowly varying amplitude, which is solely determined by the configuration vector β, must also be equal to an integer number times the period of the non-diagonal element of the incoming atom's density matrix. Since β does not include ν as an independent parameter (it only includes $\Delta = \frac{\omega_0 - \nu}{\Gamma}$) this condition Eq. (4.75) can not be guarantied to be satisfied at all. Which also means the possibility of obtaining a steady state solution in the case when the Jordan decomposition of A(β) resulted in κ values located on the imaginary axis is very small, almost zero.

In cases other than the two that we have discussed we will not have a steady state solution, since the density matrix describing the field inside the micromaser cavity in those cases would change over time without any periodicity.

5

Trapping states of the coherently pumped micromaser

In this chapter we extend the theory of the trapping states which was first introduced for the incoherently pumped micromaser by Filipowicz *et al.* [1] and Meystre *et al.* [14]. We will show how trapping states can be formed in a coherently pumped micromaser and derive the condition under which they occur. Then we will examine the steady state solutions formed under trapping state condition and provide two examples of how the steady state solution is determined by β and the initial state of the cavity field.

A steady state formed in a micromaser is the result of two competing processes, the pumping and the decay due to the cavity losses. Under general conditions in the absence of either process steady state cannot be reached (except of course the vacuum state). However, a steady state can be obtained in the absence of the decay process if we restrict the interaction phase Θ in such a way that we cancel the coupling between given rows and columns of the field density matrix. In this case the density matrix is split into non-interacting blocks illustrated in Fig. 30. Since there is no interaction between these blocks they all evolve independently, therefore each normal mode of the original density matrix is localized to only one of the blocks. This means, that

an initial state which was originally localized to one of the blocks will never escape from the block, the state is trapped there. The condition under which this situation occurs is called the trapping state condition. To derive the trapping state condition

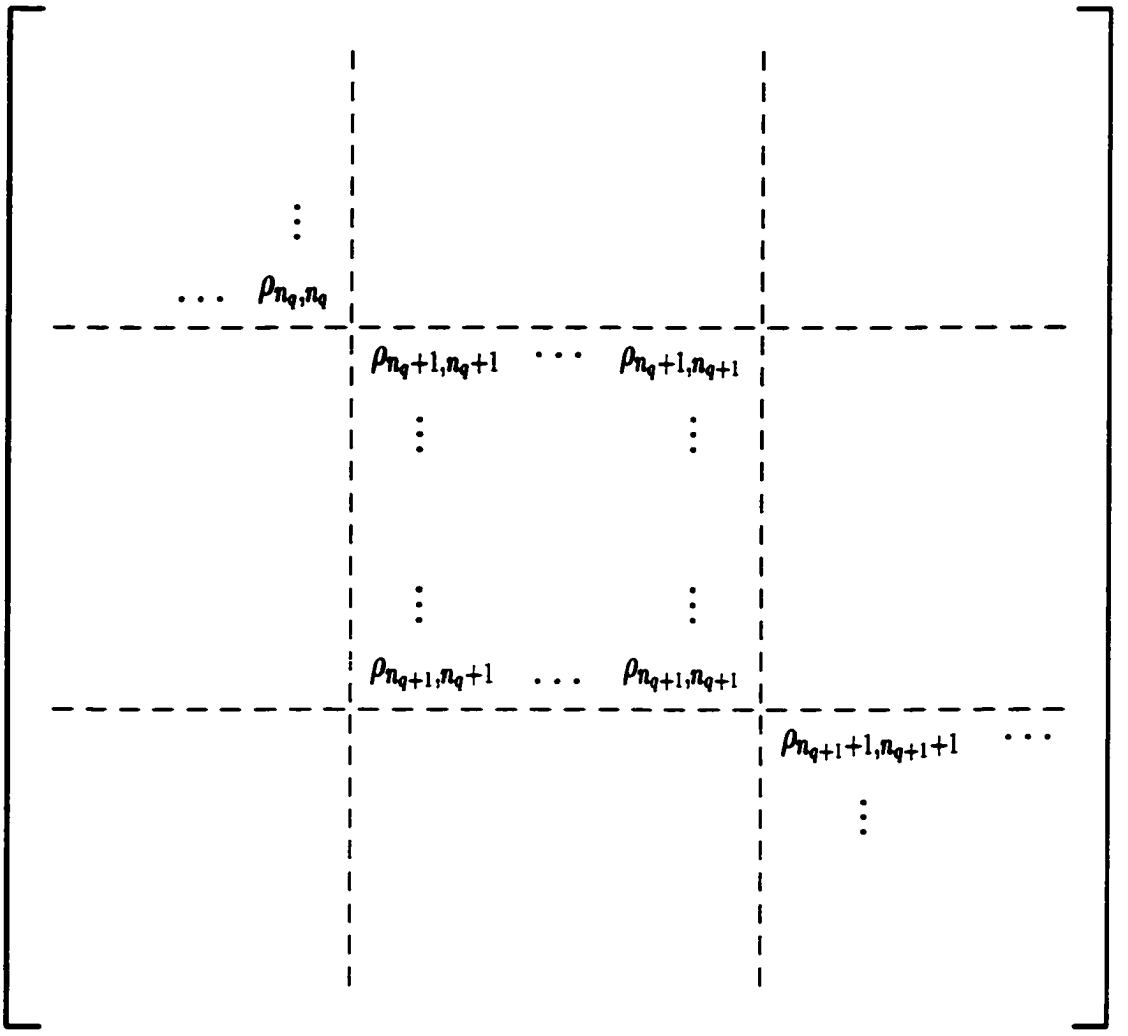

Figure 30: The blocks formed in the field density matrix of a coherently pumped micromaser under trapping state condition. The dashed lines are indicating the positions where the interaction is severed between neighboring elements.

we use Eq. (4.1). Here we can see, to severe the interaction between given rows and

columns of the field density matrix we must satisfy

$$S_{n_q+1} = 0, \qquad q = 1, 2, 3, \ldots, \tag{5.1}$$

where n_q represent the index where the termination takes place. Using the definition of S_k, Eq. (4.2b), this can also be written as

$$\sqrt{n_0^2 + (n_q + 1)}\Theta = q\pi, \qquad q = 1, 2, 3, \ldots. \tag{5.2}$$

Based on Eq. (5.2), the trapping state condition imposed on the interaction phase is

$$\Theta = \frac{q\pi}{\sqrt{n_0^2 + (n_q + 1)}}, \qquad q = 1, 2, 3, \ldots. \tag{5.3}$$

From Eq. (5.3) we can see the role of the q variable introduced in Eq. (5.1). For fixed values of Θ and n_0, q is indexing the trapping state blocks in the diagonal of the field density matrix as shown in Fig. 30. From Eq. (5.3) we can also read out how, for fixed values of Θ and n_0, the different values of n_q are related to each other and to q:

$$(n_{q'} + 1) = \left(\left(\frac{q'}{q}\right)^2 - 1\right) n_0^2 + \left(\frac{q'}{q}\right)^2 (n_q + 1). \tag{5.4}$$

Since all couplings between the n_qth and $n_q + 1$st rows and columns are canceled, each partition of the density matrix shown in Fig. 30 is independent of the others. The downward and upward trapping states known from the theory of the incoherently pumped micromasers [14] are located at the upper left and the lower right corners of the diagonal partitions. It is also clear that initial states solely located in different diagonal partitions must produce different steady state solutions located in the partition of the initial state. Therefore, for each diagonal partition, there must be

at least one corresponding steady state solution. This means, that just specifying $\boldsymbol{\beta}$ does not uniquely determine the steady state of the system. To do so we would also need information about the initial state of the cavity field. This is an example where the steady state is determined by the configuration vector $\boldsymbol{\beta}$ and the initial state of the cavity field together.

As our second example, we now investigate the situation when we add the decay process to our previous system while we keep the trapping state condition satisfied. By doing so we have introduced a diagonal coupling between the elements of the same diagonal. Since our thermal reservoir is at $T = 0$K, the introduced coupling only provides a decay channel to all but the $\tilde{\rho}_{0,0}(\boldsymbol{\beta}, t)$ element of the field density matrix resulting in the situation when all but the first trapping state, which includes the vacuum state, will decay over time. This means in the case our system is coupled to a thermal reservoir at $T = 0$K specifying $\boldsymbol{\beta}$ unambiguously determines the steady state of the system, regardless of the initial field inside the micromasers cavity.

6

Understanding the results of the quantum model

In the previous two chapters, 4 and 5, we have investigated the field inside the cavity of a coherently pumped micromaser using strict mathematical tools. The results of those calculations might be overwhelmingly full of mathematical details. Therefore in this chapter we would like to provide a clear physical understanding of what is really happening inside the cavity of the coherently pumped micromaser during the time it reaches steady state.

To start, we define our goal which is to understand the changes taking place in the density matrix describing the field inside the cavity of the micromaser. To visualize the changes we will use the slowly varying part of the field density matrix $\tilde{\rho}(\beta, t')$, and think of it as a matrix describing the displacement of the elements of a two dimensional lattice. From Eq. (2.48) we can see that the time evolution of each element of the lattice is connected to its specific neighbors through an interaction illustrated in Fig. 31. The strength of the interactions in which a specific element is involved, in general, is a complicated function of the given element's position in the lattice and the parameter vector β describing the excitation (pumping) of the lattice (field). However these couplings have some simple and easy to understand properties

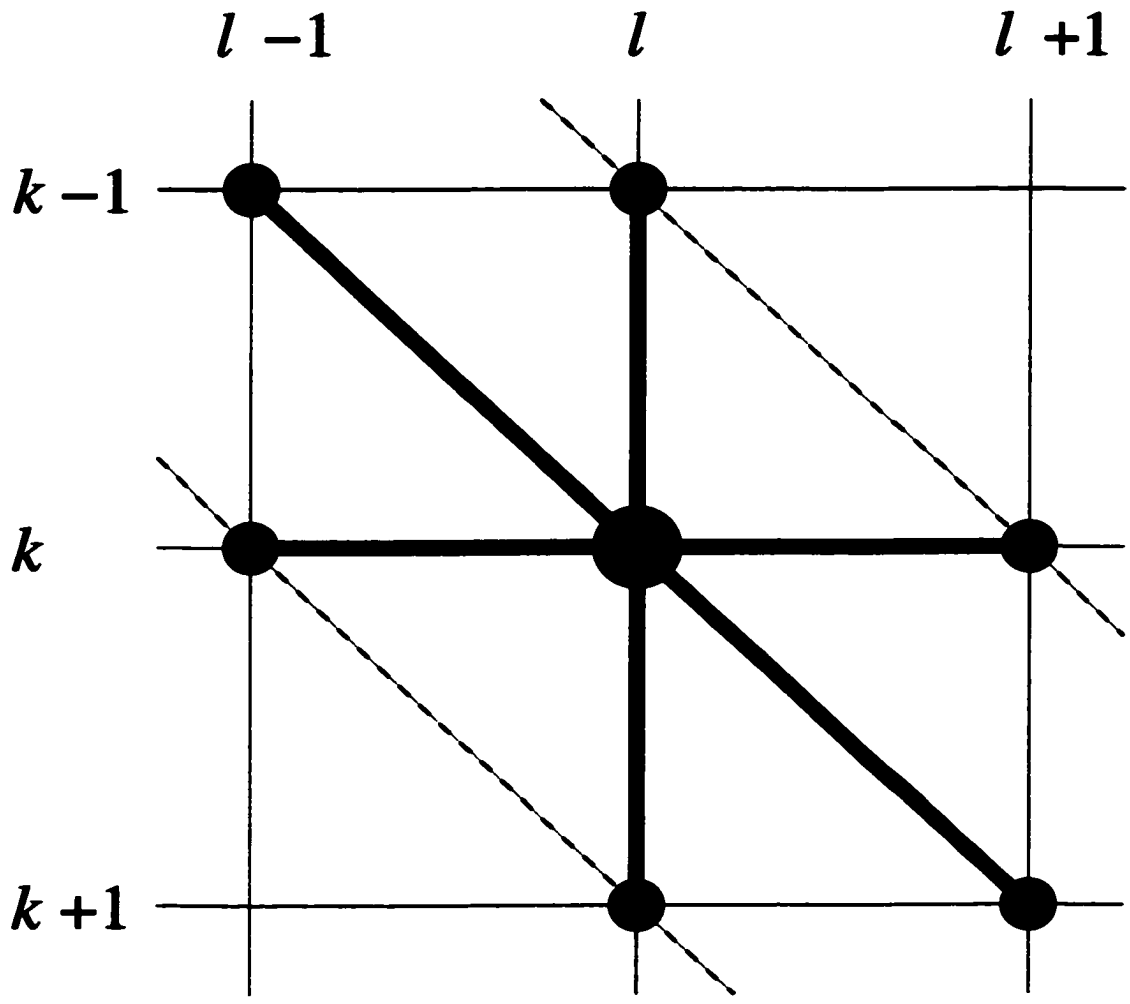

Figure 31: Couplings of the (k, l)th element of the lattice (density matrix) to its next neighbors. The thick lines represent the interaction between the elements. As a result, different diagonals of the lattice indicated with dashed lines, are coupled.

which we will summarize now:

1. The couplings introduced by the decay process only act between the elements of the same diagonal of the lattice.

2. The strength of the coupling between elements in neighboring diagonals is proportional to $\lambda\sqrt{1-u^2}$, also the strength of the coupling goes to zero if n_0 goes

to infinity.

Based on these properties of the interaction, we can say the different diagonals of our lattice will have no effect on each other in the following cases:

- $\lambda = 0$, the case of the incoherent pumping,
- $u = \pm 1$, the incoming atoms are either in their upper or lower states,
- $n_0 \to \infty$, the detuning between the empty cavity frequency ω_0, and the atomic transition frequency ω_{ab}, is too high.

In any other case the different diagonals of our lattice will strongly interact through the next neighbor interaction shown in Fig. 31, forming collective excitations of the lattice. To describe the time evolution of the whole lattice in the strongly interacting case in chapter 4 we have introduced the normal modes, and the Hermitian normal modes of the 'vibration' of the lattice. These normal modes, as we have shown, are evolving independently from each other and they form a basis in the sense that any other excitation of the lattice can be written as a superposition of these normal modes. We have also shown in chapter 4 that the time evolution of each normal mode is controlled by $e^{\kappa t'}$, where κ is a complex number specific to the given normal mode. We proved that for all normal modes but one, $\mathrm{Re}\kappa < 0$. Therefore, these normal modes decay over time. The single normal mode which had $\mathrm{Re}\kappa = 0$, however, is not decaying. It forms the unique steady state solution determined by the excitation of the lattice.

The dynamics of the model can now be easily summarized using the normal modes. By setting up an experiment involving a coherently pumped micromaser we determine the parameter vector β which determines the basis of the normal modes of our lattice. The initial state of the field is then decomposed into the normal modes which evolve independently over time. After some time all but one of the normal modes decay reducing the field inside the micromaser cavity to its steady state. The steady state of the field is, therefore, determined by the only normal mode which had not decayed.

In the following set of pictures we show two examples corresponding to two different cases of the time evolution of the lattice. In the figures we print the κ's and the normal modes, we highlight the κ which belongs to the given mode. In Figs. 32–40 we list all normal modes corresponding to a 3×3 trapping state of the coherently pumped micromaser. In this example Δ, as well as n_0, are large, therefore the coupling between the diagonals of the lattice is severed. This we can recognize in the graphs, Figs. 32–40, since in this case the normal modes are all confined to a single diagonal of the lattice. Also note, because of the large detuning the only excited element of the lattice is the one corresponding to the vacuum state $\tilde{\rho}_{00}(\beta, t')$.

In Figs. 41–49 we list all normal modes corresponding to the same 3×3 trapping state of the coherently pumped micromaser, however, in this example $\Delta = 0$ and $n_0 = 0$. From the figures we can see clearly, in this case the coupling between the diagonals of the lattice is strong resulting in normal modes which extend throughout the whole lattice. The steady state of the micromaser in this case extend to the whole trapping state.

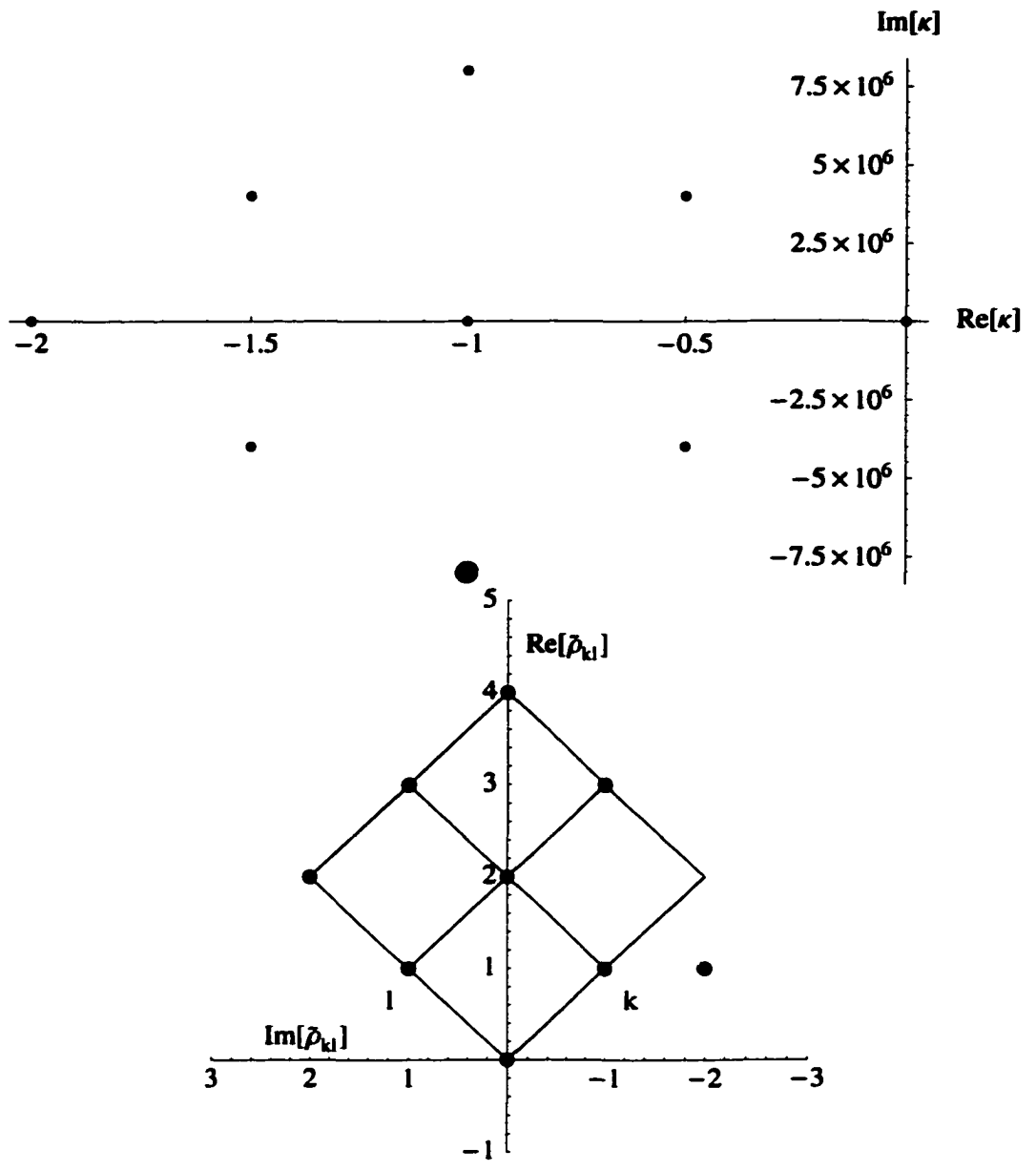

Figure 32: On the top the κ's, highlighted the one corresponding to the normal mode pictured on the bottom. Since Reκ < 0, this normal mode decays over time.

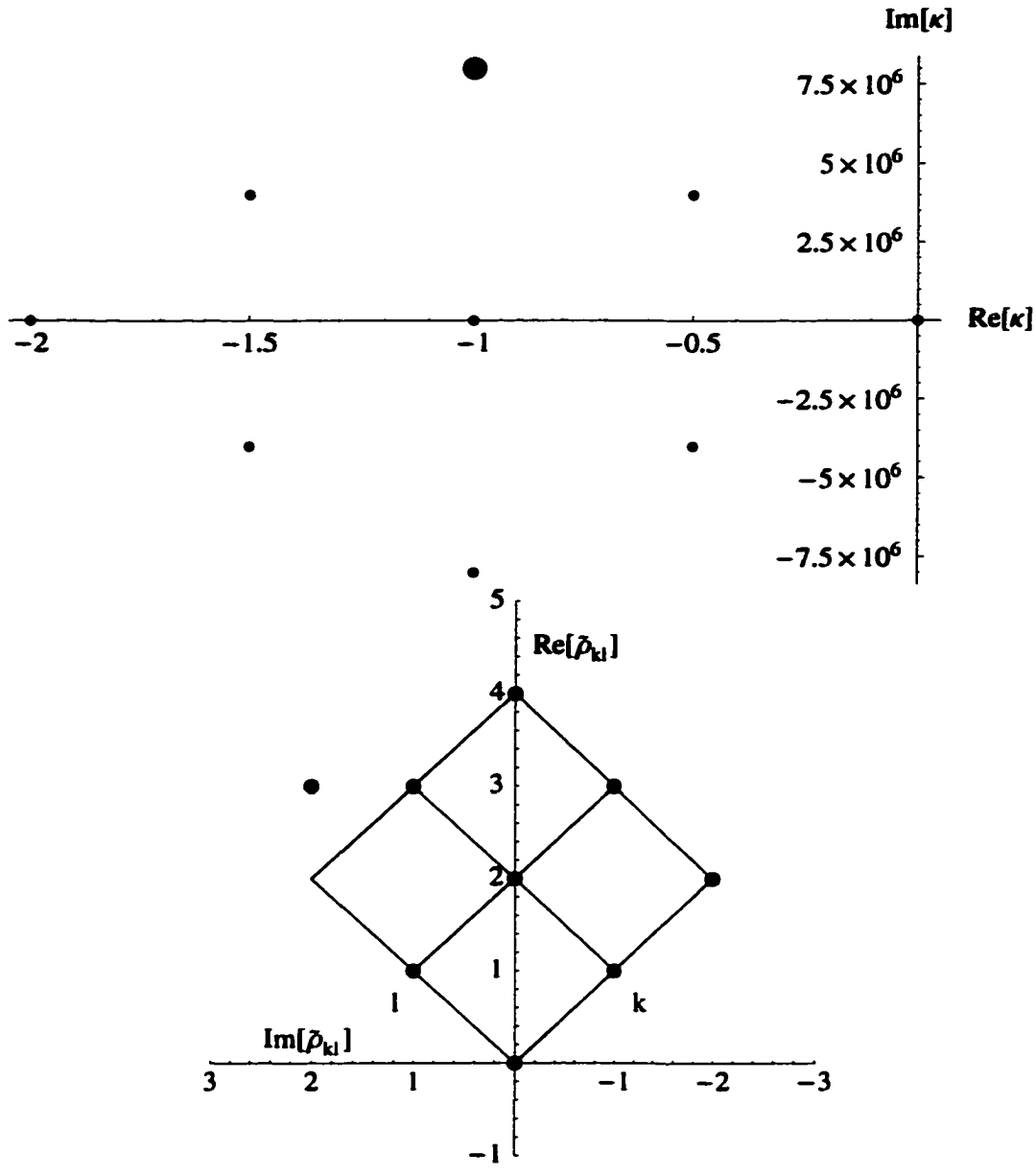

Figure 33: On the top the κ's, highlighted the one corresponding to the normal mode pictured on the bottom. Since Reκ < 0, this normal mode decays over time.

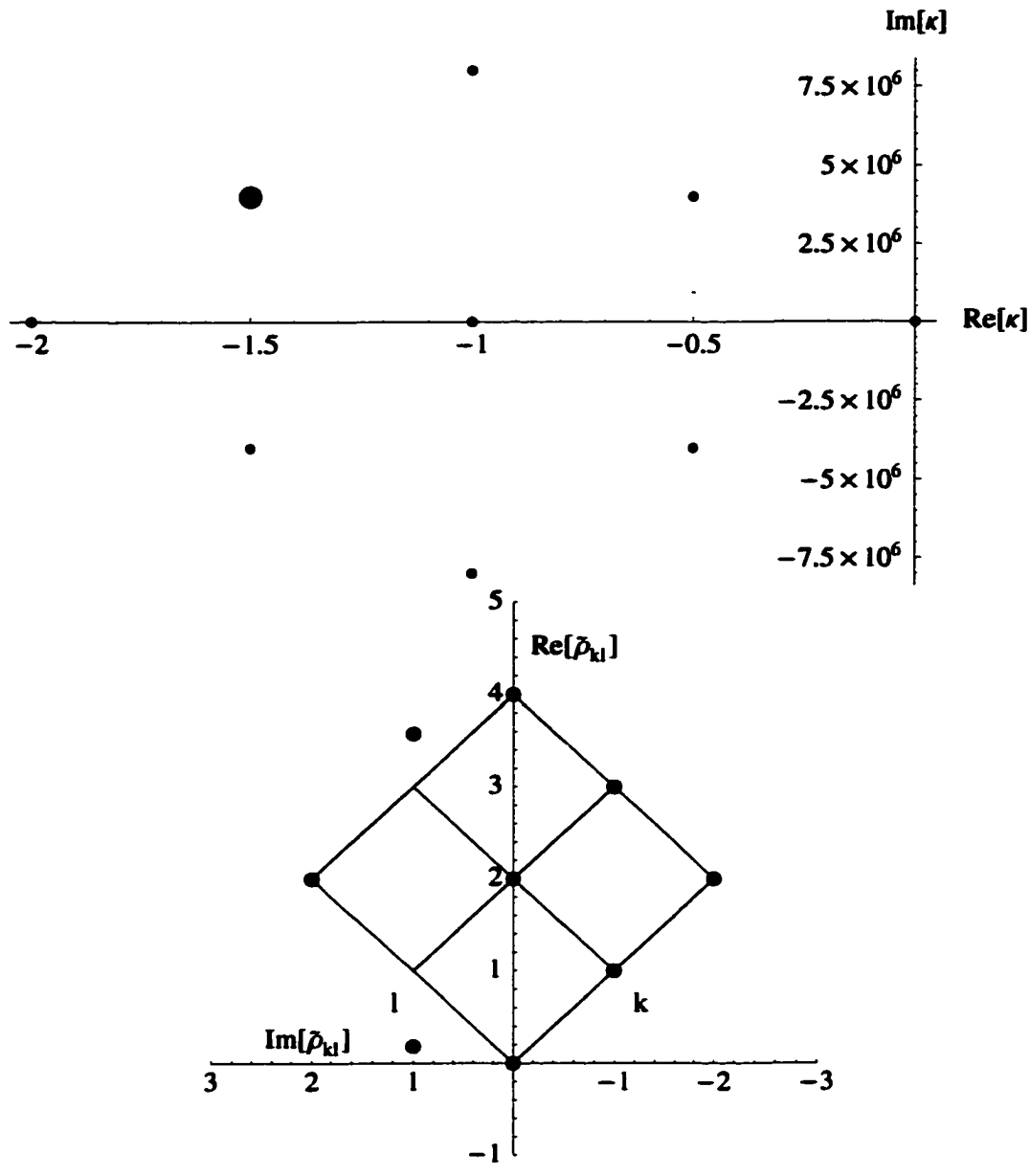

Figure 34: On the top the κ's, highlighted the one corresponding to the normal mode pictured on the bottom. Since Reκ < 0, this normal mode decays over time.

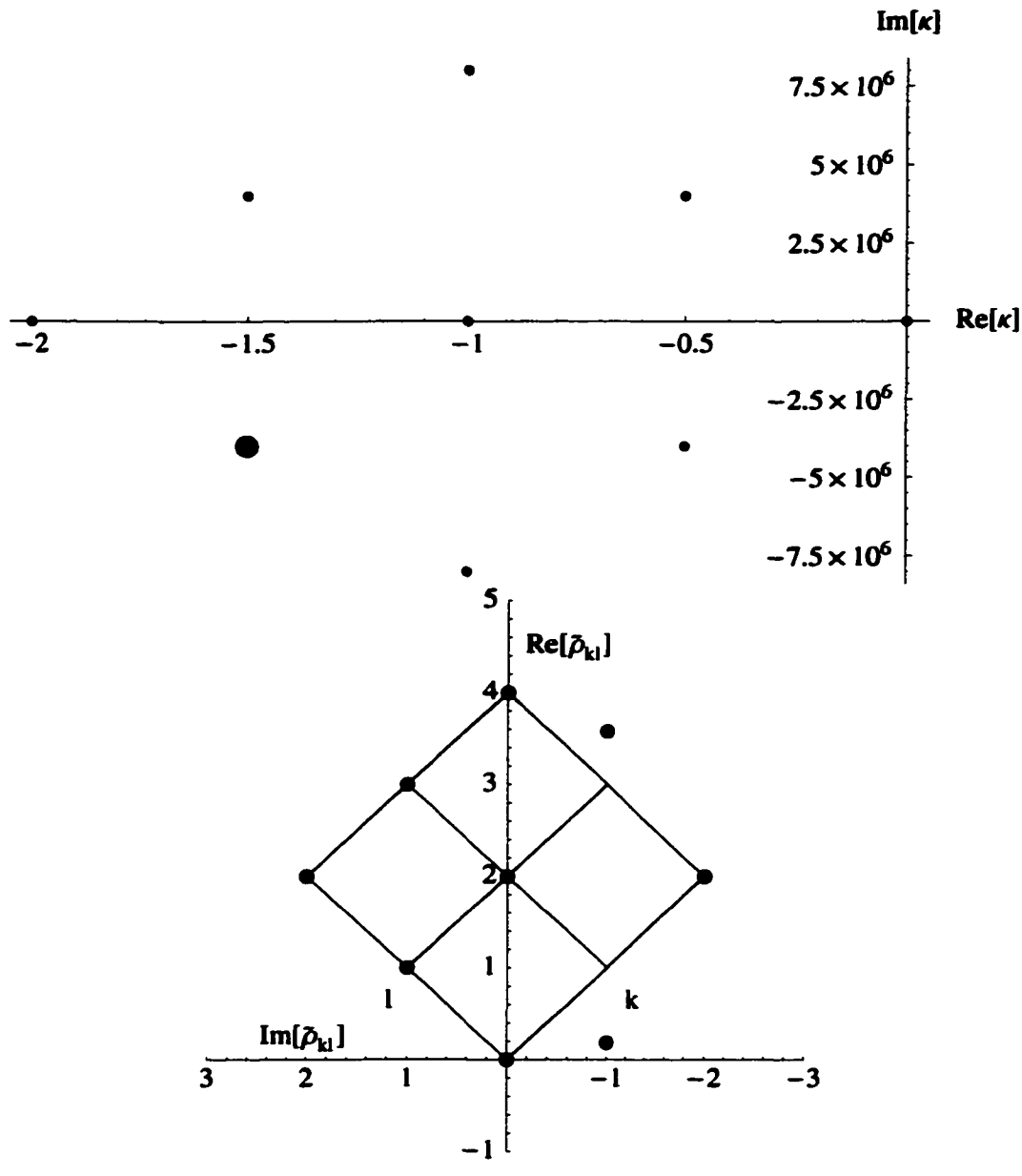

Figure 35: On the top the κ's, highlighted the one corresponding to the normal mode pictured on the bottom. Since Reκ < 0, this normal mode decays over time.

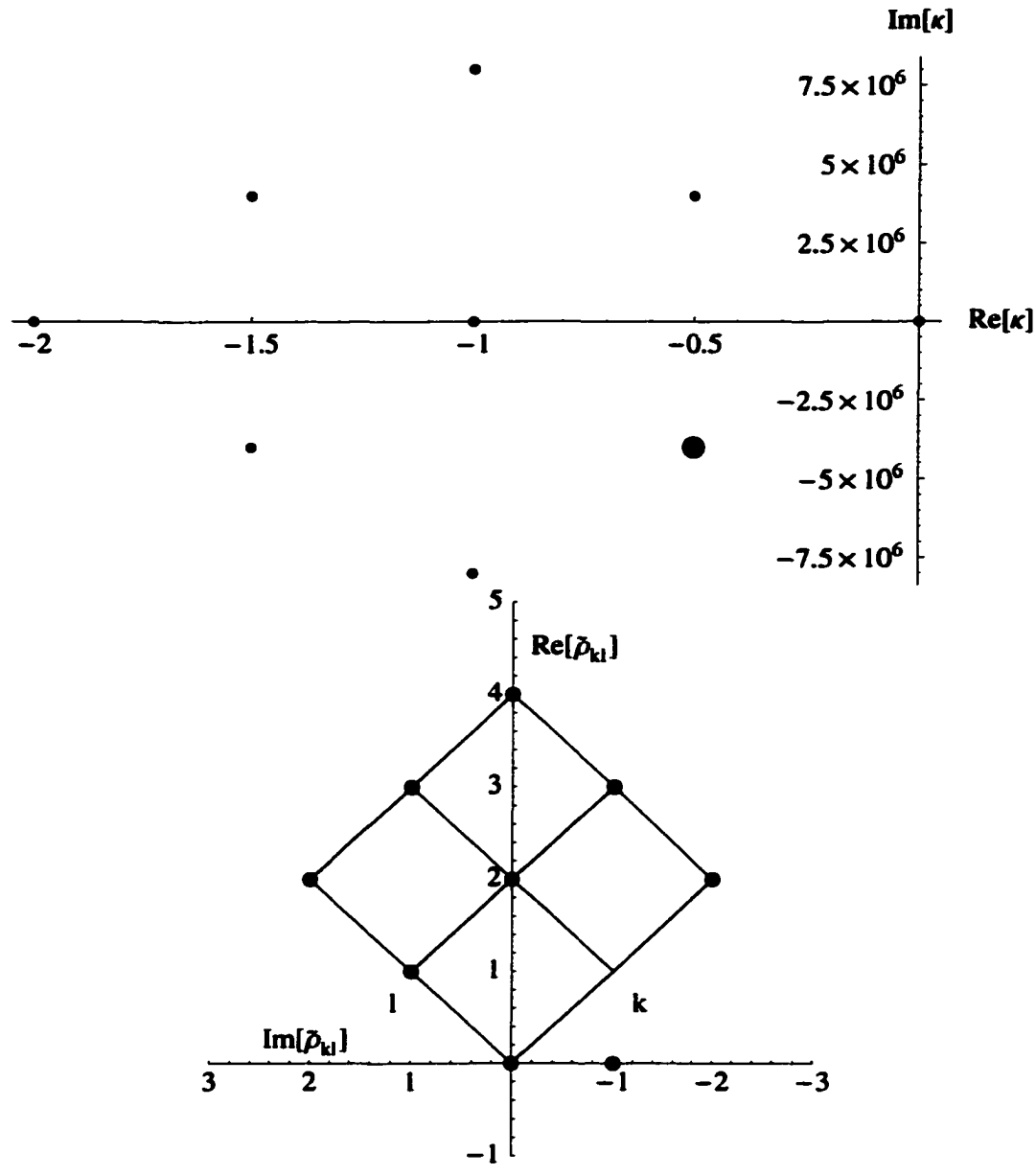

Figure 36: On the top the κ's, highlighted the one corresponding to the normal mode pictured on the bottom. Since Reκ < 0, this normal mode decays over time.

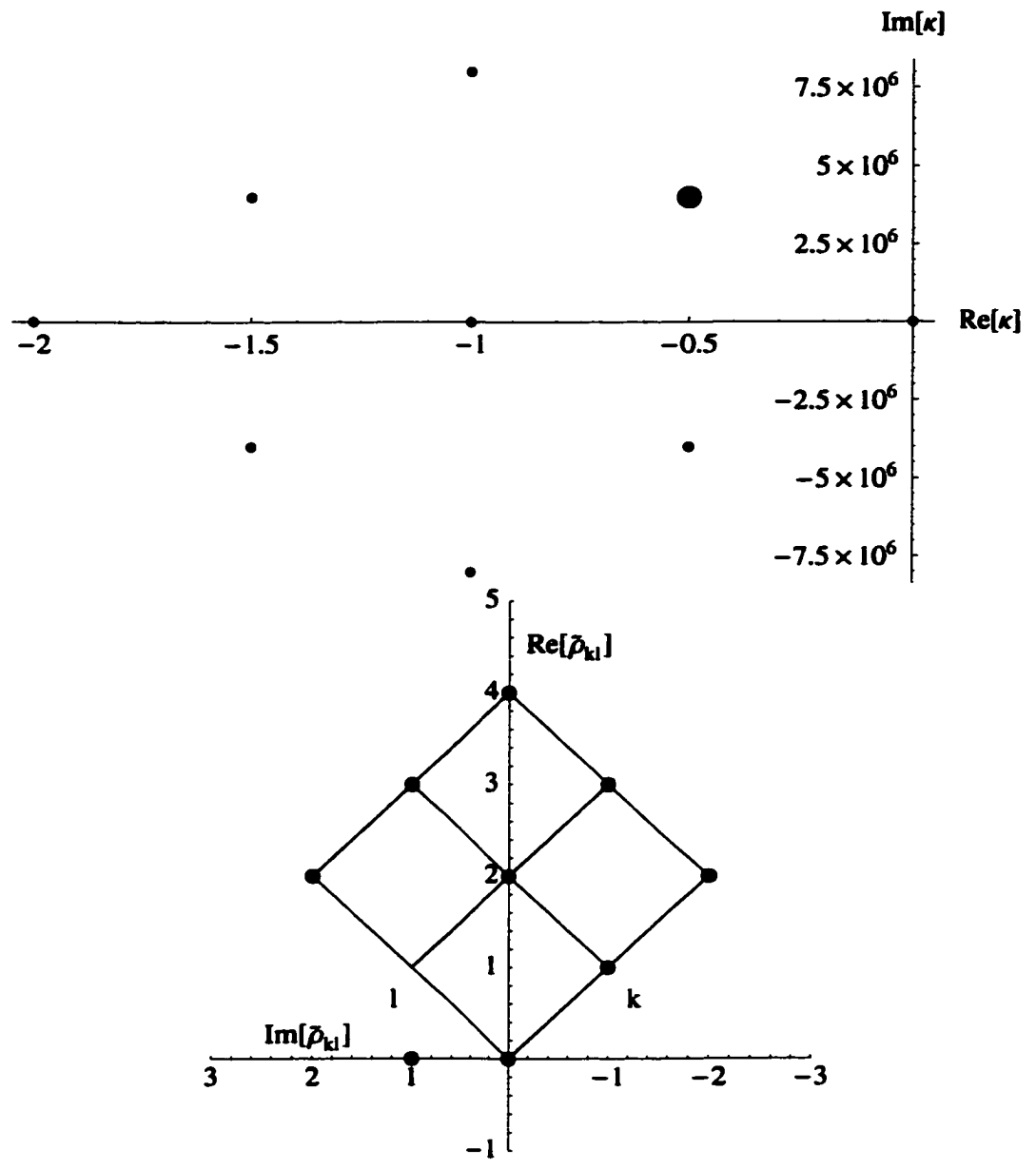

Figure 37: On the top the κ's, highlighted the one corresponding to the normal mode pictured on the bottom. Since Re$\kappa < 0$, this normal mode decays over time.

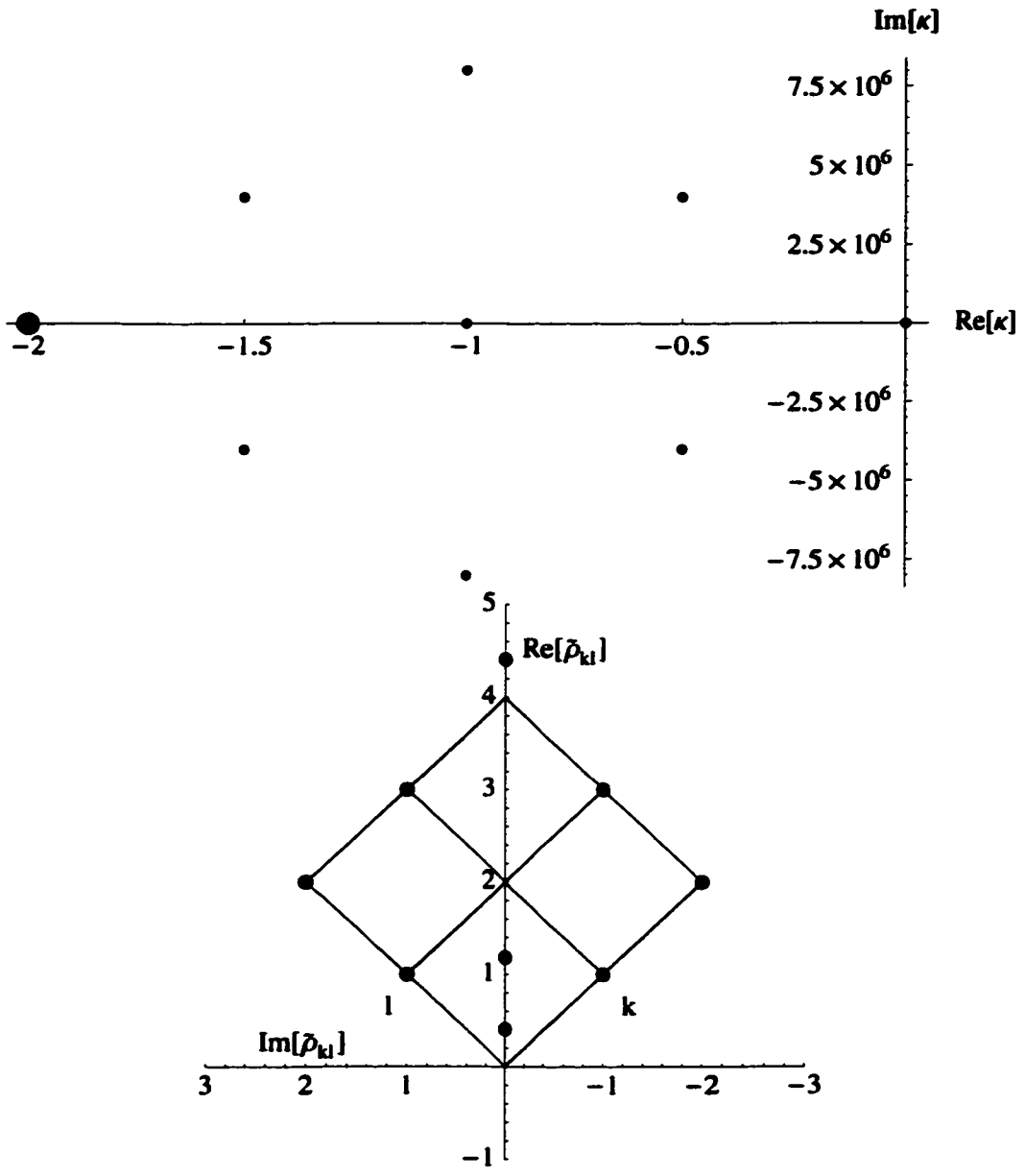

Figure 38: On the top the κ's, highlighted the one corresponding to the normal mode pictured on the bottom. Since Re$\kappa < 0$, this normal mode decays over time.

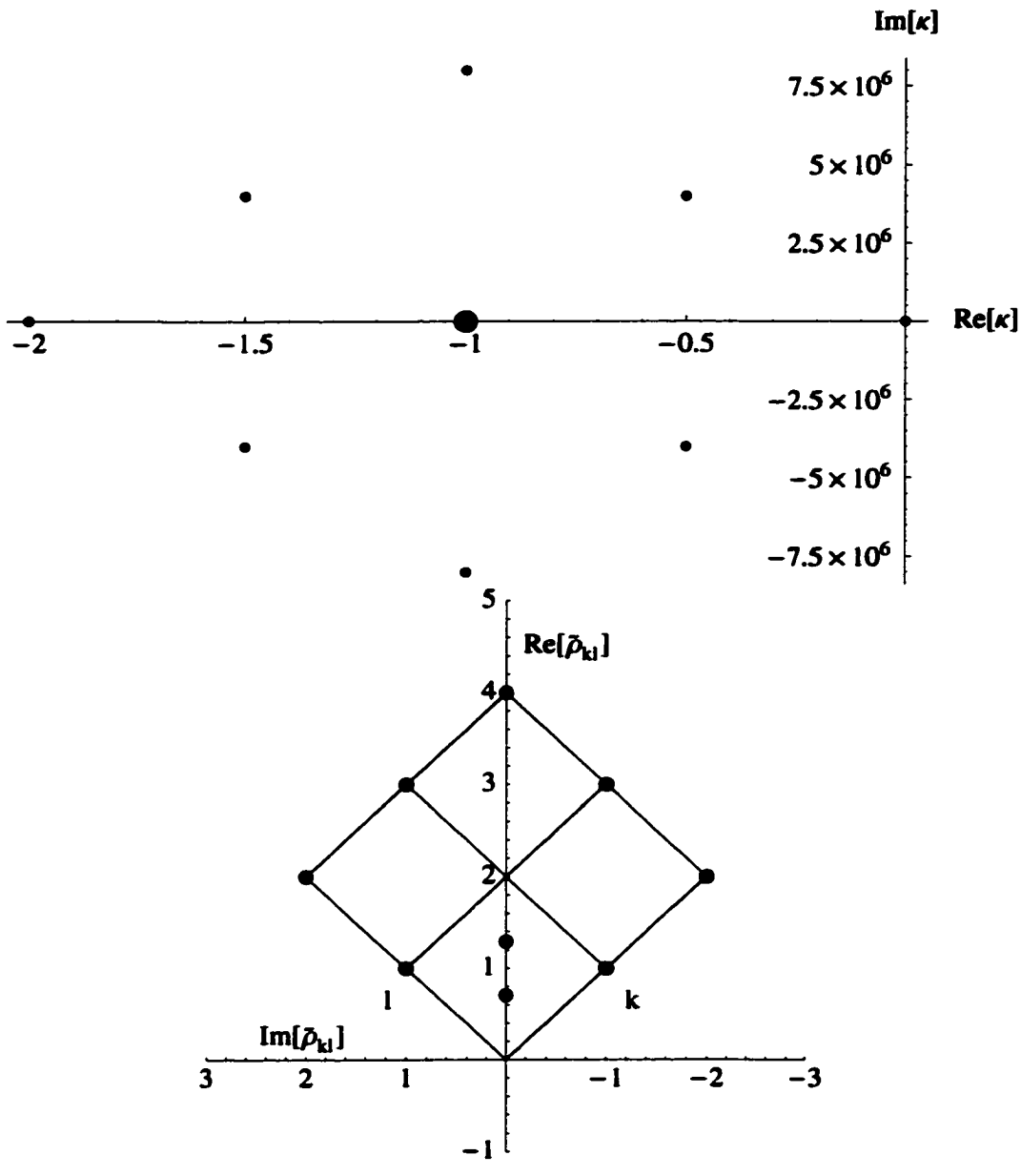

Figure 39: On the top the κ's, highlighted the one corresponding to the normal mode pictured on the bottom. Since Reκ < 0, this normal mode decays over time.

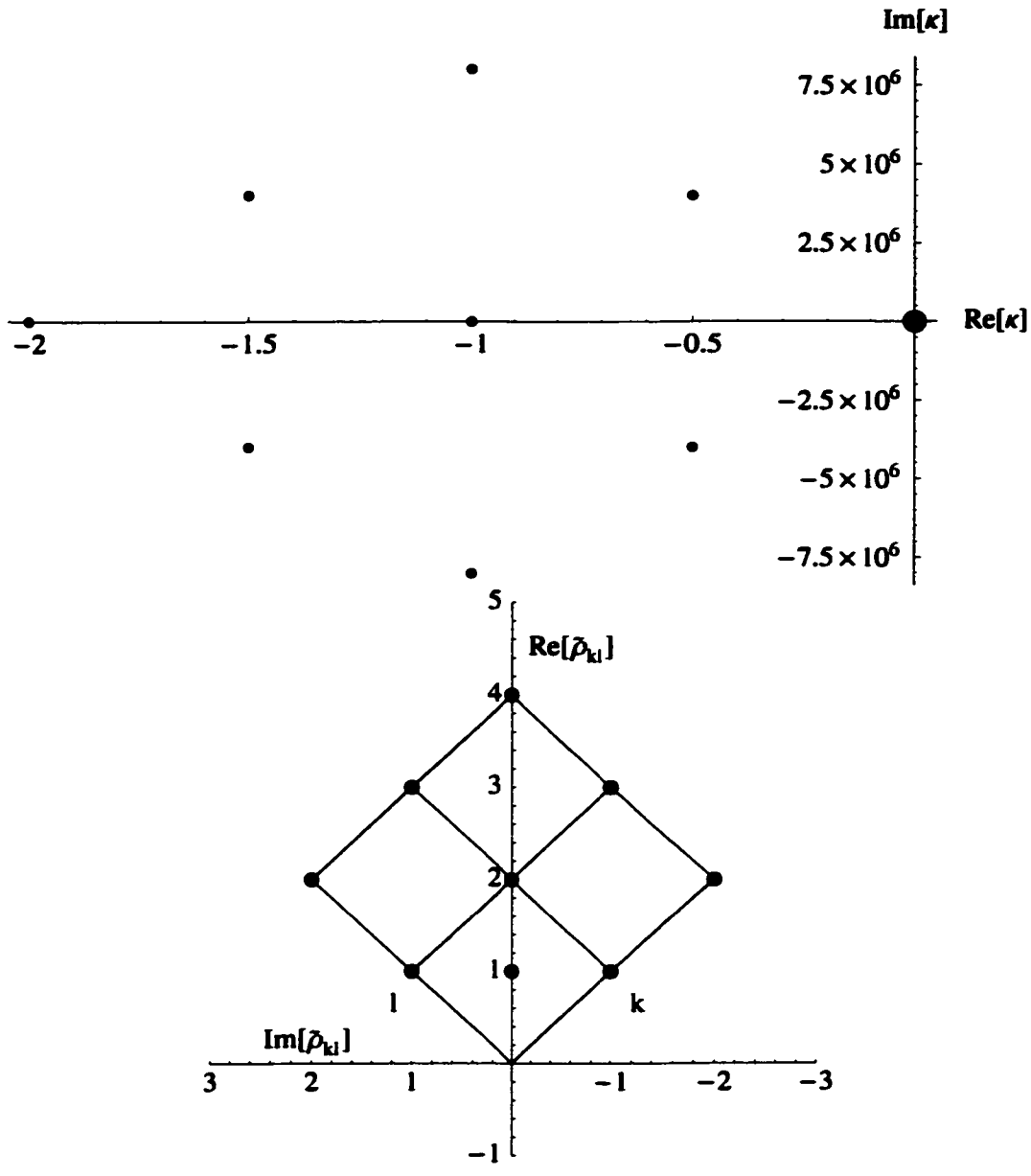

Figure 40: On the top the κ's, highlighted the one corresponding to the normal mode pictured on the bottom. Since Reκ = 0, this normal mode forms the steady state of the coherently pumped micromaser.

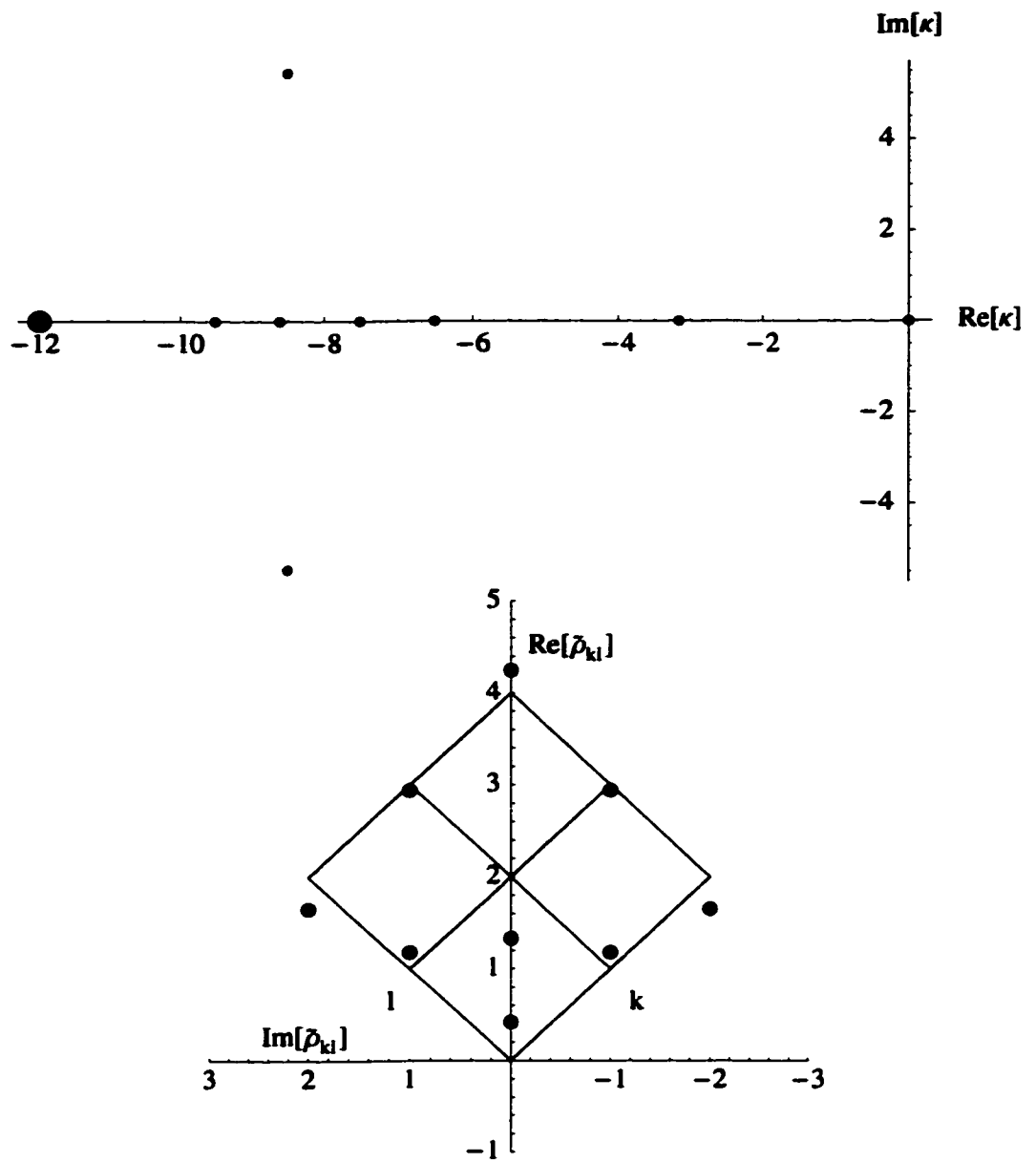

Figure 41: On the top the κ's, highlighted the one corresponding to the normal mode pictured on the bottom. Since Re$\kappa < 0$, this normal mode decays over time.

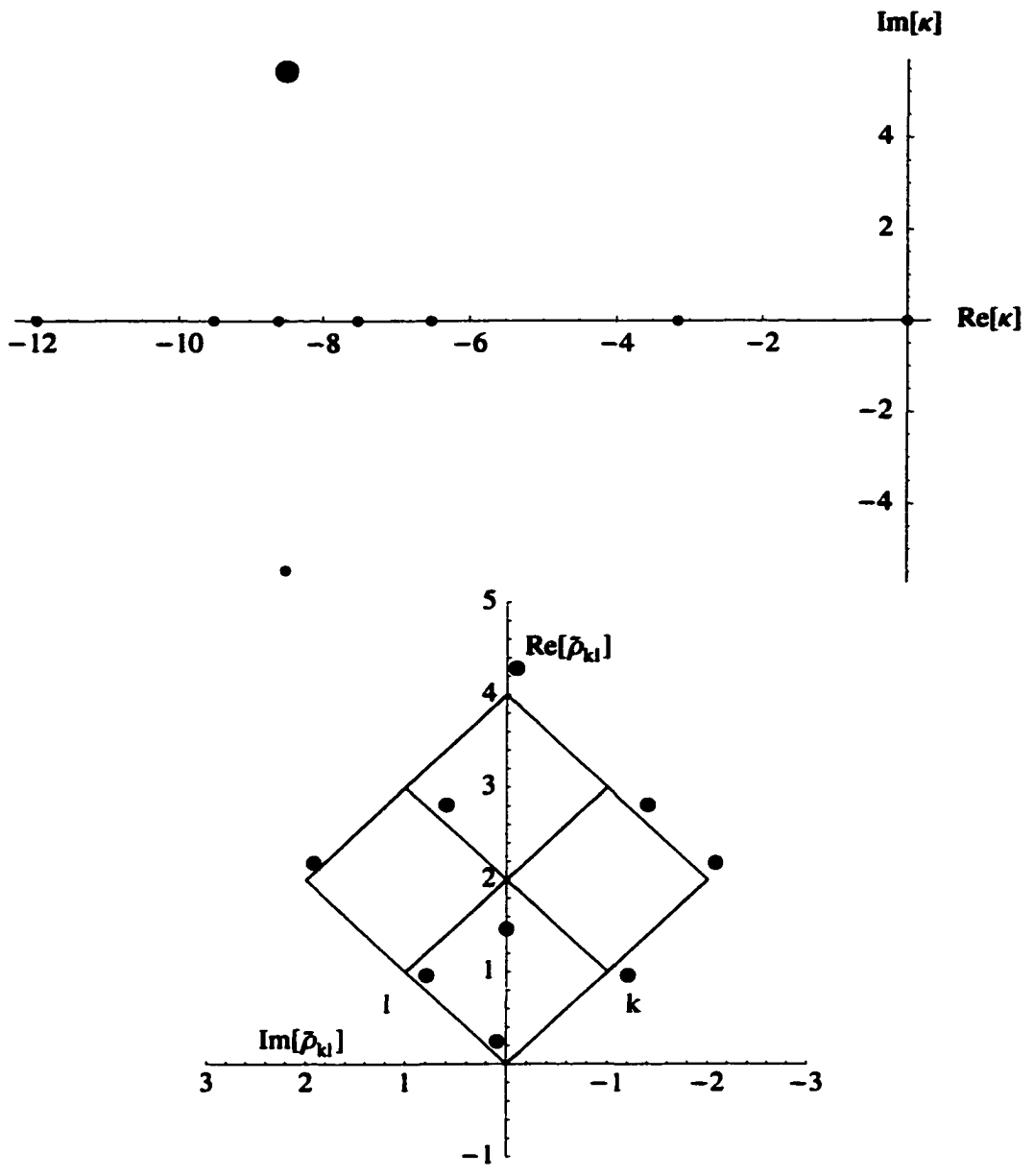

Figure 42: On the top the κ's, highlighted the one corresponding to the normal mode pictured on the bottom. Since Reκ < 0, this normal mode decays over time.

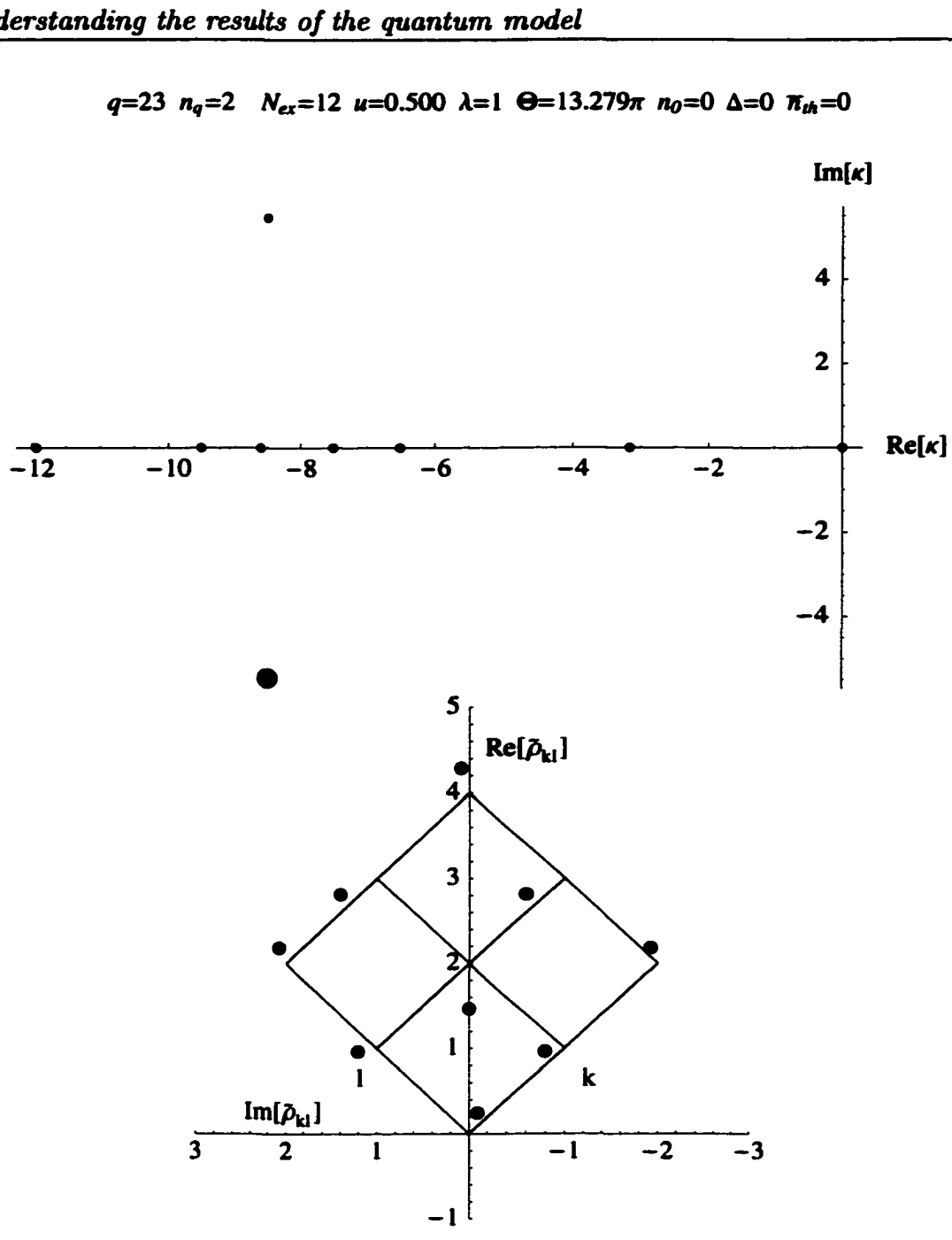

Figure 43: On the top the κ's, highlighted the one corresponding to the normal mode pictured on the bottom. Since Reκ < 0, this normal mode decays over time.

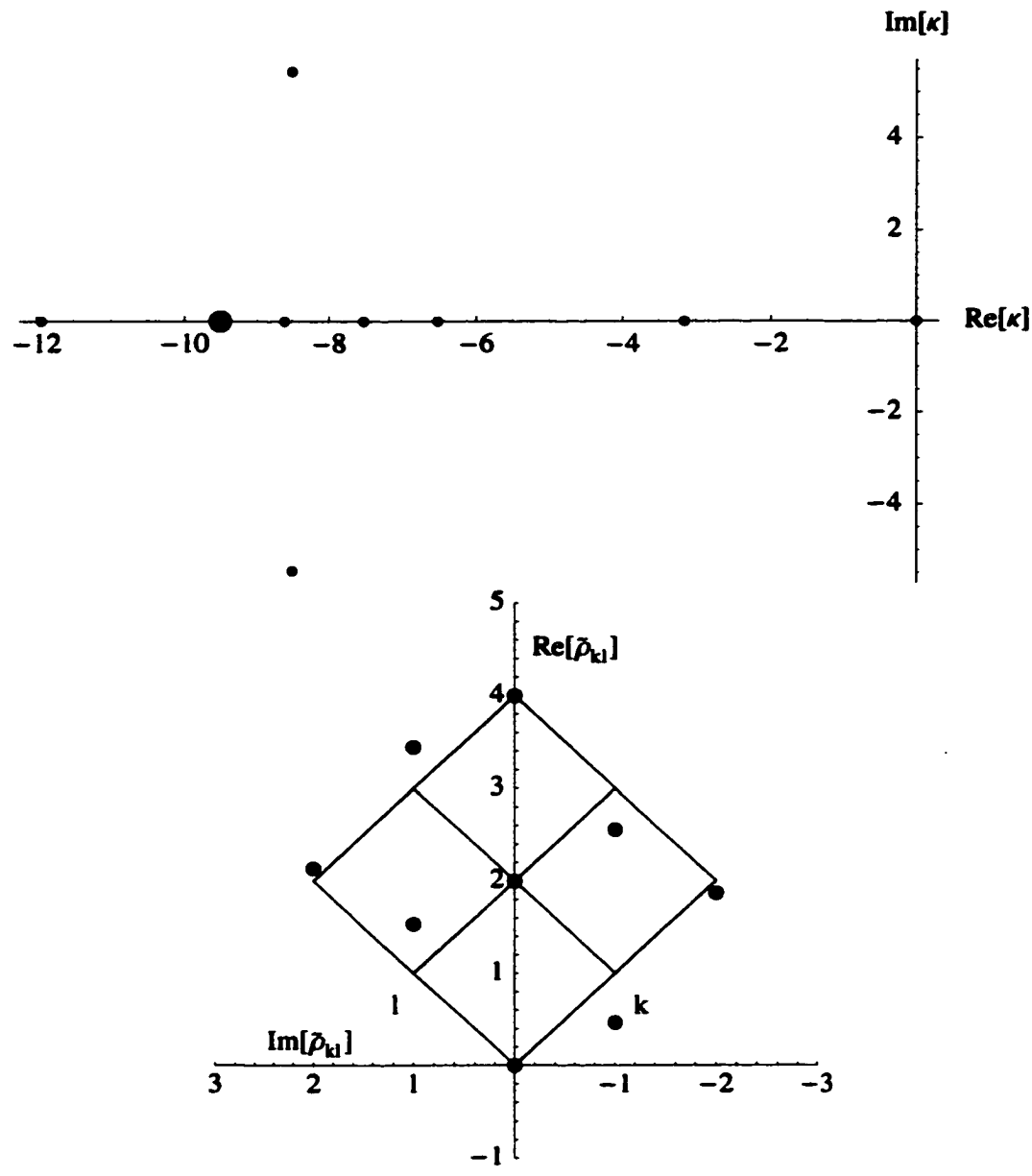

Figure 44: On the top the κ's, highlighted the one corresponding to the normal mode pictured on the bottom. Since Reκ < 0, this normal mode decays over time.

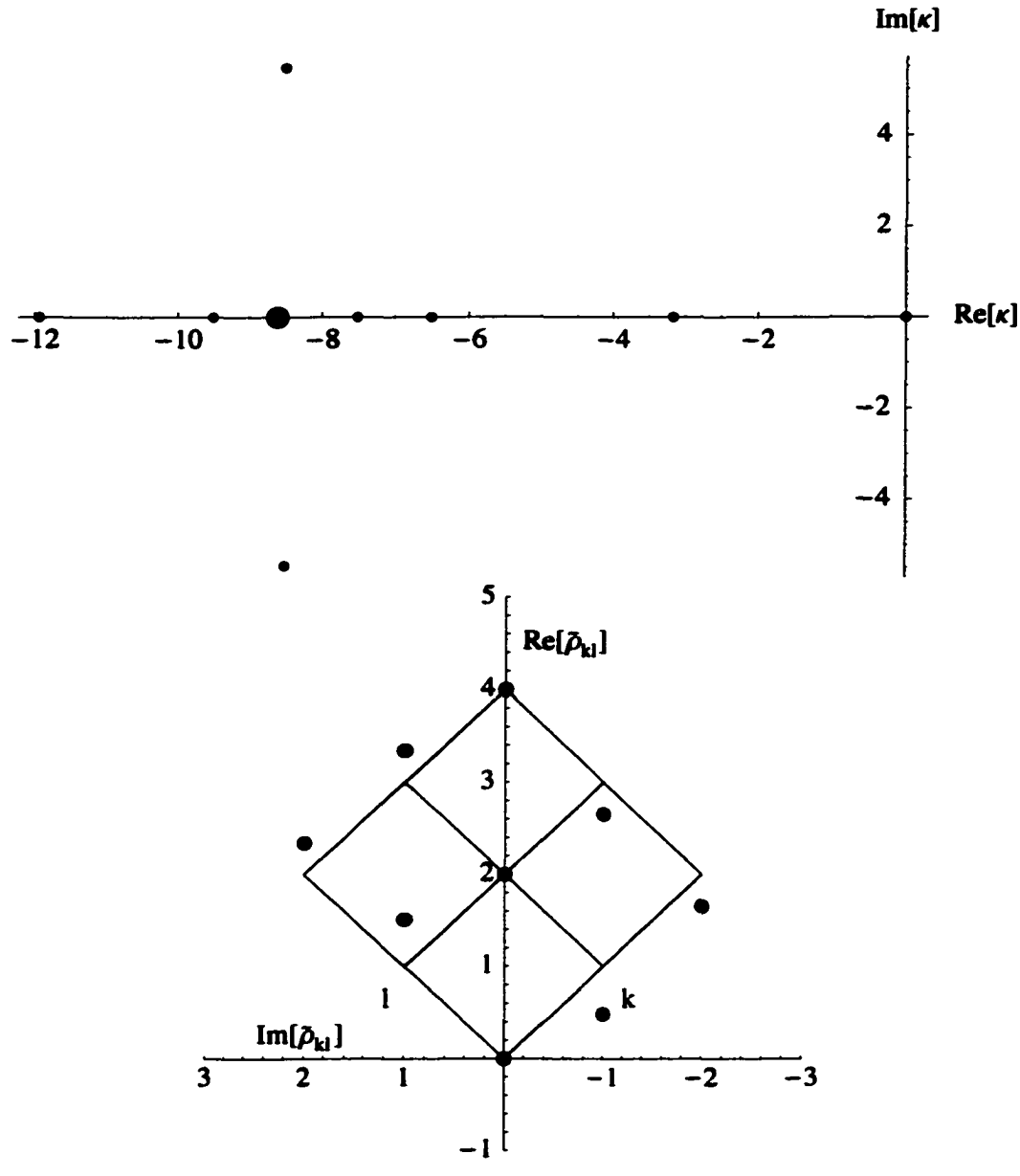

Figure 45: On the top the κ's, highlighted the one corresponding to the normal mode pictured on the bottom. Since Reκ < 0, this normal mode decays over time.

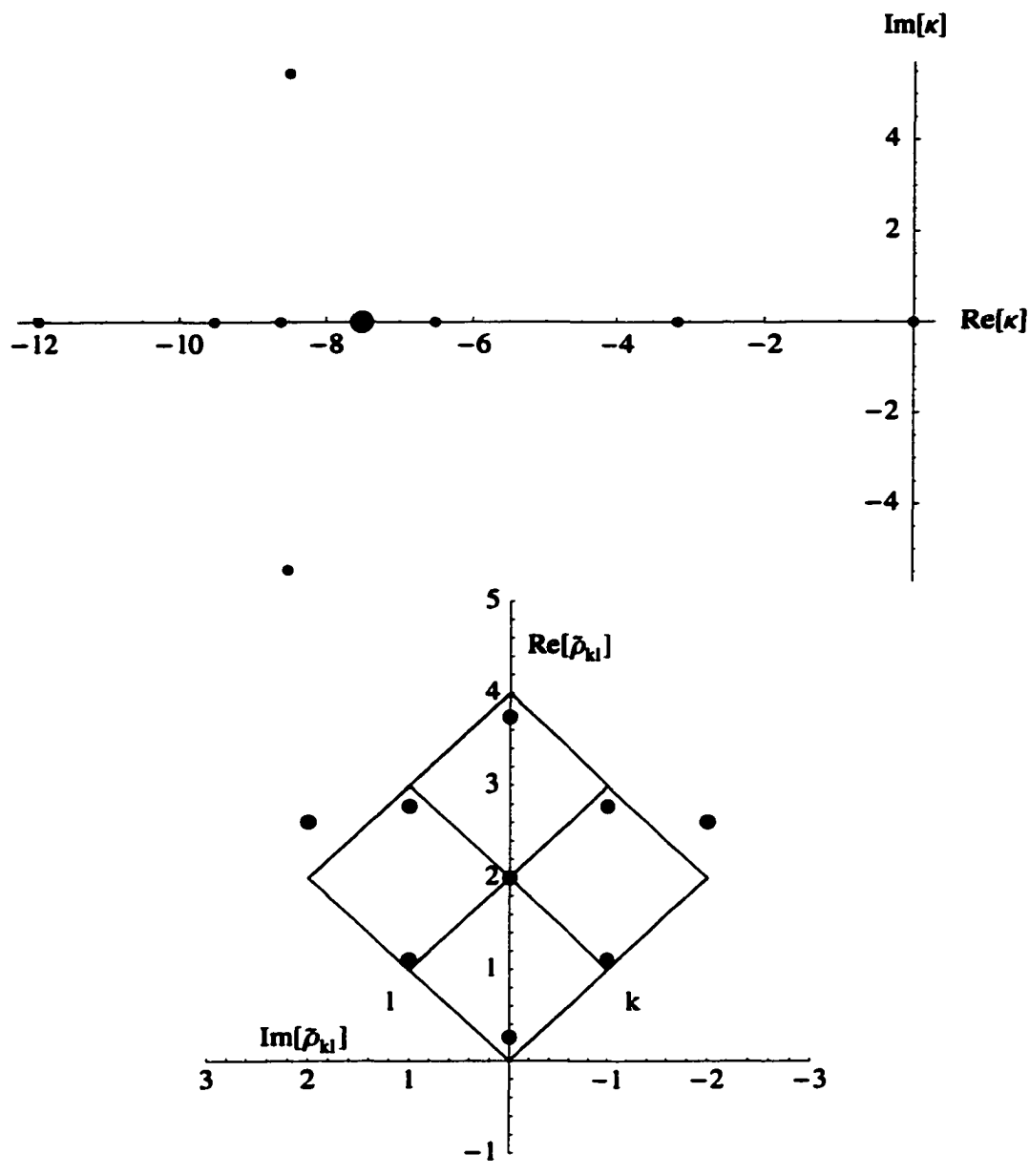

Figure 46: On the top the κ's, highlighted the one corresponding to the normal mode pictured on the bottom. Since Reκ < 0, this normal mode decays over time.

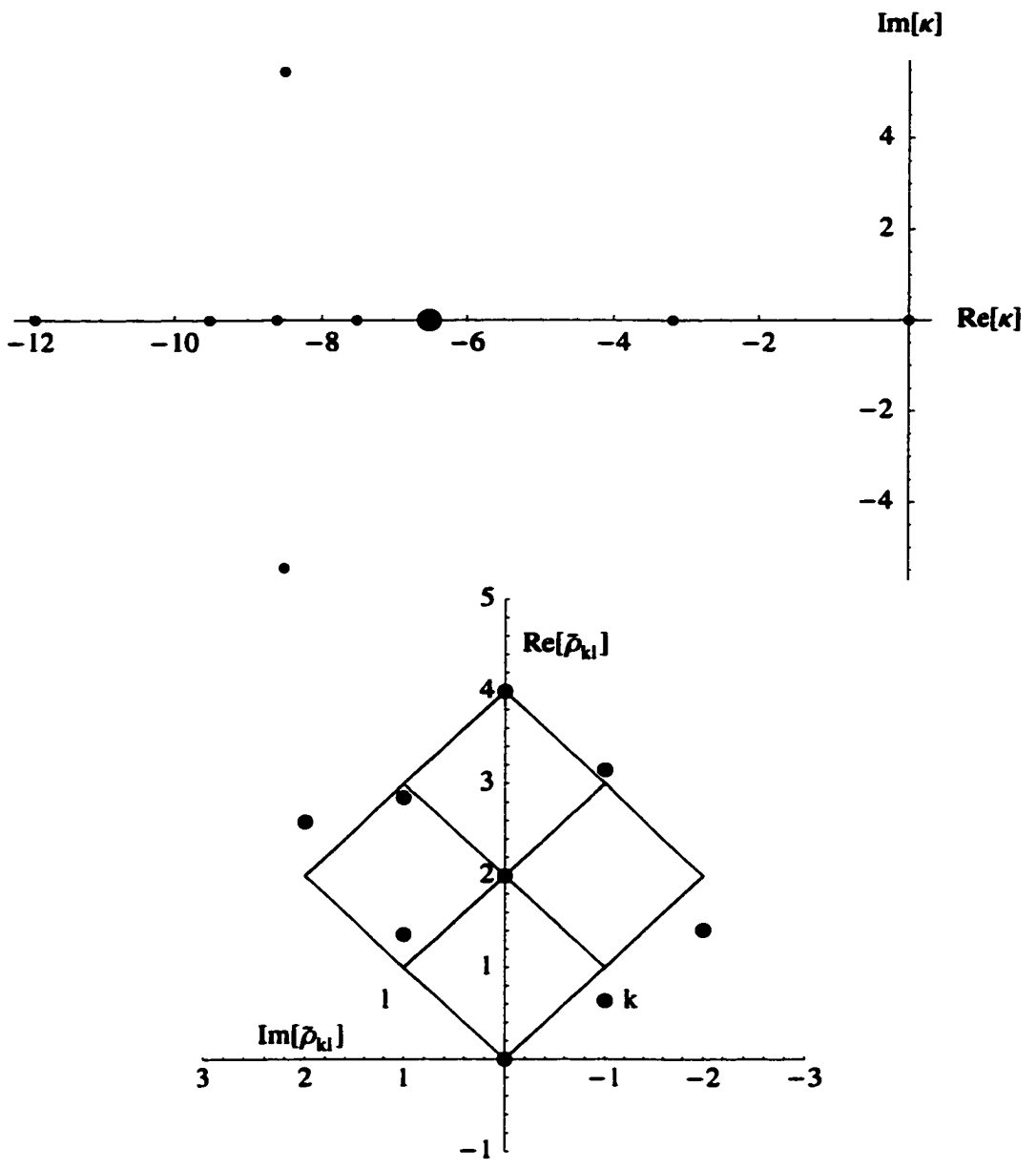

Figure 47: On the top the κ's, highlighted the one corresponding to the normal mode pictured on the bottom. Since Re$\kappa < 0$, this normal mode decays over time.

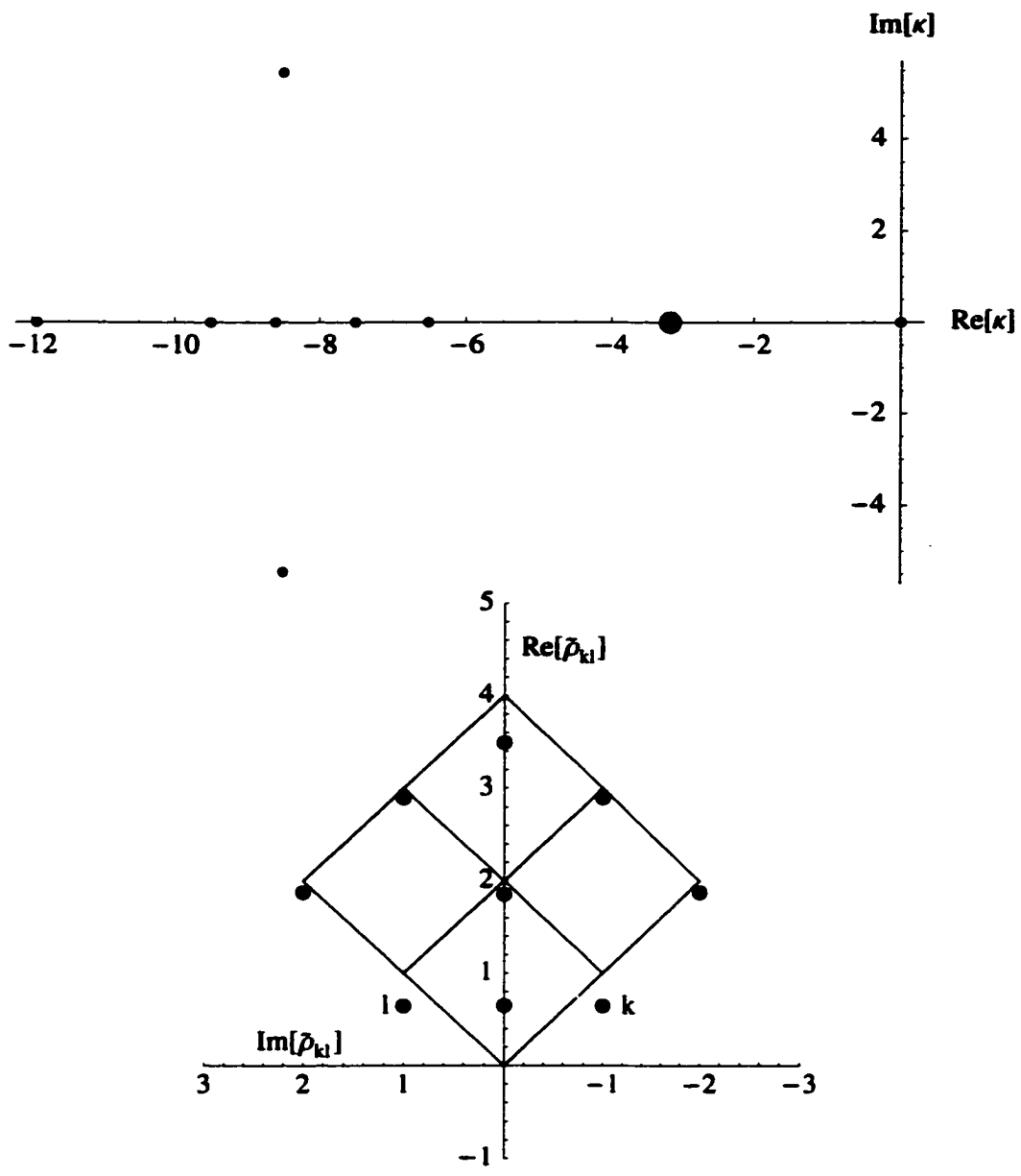

Figure 48: On the top the κ's, highlighted the one corresponding to the normal mode pictured on the bottom. Since Reκ < 0, this normal mode decays over time.

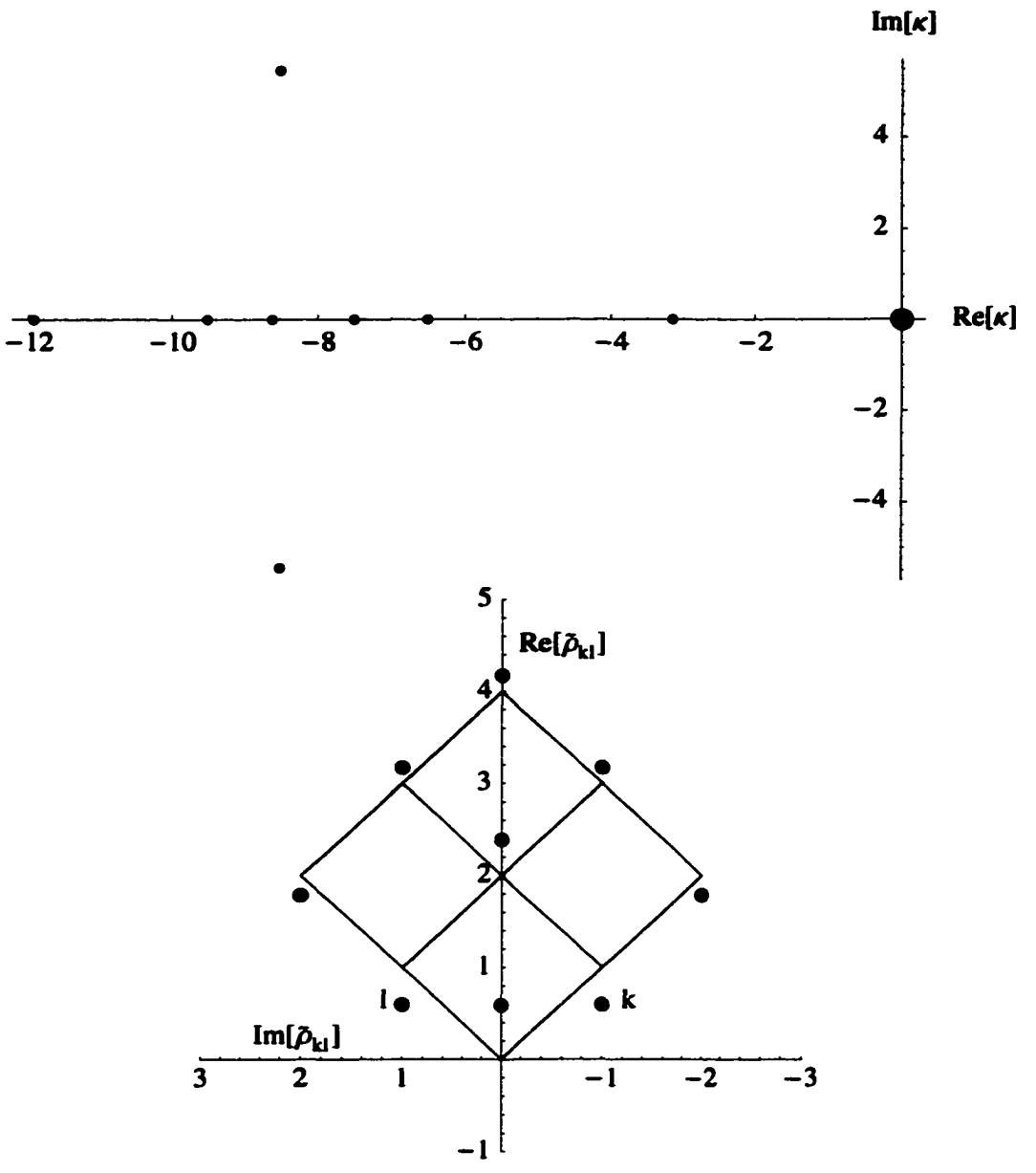

Figure 49: On the top the κ's, highlighted the one corresponding to the normal mode pictured on the bottom. Since Re$\kappa = 0$, this normal mode forms the steady state of the coherently pumped micromaser.

7

Phase density function of the coherently pumped micromaser

In this chapter we focus our attention on the phase properties of the field inside the coherently pumped micromaser in its steady state. First, we review Pegg and Barnett's definition of phase states and the phase distribution function [41], then we derive a general formula which will provide the phase density function describing an ideal phase measurement executed on a state given by the density matrix $\rho(t)$. Using our general result, finally, we will discuss the phase properties of the field inside the cavity of a coherently pumped micromaser.

To start the investigation we have to choose an operator which will represent the phase throughout our calculations. We have chosen the *Pegg-Barnett* Hermitian phase operator for this purpose. The reason behind our decision lies in the fact that the *Pegg-Barnett* phase operator is defined on a truncated Hilbert space. Therefore it is very suitable to describe the phase distribution of micromasers operating under trapping state conditions. Furthermore it is also easy to see from Eq. (5.2) that

$$\left(\frac{\pi}{\Theta}\right)^2 = \frac{n_0^2}{q^2} + \frac{n_q + 1}{q^2}, \tag{7.1}$$

which tells us that even in the case when the interaction phase variable Θ does

not satisfy the trapping state condition we will still be able to find an appropriate trapping state, with interaction phase variable Θ_T such that $|\Theta - \Theta_T| < \varepsilon$, which will. This means we can approximate any state of the field inside the coherently pumped micromaser with an appropriately chosen trapping state. Thus our main goal throughout this chapter will be to describe the phase properties of micromasers operating under trapping state conditions.

Let us review now the basic properties of the *Pegg-Barnett* Hermitian phase operator. It is defined on the truncated $(s+1)$ dimensional Hilbert space as

$$\Phi_{PB} = \sum_{m=0}^{s} \Phi_m |\Phi_m\rangle \langle\Phi_m| , \tag{7.2}$$

where

$$\Phi_m = \Phi_0 + \frac{2\pi m}{s+1}, \tag{7.3}$$

and

$$|\Phi_m\rangle = \frac{e^{ia^\dagger a \Phi_m}}{\sqrt{s+1}} \sum_{n=0}^{s} |n\rangle . \tag{7.4}$$

Φ_0 in Eq. (7.3) designates an arbitrary reference point so that $\Phi_0 \leq \Phi_m < \Phi_0 + 2\pi$. Using the definition of the eigenstates of the *Pegg-Barnett* phase operator, Eq. (7.4), it is easy to show that these states form a complete orthonormal set on the truncated $(s+1)$ dimensional Hilbert space

$$\sum_{m=0}^{s} |\Phi_m\rangle \langle\Phi_m| = \mathbf{1}. \tag{7.5}$$

Using Eq. (7.5), the discrete distribution $P^s_{\Phi_m}$ representing the measurement statistic of Φ_{PB} for systems in the state $\rho(t)$ which is restricted to the $(s+1)$ dimensional

truncated Hilbert space can be obtained from

$$1 = \mathrm{Tr}_{field}[\mathbb{1}\rho(t)] = \sum_{m=0}^{s}\left(\frac{1}{s+1}\sum_{k,l=0}^{s}\rho_{k,l}(t)\mathrm{e}^{-i(k-l)\Phi_m}\right) = \sum_{m=0}^{s}P^{s}_{\Phi_m}(t). \tag{7.6}$$

Thus

$$P^{s}_{\Phi_m}(t) = \frac{1}{s+1}\sum_{k,l=0}^{s}\rho_{k,l}(t)\mathrm{e}^{-i(k-l)\Phi_m} \tag{7.7}$$

is the probability of obtaining Φ_m as the result of a measurement of Φ_{PB} on a system in the state $\rho(t)$. Using the fact that $\rho(t)$ is restricted to the $(s+1)$ dimensional truncated Hilbert space and therefore $\rho_{k,l}(t) = 0$ for all $k > s$ or $l > s$ indexes we now extend the upper limit of the summation over k and l to ∞ in Eq. (7.7) and simplify $P^{s}_{\Phi_m}(t)$ to

$$P^{s}_{\Phi_m}(t) = \frac{1}{s+1}\sum_{N=-\infty}^{\infty}\rho_N(t)\mathrm{e}^{-iN\Phi_m}. \tag{7.8}$$

Here we introduced the following quantities

$$\rho_N(t) = \begin{cases}\displaystyle\sum_{k=N}^{\infty}\rho_{k,k-N}(t) & \text{for } N = 0,1,2,\ldots \\ \displaystyle\sum_{k=0}^{\infty}\rho_{k,k-N}(t) & \text{for } N = -1,-2,\ldots.\end{cases} \tag{7.9}$$

They represent the sum of the elements in the Nth diagonal of $\rho(t)$ ($N > 0$ for diagonals below the main diagonal, $N < 0$ for diagonals above the main diagonal and $N = 0$ refers to the main diagonal). From the definition Eq. (7.9) it is also clear that

$$(\rho_N(t))^* = \rho_{-N}(t), \tag{7.10}$$

and since $\rho(t)$ is normalized

$$\rho_0(t) = 1. \tag{7.11}$$

We would expect now that in order to obtain the Hermitian phase operator valid in the infinite dimensional Hilbert space we only need to take the limit $s \to \infty$ in Eqs. (7.2) and (7.4). However, in this limit the *Pegg-Barnett* phase operator, Eq. (7.2), does not converge to an Hermitian phase operator but the discrete phase distribution determined by it and given in Eq. (7.8) does converge to a probability density function $P(\Phi, t)$ where

$$\Phi = \lim_{s\to\infty} \Phi_m \tag{7.12}$$

and $\Phi_0 \leq \Phi \leq \Phi_0 + 2\pi$. To determine the actual form of $P(\Phi, t)$ let us use that, since $P^s_{\Phi_m}(t)$ was properly normalized, $P(\Phi, t)$ should be normalized as well, thus

$$\begin{aligned} 1 = \lim_{s\to\infty} \sum_{m=0}^{s} P^s_{\Phi_m}(t) &= \lim_{s\to\infty} \sum_{m=0}^{s} \left(\frac{1}{2\pi} \sum_{N=-\infty}^{\infty} \rho_N(t) \mathrm{e}^{-iN\Phi_m} \right) \left(\frac{2\pi\Delta m}{s+1} \right) \\ &= \int_{\Phi_0}^{\Phi_0+2\pi} P(\Phi, t) d\Phi. \end{aligned} \tag{7.13}$$

From Eq. (7.13) now we can read out the probability density function $P^s_{\Phi_m}(t)$ converges to, in the limit $s \to \infty$, namely

$$\begin{aligned} P(\Phi, t) &= \frac{1}{2\pi} \sum_{N=-\infty}^{\infty} \rho_N(t) \mathrm{e}^{-iN\Phi} \\ &= \frac{1}{2\pi} + \frac{1}{\pi} \sum_{N=1}^{\infty} \Big(\rho_N^{\mathrm{Re}}(t) \cos(N\Phi) + \rho_N^{\mathrm{Im}}(t) \sin(N\Phi) \Big), \end{aligned} \tag{7.14}$$

where ρ_N^{Re} (ρ_N^{Im}) denotes the real (imaginary) part of ρ_N. The probability density function given in Eq. (7.14) is defined now for all phase values in the $[\Phi_0, \Phi_0 + 2\pi]$ interval and represents the measurement statistic of an optimal phase measurement executed on a system in the state $\rho(t)$ which is not necessarily restricted to the truncated Hilbert space any longer. This also means the probability of obtaining a

phase value at time $t = t'$ which falls between Φ and $\Phi + d\Phi$ is equal to $P(\Phi, t')d\Phi$. It can also be easily shown that Eq. (7.14) represents the probability density function corresponding to the *Susskind-Glogower* non Hermitian phase operator [42] which is defined as

$$e^{i\Phi_{SG}} = \frac{1}{\sqrt{aa^\dagger}}a. \tag{7.15}$$

The probability density function, $P(\Phi, t)$, in Eq. (7.14) is defined by a Fourier series, hence $P(\Phi, t)$ has to have only a finite number of finite discontinuities and only a finite number of extrema. In other words $P(\Phi, t)$ must be a piecewise regular function. Furthermore, from Eq. (7.14) we see that we can extend the definition of $P(\Phi, t)$ to arbitrary Φ values outside the $[\Phi_0, \Phi_0 + 2\pi]$ interval and obtain a periodic probability density function valid for all phase values. However, caution must be taken using the periodic probability density function. In the case when we evaluate the moments of $P(\Phi, t)$ we must always restrict its domain to a 2π interval. This interval, however, can be chosen arbitrarily. The characteristic function $f(k, t)$ corresponding to the periodic probability density function $P(\Phi, t)$ can also be determined (for further reference on the characteristic functions see [35]). Using its definition,

$$f(k,t) = \langle e^{ik\Phi} \rangle = \int_{-\infty}^{\infty} P(\Phi, t) e^{ik\Phi} d\Phi = \sum_{N=-\infty}^{\infty} \rho_N(t)\delta(k - N). \tag{7.16}$$

From here we see the role of the diagonal sums. For the non-periodic probability density function (restricted to $[\Phi_0, \Phi_0 + 2\pi]$) the relationship is even more obvious

$$f_k = \rho_k(t) \qquad k = \ldots, -2, -1, 0, 1, 2, \ldots. \tag{7.17}$$

Here now the characteristic function is defined only for discrete values of k and it

is equal to the diagonal sums. Using $P(\Phi,t)$, the expectation value of the phase operator can be given as

$$\langle \Phi_{PB} \rangle = \lim_{s\to\infty} \mathrm{Tr}_{field}[\rho(t)\Phi_{PB}] = \int_{\Phi_0}^{\Phi_0+2\pi} \Phi P(\Phi,t)d\Phi = \langle \Phi \rangle, \tag{7.18}$$

and similarly the variance of the phase operator can be written as

$$V(\Phi_{PB}) = V(\Phi) = \left\langle \left(\Phi - \langle\Phi\rangle\right)^2 \right\rangle = \int_{\Phi_0}^{\Phi_0+2\pi} \left(\Phi - \langle\Phi\rangle\right)^2 P(\Phi,t)d\Phi. \tag{7.19}$$

To summarize, we can say that an optimal phase measurement executed on a system in the state $\rho(t)$ would result in the probability density function $P(\Phi,t)$, the mean value $\langle\Phi\rangle$, and the variance $V(\Phi)$, defined by Eqs. (7.14), (7.18) and (7.19), respectively. To complete our general results now we determine the probability density function corresponding to a relative phase measurement. Let us suppose that we have a signal designating a reference phase Φ_A and we are looking for the probability density function $\bar{P}(\Phi_R,t)$ corresponding to the measurement of the relative phase

$$\Phi_R = \Phi - \Phi_A \tag{7.20}$$

given by the difference between the phase of the micromaser's field and our reference signal's phase. Using the general rule of transforming probability density functions we obtain $\bar{P}(\Phi_R,t)$ from $P(\Phi,t)$ as

$$\bar{P}(\Phi_R,t) = \langle \delta\left(\Phi_R - (\Phi - \Phi_A)\right)\rangle = \int_{-\infty}^{\infty} \delta\left(\Phi_R - (\Phi - \Phi_A)\right) P(\Phi,t)d\Phi. \tag{7.21}$$

Next, based on the general results we have discussed so far, we will determine the probability density function $P(\Phi,\beta,t)$ corresponding to the optimal phase measurement on the state of the field given by Eq. (2.37). Then we will identify a

'natural' reference signal in our model and determine the probability density function $\bar{P}(\Phi_R, \beta, t)$ corresponding to the relative phase measurement where now Φ_A is the phase of the reference signal. Finally we will determine the phase density function $\bar{P}_S(\Phi_R, \beta)$ corresponding to the relative phase measurement on the steady state of the field and calculate the values of $\langle \Phi_R \rangle$ and $V(\Phi_R)$ in this state. From Eq. (2.37), the density matrix describing the field inside of a coherently pumped micromaser at time t' can be given as

$$\bar{\rho}(\beta, t') = \mathrm{e}^{-i a^\dagger a(\frac{\nu}{\Gamma}t' + \varphi_g - \varphi_{ab} + \pi/2)} \tilde{\rho}(\beta, t') \mathrm{e}^{i a^\dagger a(\frac{\nu}{\Gamma}t' + \varphi_g - \varphi_{ab} + \pi/2)}, \tag{7.22}$$

where $\tilde{\rho}(\beta, t')$ represents the slowly varying part of the field density matrix. Now substituting $\bar{\rho}(\beta, t')$ in Eq. (7.6) as $\rho(t)$ and using the relation

$$\mathrm{e}^{i a^\dagger a(\frac{\nu}{\Gamma}t' + \varphi_g - \varphi_{ab} + \pi/2)} |\Phi_m\rangle = \left| \Phi_m + \frac{\nu}{\Gamma}t' + \varphi_g - \varphi_{ab} + \pi/2 \right\rangle, \tag{7.23}$$

we obtain the periodic probability density function corresponding to an optimal phase measurement on a system in the state $\bar{\rho}(\beta, t')$ as

$$P(\Phi, \beta, t') = \frac{1}{2\pi} \sum_{N=-\infty}^{\infty} \tilde{\rho}_N(\beta, t') \mathrm{e}^{-iN\left(\Phi + \frac{\nu}{\Gamma}t' + \varphi_g - \varphi_{ab} + \pi/2\right)}. \tag{7.24}$$

In the argument of the exponential one can recognize the phase carried by the atoms entering into the micromaser cavity, namely

$$-\left(\frac{\nu}{\Gamma}t' + \varphi_g - \varphi_{ab}\right). \tag{7.25}$$

Borrowing the term from the theory of the classical forced oscillations, we could say that the incoming atoms represent the 'driving force' on our system which, in

turn, is represented by the field inside the micromaser cavity. Therefore it would be useful, just like in the classical case, to describe the phase of our system with respect to the phase of this 'driving force', Eq. (7.25). This description in quantum mechanics is given by the probability density function $\bar{P}(\Phi_R, \beta, t)$ corresponding to the measurement statistic of the relative phase,

$$\Phi_R = \Phi - \Phi_A = \Phi + \frac{\nu}{\Gamma}t' + \varphi_g - \varphi_{ab}. \tag{7.26}$$

Using Eqs. (7.24) and (7.21), now we obtain this probability density function as

$$\begin{aligned}\bar{P}(\Phi_R, \beta, t) &= \frac{1}{2\pi}\sum_{N=-\infty}^{\infty}\tilde{\rho}_N(\beta, t')\mathrm{e}^{-iN(\Phi_R+\pi/2)} \\ &= \frac{1}{2\pi} + \frac{1}{\pi}\sum_{N=1}^{\infty}\Big(\tilde{\rho}_N^{\mathrm{Re}}(\beta, t')\cos(N(\Phi_R + \pi/2)) \\ &+ \tilde{\rho}_N^{\mathrm{Im}}(\beta, t')\sin(N(\Phi_R + \pi/2))\Big).\end{aligned} \tag{7.27}$$

In order to calculate the proper moments corresponding to $\bar{P}(\Phi_R, \beta, t)$, we now restrict Φ_R to the $[-\pi, \pi]$ symmetric interval. In this case the expectation value of the relative phase measurement can be given as

$$\begin{aligned}\langle\Phi_R\rangle &= \int_{-\pi}^{\pi}\Phi_R\bar{P}(\Phi_R, \beta, t)d\Phi_R \\ &= 2\sum_{N=1}^{\infty}\mathrm{Re}\left[\tilde{\rho}_N(\beta, t')\frac{i^{N+1}}{N}\right] \\ &= -2\sum_{N=1}^{\infty}\left(\tilde{\rho}_N^{\mathrm{Re}}(\beta, t')\frac{\sin(N\pi/2)}{N} + \tilde{\rho}_N^{\mathrm{Im}}(\beta, t')\frac{\cos(N\pi/2)}{N}\right).\end{aligned} \tag{7.28}$$

Roughly speaking the value of $|\langle\Phi_R\rangle|$ gives us by how much the phase of the field inside the cavity is behind ($\langle\Phi_R\rangle > 0$) or ahead ($\langle\Phi_R\rangle < 0$) of the phase of the

injected atoms, on the average. The variance corresponding to this measurement can also be calculated, yielding

$$\begin{aligned} V(\Phi_R) &= \langle \Phi_R^2 \rangle - \langle \Phi_R \rangle^2 \\ &= \frac{\pi^2}{3} + 4\sum_{N=1}^{\infty} \mathrm{Re}\left[\tilde{\rho}_N(\beta,t')\frac{i^N}{N^2}\right] - \left(2\sum_{N=1}^{\infty} \mathrm{Re}\left[\tilde{\rho}_N(\beta,t')\frac{i^{N+1}}{N}\right]\right)^2 \\ &= \frac{\pi^2}{3} + 4\sum_{N=1}^{\infty}\left(\tilde{\rho}_N^{\mathrm{Re}}(\beta,t')\frac{\cos(N\pi/2)}{N^2} - \tilde{\rho}_N^{\mathrm{Im}}(\beta,t')\frac{\sin(N\pi/2)}{N^2}\right) \\ &\quad - \left(-2\sum_{N=1}^{\infty}\left(\tilde{\rho}_N^{\mathrm{Re}}(\beta,t')\frac{\sin(N\pi/2)}{N} + \tilde{\rho}_N^{\mathrm{Im}}(\beta,t')\frac{\cos(N\pi/2)}{N}\right)\right)^2 . \end{aligned} \tag{7.29}$$

To complete this chapter now we will determine the probability density function corresponding to the relative phase measurement on the steady state of the field. Taking the limit $t' \to \infty$ in Eq. (7.27), we obtain

$$\begin{aligned} \tilde{P}_S(\Phi_R,\beta) &= \frac{1}{2\pi}\lim_{t'\to\infty}\sum_{N=-\infty}^{\infty}\tilde{\rho}_N(\beta,t')\mathrm{e}^{-iN(\Phi_R+\pi/2)} \\ &= \frac{1}{2\pi} + \frac{1}{\pi}\lim_{t'\to\infty}\sum_{N=1}^{\infty}\Big(\tilde{\rho}_N^{\mathrm{Re}}(\beta,t')\cos\big(N(\Phi_R+\pi/2)\big) \\ &\quad + \tilde{\rho}_N^{\mathrm{Im}}(\beta,t')\sin\big(N(\Phi_R+\pi/2)\big)\Big). \end{aligned} \tag{7.30}$$

Here we did not exchange the limit and the infinite sum operations yet because we have to discuss under what conditions we are allowed to do that. In general, we know the limit and the infinite sum operations can be exchanged only if the series is uniformly convergent. However, the conditions so far, imposed on the general probability density functions ($P(\Phi,t)$) in order to make Eq. (7.14) valid, are far less restrictive. They allow functions with finite number of finite discontinuities to be present. Thus, we should not expect Eq. (7.27) to be uniformly convergent since a uniformly convergent series of continuous functions ($\sin(N\Phi_R)$, $\cos(N\Phi_R)$) would always yield a

continuous function. Therefore in the following we restrict the possible probability density functions, describing phase measurement statistics, to those which are continuous and differentiable, assuring that the Fourier series in Eq. (7.27) is always uniformly convergent. In particular, the phase probability density functions corresponding to trapping states always satisfy these conditions. Then we can exchange the limit and the infinite sum operation in Eq. (7.30) and obtain

$$\begin{aligned}\bar{P}_S(\Phi_R,\boldsymbol{\beta}) &= \frac{1}{2\pi}\sum_{N=-\infty}^{\infty}\left(\tilde{\rho}_S(\boldsymbol{\beta})\right)_N e^{-iN(\Phi_R+\pi/2)} \\ &= \frac{1}{2\pi}+\frac{1}{\pi}\sum_{N=1}^{\infty}\Big(\left(\tilde{\rho}_S(\boldsymbol{\beta})\right)_N^{\mathrm{Re}}\cos\big(N(\Phi_R+\pi/2)\big) \\ &+ \left(\tilde{\rho}_S(\boldsymbol{\beta})\right)_N^{\mathrm{Im}}\sin\big(N(\Phi_R+\pi/2)\big)\Big), \end{aligned} \tag{7.31}$$

where $\left(\tilde{\rho}_S(\boldsymbol{\beta})\right)_N$ represents the steady state value of the Nth diagonal sum and it is given by Eq. (4.68). The probability density function in Eq. (7.31) therefore gives us the measurement statistic of the optimal relative phase (Φ_R) measurement executed on the steady state of the field corresponding to the configuration vector $\boldsymbol{\beta}$. In the case of the incoherent pumping the steady state values of the off-diagonal sums can be given as

$$\left(\tilde{\rho}_S(\boldsymbol{\beta})\right)_N = 0 \qquad N = 1,2,\ldots, \tag{7.32}$$

therefore the phase density function reduces to $\bar{P}_S(\Phi',\boldsymbol{\beta}) = \frac{1}{2\pi}$. This represents uniformly distributed phase over the $[-\pi,\pi]$ interval. This also means the phase of an incoherently pumped micromaser is completely undetermined. Finally, using Eq. (7.31), we determine the mean value and the variance associated with the optimal relative phase (Φ_R) measurement performed on the steady state of the field. These

values can be easily obtained from Eqs. (7.28) and (7.29), respectively, by replacing the diagonal sums $\tilde{\rho}_N(\beta, t')$ in the equations with their steady state value $\left(\tilde{\rho}_S(\beta)\right)_N$. In the case of the incoherent pumping these values reduce to

$$\langle \Phi_R \rangle = 0, \tag{7.33a}$$

$$V(\Phi_R) = \frac{\pi^2}{3}, \tag{7.33b}$$

which are again the characteristics of a state with uniformly distributed phase.

In the next chapter we will examine how the phase properties of the steady state field, we discussed in this chapter, depend on the configuration vector β.

8

Study of the phase of a coherently pumped micromaser in steady state

In this chapter our goal is to understand how the probability density function corresponding to an optimal relative phase measurement on the steady state of the field depends on the configuration vector of the model $\boldsymbol{\beta}$. Especially we are interested in how the phase of the steady state field depend on the two parameter, λ and Δ, which are exclusive to the coherent pumping. First, however, we briefly recall the steady state of a classical forced oscillation as a reference for our investigation (see for example [37]). The equation of motion describing a classical forced oscillator is given by

$$\frac{d^2z}{dt^2} + \frac{\Gamma}{2}\frac{dz}{dt} + \omega_0^2 z = f_0 \mathrm{e}^{-i\nu t} \tag{8.1}$$

where z represents the complex amplitude and ω_0 is the eigenfrequency of the driven system. Furthermore ν is the frequency and f_0 the complex amplitude of the external driving force and $\Gamma > 0$ is the damping constant, describing the energy dissipation of the system. To be in accordance with our quantum mechanical model let us now

rescale the time according to Eq. (2.41) and rewrite Eq. (8.1) as

$$\frac{d^2z}{dt'^2} + \frac{1}{2}\frac{dz}{dt'} + \left(\frac{\omega_0}{\Gamma}\right)^2 z = \frac{f_0}{\Gamma^2}e^{-i\frac{\nu}{\Gamma}t'}. \tag{8.2}$$

The steady state solution of Eq. (8.2) is well known and can be given in the following form

$$z_S(t) = Ae^{-i(\nu t-\varphi')}, \tag{8.3}$$

where A, the complex amplitude of the steady state oscillation, is given by

$$A = \frac{f_0}{\sqrt{(\omega_0^2-\nu^2)^2 + \left(\frac{\Gamma\nu}{2}\right)^2}} \tag{8.4}$$

and φ', the phase shift of the driven system relative to the phase of the driving, is given by

$$\varphi' = \mathrm{Arg}\left[(\omega_0^2-\nu^2) + i\frac{\Gamma}{2}\nu\right]. \tag{8.5}$$

From Eq. (8.5) we can see that the phase shift, in the case of the classical forced oscillations, is always between 0 and π,

$$0 \leq \varphi' \leq \pi. \tag{8.6}$$

Introducing Δ, as in Eq. (2.47), we can rewrite the phase shift in the following form

$$\varphi' = \mathrm{Arg}\left[\Delta\left(\Delta + 2\frac{\nu}{\Gamma}\right) + i\frac{\nu}{2\Gamma}\right], \tag{8.7}$$

which contains no approximations. In Eq. (8.7) since $\nu \geq 0$ and $\omega_0 \geq 0$

$$-\frac{\nu}{\Gamma} \leq \Delta. \tag{8.8}$$

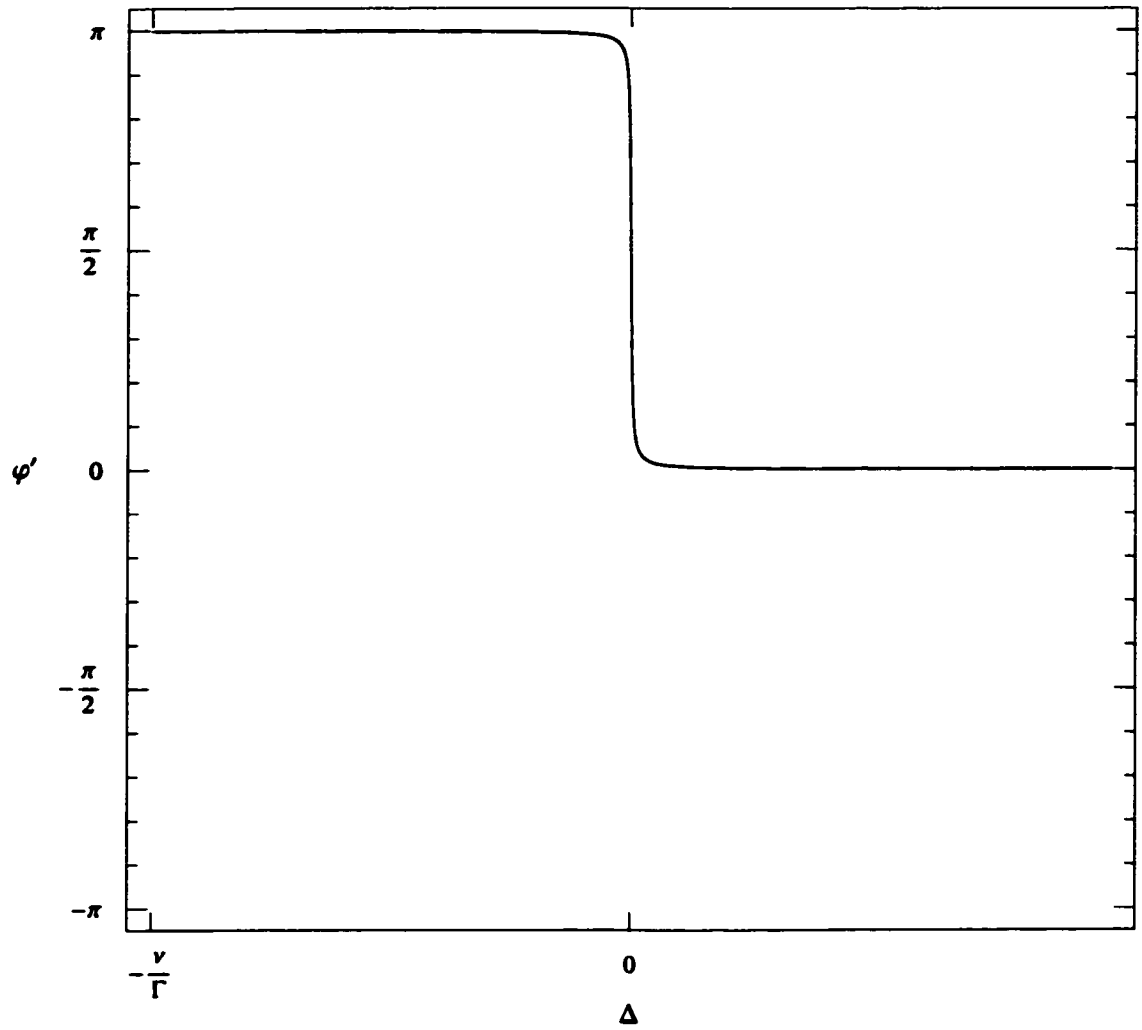

Figure 50: The phase shift of the driven classical oscillator relative to the phase of the driving is a function of Δ for a fixed value of the $\frac{\nu}{\Gamma}$ parameter.

Please note that φ' is only the function of two parameters Δ and $\frac{\nu}{\Gamma}$ thus it can be written as $\varphi'\left(\Delta, \frac{\nu}{\Gamma}\right)$. For a fixed value of the $\frac{\nu}{\Gamma}$ parameter this function $\varphi'\left(\Delta, \frac{\nu}{\Gamma} = \text{const.}\right)$ is displayed in Fig. 50. From the figure we can see the most important features of the driven classical oscillator's phase, namely that it makes a quick transition from π to 0 around $\Delta = 0$ and has the value of $\frac{\pi}{2}$ at $\Delta = 0$. In the following we will address the question whether these simple features, describing the phase of a classical forced

oscillation, can be still observed in the quantum case.

To answer this and the more general question we started this section with, now we will study the phase properties of the steady state formed in a coherently pumped micromaser. Before we proceed any further however, we recall that the relative phase of the steady state field— unlike in the classical case—now can not be given by a single parameter φ'. Rather, it is given by a probability density function $\bar{P}_S(\Phi_R, \boldsymbol{\beta})$, shown in Eq. (7.31). In addition, $\bar{P}_S(\Phi_R, \boldsymbol{\beta})$ represents the measurement statistic of an optimal relative phase measurement executed on the steady state of the field. To plot $\bar{P}_S(\Phi_R, \boldsymbol{\beta})$, however, we would need to draw a surface over the 7 dimensional region spanned by Φ_R and $\boldsymbol{\beta}$. Since we can only draw 3 dimensional diagrams we will be able to see only certain projections of this hyper surface, determined by $\bar{P}_S(\Phi_R, \boldsymbol{\beta})$. The most important projections will be those 3-dimensional surfaces which are drawn over any 2 dimensional region spanned by Φ_R and a component β_i (either N_{ex}, u, λ, Θ, n_0 or Δ) of the parameter vector $\boldsymbol{\beta}$. We will show these $\bar{P}_S(\Phi_R, \beta_i)$ surfaces throughout this chapter by drawing a contour plot of them on which we will also indicate the exact positions of the local and global maxima and minima of the $\bar{P}_S(\Phi_R, \beta_i = \text{const.})$ function. The positions of the local (global) minima will be indicated by small (big) black dots, the maxima will be shown similarly but with white dots instead of black ones. Also shown on the contour graphs are the position and the value of the maximum and the minimum of the plotted region of $\bar{P}_S(\Phi_R, \beta_i)$. Furthermore in each graph we will also provide the constant values of the remaining parameters of the model and the value of $\mathrm{Tr}\,[\vec{\rho}^2]$ indicating the purity of the steady

state. We discuss two examples here, in both examples we maximize the atomic coherence injected into the micromaser cavity by requiring Eq. (2.49). We used the value $\frac{\Gamma}{2|g|} = 6.25 \times 10^{-5}$ based on the parameters of most recent experiments.

In the first example we show that the injected atomic coherence creates multistability. In Figs. 51 and 52 we present a system which locks its phase to $\frac{\pi}{2}$ for small values of λ, this indicates unique selection of phase for small values of the injected atomic coherence. Increasing the injected atomic coherence, however, leads to the splitting of the phase density function as we can see in Fig. 51. The explanation based on the semiclassical theory, chapter 3, is the following, as we increase λ we create stable points of n and $|\hat{\varepsilon}|^2$ which belong to different phase locking values. The quantum mechanical solution which is the coherent superposition of all phase locking scheme, therefore, has a multiple peaked phase density function. Also, please note in Figs. 53–56 the case of the off-resonant pumping ($\Delta \neq 0$). In this case the symmetry of the phase density function, present while $\Delta = 0$, is broken. Selecting the sign of Δ, in the case of the off-resonant pumping, means selecting a specific branch of the phase density function pictured in Figs. 53 and 55.

In our second example we would like to demonstrate how simple features, describing the phase of a classical forced oscillation, can be still observed in the quantum case. In Figs. 57–70 we present the phase density function of a system where we control the atomic inversion. The system shows rich multistable behavior at resonance ($\Delta = 0$). As we increase the detuning ($|\Delta| > 0$) we observe the branch selection we explained above as well as the overall shift of the phase density function. The

direction of the shift follows exactly the same pattern as the relative phase of a classical forced oscillation shown in Fig. 50. Namely, in the case $\Delta < 0$ ($\Delta > 0$) the whole phase density function shifts toward π (0) just as the relative phase of a the classical forced oscillation under the same condition. This is a remarkable feature of the coherently pumped micromaser.

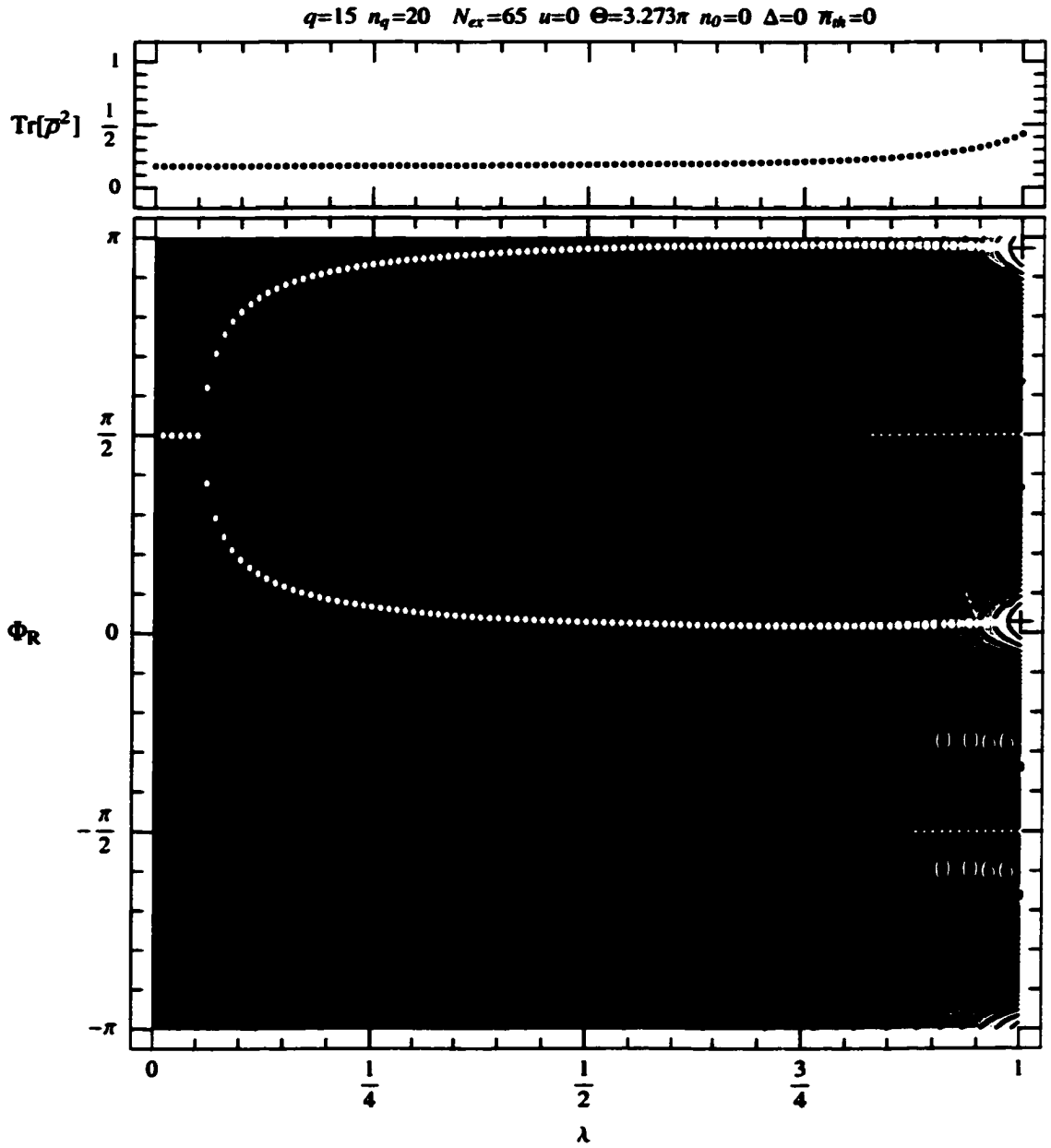

Figure 51: On the top the value of $\mathrm{Tr}\,[\bar{\rho}^2]$ indicating the purity of the steady state. On the bottom is the contour plot of the phase density function $\bar{P}_S(\Phi_R, \lambda)$.

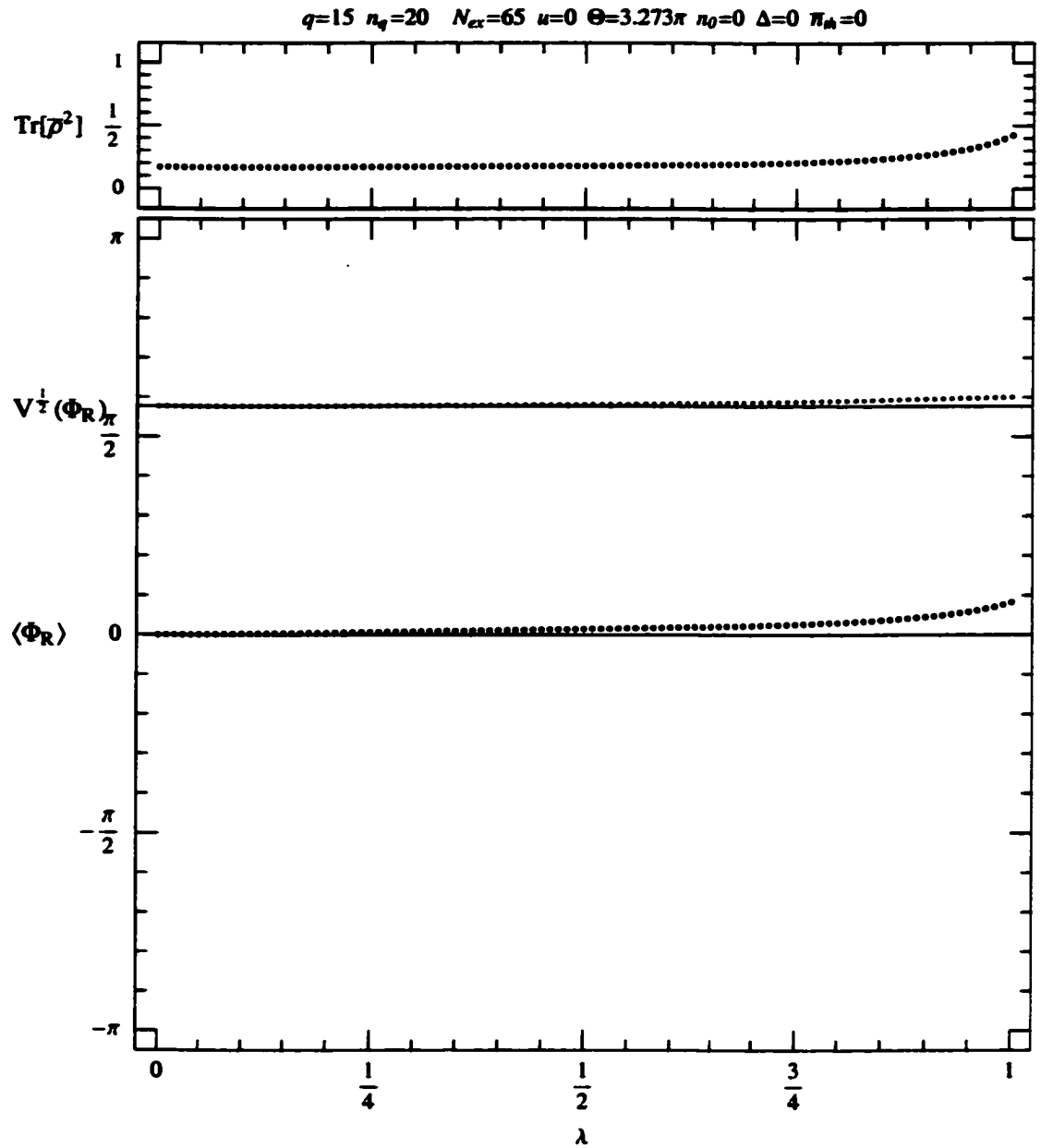

Figure 52: On the top the value of Tr $[\bar{\rho}^2]$ indicating the purity of the steady state. On the bottom is the value of $\langle\Phi_R\rangle$ and the value of $V^{\frac{1}{2}}(\Phi_R)$ corresponding to the probability density function $\bar{P}_S(\Phi_R, \lambda)$. The solid lines are representing the average phase and the square root of the variance corresponding to the uniform distribution.

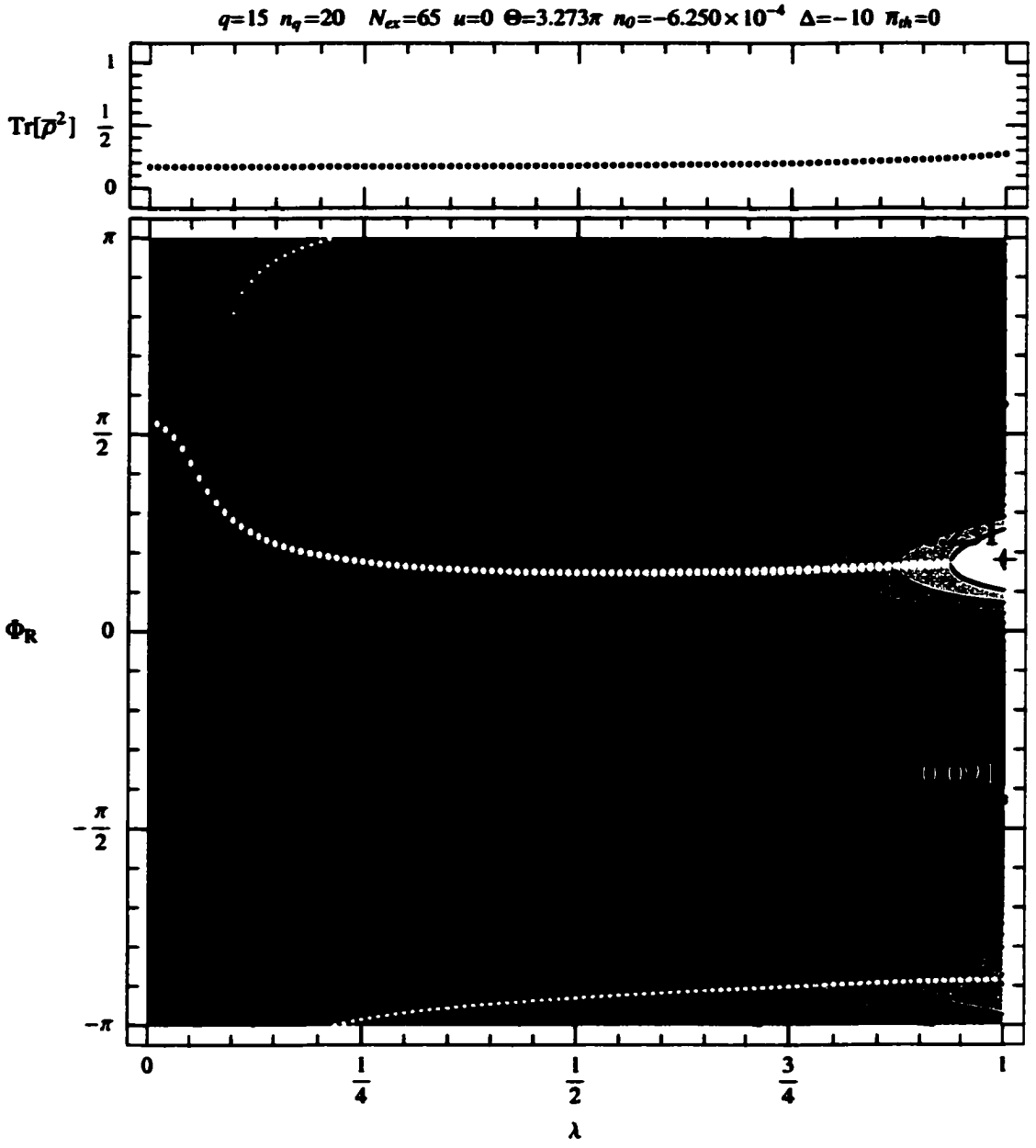

Figure 53: On the top the value of $\mathrm{Tr}\,[\bar{\rho}^2]$ indicating the purity of the steady state. On the bottom is the contour plot of the phase density function $\bar{P}_S(\Phi_R, \lambda)$.

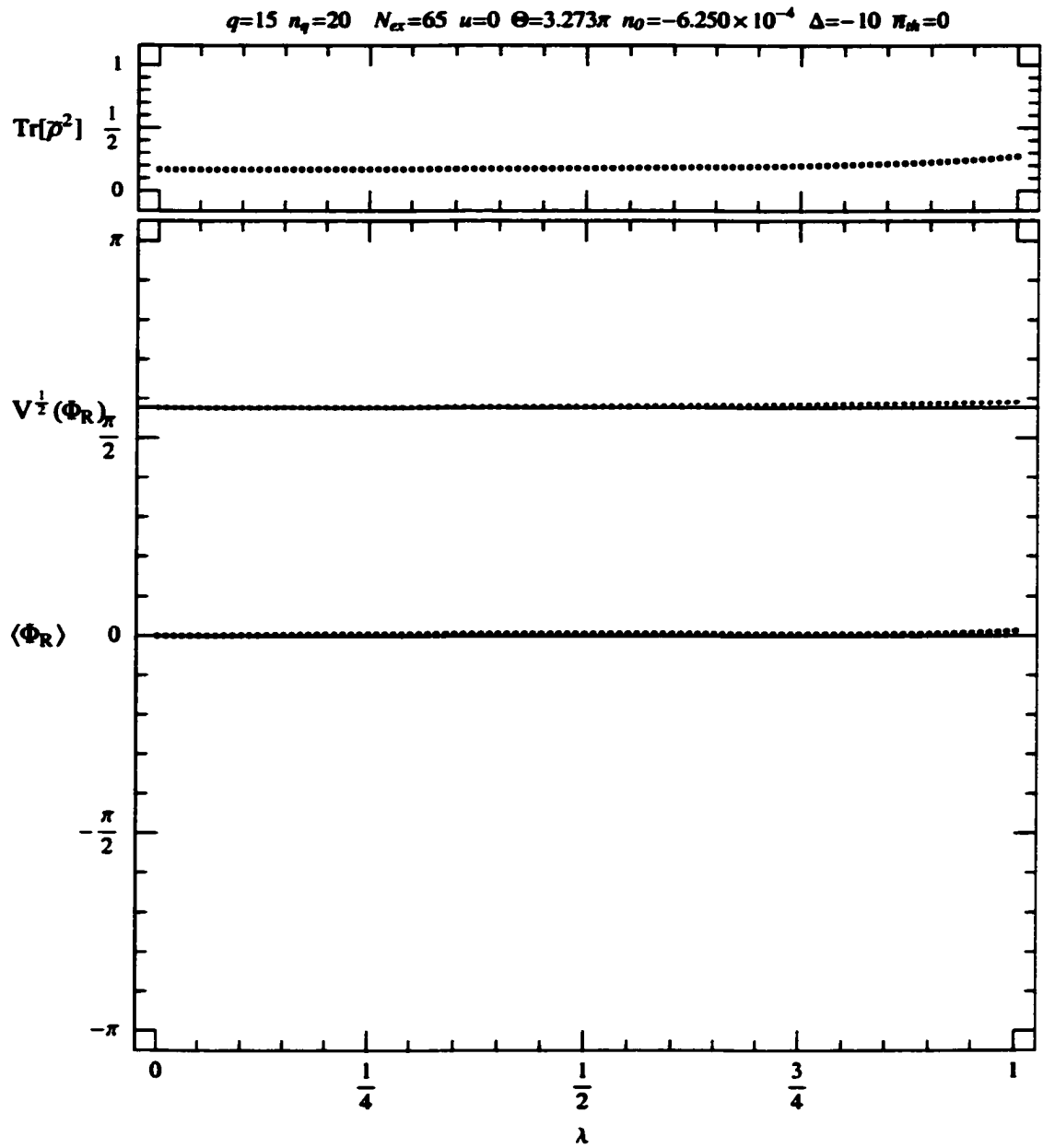

Figure 54: On the top the value of $\mathrm{Tr}\,[\bar{\rho}^2]$ indicating the purity of the steady state. On the bottom is the value of $\langle\Phi_R\rangle$ and the value of $V^{\frac{1}{2}}(\Phi_R)$ corresponding to the probability density function $\bar{P}_S(\Phi_R, \lambda)$. The solid lines are representing the average phase and the square root of the variance corresponding to the uniform distribution.

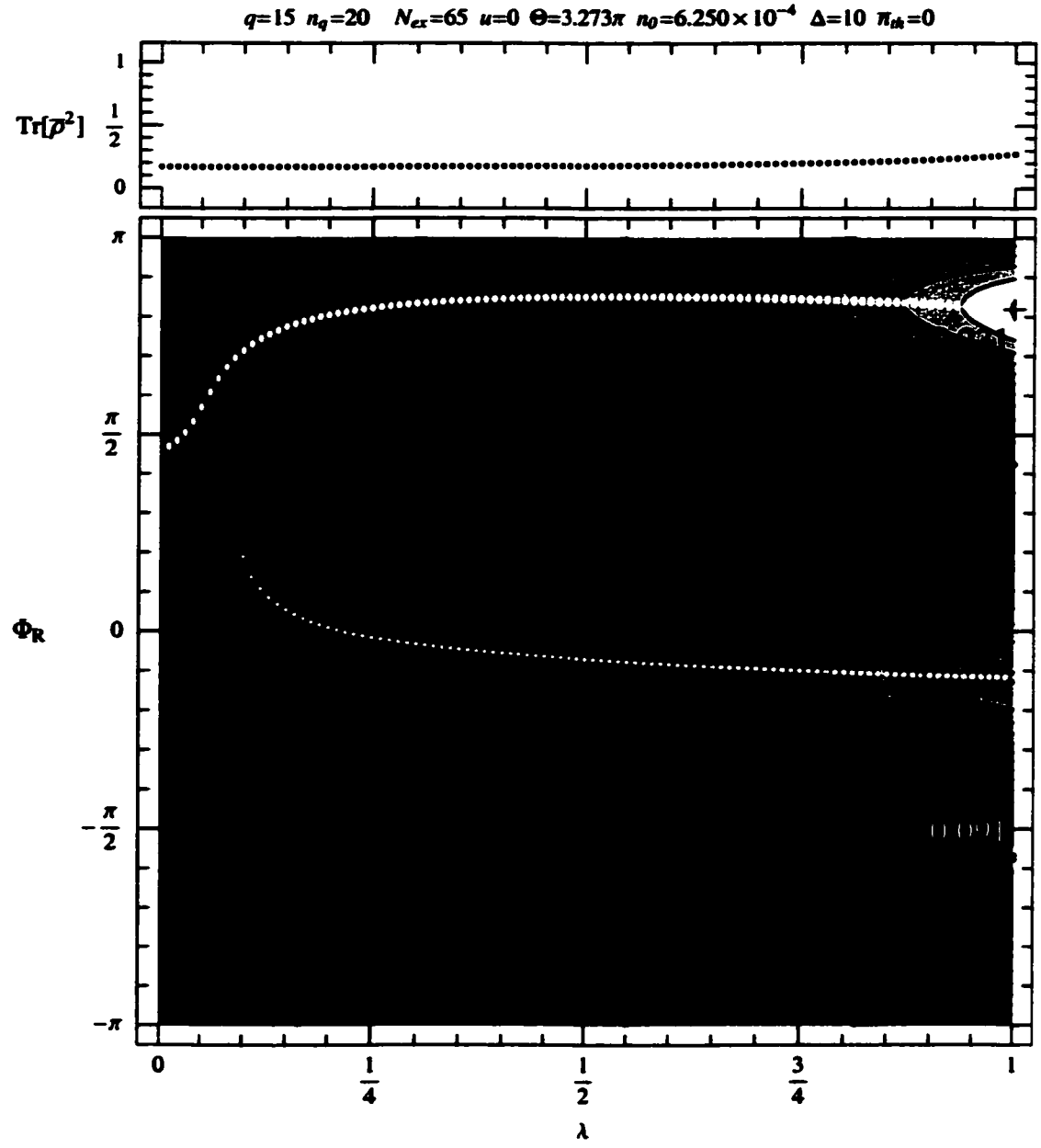

Figure 55: On the top the value of Tr $[\bar{\rho}^2]$ indicating the purity of the steady state. On the bottom is the contour plot of the phase density function $\bar{P}_S(\Phi_R, \lambda)$.

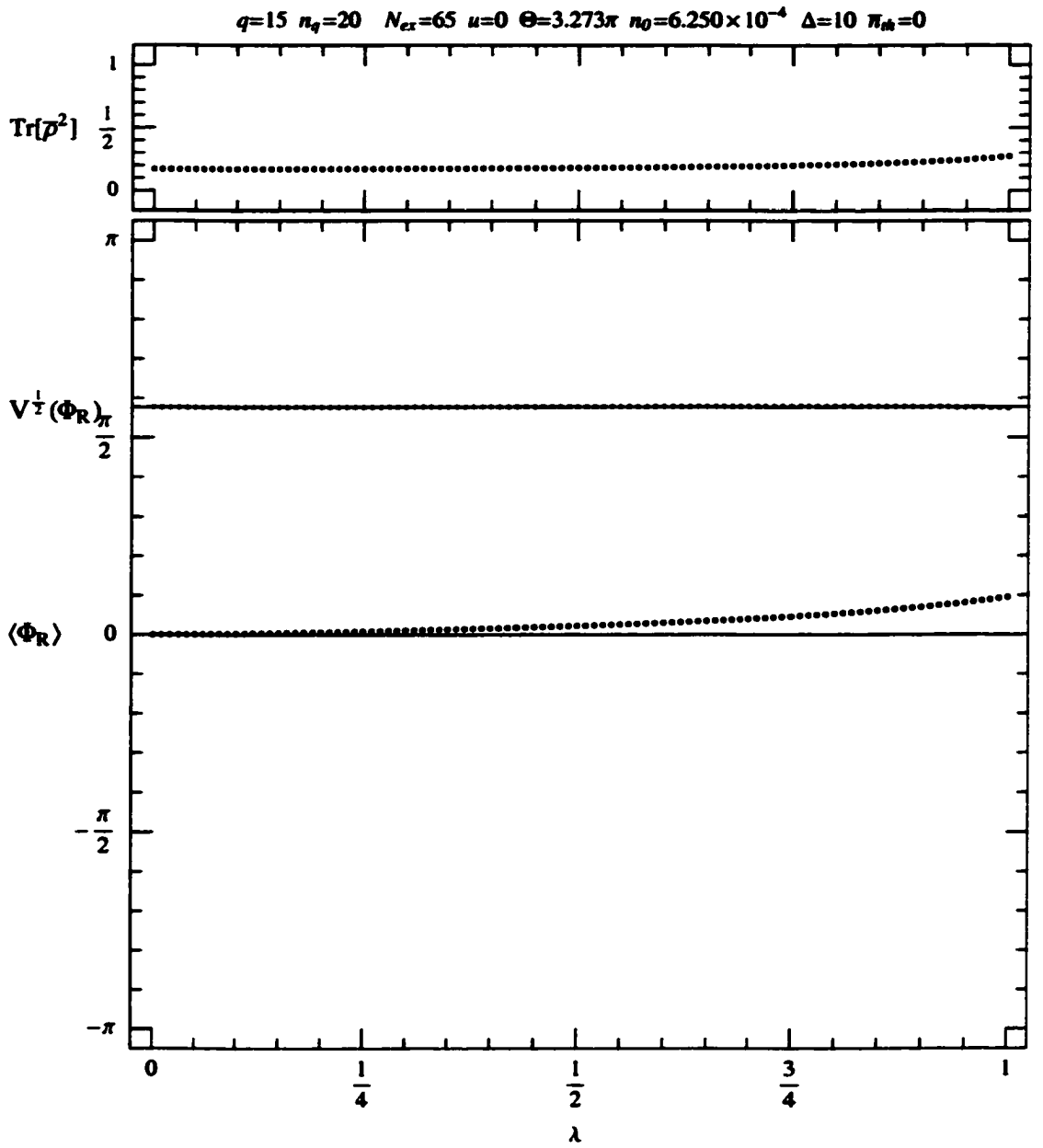

Figure 56: On the top the value of $\mathrm{Tr}\,[\bar{\rho}^2]$ indicating the purity of the steady state. On the bottom is the value of $\langle\Phi_R\rangle$ and the value of $V^{\frac{1}{2}}(\Phi_R)$ corresponding to the probability density function $\bar{P}_S(\Phi_R, \lambda)$. The solid lines are representing the average phase and the square root of the variance corresponding to the uniform distribution.

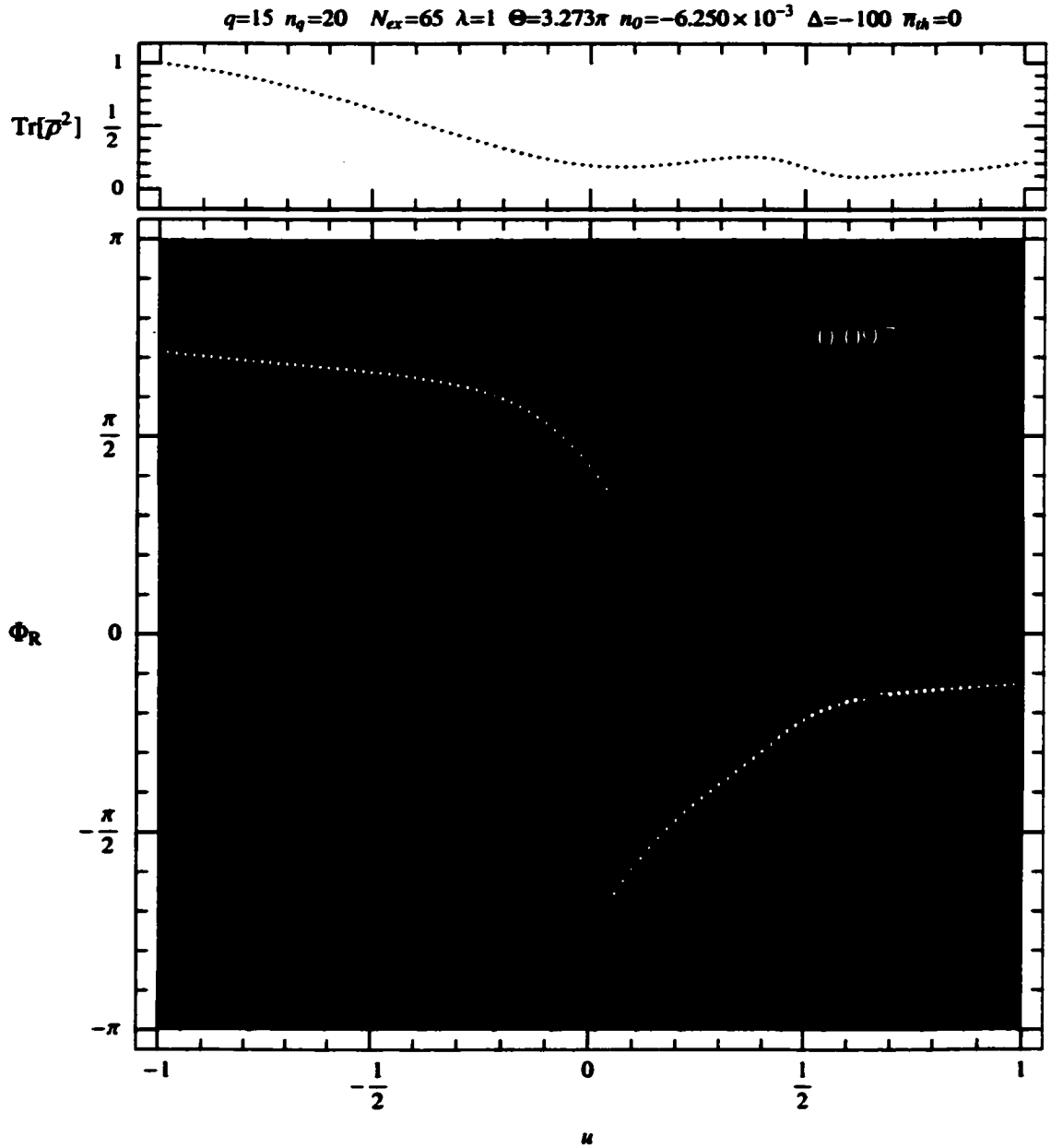

Figure 57: On the top the value of Tr $[\bar{\rho}^2]$ indicating the purity of the steady state. On the bottom is the contour plot of the phase density function $\bar{P}_S(\Phi_R, u)$.

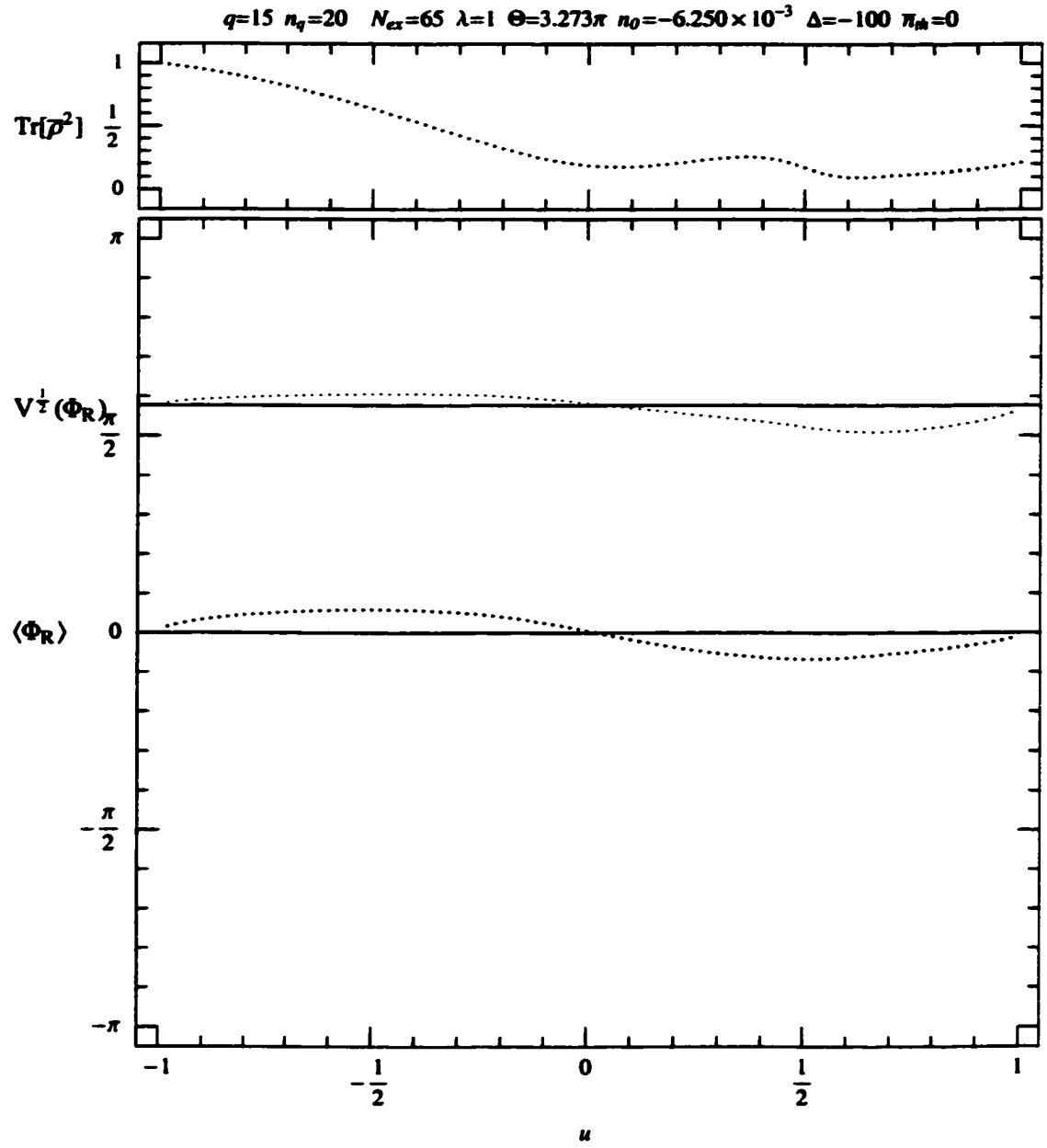

Figure 58: On the top the value of $\mathrm{Tr}\,[\tilde{\rho}^2]$ indicating the purity of the steady state. On the bottom is the value of $\langle \Phi_R \rangle$ and the value of $V^{\frac{1}{2}}(\Phi_R)$ corresponding to the probability density function $\tilde{P}_S(\Phi_R, u)$. The solid lines are representing the average phase and the square root of the variance corresponding to the uniform distribution.

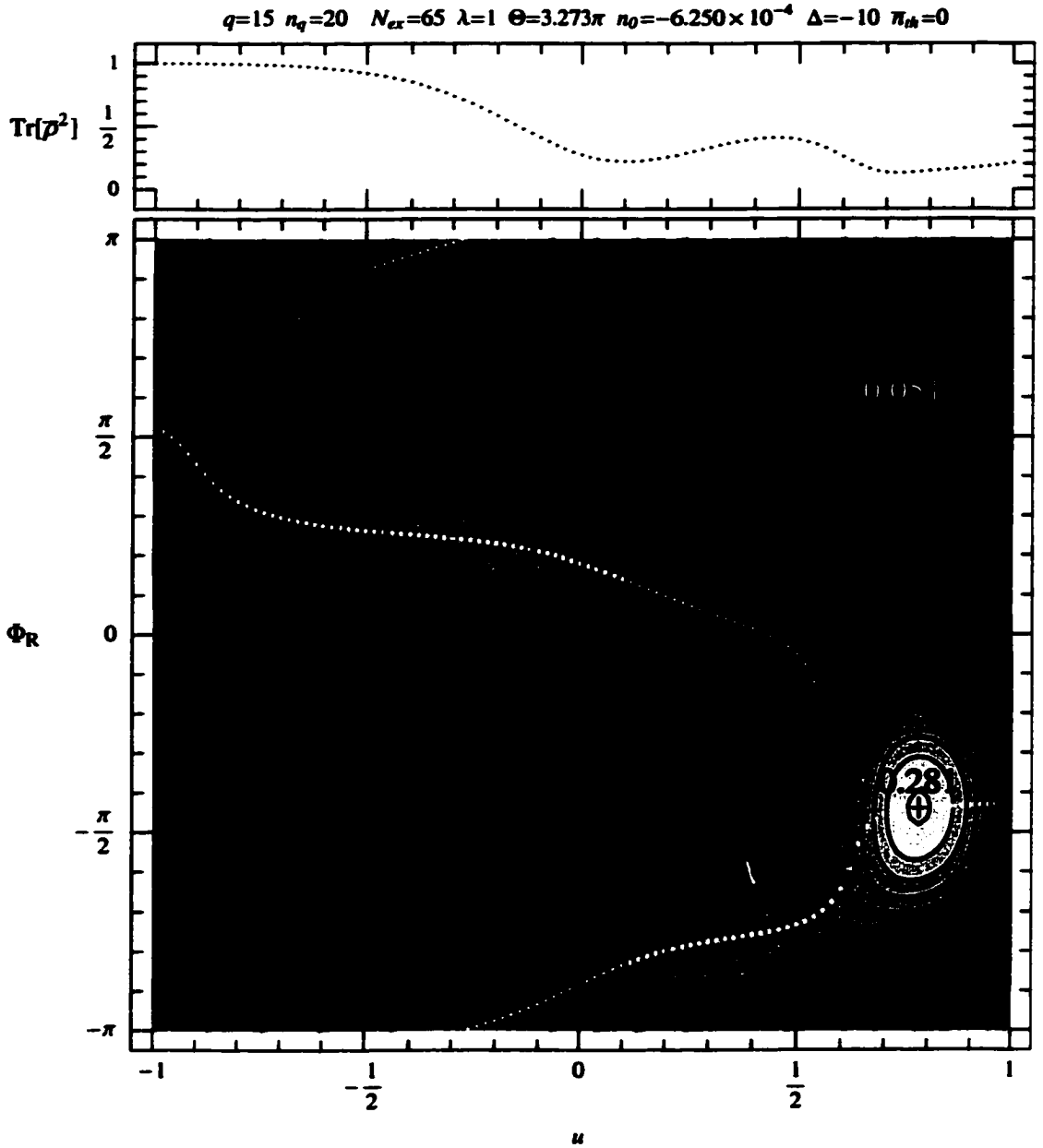

Figure 59: On the top the value of Tr $[\bar{\rho}^2]$ indicating the purity of the steady state. On the bottom is the contour plot of the phase density function $\bar{P}_S(\Phi_R, u)$.

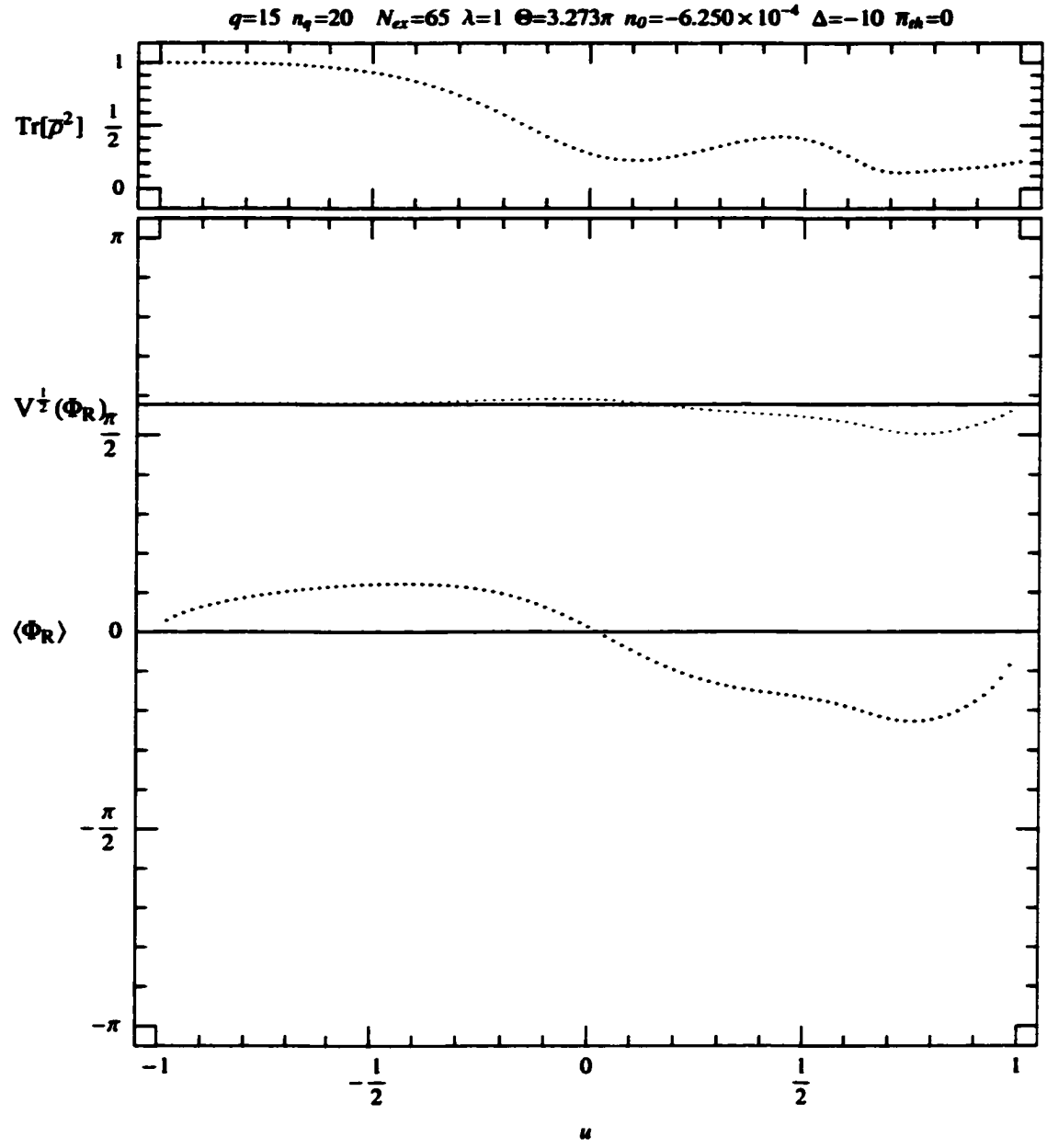

Figure 60: On the top the value of Tr $[\bar{\rho}^2]$ indicating the purity of the steady state. On the bottom is the value of $\langle \Phi_R \rangle$ and the value of $V^{\frac{1}{2}}(\Phi_R)$ corresponding to the probability density function $\bar{P}_S(\Phi_R, u)$. The solid lines are representing the average phase and the square root of the variance corresponding to the uniform distribution.

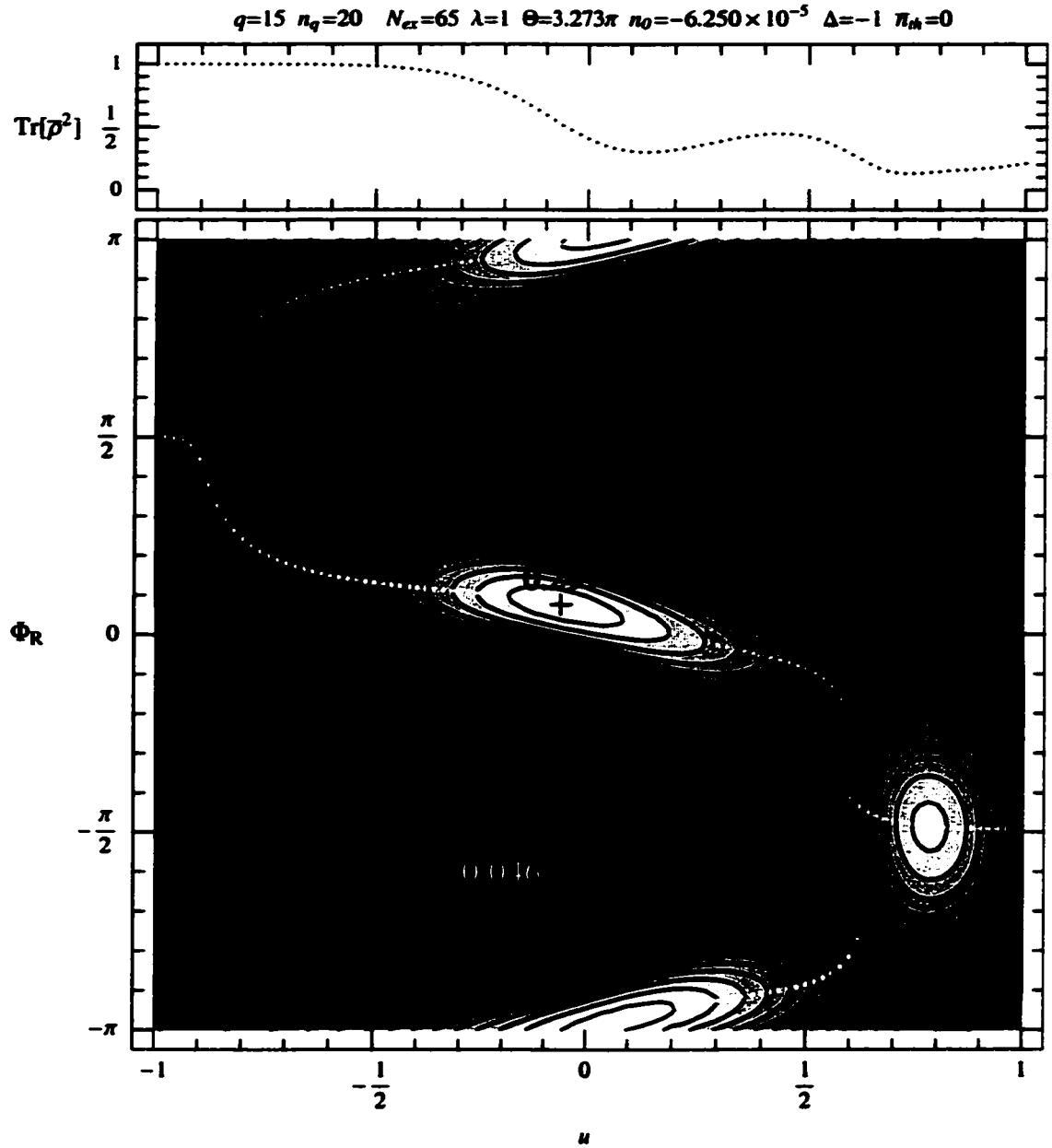

Figure 61: On the top the value of Tr $[\bar{\rho}^2]$ indicating the purity of the steady state. On the bottom is the contour plot of the phase density function $\bar{P}_S(\Phi_R, u)$.

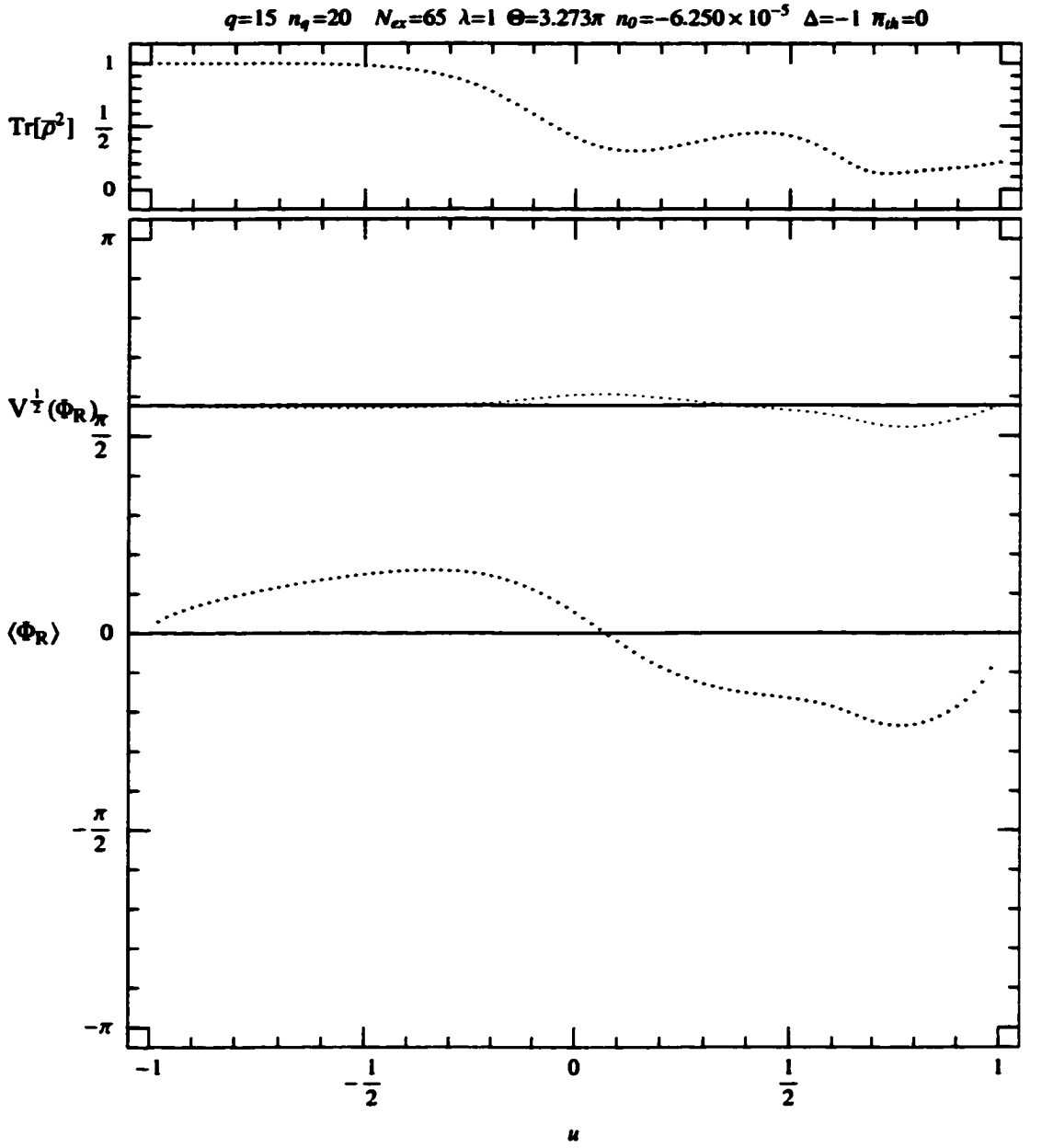

Figure 62: On the top the value of $\mathrm{Tr}\,[\bar{\rho}^2]$ indicating the purity of the steady state. On the bottom is the value of $\langle\Phi_R\rangle$ and the value of $V^{\frac{1}{2}}(\Phi_R)$ corresponding to the probability density function $\bar{P}_S(\Phi_R, u)$. The solid lines are representing the average phase and the square root of the variance corresponding to the uniform distribution.

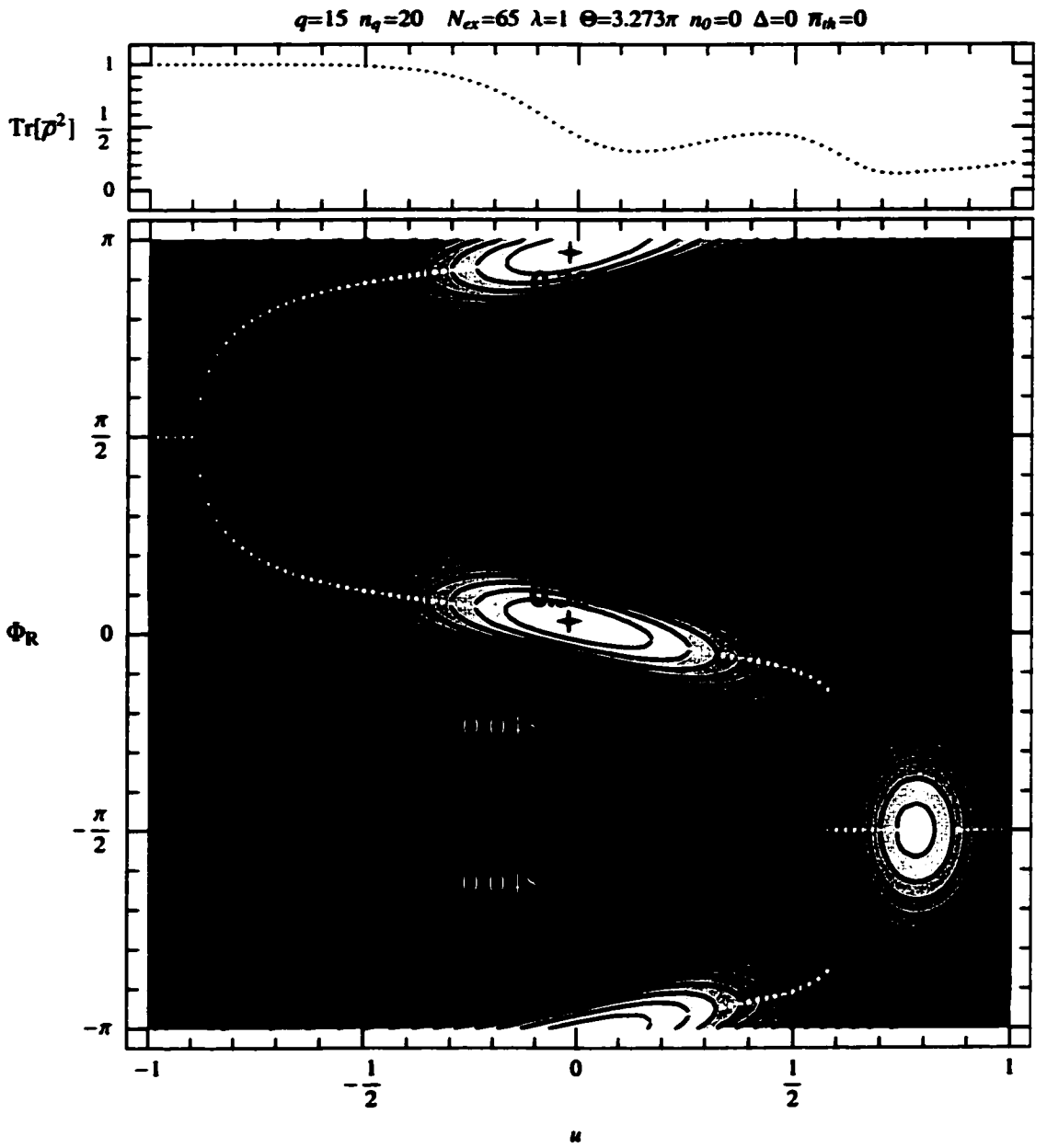

Figure 63: On the top the value of $\mathrm{Tr}\,[\bar{\rho}^2]$ indicating the purity of the steady state. On the bottom is the contour plot of the phase density function $\bar{P}_S(\Phi_R, u)$.

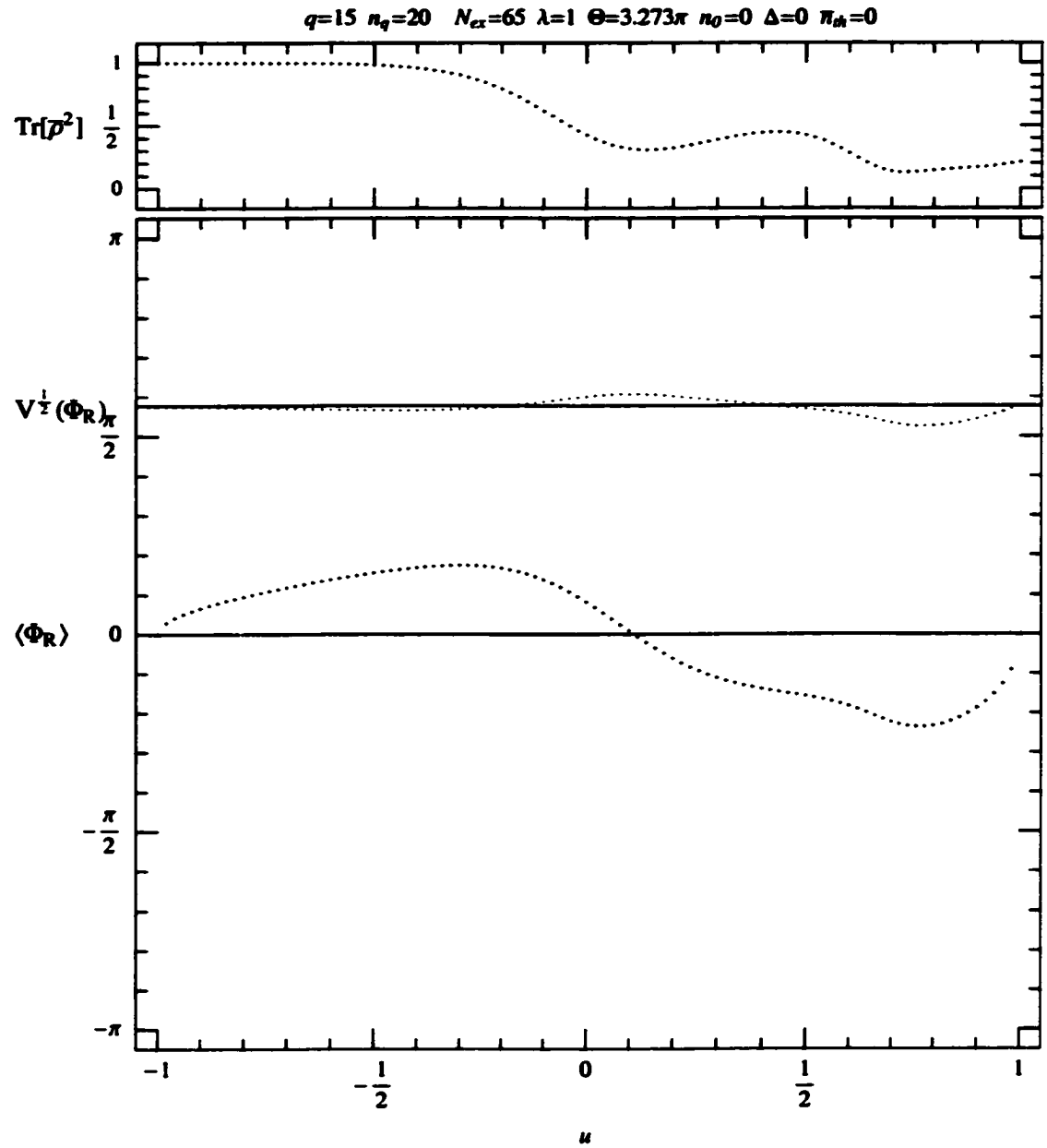

Figure 64: On the top the value of $\mathrm{Tr}\,[\bar{\rho}^2]$ indicating the purity of the steady state. On the bottom is the value of $\langle\Phi_R\rangle$ and the value of $V^{\frac{1}{2}}(\Phi_R)$ corresponding to the probability density function $\bar{P}_S(\Phi_R, u)$. The solid lines are representing the average phase and the square root of the variance corresponding to the uniform distribution.

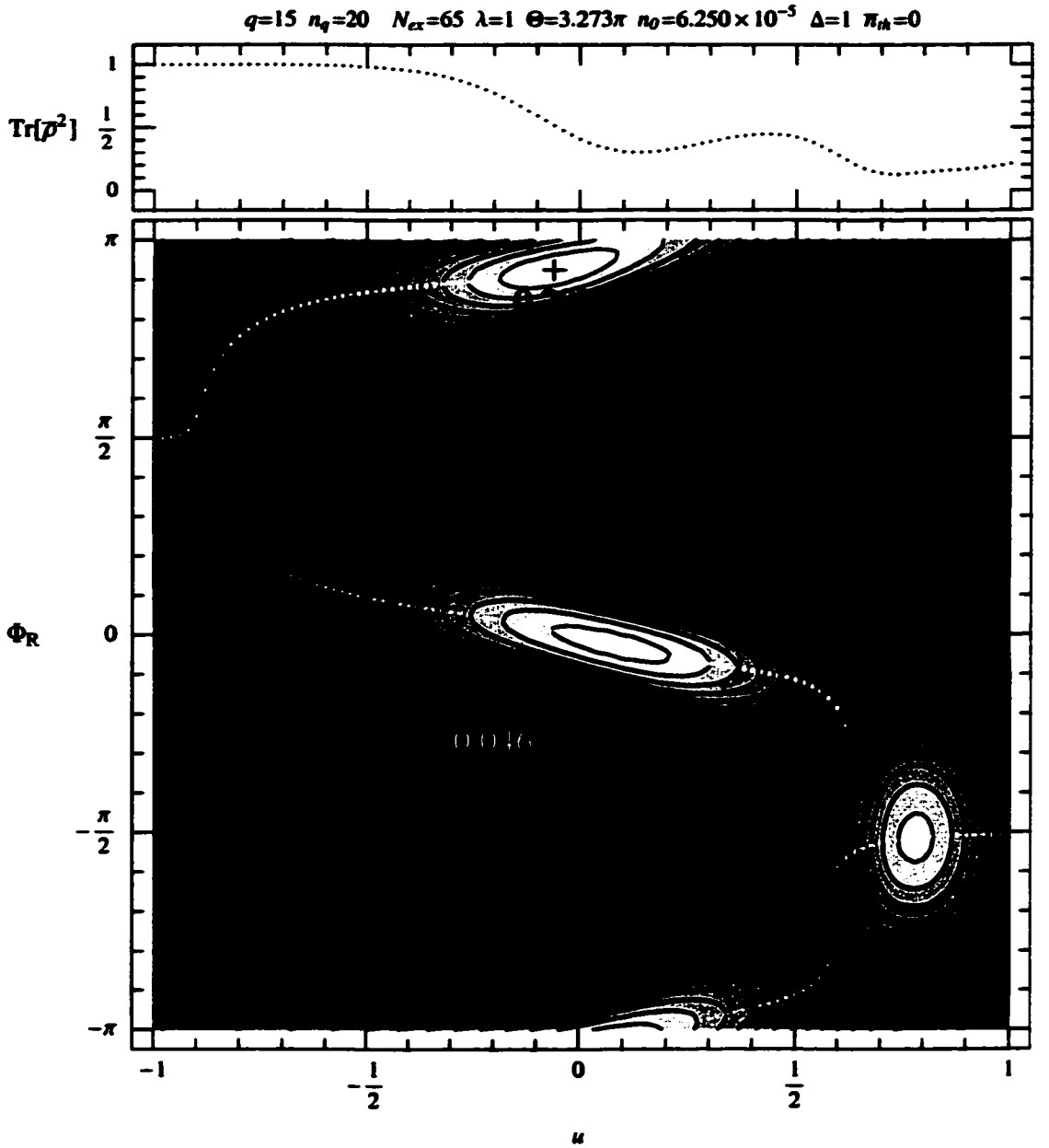

Figure 65: On the top the value of $\mathrm{Tr}\,[\bar{\rho}^2]$ indicating the purity of the steady state. On the bottom is the contour plot of the phase density function $\bar{P}_S(\Phi_R, u)$.

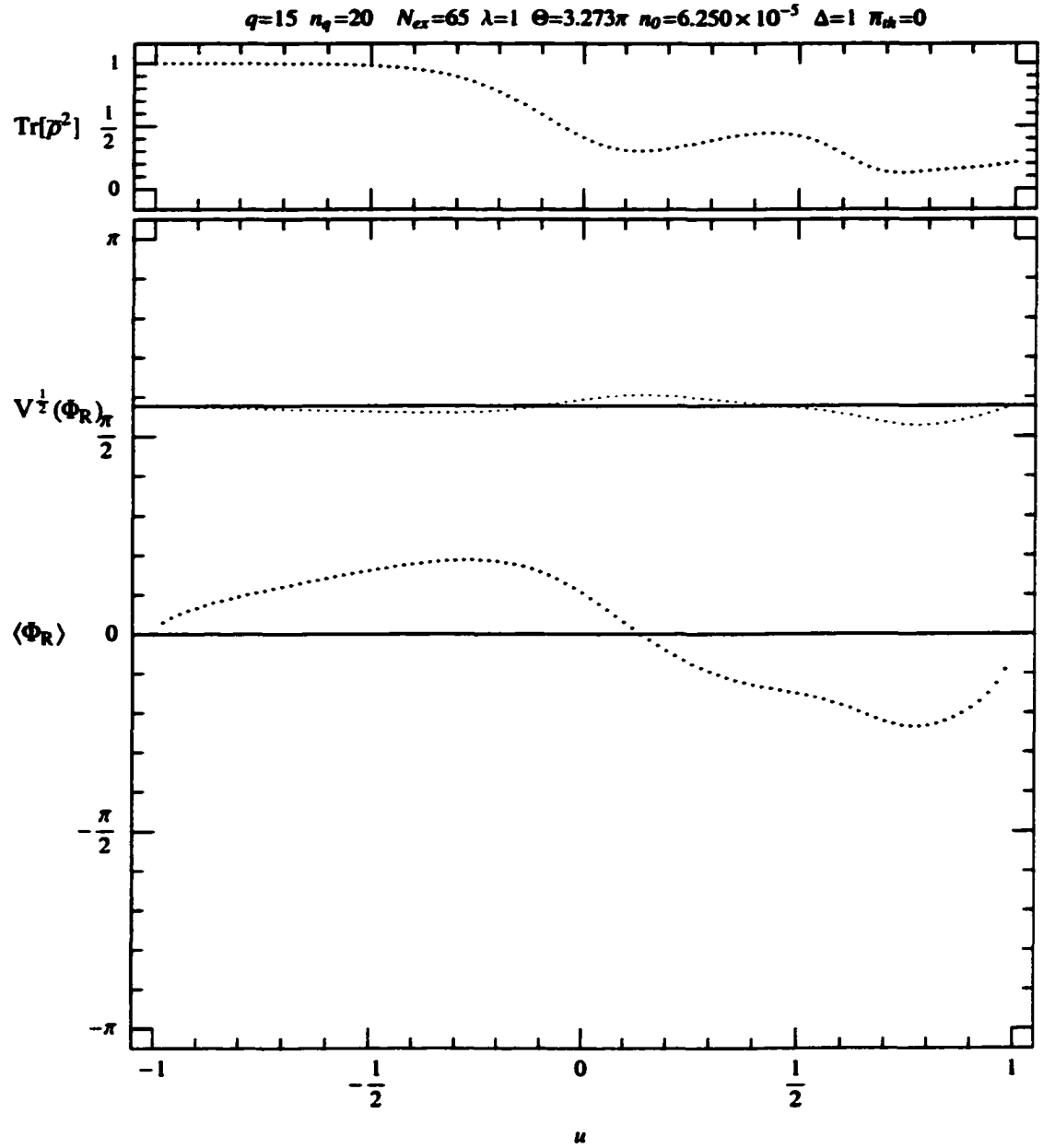

Figure 66: On the top the value of $\mathrm{Tr}[\bar{\rho}^2]$ indicating the purity of the steady state. On the bottom is the value of $\langle \Phi_R \rangle$ and the value of $V^{\frac{1}{2}}(\Phi_R)$ corresponding to the probability density function $\bar{P}_S(\Phi_R, u)$. The solid lines are representing the average phase and the square root of the variance corresponding to the uniform distribution.

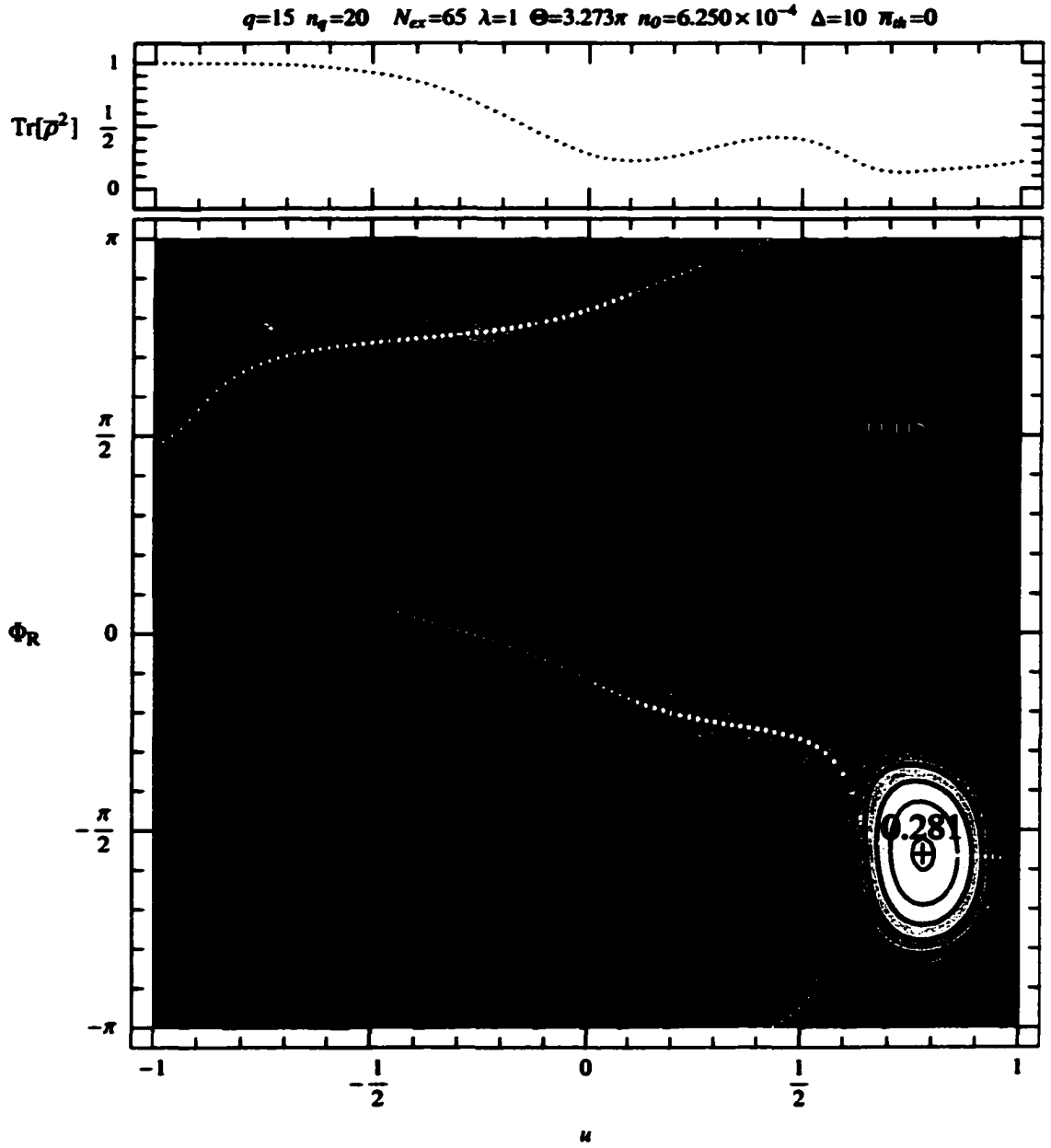

Figure 67: On the top the value of $\mathrm{Tr}\,[\bar{\rho}^2]$ indicating the purity of the steady state. On the bottom is the contour plot of the phase density function $\bar{P}_S(\Phi_R, u)$.

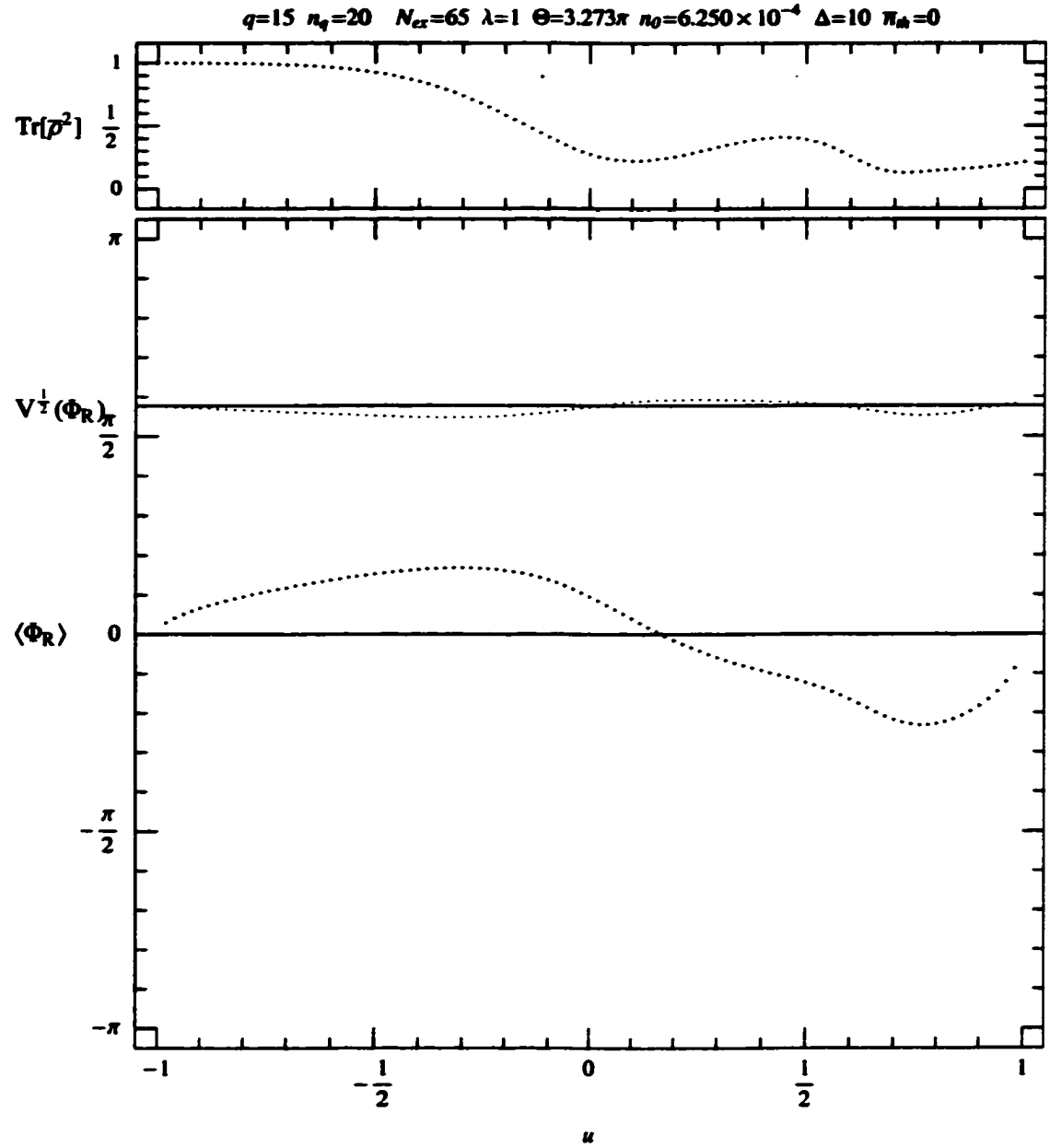

Figure 68: On the top the value of $\mathrm{Tr}\,[\bar{\rho}^2]$ indicating the purity of the steady state. On the bottom is the value of $\langle \Phi_R \rangle$ and the value of $V^{\frac{1}{2}}(\Phi_R)$ corresponding to the probability density function $\bar{P}_S(\Phi_R, u)$. The solid lines are representing the average phase and the square root of the variance corresponding to the uniform distribution.

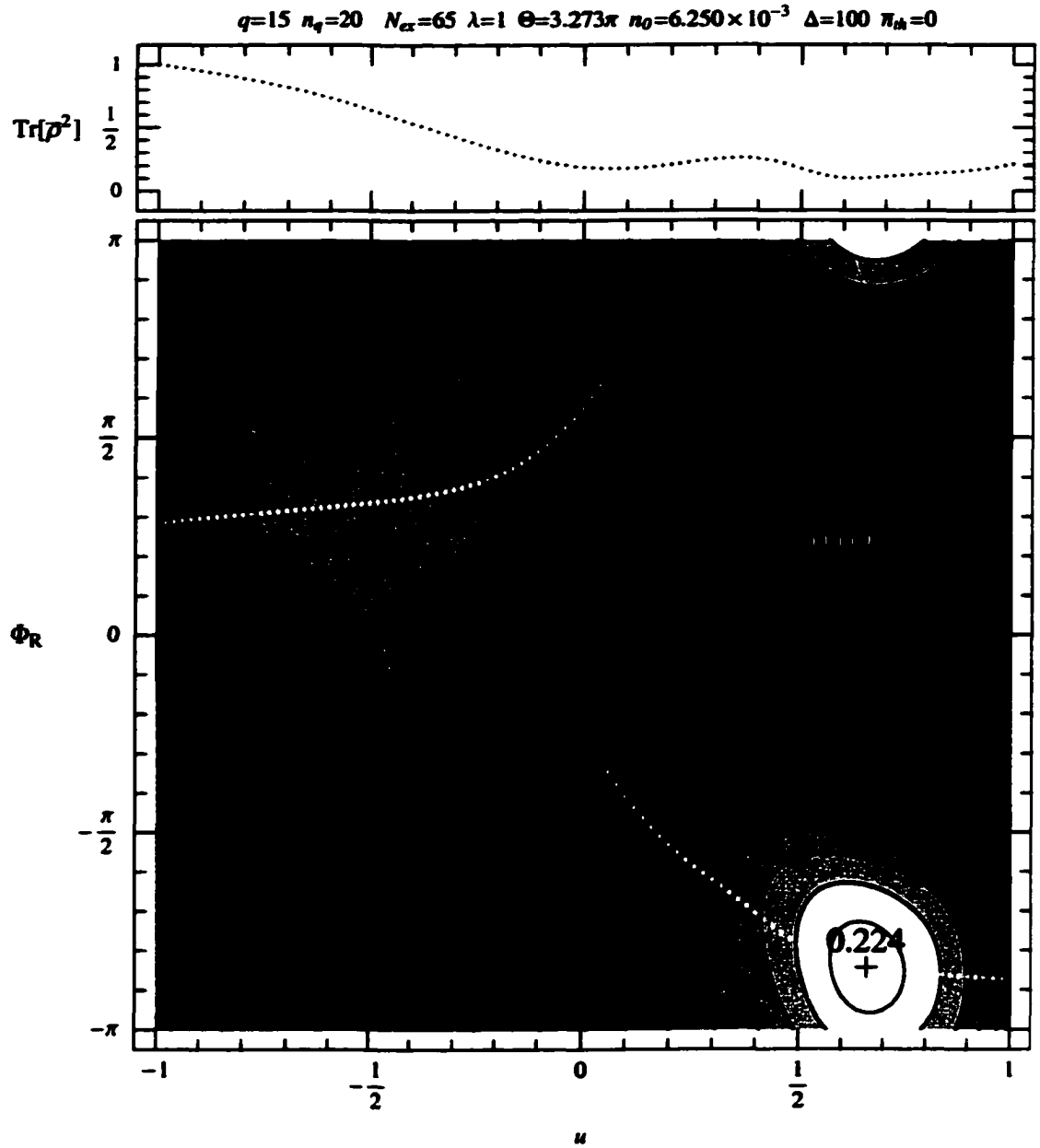

Figure 69: On the top the value of $\mathrm{Tr}\,[\bar{\rho}^2]$ indicating the purity of the steady state. On the bottom is the contour plot of the phase density function $\bar{P}_S(\Phi_R, u)$.

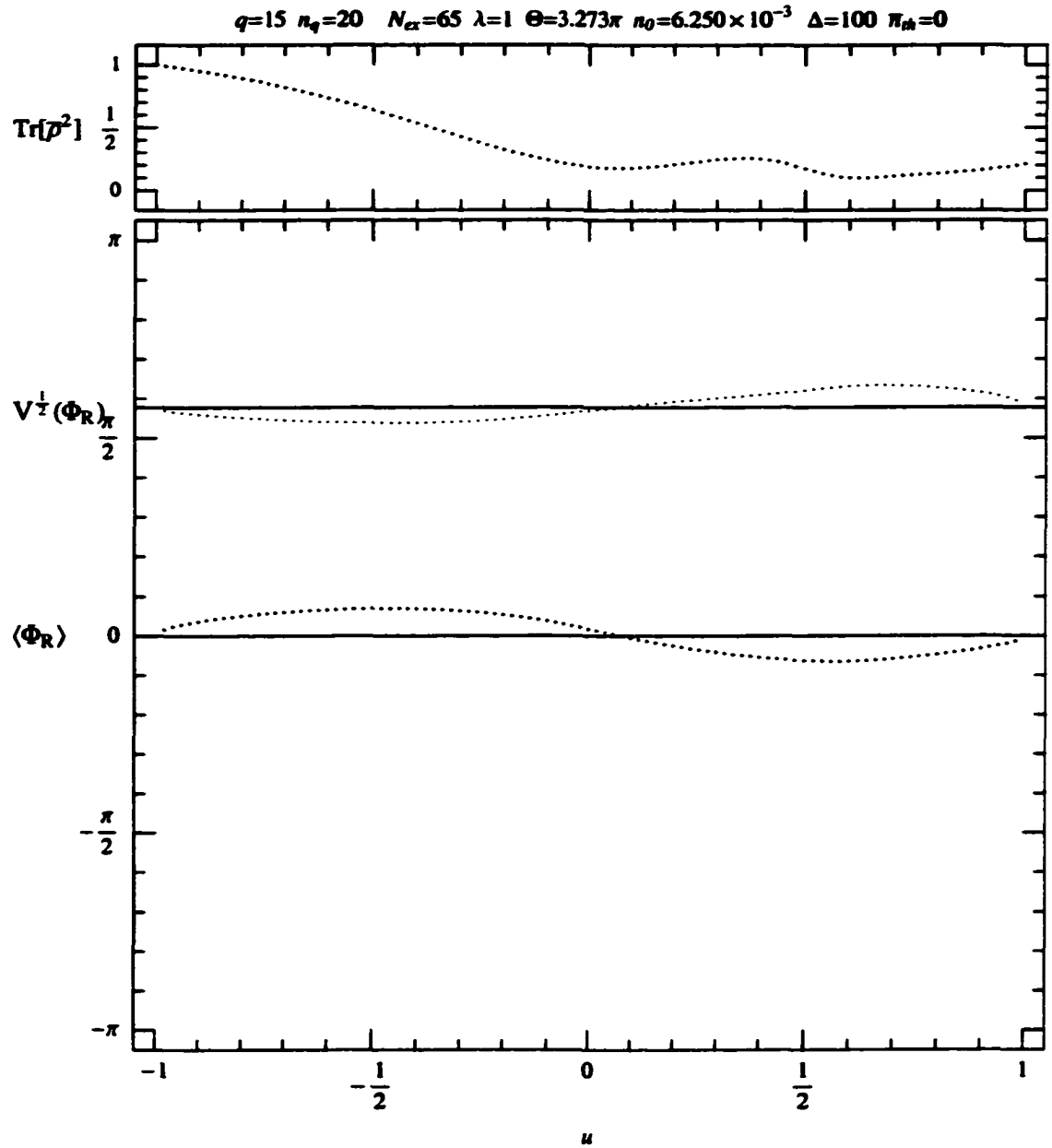

Figure 70: On the top the value of $\mathrm{Tr}\,[\bar{\rho}^2]$ indicating the purity of the steady state. On the bottom is the value of $\langle\Phi_R\rangle$ and the value of $V^{\frac{1}{2}}(\Phi_R)$ corresponding to the probability density function $\bar{P}_S(\Phi_R, u)$. The solid lines are representing the average phase and the square root of the variance corresponding to the uniform distribution.

Bibliography

[1] P. Filipowicz, J. Javanainen, and P. Meystre, J. Opt. Soc. Am. B **3**, 906 (1986).

[2] P. Filipowicz, J. Javanainen, and P. Meystre, Phys. Rev. A **34**, 3077 (1986).

[3] J. A. Bergou, B.-G. Englert, M. Lax, M. O. Scully, H. Walther, and M. S. Zubairy, in *Handbook of Optics*, edited by M. Bass (McGraw-Hill, New York, 2001), vol. IV, chap. 26, 2nd ed.

[4] D. Meschede, H. Walther, and G. Muller, Phys. Rev. Lett. **54**, 551 (1985).

[5] M. Brune, J. M. Raimond, P. Goy, L. Davidovitch, and S. Haroche, Phys. Rev. Lett. **59**, 1899 (1987).

[6] G. Rempe, H. Walther, and J. Klein, Phys. Rev. Lett. **58**, 353 (1987).

[7] G. Rempe, F. Schmidt-Kaler, and H. Walther, Phys. Rev. Lett. **64**, 2783 (1990).

[8] G. Rempe and H. Walther, Phys. Rev. A **42**, 1650 (1990).

[9] B. W. Shore and P. L. Knight, J. Mod. Opt. **40**, 1195 (1993).

[10] E. T. Jaynes and F. W. Cummings, Proc. IEEE **51**, 89 (1963).

[11] C. Bracher, J. Phys. B **30**, 2717 (1997).

[12] P. Masiak, K. Rzazewski, and L. Roso, Phys. Rev. A **51**, 3267 (1995).

[13] J. A. Bergou and M. Hillery, Phys. Rev. A **55**, 4585 (1997).

[14] P. Meystre, G. Rempe, and H. Walther, Opt. Lett. **13**, 1078 (1988).

[15] J. J. Slosser and P. Meystre, Phys. Rev. A **41**, 3867 (1990).

[16] J. J. Slosser, P. Meystre, and S. Braunstein, Phys. Rev. Lett. **63**, 934 (1989).

[17] S. Brattke, B. T. Varcoe, and H. Walther, Optics Express **8**, 131 (2001).

[18] M. O. Scully, H. Walther, G. S. Agarwal, T. Quang, and W. Schleich, Phys. Rev. A **44**, 5992 (1991).

[19] W. C. Schieve and R. R. McGowan, Phys. Rev. A **48**, 2315 (1993).

[20] T. Quang, G. S. Agarwal, J. A. Bergou, M. O. Scully, and H. Walther, Phys. Rev. A **48**, 803 (1993).

[21] N. Lu, Opt. Commun. **103**, 315 (1993).

[22] N. Lu, Phys. Rev. A **47**, 1347 (1993).

[23] K. Vogel, W. P. Schleich, M. O. Scully, and H. Walther, Phys. Rev. A **48**, 813 (1993).

[24] W. C. Schieve and R. R. McGowan, Phys. Rev. A **55**, 3813 (1997).

[25] R. R. McGowan and W. C. Schieve, Phys. Rev. A **59**, 778 (1999).

[26] U. Herzog and J. Bergou, Phys. Rev. A **62**, 063814 (2000).

[27] R. J. Brecha, A. Peters, C. Wagner, and H. Walther, Phys. Rev. A **46**, 567 (1992).

[28] H.-J. Briegel, B.-G. Englert, N. Sterpi, and H. Walther, Phys. Rev. A **49**, 2962 (1994).

[29] B.-G. Englert, T. Gantsog, A. Schenzle, C. Wagner, and H. Walther, Phys. Rev. A **53**, 4386 (1996).

[30] J. Krause, M. O. Scully, and H. Walther, Phys. Rev. A **34**, 2032 (1986).

[31] A. M. Guzman, P. Meystre, and E. M. Wright, Phys. Rev. A **40**, 2471 (1989).

[32] J. Skvarcek and M. Hillery, Phys. Rev. A **62**, 013807 (2000).

[33] N. Lu and J. A. Bergou, Phys. Rev. A **40**, 237 (1989).

[34] J. D. Cresser, Phys. Rev. A **46**, 5913 (1992).

[35] L. E. Reichl, *A modern course in statistical physics* (John Wiley & Sons, New York, 1998), 2nd ed.

[36] Z. Liu, L. Zeng, S. Zhu, and T. F. George, J. Mod. Opt. **45**, 2473 (1998).

[37] L. D. Landau and E. M. Lifshitz, *Mechanics* (Pergamon Press, Oxford, 1976).

[38] M. W. Hirsch and S. Smale, *Differential Equations, Dynamical Systems, and Linear Algebra* (Academic Press, New York, 1974).

[39] H. Goldstein, *Classical Mechanics* (Addison-Wesley, Reading, MA, 1980), 2nd ed.

[40] M. Artin, *Algebra* (Prentice Hall, Englewood Cliffs, NJ, 1991).

[41] D. T. Pegg and S. M. Barnett, Phys. Rev. A **39**, 1665 (1989).

[42] L. Susskind and J. Glogower, Physics **1**, 49 (1964).